International Conference
“Micro- and nanoelectronics – 2009”

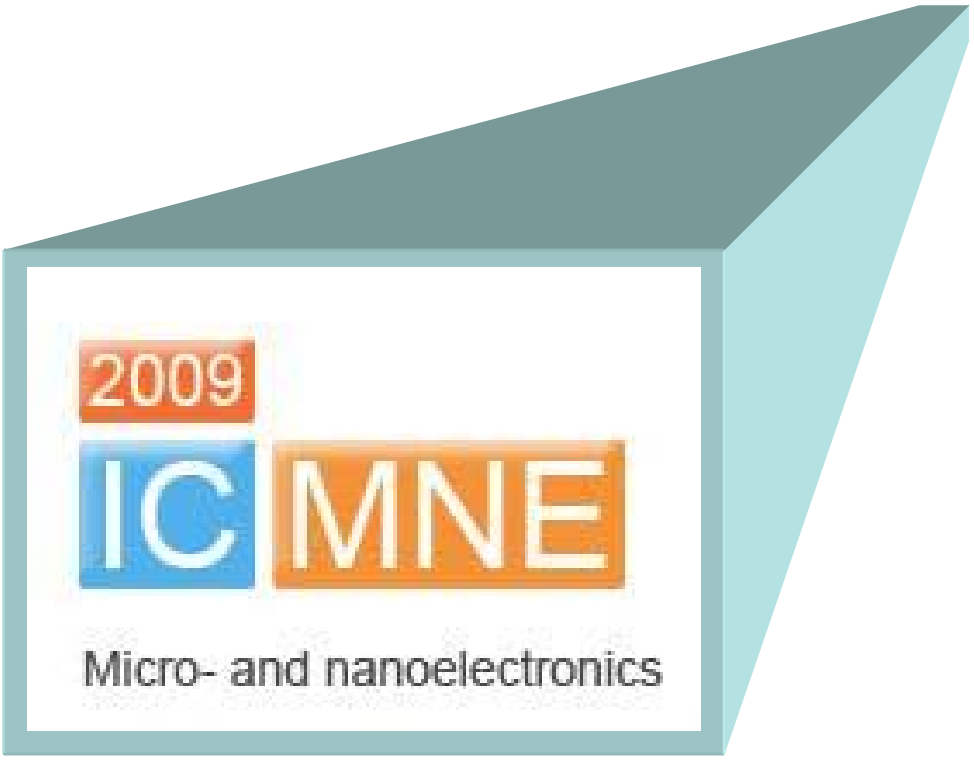

Book of

ABSTRACTS

October 5th - 9th, 2009
Moscow – Zvenigorod, Russia

Russian Academy of Sciences (RAS)

Russian Foundation for Basic Research

The International Society for Optical Engineering (SPIE), Cooperating Organization

- Insitute of Physics & Technology (IPT) of RAS, Moscow, Russia
- Institute of Semiconductor Physics (ISP) of Siberian Brahch of RAS, Novosibirsk, Russia
- Lomonosov Moscow State University, Moscow, Russia
- Moscow Institute of Electronic Engineering (TU) (MIEE), Zelenograd, Russia
- International Microelectronic Centre (IMEC), Leuven, Belgium

International Conference "Micro- and nanoelectronics – 2009" ICMNE-2009

October, 5th - 9th, 2009
Moscow – Zvenigorod, Russia

Supported by:

TABLE OF CONTENTS

How to search for necessary abstract?

The sheets of paper abstracts in this issue are colored according to the day of presentation at Conference. Every Abstract has its own identification number (for instance L1-04, O1-07, q2-09, P2-28 and so on), which is marked in the right bottom corner of page. This number is corresponding to the one in *Conference Programme*. If you don't know the number of paper in Scientific Program and one of the authors of paper is known it is possible to search for necessary Abstract by *Author Index* located at the end of the *Book of Abstracts*.

Как отыскать интересующие Вас тезисы доклада?

Страница сборника, содержащая искомые тезисы доклада, имеет цвет, соответствующий дню представления доклада на Конференции. Каждый доклад имеет собственный идентификационный номер (например, L1-04, O1-07, q2-09 P2-28 и т.д.), который указан в правом нижнем углу страницы. Этот номер совпадает с номером, присвоенным докладу в *Программе Конференции*. Если Вы не знаете номера доклада, но Вам известен хотя бы один из авторов, вы можете воспользоваться *Авторским Указателем*, расположенным в конце *Сборника Тезисов.*

Carl Zeiss SMT/NTS - Департамент нанотехнологических систем и электронной микроскопии

MERLIN™

Аналитические возможности для наноисследований

- Получение полной информации об образце
- Анализ на уровне наноразмеров
- Возможность дооснащения
- Легкость управления

Новое поколение аналитических автоэмиссионных электронных микроскопов

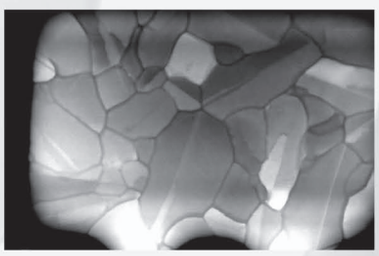

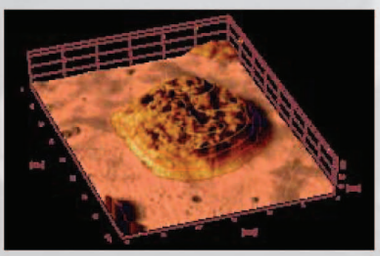

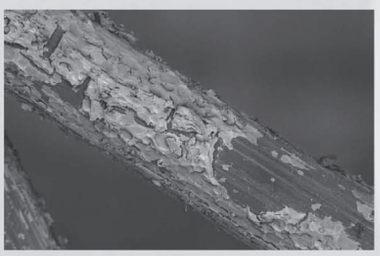

Carl Zeiss SMT
Enabling the Nano-Age World®

105005, Москва
Денисовский пер., 26,
Тел.: +7 (495) 933-51-51
+7 (495) 933-51-56
Факс: +7 (495) 933-51-55,
office@zeiss.ru
www.zeiss.ru
Горячая линия: 8-800-2000-567

ZEISS

We make it visible.

Компания **Technoinfo Ltd.** предлагает широкий спектр аналитического, лабораторного, испытательного и технологического оборудования, обеспечивает гарантийное и послегарантийное обслуживание, обучение персонала и методическую поддержку.

TechnoInfo
Your partner in nanoscience research

121248 Москва, Кутузовский проспект, д. 9, корп. 2а, офис 75
тел./факс: +7 (499) 243-66-26 эл. почта: sales@technoinfo.ru

IONTOF

TOF.SIMS 5 — времяпролетный масс-спектрометр вторичных ионов
Qtac 100 — высокочувствительный спектрометр рассеяния ионов с малой энергией
NanoScan — магнитно-силовой микроскоп высокого разрешения

KRATOS ANALYTICAL
A SHIMADZU GROUP COMPANY

AXIS Nova — автоматизированный РФС-спектрометр
AXIS Ultra DLD — высокочувствительный многофункциональный электронный спектрометр с параллельным режимом визуализации
AXIS Ultra HSA — многофункциональный РФС-спектрометр с РФС-картированием
AMICUS / ESCA 3400 — высококлассный РФС-спектрометр для повседневного использования

ICE
Innovative Cryogenic Engineering

ICE^{CF} — проточный гелиевый криостат
^{OPTI}**ICE^{CF}** — криостат для спектроскопии
^{3}**ICE^{VT32}** — He3 система
^{D}**ICE^{EASYFIT450}** — рефрижератор растворения
^{4}**ICE** — вставка VTI
^{DRY}**ICE^{4K}** — безгелиевые криостаты
^{DRY}**ICE^{OPTI4K}** — безгелиевые криостаты для спектроскопии
^{DRY}**ICE^{3}** — безгелиевые He3 системы
^{DRY}**ICE^{EASYFIT}** — безгелиевые рефрижераторы растворения
^{DRY}**ICE^{VTI}** — безгелиевые вставки VTI
Cryo-bitz — запчасти, приспособления и расходные материалы для криогенной техники, восстановление и ремонт криостатов, включая системы известных производителей

OXFORD INSTRUMENTS
Plasma Technology

FlexAL / OpAL — атомно-слоевое осаждение (ALD)
Plasmalab 80Plus / Plasmalab System 100 — плазменные процессы осаждения/травления (PECVD, RIE, ICP-RIE, PE)
Optofab 3000 / Ionfab 300Plus — ионно-лучевое осаждение/травление (IBE, IBS, RIBE, CAIBE/IBS, DIBD)
Plasmalab 400 — магнетронное напыление
Nanofab 700 / Nanofab 800 Agile — выращивание наноструктур
CrystalFlex — гидридная эпитаксия (HVPE)

THERMAL TECHNOLOGY LLC
HIGH TEMPERATURE EXPERTS

- вакуумные печи
- высокотемпературные печи
- системы выращивания кристаллов
- системы искрового плазменного спекания
- печи горячего прессования
- печи дугового спекания
- печи для лабораторного и промышленного использования.

Евротек

Компания Евротек создана для взаимного обмена технологиями между Западом и Востоком. Мы поставляем как научное оборудование, изготовленное в США и Германии в Польшу и Россию, так и продукцию российского и польского производства - в США и Германию.

Общие сведения:

Название комапании: Eurotek Inc., компания зарегистрирована в сентябре 1989г.

Президент: Джек Росс

Представительство в Российской Федерации: ООО «Евротек»

Генеральный директор: А.А. Пастор

Цели компании:

Разработка и поставка высокотехнологичного оборудования и комплексных установок для научных лабораторий в высших учебных заведениях, НИИ и исследовательских отделах коммерческих фирм. Мы также сотрудничаем с различными компаниями, которые работают в области лазерных технологий, оптоэлектроники, аналитики и вакуумной технологии.

Поставки продукции:

Поставки оборудования осуществляются через наши офисы в России (в Москве и Санкт-Петербурге), в Польше (в Варшаве) и в Германии (в Бад-Хомбурге).

Услуги

Высококвалифицированные и опытные команды специалистов в России и Польше осуществляют настройку и обслуживание оборудования и иную поддержку клиентов нашей фирмы, которые приобрели продукцию на территории этих стран.

Мы находимся в контакте со многими производителями в сфере электрооптики, биоаналитики, полупроводниковых технологий, наноэлектроники и вакуумного оборудования.
Компания Евротек занимается поставками и продажей высокотехнологичного оборудования (электронные микроскопы, вакуумное оборудование и прочее оборудование для микроэлектронной промышленности).
Мы сотрудничаем с такими компаниями, как Prevac (www.prevac.eu), Novelx (www.novelx.com), Obducat (www.obducat.com) и др.

Контактная информация

ООО «Евротек»
Санкт-Петербург, ул. Седова, 37-А, бизнес центр «Кристалл», 192148
тел: +7 (812) 448 56 65, доб. 246
E-mail: alexanderp@eurotek.com lenap@eurotek.com
А.А.Пастор, генеральный директор
Е.А.Пастор, гл. менеджер по продажам)

НИКС
КОМПЬЮТЕРЫ

БИЗНЕС, ОСНОВАННЫЙ НА НАУЧНОМ ПОДХОДЕ

Спонсор конференций ICMNE2003, Qi2004, ICMNE2005, 2007, 2009

Год основания: **1991**

Профиль: **компьютеры,**
- комплектующие,
- программное обеспечение,
- бизнес-анализ

Учредители: **выпускники МФТИ**

Сотрудники: **600 человек,**
- из них 20% выпускников МФТИ и других физико-математических вузов России

Годовой оборот: **$280млн**

Сайт: www.nix.ru
- **80 тыс. уникальных посетителей в день**

Компьютерный супермаркет НИКС в рамках собственного проекта NANOSOFT® занимается всесторонней поддержкой российской науки и образования, исследований в области квантовой информатики. На гранты нашей компании многие талантливые студенты, преподаватели и российские учёные смогли успешно развивать свою научную деятельность.

NANOSOFT.RU

ваш шанс на прорыв в будущее

Nanosoft® - собственная программа Компьютерного супермаркета НИКС по поддержке российских ученых, занимающихся теоретическими и экспериментальными исследованиями квантовых приборов и нанотехнологий.

http://www.nanosoft.ru, science@nix.ru

Colours do not play at nanometer scale

But you can colour molecules by their Raman spectra.

Raman mapping by TERS with ultra-high resolution

NTEGRA Spectra

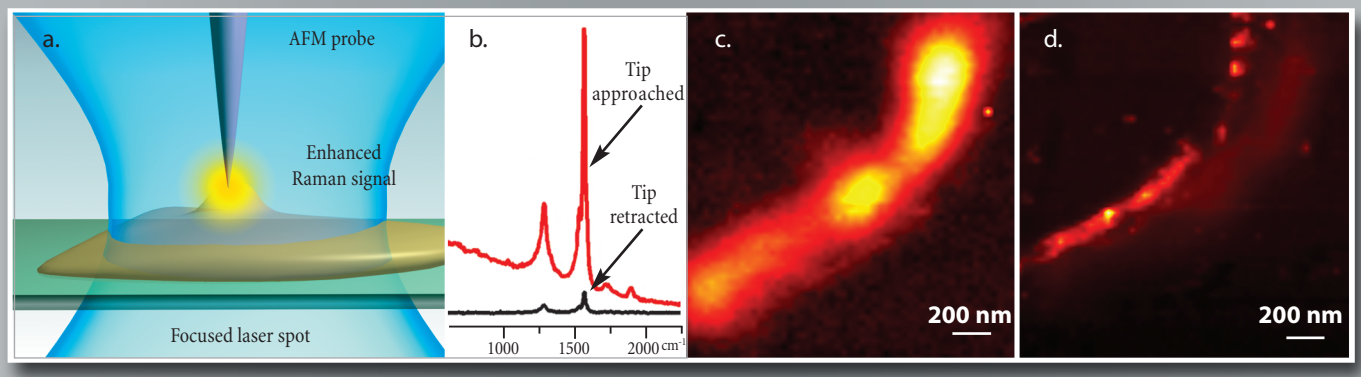

a — a specially prepared AFM probe (metal coated cantilever or etched metal wire) is precisely positioned inside a tightly focused laser spot. b — intensity of carbon nanotube G- and D- Raman bands increases by several orders of magnitude when the special AFM probe is landed and positioned over a small (5 nm height) nanotube bundle - the effect of Tip enhanced Raman scattering (TERS). c — "conventional" confocal Raman image of the nanotube bundle, the observed width of the bundle is ~250 nm (diffraction limit of confocal microscopy, laser wavelength - 633 nm). d — TERS image of the same bundle - now the observed width is ~70 nm.
Note, in this example, TERS provides more than 4-times better spatial resolution as compared to confocal microscopy. Resolution down to 10 nm and less is theoretically possible. Measurements are done with NTEGRA Spectra in Inverted configuration.
Data courtesy of Dr. S. Kharintsev, Dr. J. Loos, Dr. G. Hoffmann, Prof. G. de With, TUE, the Netherlands and Dr. P. Dorozhkin, NT-MDT Co.

*** Enter the Gift code at www.nt-mdt.com and get a present from NT-MDT Co. Attention: limited quantity! Be in time to get your gift!**

NT-MDT
Molecular Devices and Tools for NanoTechnology

NT-MDT Co., building 100, Zelenograd,
124482, Moscow, Russia.
Tel: +7 (499) 735-0305, +7 (495) 913-5736
Fax: +7 (499) 735-6410, +7 (495) 913-5739
E-mail: spm@ntmdt.ru; www.ntmdt.com

Technological complexes for MEMS and NEMS research and development

V. Bykov
NT-MDT Co., Build. 100, Zelenograd Moscow, 124460 Russia

Range of AFM applications nowadays cover almost all scientific areas starting from material science, nanoelectronics and polymers up to biology, pharmacy and medicine. When basic AFM methods applied to these objects are the same, each application area requires its own cutting edge technical solutions for optimal performance and critical results.

Polymer sciences applications require extreme stability of the AFM experiments conducted with variable temperature and in long-term experiments. Molecular biology applications require highest achievable resolution with high sensitivity of measurements and precise probe positioning system. Cell biology requires precision environmental conditions control simultaneously with free optical access to the sample. All these requirements can be achieved in one single instrument only if it is based on a completely modular design platform allowing quick and reliable system reconfiguration.

Newcomers in analytical equipment like integrated Raman-SPM instrument, integrated Tomography-SPM instruments and integrated Nanoindentation-SPM instruments open new horizons for simultaneous complementary measurements of different properties of matter on a nanometer scale level from the same object of investigation.

Critical results have been achieved on DNA molecules, carbon nanotubes, magnetic nanoparticles, single molecules interactions, polymer materials and many other objects.

Nanoelectronic devices and materials for the end of the roadmap

G. Ghibaudo and F. Balestra
IMEP-LAHC, Minatec (CNRS-Grenoble INP, UJF, US), 3 Parvis Louis Neel, 38016 Grenoble, France

For the end of the ITRS, very innovative materials, nanotechnologies and device architectures will be needed for nanoscale CMOS and beyond-CMOS [1]. Silicon On Insulator-based devices seem to be very promising for the ultimate integration of electronic circuits on silicon [1,2]. The performance and physical mechanisms are investigated in single- and multi-gate thin film MOSFETs. A comparison between Si, Ge and III-V semiconductors on insulator is given. The impact of strain in the channel, of high k materials as well as Schottky source-drain architectures is discussed. The interest of beyond-CMOS nanodevices for long term applications, based on nanowires or tunnel FETs is also presented. Finally, an overview of advanced memory architectures allowing to overcome integration challenges in the nm range is outlined.

Strain silicon-on-insulator is very interesting for boosting the transport properties and the scalability of nanoCMOS. The electron mobility has been shown to be enhanced down to ultra-thin 2.3nm Si layer under uniaxial tensile strain, and the hole mobility increases in 2.5nm film under uniaxial compressive strain [3]. Source/drain (S/D) engineering takes an increasing importance in the development of leading edge CMOS generations. It has recently been shown that sub-100 meV Schottky barrier can be obtained consistently with the boron pile-up observed at the PtSi/Si S/D-channel interface, leading to high driving current and record RF performance for a 30-nm p-type thin-film fully depleted SOI SB MOSFET [4]. The combination of dielectric constant, k, and the energy barrier offset, ΔE, between the energy bands of the insulator and silicon is crucial for reducing the gate tunnelling current. For the LSTP 22nm bulk CMOS node, $\Delta E \times k \approx 70$ eV, while the corresponding requirement for double gate SOI can be set to 30 eV. The lower value mentioned above for SOI offers a large number of possibilities for gate dielectrics [5]. Multi-gate architectures based on the concept of volume inversion are very promising in order to overcome the number of challenges for CMOS integration down to sub-10nm gate length (higher driving and reduced leakage currents) [6]. Multi-gate SOI devices seem to lead to the best Ion/Ioff trade-off compared with its Ge or III-V counterparts, due to reduced source-drain and band-to-band tunneling currents [7]. Multi-bridge-channel MOSFETs (MBCFET) [8], 3D GAA and independent gate ΦFET semiconductors nanowires on SOI (highest current ever reported and possibility of VT tuning [9]) can be seen as the ultimate integration of these innovative nanodevices and present very interesting electrical properties.

It is also becoming difficult for memories to be scaled down. Double gate capacitorless 1T-FinDRAMs have been proposed showing very good memory characteristics [10]. FinFlash, SiN-based FinFlash and Nano-crystal Finflash/SOI have shown very good performance: increased driving current inducing reduced access time, smaller short channel effects leading to better scalability, higher number of stored electrons improving variability [11]. Independent double-gate FinFET are also interesting candidates for enhancing SRAM performance: reduction of leakage current and enhancement of read/write noise margins [12].

One other interesting class of Beyond-CMOS devices are the small slope switches (swing < 60mV/decade) for very low power applications. Tunnelling devices seem very promising, especially 2G high-K TFETs, feedback TFETs and strain Ge Double Gate TFETs with asymmetric source/drain, which led to excellent electrical properties (swing down to 2mV/dec together with Ion/Ioff of 10^8) [13-15].

This work has been supported by the Nanosil European Network of Excellence and the Sinano Institute.

1. ITRS Roadmap - **2.** F. Balestra, SOI devices, Wiley Encyclopedia of EEE, 1999 - S . Cristoloveanu and F. Balestra, in advanced Semiconductor and Organic Nano-techniques, Academic Press, 2003 - **3.** K. Uchida, IEDM'04 - **4.** G. Larrie, IEDM'07 - **5.** O. Engström, *Solid St. Electron., 51, 622, 2007* - ***6***. F. Balestra, IEEE EDL 8, 410, 1987 - **7.** Q. Rafhay, Solid-St. Electron., Oct. 2008 - **8.** E.-J. Yoon, IEDM'04 ; Bernard, VLSI'08 - **9.** C. Dupré, Proc. IEDM'08 - **10.** T. Tanaka, IEDM'04, p. 919 - **11.** B. DeSalvo, IEDM'08 - **12.** K. Endo, IEDM'08 - **13.** K. Boucart and A.M. Ionescu, IEEE TED, 1725, 2007 - **14.** A. Padilla, IEDM'08 - **15.** T. Krishnamohan, IEDM'08.

Challenges of Advanced Interconnects: from Cu/low-k to Wireless

Takamaro Kikkawa
Research Institute for Nanodevice and Bio Systems, Hiroshima University,
Higashi-Hiroshima, 739-8527 Japan,
kikkawat@hiroshima-u.ac.jp

According to the scaling rule for metal-oxide-semiconductor (MOS) transistors in silicon large scale integrated circuits (LSI), both operating frequency and power consumption can be improved by reducing the feature sizes of MOS transistors. On the other hand, the scaling of metal interconnects deteriorates the performances of LSI chips in terms of operating frequency and power consumption due to resistance-capacitance (RC) time constants. Bonding wires of LSI packaging also limit high-speed signal transmission between LSI chips due to their parasitic inductances (L).

In order to reduce the RC delay, the copper (Cu) interconnect and low-dielectric constant (low-k) materials have been developed for 90 nm CMOS and beyond. A novel scalable low dielectric constant (low-k) film technology was developed by use of self-assembled porous silica. Periodic two-dimensional hexagonal porous silica film structures were formed by electrostatic interaction between micelles of surfactants and silica oligomers. Tetraethyl-orthosilicate (TEOS) was used as a precursor of the silica oligomer. Polyethylene-oxide/polypropylene-oxide/polyethylene-oxide tri-block copolymers were used as nonionic surfactants. Non-periodic porous silica film structures were also formed. The dielectric constant of the porous silica film was controlled by changing pore diameters of micelles which were determined by the molecular weight of the surfactant as well as the surfactant/Si molar ratio in the precursor solution. A novel tetramethyl-cyclo-tetra-siloxane gas treatment process was developed for enhancing the elastic modulus (E) and hydrophobicity of the porous silica. Porous ultra-low-k silica films having the E = 8 GPa and k = 2.07 were obtained. [1] Ultra-low-k/Cu damascene with sufficient mechanical strength was successfully demonstrated for 45 nm technology node of ULSI.

Although the Cu/low-k technology can solve the existing problems, it cannot be an ultimate solution. To eliminate the parasitic L, C and R of the metal interconnects, wireless interconnects have been proposed for inter-chip link, stacked multi-chip packaging and three-dimensional (3D) integrated circuits. Among wireless interconnection technologies, capacitance coupling, inductance coupling and transverse electromagnetic (TEM) wave propagation using on-chip antennas have been developed for LSI [2]. The practical antenna length is designed as a half of the wavelength which corresponds to the frequency of approximately 1/20 of CMOS cut-off frequency (f_T) and maximum frequency (f_{max}). The dipole antenna length is approximately 15 mm for the center frequency of 3.5 GHz by use of 180 nm CMOS technology (f_T = 60 GHz, f_{max} = 70 GHz). The antenna length will be scaled down to approximately 3 mm for the center frequency of 30 GHz using 32 nm CMOS technology (f_T = 400 GHz, f_{max} = 590 GHz).

A single-chip ultrawideband (UWB) transmitter circuit of ultra short Gaussian monocycle pulse (GMP) of 280 ps was successfully demonstrated using 180 nm CMOS technology with the on-chip integrated antennas. The transmission and reception of generated GMP at the rate of 1.16 Gbps were demonstrated by the meander dipole antennas which were integrated on the same Si chip for intra/interchip communication as shown in Fig. 1.

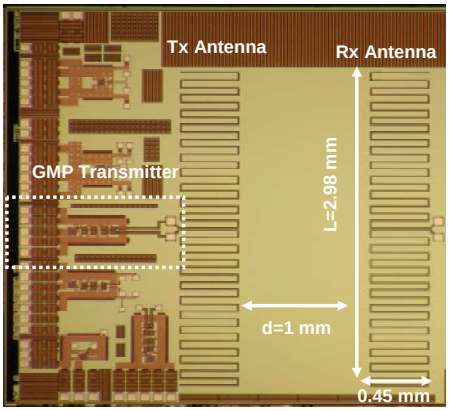

Fig. 1. A photomicrograph of 180 nm CMOS with integrated on-chip antennas.

References
1. T. Kikkawa, et al., "Advanced Scalable Ultra low-k/Cu interconnect Technology for 32nm CMOS ULSI Using Self-Assembled Porous Silica and Self-Aligned CoWP Barrier", in IEEE International Electron Devices Meeting Technical Digest, Washington DC, Dec.5, pp.99-102, 2005.
2 . T. Kikkawa, et al., "Gaussian Monocycle Pulse Transmitter Using 0.18 μm CMOS Technology With On-Chip Integrated Antennas for Inter-Chip UWB Communication," IEEE Journal of Solid-State Circuits, Vol. 43, No. 5, pp.1303-1312, 2008.

Emerging non-volatile semiconductor memories in deep submicron technologies

Yakov Roizin
Tower Semiconductor Ltd. P.O.Box 619, Migdal HaEmek 23105, Israel

Non-volatile memory (NVM) miniaturization and multi-level cell designs (MLC) resulted in the dramatic growth of the memory volume on a single chip and drastic price decrease. The main players in the NVM market announced shipping of 32Gbit chips on 30nm processes. Nevertheless, there are principal physical and commercial limitations in the roadmap of conventional memories scaling down. None of the solutions alone can satisfy the diverse requirements dictated by applications. For example, the densest and cheapest NAND memories have low writing speed, endurance/retention limitations (especially MLC) and need high voltages for programming and erase, while advanced NOR memories have high power consumption and long erase times (most NAND and NOR operate in the Flash regime when large amounts of cells are erased simultaneously). There is a compromise between the parameters of the embedded memory in system-on-chip designs and the chip cost.

The majority of the commercial semiconductor memories is based on electric charge storage in the floating gate (FG) of a MOSFET. Electrically erasable read only memory (EEPROM), where charge is stored in the polysilicon FG, and silicon-oxide-nitride-oxide-silicon (SONOS) devices with charge trapping in the silicon nitride, are employed in most cases.

There have been concerns about whether the current progress in both polysilicon FG and NROM memories can be maintained in the Nano era. Moreover, there is a dream of the Universal memory, that operates as an NVM but is as fast as SRAM (static random access memory). This stimulates the attempts to develop alternative, revolutionary NVM based on different physical principles, which are expected to have both high density, high speed, high retention and low power, that none of the scaled down conventional memories have at the same time.

Solutions that allow improved performance and further scaling of NVM can be divided into evolutionary and revolutionary. The main directions in the evolutional approach are (i) NVM with transistor floating gates consisting of nanodots, which allows more efficient erase and improved retention, (ii) using of high-k materials to obtain lower memory stack effective thickness and more efficient programming; (iii) special geometries of the memory transistors, e.g. FinFets allowing denser arrays; (iv) MLC designs. In particular, scaling challenges of NROM (nitride read only memories) include application of high-k materials as a part of the ONO stack . NROM currently dominates among the SONOS memories. NROM was first moved into production in Tower Semiconductor (*micro*Flash®), and now reached record for NOR memory densities of 2Gbit (e.g., Spansion MirrorBit 65nm chips).

Revolutionary approaches employ physical principles different from charge trapping. The solutions entering the market or already existing in the market in small volumes include MRAM (magnetoresistive RAM), PCM (phase change memory), FeRAM(ferroelectric RAM) and several others.

Different options of MRAM are reviewed with the stress on their performance and scalability. In particular, the advantages and limitations of thermally assisted TA MRAM and spin torque transfer STT MRAM devices (targeting the 45 nm technology node and beyond) are discussed.

PCM memory is based on resistance changes due to phase transitions in chalcogenide glasses. The material can be "switched" between crystalline and amorphous states with the application of heat. The memory cells are integrated between the metallization levels (placed in the Back End of the microcircuit). Recently observed PCM reliability limitations are discussed in relation to scaling.

Several less mature, but considered to have strong business potential solutions include the cross-point memories, which are also placed in the Back End. Examples of this class of memories (sometimes called RRAM-resistive RAM) include stacked between the metal electrodes metal oxide films and doped chalcogenide layers. A resistance change can be caused in a tiny region of several nanometers in size. Very small programming/erase times are demonstrated in corresponding devices. Physics behind the most PRAM technologies is not enough clear. In most cases, switching is attributed to the reproducible conductive filament formation.

Emerging embedded memory technologies deviate significantly from the dominant stand-alone memory technologies. Minimum additional masks and process steps and low programming voltages and currents (for achieving smaller CMOS periphery) are often more important than memory cell scalability. The low-cost embedded memories developed in Tower Semiconductor are presented as examples.

Electromigration theory and its applications to integrated circuit metallization

T. Makhviladze and M. Sarychev
Institute of Physics and Technology, Russian Academy of Sciences, Moscow, Russia, tarielmakh@mail.ru

To evaluate the reliability and lifetime of nano- and microelectronic structures of IC it is necessary to model their electrical and mechanical properties determined by microstructure and evolution of the IC elements. One of the main failures in integrated circuit performance occurs due to electromigration of vacancies (ions) in thin-film conducting lines, which causes their damage [1-7]. The general theory and modeling results of electromigration-induced nano- and microprocesses which result in failure of thin-film conducting elements are presented. The detailed analysis of various mechanisms of their deformations and failures that are of practical importance for different types of multilevel arrangement and microstructure of conductors, is given.
We develop here a full 3D theory of electromigration and generation of electromigration-induced mechanical stresses in IC metallization lines. It considers the electromigration failures as a set of processes occurring at the nano-, micro- and mesoscale. We give a number of physical and mechanical models combined to understand, explain and calculate the deformation and defect nucleation at electromigration in IC metal interconnects and elements. The models allow calculating the metallization lifetime and optimizing the physical and geometric parameters of densely packed integrated circuit to achieve the maximum lifetime depending on current density. Our results show that electromigration processes cause the generation of thermodynamically stable nanovoids with characteristic nanovoid size ~ 100 nm. It is the nanovoid nucleation times that often determine the order of metallization time-to-failure (even when metallization width amounts to 0.5-1 mμ).
In particular, we model the electromigration nucleation of a microvoid at a triple point of polycrystalline structure and generation of defects related to the multilevel arrangement of metallization (a microvoid at the contact boundary between the metal line and plug, and erosion of the free end of the line). The characteristic sizes of microdefects and their nucleation times for various temperatures, current densities and crystalline structure parameters of the conductors are numerically obtained and compared with experiments.
We also put forward an approach to modeling the electromigration and mechanical stresses in conductors containing impurities and consider the influence of impurities on vacancy transfer and metallization lifetime increasing.

1. T.M. Makhviladze, M.E. Sarychev, and K.A. Valiev, “Modeling of ion electromigration process in microelectronic structure”, *Proceeding of the 6th International Conference on the Numerical Analysis of Semiconductor Devices and Integrated Circuits*, Boole Press, Dublin, Ireland, pp.521-525, 1989
2. K.A. Valiev, T.M. Makhviladze, and M.E. Sarychev, “Mechanism of ion electromigration in metals and and dielectrics”, DAN (Doklady Akademii Nauk), **306**, pp.91-94, 1989 (*in Russian*)
3. K.A. Valiev, T.M. Makhviladze, and M.E. Sarychev, “Ion migration kinetics in solids”, Mikroelectronika, **19**, pp.419- 429, 1990 (*in Russian*)
4. T.M. Makhviladze and M.E. Sarychev, “Migration model for the kinetics of failure induced by electrical fields and mechanical stresses”, *Trudy FTIAN (Proceedings of IPT)*, **2**, pp.73-83, Nauka, Moscow, 1991 (*in Russian*)
5. T.M. Makhviladze, M.E Sarychev, and Yu.V. Zhitnikov, “Simulation of defects generation processes during electromigration due account of polycrystalline structure of the current lines”, *Trudy FTIAN (Proceedings of IPT)*, **13**, pp.98-114, 1997
6. T.M. Makhviladze, M.E .Sarychev *et al.,* “General model for mechanical stress evolution during electromigration”, J. Appl. Phys., **86**, pp.3068-3075, 1999
7. T.M. Makhviladze, M.E. Sarychev *et al.,* “A new, general model for mechanical stress evolution during electromigration”, Thin Solid Films, **365**, pp.211-218, 2000
8. K.A. Valiev, R.V. Goldstein, Yu.V. Zhitnikov, T.M. Makhviladze, and M.E.Sarychev, “Modeling of failure and lifetime of thin-film metal conductors in integrated circuits”, Fizicheskaja mesomekhanika, **11**, pp.57-88, 2008 (*English translation*: Physical Mesomechanics, **11**, № 3-4, 2008)

Immersion Lithography and Double Patterning in Advanced Microelectronics

T. Vandeweyer, J. Bekaert, M. Ercken, R. Gronheid, A. Miller, V. Truffert, J. Versluijs, V.Wiaux, P. Wong, G. Vandenberghe, M. Maenhoudt.
IMEC vzw, Kapeldreef 75, 3001 Heverlee, Belgium, Email: tom.vandeweyer@imec.be

As EUV lithography is late for the 32nm half pitch (HP) node, several options are being explored to extend device scaling with the current immersion lithography tools. These extension techniques all involve compromises between design and process. In this paper, several options for the extension of immersion lithography beyond the 32nm node are investigated and illustrated with experimental results.

First, Single Patterning (SP), using a single mask and exposure, can be scaled significantly if the design is made litho-friendly. Scaling down to 22nm node is demonstrated on logic devices by applying unidirectional designs [1].
Also Double Exposure (DE) can be used to push the resolution and pitch to the ultimate limits by separating horizontal and vertical features on two masks and using dipole illumination. The DE of lines in combination with image reversal techniques allow us to pattern contact holes down to 80nm pitch, which is lower than the SP limit around 110nm pitch [2].
Next, Double Patterning (DP) enables pitch scaling beyond the limits of 1.35NA. The most common technique used is litho-etch-litho-etch (LELE). The desired pattern is split over two designs and recombined through two patterning steps (fig.2a). New, cost effective materials are being developed, where the first litho pattern is frozen before applying the second litho [3]. Both resist patterns are then transferred into the underlying substrate with a single etch step (fig.2b). Several approaches are already available that allow patterning down to 26nm half pitch.
Finally, Self-Aligned Double Patterning is a pitch doubling technique for 1D applications on narrow pitches, often used for FLASH memory devices [4]. In this technique, a core sacrificial pattern at pitch 1:3 is used to sustain spacer formation at both sides of the pattern. Afterwards, the core is removed and the spacers are transferred into the substrate creating the pitch-doubled pattern. Very good CD control can be obtained for a 32nm HP gate process.

References

1. A. Veloso et al., “Full-Field EUV and Immersion Lithography Integration in 0.186µm2 FinFET 6T-SRAM cell”, IEDM. 2008. pp.861-864, San Francisco, USA, 2008
2. V. Truffert et al.,”Ultimate contact hole resolution using immersion lithography with line/space imaging”, Proceedings of SPIE, vol. 7274, San Jose, USA, 2009
3. M. Maenhoudt et al.,”Alternative process schemes for double patterning that eliminate the intermediate etch step”, Proceedings of SPIE, vol. 6924, San Jose, USA, 2008
4. C. Bencher et al.,”22nm half-pitch patterning by cvd spacer self alignment double patterning (sadp).”, Proceedings of SPIE, vol. 6924, San Jose, USA, 2008

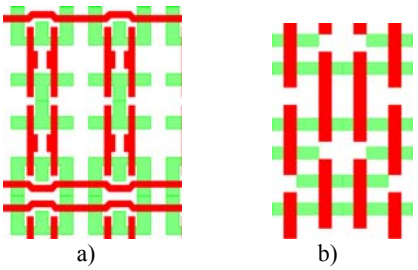

Fig.1 a) Classic 6-T SRAM b) Litho-friendly 6-T SRAM design (green = fin, red = gate).

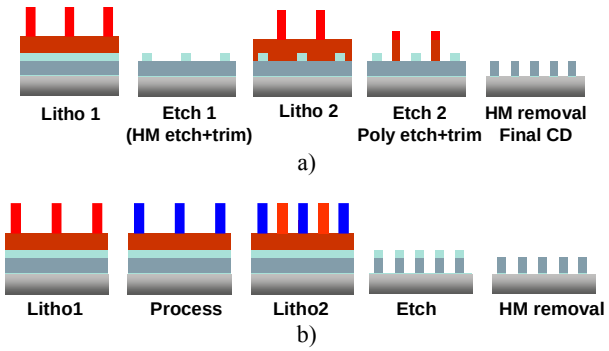

Fig.2 a) Scheme of Litho-Etch-Litho-Etch; b) Scheme of Litho-Process-Litho-Etch

Thermo-Electric Charge-to-Voltage Converter with an SIN Tunnel Junction for Bolometer Applications

Leonid Kuzmin
Chalmers University of Technology, S-41296 Gothenburg, Sweden, E-mail: leonid.kuzmin@chalmers.se

The novel type of a ***Zero-Biased Superconducting Thermo-Electric Bolometer (TEB)*** has been proposed. The bolometer is based on the Charge-to-Voltage Converter (CVC) with a Superconductor-Insulator-Normal (SIN) Tunnel Junction and a superconducting absorber. The absorption of photons in the absorber leads to excitation of quasiparticles with some fraction of charge imbalance, tunneling through the SIN junction in zero-biased mode and generation of voltage. The thermoelectric voltage is determined by accumulation of tunneling charge by an external capacitance. Conversion efficiency is very high and voltage can easy achieve values comparable with a superconducting gap. The CVC-TEB can be effectively used for multi-pixel array of bolometers.

The main goal current experiments is to prove that a radically new idea of the TEB is practical. Having a bias-free thermo-electric bolometer working at low temperatures is an old dream of scientists. However, the thermo-electric Seebeck coefficient is dramatically decreased at low temperatures for ordinary metals and semiconductors. In contrast, superconductors have been shown to have a rather large thermo-electric coefficient if they are put in contact with another, different superconductor or with a normal metal. Because the TEB is designed to work without any supplied bias, the circuitry can be kept simple. As a result it becomes much easier to avoid ground-loop interference problems and to improve noise properties. The TEB would open up the possibility to assemble large-scale arrays of bolometers, due to the absence of bias-induced overheating. In the case of its successful realization, we are confident that the TEB could challenge the current dominance of the – still under development – American TES (Transition-Edge Sensor) concept.

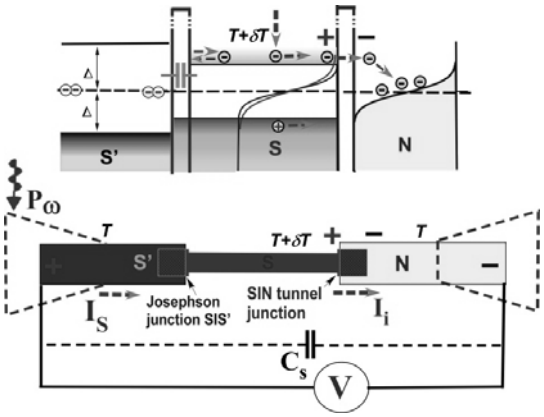

Fig 1. Sketch of the proposed **Thermo-Electric Bolometer based on a Charge-to-Voltage Converter (CVC-TEB)** with voltage readout and capacitive coupling to the antenna. The convertor will work in a novel mode as an integrator of charge that has tunneled through the SIN junction to an external capacitor. The CVC comprises an absorber coupled through an SIN tunnel junction to a normal metal and through an SIS' tunnel junction to a strong superconductor. The self-biased SIN tunnel junction is used for the generation of a voltage which appears due to the tunneling of imbalanced quasiparticles to the normal metal while back-tunneling is prohibited.

We believe that novel and important applications will emerge, based on sensors of this type, showing reasonable thermoelectric coefficients at low temperatures. A new type of zero-biased bolometers could be developed using SIN or SS' (Weak Superconductor-Superconductor) contacts. The TEB can work as a voltage source (converting incoming radiation power to voltage) with a JFET readout and as a current source with a SQUID readout.

The main problem in realization of the CVC concept is related to the uncertainty of the degree of charge imbalance achieved during the absorption of an RF signal. The value of this parameter is hard to estimate theoretically, so extensive experimental tests are needed. Due to the asymmetry of the device structure (containing SIN and SIS' junctions) we expect a substational imbalance of quasiparticle excitations. This imbalance should be increased for the CVC concept due to voltage self-biasing of the SIN tunnel junction by an accumulated charge.

The novel concept of a ***Zero-Power Cold-Electron Bolometer (ZP-CEB)*** has been proposed. In addition to classical concept of the CEB based on direct electron cooling of the absorber [2], a self-biasing of the bolometer using thermo-electric effect is proposed. This revolutionary step would help to avoid additional electronics for CEB biasing, and additional interferences due to ground loops. The energy will be harvested from cold-hot parts of a cryostat with efficiency close to 100%. The concept could be useful for space and balloon-based telescopes:

1. L. Kuzmin, "Thermo-Electric Charge-to-Voltage Converter based on SIN Tunnel Junction", submitted to Applied Physics Letters, (August 2009).
2. L. Kuzmin, "Ultimate Cold-Electron Bolometer with Strong Electrothermal Feedback", Proc. of SPIE conference "Millimeters and Submillimeter Detectors", Vol. 5498, pp 349-361, Glasgow, June 21-25, 2004.

Projection photolithography modeling using the finite-difference time-domain approach

T. Makhviladze and M. Sarychev
Institute of Physics and Technology, Russian Academy of Sciences, Moscow, Russia, tarielmakh@mail.ru

The achievement of the minimal topological sizes is defined currently by highly productive photolithography, mathematical modeling being of great and as a rule advanced importance for investigation and optimization of photolithography processes. The well known software packages used by leading manufactures and R&D centers, including our own package, contributed to achievement of resolutions less than 50 nm by using modern 193 nm - lithographers. Further progress up to 22 nm turned out to be possible by using special techniques (like immersion, OPC, off-axis sources and double patterning), the most advanced packages providing modeling and optimization of these special methods too.
The achievement of the critical dimensions that are several times less than the radiation wave-length (in the case of ArF-laser as a radiation source and with the use of special techniques to improve resolution, the 8-9-fold reduction can be obtained) requires careful study and intensive analysis of physical models' fundamentals themselves, that the software packages and tools are based on. We imply analysis of approximations and limitations, which are used in deriving the main equations and relations, as well as a study of applicability of numerical methods and algorithms. Sometimes it is necessary even to revise entirely and to replace physical, mathematical and computational models by more appropriate and accurate ones. New challenges in modeling arise if more short-wave radiation, for example extreme ultraviolet, is used.
In order to improve reliable methods of photolithographic processes modeling and optimization for the purpose of achievement of maximum possible values of resolution we develop the photolithographic finite-difference time-domain (PFDTD) approach to the modeling of 3D electromagnetic fields and photolithographic structures for projection photolithography in sub-0.2μm and nanometer ranges. The essence of this approach is adaptation and application of advanced methods [1] of the Maxwell equations' solution to photolithography problems. These state-of-the-art methods are often free of limitations that put obstacles in the way of further limiting-resolution-lithography developments by modeling and simulation methods. Within the framework of the photolithographic FDTD approach developed by the authors [2], the appropriate computational methods and modeling algorithms are presented and discussed.
Contrary to the rigorous coupled-waves analysis (RCWA-method [3]) generally accepted and everywhere used, we apply the PFDTD-method, by means of which the Maxwell's equations are directly solved numerically in the time domain. It is not assumed in advance (as it usually is adopted), that the electromagnetic fields at each sample point are in harmonic oscillation states, and the standard Fourier expansion in spatial coordinates is not performed (see e.g. [1,2,4]).
It is shown that developments of the direct procedures of numerical solution of electromagnetic field equations are necessary in many practical cases, when well approved modeling methods lose their accuracy or even become inoperative. It is important especially for short-length radiation sources.
Within the PFDTD-method the results of computing experiments for sub-100nm-resolution photolithography schemes with the different wave length sources and different phase shifting masks, including off-axes radiations, were carried out and analyzed. The comprehensive analyses of resolution values, focus depths and contrasts in dependence on exposure conditions, masks' parameters and geometrical characteristics of the schemes for PFDTD-method and RCWA-method were given. The ranges of applicability of the PFDTD-method were investigated in detail.

1. H. Ichikawa, "Electromagnetic analysis of diffraction gratings by the finite-difference time-domain method", J. Opt. Soc. Am. A, **15**, pp.152-157, 1998
2. T.M. Makhviladze, M.E. Sarychev, "New results of modeling in micro- and nanoelectronics", *IC MNE-2007, Book of Absracts*, p.L1-06, IPT RAN, Moscow, 2007
3. M. Moharam *et al*., "Formulation for stable and efficient implementation of the rigorous coupled-wave analyses of binary gratings", J. Opt. Soc. Am. A, **12**, pp.1068-1076, 1995
4. A. Taflove, S.C. Hagness. *Computational Electrodynamics: the finite-difference time-domain method.* Artech House, Norwood, MA, 2005

The metal hard-mask approach for contact patterning

J.-F. de Marneffe , D. Goossens , D. Shamiryan, F. Lazzarino, Th. Conard, I. Hoflijk, H. Struyf and W. Boullart

Interuniversitair Microelectronica Centrum (IMEC v.z.w.), Kapeldreef 75, B-3001 Leuven, Belgium.
marneffe@imec.be

In order to overcome patterning challenges brought by dimensional scaling and aggressive pitches, extreme ultra-violet lithography (EUVL) has been recently pushed forward as a possible solution for IC manufacturing, allowing extended exposure latitude at sub-50nm dimensions [1]. A major issue with EUVL is the necessity to use very thin photoresist (PR) films, because of resolution requirements and limited depth of focus. This introduces difficulties during the plasma etch process, which, as a consequence, requires a higher selectivity towards the photoresist. This problem is enhanced by the fact that, as feature dimensions go down, the typical dielectric etch rate drops in a similar way. Another point of concern is plasma-induced photoresist roughness, which occurs through deformation of the photopolymer by UV radiation and ion bombardment. This mask roughness transfers into the underlying substrate, leading to edge roughness and striations appearing in the pattern sidewalls. As the dimensions of etched features go down, the relative scale of these defects goes up and becomes a serious limiting factor for the metallization.

A solution to overcome the issues introduced above is to use a hard-mask approach, that consists in limiting the photoresist-based patterning step to the etch of a thin "hard" mask, which shows a high etch-resistance to the subsequent fluorocarbon-based plasma used for dielectric etch. Careful selection of a mask material is crucial and it is foreseen that typical plasma processes used for PR-based SiO_2 patterning will require specific adjustments as a consequence of the replacement of the photoresist by the hard-mask.

In this work, the selected hard-mask is titanium nitride (TiN). Based on the specific requirements of a modern contact etch process (self-alignment, high aspect-ratio, smooth circular shape, vertical sidewalls), the first part of this study describes the etch mechanisms for an $Ar/C_4F_8/CO/O_2$ plasma, with a particular emphasis on the effect of the O_2 flow and plasma power on the observed blanket selectivities for SiO_2 towards TiN and Si_3N_4. Results show that the presence of O_2 in the plasma is detrimental to both TiN and Si_3N_4 etch rates, while the use of 2 MHz driving power decreases the Si_3N_4 etch rate but enhances the TiN removal rate. The etch mechanism of both nitrides, and their dependence on 2 MHz driving power and O_2 addition will be discussed in detail.

The second part of this work studies the effect of intermixing metallic (TiN) and dielectric surfaces (SiO_2, Si_3N_4) on the general characteristics of the etch process. Indeed, opposite to the case of blanket wafers tests, real device masks for contact patterning show > 99% surface covered by the mask, which may drastically modify the plasma chemical loading.

Finally, the third part describes the contact patterning characteristics, with a focus on aspect–ratio (depth/diameter) dependent effects. For contact stacks with an aspect-ratio of around 5, vertical profile is a key parameter in order to ensure good metal filling and low electrical resistance. Various aspects of the profile optimization will be tackled and analyzed in terms of the polymerizing nature of the discharge.

In conclusion, the metal hard-mask approach has been studied for advanced contact patterning. This work demonstrates that the use of a metal hard-mask allows circumvention of photoresist-driven issues (thickness, plasma-induced deformations), by decoupling the dielectric etch and lithography processes. Modifications of the plasma etch process allows the patterning of contacts with high aspect-ratio, smooth and almost vertical (> 85°) sidewalls, and SiO_2:Si_3N_4 selectivity compatible with a Self-Aligned Contact design.

1. A. Veloso *et al.*, “Full-Field EUV and Immersion Lithography Integration in 0.186μm^2 FinFET 6T-SRAM cell”, Proceedings of the IEEE Electron Device Meeting, IEEE, San Francisco, 2008

Manufacturing of diffraction quality optical elements for high resolution optical systems

N.I. Chkhalo, A.E. Pestov, N.N. Salashchenko, M.N. Toropov

Institute for Physics of Microstructures, Russian Academy of Sciences, Nizhny Novgorod, Russia, E-mail address: chkhalo@ipm.sci-nnov.ru

This report is an extension of investigations started in [1, 2] on manufacturing of optical units and systems providing diffraction quality imaging (in concordance with the Rayleigh criterion the space resolution is an order of a wavelength) in soft X-ray and extreme ultraviolet ranges, λ=3-50 nm. The interest in super-high-resolution optical systems is related to the development of a number of fundamental and applied fields, primarily such as high resolution, 10-20 nm, X-ray microscopy in the «Water window» and projection nanolithography in the extreme ultraviolet spectral range. As an example of projective objective for nanolithography at 13.5 nm operating wavelength the requirements imposed to the surface shape and microroughness of substrates for mirrors are discussed. Basic problems and critical technologies providing required quality of the substrates for the mirrors are considered. Much attention is given to investigations in the field of characterization of the optical units and systems wave aberrations. In particular a new type of point diffraction interferometer utilizing a tipped down to 0.2-0.3 μm fiber as a source of a reference spherical wave is reported [3]. The last results on the reference wave front aberration studies made with a wavelength of λ=530 nm are presented. In particular the measured aberrations of the fiber based source as compared with a conventional one, based on a pin-hole in an opaque screen, indicates advantage of the source [4].

Recent developments and investigations curried out in IPM RAS in a field of subnanometer accurate surface shape correction methods are described. Particularly experimental data of achieved parameters on microroughness and surface shape of aspherical substrates for a nanolithographer operating at a wavelength of λ=13.5 nm are given. It is shown that these methods and technologies are applicable in manufacturing and characterization a refracting optics too.

A problem of intrinsic stress in the reflecting multilayer interference mirrors which becomes extremely important at the subnanometer level the surface shape precision is discussed. A solution of the problem for Mo/Si and Cr/Sc multilayer structures which are of prime interest for the projective nanolithography at λ=13.5 nm and the X-ray microscopy in the “Water window” region, λ=2-5 nm, is reported.

In conclusion the main problems that have to be solved at the way of manufacturing atomic-smooth super-accurate imaging optics are discussed.

This work is supported by RFBR grants 07-02-00190, 08-02-00873, 09-02-00912.

1. N. Chkhalo, L. Paramonov, A. Pestov, D. Raskin, and N. Salashchenko, “Correction of the EUV mirror substrate shape by ion beam”, Proc. SPIE 7025, 702503 (2008).
2. N.I. Chkhalo, E.B. Kluenkov, A.E. Pestov, D.G. Raskin, N.N. Salashchenko, and M.N. Toropov, “Manufacturing and investigation of objective lens for ultrahigh resolution lithography facilities”, Proc. SPIE 7025, 702505 (2008).
3. N.I. Chkhalo, A.Yu. Klimov, V.V. Rogov, et al., “A source of a reference spherical wave based on a single mode optical fiber with a narrowed exit aperture”, Rev. Sci. Instrum., v. 79, 033107 (2008).
4. P.P. Naulleau, K.A. Goldberg, S.H. Lee, et al., “Extreme-ultraviolet phase-shifting point-diffraction interferometer: a wave-front metrology tool with subangstrom reference-wave accuracy”, Appl. Opt., v. 38, no. 35, p. 7252-7263 (1999).

A nanoelectronic device simulation software system NANODEV: New opportunities

I.I. Abramov, A.L. Baranoff, I.A. Goncharenko, N.V. Kolomejtseva, Y.L. Bely
Belarusian State University of Informatics and Radioelectronics, Minsk, Belarus, E-mail: nanodev@bsuir.edu.by

The system NANODEV [1,2] consists of three subsystems: SET-NANODEV for simulation of single-electron structures, RTS-NANODEV for simulation of resonant-tunneling structures, and QW-NANODEV for simulation of quantum wire devices. The new models of nanoelectronic devices on single-electron tunneling, resonant-tunneling effects have been included in the NANODEV system.

In this paper we described results for RTD's based on GaAs/AlAs and InAs/AlSb/GaSb/AlSb/InAs material systems which were obtained with the use of two-band combined numerical models of wave function formalism. It was shown that it is necessary to take into account many of factors for adequate simulation of these devices [3]. Accounting of more complex band structure of investigated material systems on the basis of multiband models is one of the most important factor [4]. The influence of conduction band X-valley on electrical characteristics of RTD based on GaAs/AlAs was investigated with the use of model including Γ-X intervalley scattering effect. Adequacy of the models is proved by comparison with experimental data. The use of the models confirms the importance of taking into account band structure of materials for calculating RTD I-V characteristics.

Physical model of single-electron devices with spatial quantization on islands was also proposed. It was shown that effect is important on IV-characteristics of devices not only for small islands but with increasing of number of islands, applied voltages and decreasing of temperature. The physical model allows to calculate single-electron transistor IV-characteristics depending on the geometrical sizes and parameters of materials. The following approximations are included in the modified models: 1) infinite quantum well; 2) rectangular quantum well; 3) parabolic quantum well. A good agreement of the results with the experimental data was obtained too.

1. I.I. Abramov, I.A. Goncharenko, S.A. Ignatenko, A.V. Korolev, E.G. Novik and A.I. Rogachev, "NANODEV: A Nanoelectronic-Device Simulation Software System", Russian Microelectronics, 2003, v. 32, N 2, p. 124-133.
2. I.I. Abramov, K.I. Abramov, I.A. Goncharenko, S.A. Ignatenko, A.P. Kazantsev, N.V. Kolomejtseva, A.M. Lavrinovich, S.N. Pavlenok, A.S. Strogova, "Simulation of physical processes in nanoelectronic devices with the use NANODEV system", Proc. SPIE, 2006, v. 6260, p. 62601Q-1-62601Q-8.
3. I.I. Abramov, "Problems and principles of physics and simulation of micro- and nanoelectronics devices. V. Resonant-tunneling structures", Nano- and microsystemnaya technika, 2007, № 3, p. 57-70.
4. I.I. Abramov, I.A. Goncharenko, N.V.Kolomejtseva, "Simulation of resonant tunneling diodes based on GaAs/AlAs with the use of combined two-band model", Nano- and microsystemnaya technika, 2009, v. 3, p. 10-13.

The charge sharing inside the layers of nano- CMOS integrated structures under controllable substrate biasing

T. Krupkina, D. Rodionov, A. Shvets, I. Titova
Moscow Institute of Electronic Engineering, Moscow, Russia, ieem@miee.ru

The problem of scaledown of nano- MOS transistors becomes the urgent issue again, as the design rules are reduced below 40 nm. The simple scaling of device geometry leads in this case to extremely rigorous and awkward requirements for equivalent gate-oxide thickness for example. The nano- MOS transistors engineering is getting more and more complex task, inclusive of special consideration and design of device parasitics elements [1].

Appropriately, there is a growing substrate significance in such structures. The charge fluctuations, related to avalanche multiplication near the drain and capacitive relations, are capable to change the functional characteristics of neighboring elements, threshold voltage for example, during the propagation through the substrate volume. The opportunity of the well-behaved nano system-on-chip design depends on the charge distribution and propagation inside the integrated layers, leading to substrate noise problem. The substrate bias guidance in nano CMOS structures could be considered as a possible direction of the threshold voltage scaling [2]. In this case a forward body biasing allows at the same time to reduce the threshold voltage and to weaken the short-channel effects.

The analysis of CMOS structures layers was implemented for 45 nm CMOS process, characterized and performed as a result of development and scaling of technological processes from 0.35 mkm level and below. The main process features were STI, two wells, two spacers, LDD and halo formation. The possibilities of the precise numerical simulation by TCAD Synopsys were used for this investigation. The main structure was generated by Sentaurus Process and then characterised by Sentaurus Device.

The Fig. 1,a shows technological cross-section resulted from the alternation of n- and p-channel MOS transistors. For such set of layers the fields of the enhanced impact ionization, the possible substrate noise sources during the circuits operation, have been dedicated. The usage of forward body biasing (Fig. 1,c) reduces the size of these fields, although the maximal rate of impact ionization has been rather increased. Analysis of carriers and substrate currents distributions shows the strong dependence on the combinations of neighboring MOS transistors operation regimes, including the areas of substrate/wells contacts.

It should be noted, that the optimization of such structures and technology demands to analyse different variations of fabrication process parameters and their effect on the device electrical characteristics[3].

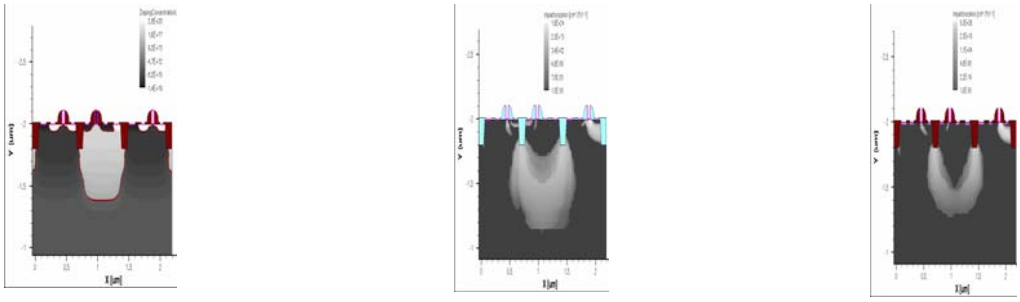

a) b) c)

Fig.1 Results of numerical modeling: the technological cross-section (a) and the fields of impact ionization under zero (b) and forward (c) substrate biasing.

1. L.Wei *et al.* “Selective device structure scaling and parasitics engineering: a way to extend the technology roadmap” IEEE Trans. on Electron Devices, V.56, No 2, pp. 312-319, 2009.
2. A.Hokazono, *et al.* “Forward body biasing as a bulk-Si CMOS technology scaling strategy” IEEE Trans. on Electron Devices, V.55, No 10, pp. 2657-2664, 2009.
3. Y. Chaplygin, M. Korolev, T. Krupkina “The process window TCAD methodology for DFM in the field of deep submicron nodes and nanoscale transistors”International conference “Micro- and nanoelectronics 2007”.- Zvenigorod, Russia.- P. O1-05.

Analysis of lateral thermal SOA for smart power IC's

Yu. Chaplygin, A. Krasukov, E. Artamonova[1]
1. Moscow Institute of Electronic Technology (Technical University), a_kras@rambler.ru

A current trend in power IC technology is the integration of power devices together with complex digital and high-performance analog circuits on the same chip - Smart power IC's. For such circuits Silicon-On-Insulator (SOI) technology provides clear advantages over the commonly used Junction-Isolation technology. In SOI – technology, the full dielectric isolation between devices completely suppresses the substrate current. However, because of the low thermal conductive of buried oxide (BOX), heat generated in the SOI device cannot be efficiently dissipated to the substrate via BOX. This yields high device temperature. This temperature can affect the low voltage part of the smart power IC [1].

In this article self-heating and thermal Safe Operating Area (SOA) of the whole smart power chip have been observed. Such chip (4x3 mm) has two power MOSFETs (power part) and low voltage CMOSFETs (Low voltage part) as shown at fig.1 (a). Each power transistor consists of 9 blocks.

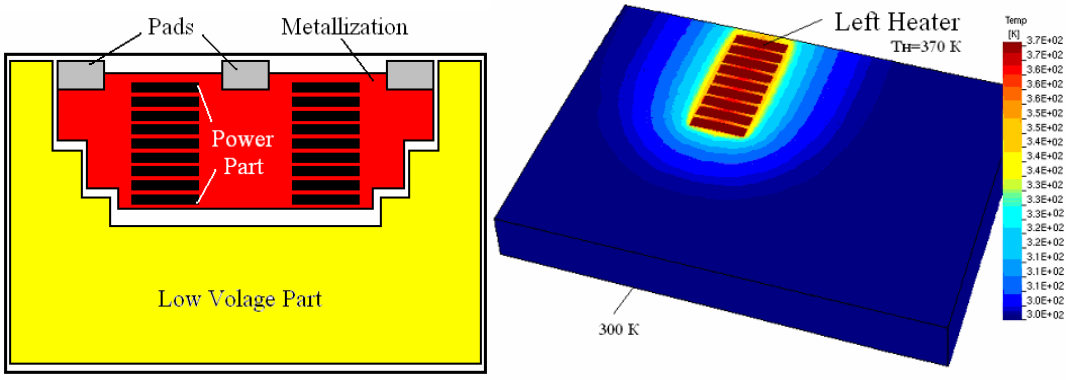

a b

Fig.1 Simplified layout of smart power IC (a) and simulated temperature distribution for one active device (b)

In order to calculate thermal SOA it is necessary to solve static heat-flow equation within every layer of our chip using TCAD tools [2]. Each power transistor (Heater) is a boundary condition with fixed temperature. The bottom chip and pad temperature is set to 300 K (fig.1 (b)). Then it is necessary to plot dependences of dissipated power versus heater temperature $P_H(T_H)$. Simulation was shown that such dependences are almost linear for T_H=310-490 K. In this range we can approximate $P_H(T_H)$ as straight-line equation and define the thermal SOA boundary as the following

$$I_d = \frac{P_H(T)}{U_{ds}} = (P_H{}^{310} + \frac{T_H - 310}{R_T}) \cdot \frac{1}{U_{ds}} \qquad (1)$$

Parameters of this equation for different substrates (SOI, bulk), different devices (one or two active power transistors; with and without heat sink though metallization) are listed in the Table 1.

Table 1 Parameters for the thermal SOA

Structure	R_T, K/W	P_{310}, W
SOI, 1 power transistor, no metallization	6,75	1,7418
SOI, 2 power transistors, no metallization	6,966	1,69
SOI, 1 power transistor, metallization	6,45	1,827
SOI, 2 power transistors, metallization	6,61	1,78
BULK, 1 power transistor, no metallization	6,31	1,9
BULK, 2 power transistors, no metallization	6,69	1,86
BULK, 1 power transistor, metallization	6,16	1,9788
BULK, 2 power transistors, metallization	6,41	1,92

1. Feixia Yu, Ming-C. Cheng, Peter Habitz, and Goodarz Ahmadi, “Modeling of Thermal Behavior in SOI Structures”, IEEE transactions on electron devices, vol. 51, no.1, pp. 83, 2004.
2. Funk J.M., Korvink J.G., Buhler J., Bachtold M., Baltes H., “SOLIDIS: a tool for microactuator simulation in 3D”, Journal of microelectromechanical systems, no.3, pp.70-82, 1997.

Advanced atomic-scale simulation of silicon nitride CVD from dichlorosilane and ammonia

T. Makhviladze, A.Minushev
Institute of Physics and Technology, Russian Academy of Sciences, Moscow, Russia, minakh@mail.ru.

Thin silicon nitride films are of considerable current use in the fabrication of integrated circuits and dynamic random access memory devices as a dielectric material. Low-pressure chemical vapor deposition (CVD) using the reaction of dichlorosilane (DCS, SiCl2H2) and ammonia (NH3) is one of the most common technique for producing silicon nitride thin films. Properties of films obtained in CVD process highly depend on the deposition conditions, first of all on the pressure and temperature of the reactor and the composition of the gas phase mixture fed into reactor. Therefore, an improved understanding of the film growth mechanism and kinetics is very helpful for selecting the best deposition conditions.

Over many years a serious experimental and theoretical effort has been directed toward studying the mechanism and kinetics of the silicon nitride CVD from DCS and NH3 and related processes. Although these studies have provided some insight into the film growth mechanism, a comprehensive model of silicon nitride deposition has not yet been developed. These approaches don't provide detail information regarding films growth mechanism and properties of deposited films. On the other hand the application of these films in future devices needs atomic scale knowledge regarding the structure of thin films.

About in the last decade the microscopic model of the chemical mechanism of S3N4 CVD has come under scrutiny of investigators (see for example [1-4]). This atomic-scale model based mainly on the first principles and on consistent application of *ab initio* approach to both gas phase and surface reactions.

In the present work we extend the range of molecules under consideration in order to analyze systematically substitution effects on the calculated reaction and activation energies. We also attempted to construct a comprehensive open-end kinetic scheme of gas-phase chemical reactions that would include all significant stoichiometric and nonstoichiometric reactions and could be further refined and augmented. All gas-phase rate constants for these reactions were calculated using the transition state (TS) and RRKM theories. The film growth model also has been enhanced in the present work in order to take into account the amorphism of the film. In this way the kinetic Monte-Carlo approach that widely used for the modeling of processes leading to crystal growth was supplemented with MD relaxation after each elementary chemical event. This comprehensive *ab initio* simulation allowed us to obtain the atomic scale amorphous structure of the deposited film. The analysis of the film structure has provided important data related to the macroscopic properties of the film for given deposition conditions, such as the stoichiometric composition and the concentration of the lattice defects.

1. A.A. Bagatur'yants, A.Kh. Minushev, K.P. Novoselov *et al*.," Theoretical study of the mechanism and kinetics of gas phase reactions in dichlorosilane and ammonia mixture", *Preprint FTIAN*, № 24, pp.1-27, MAX Press, Moscow, 2000 (*in Russian*)

1. K.P. Novoselov, "Theoretical study of the mechanism of silicon nitride CVD from dichlorosilane and ammonia mixture", *Trudy FTIAN (Proceedings of IPT)*, **17,** pp.54-81, Nauka, Moscow, 2001 (*in Russian*)

2. A.A. Bagatur'yants, K.P. Novoselov, A.A. Safonov *et al.*, "Silicon nitride chemical vapor deposition dichlorosilane and ammonia: theoretical study of surface structures and reaction mechanism", Surface Science, **486**, pp.213-225, 2001

3. A.A. Bagatur'yants, A.Kh. Minushev, K.P. Novoselov, S. Ya. Umanski *et.al.*, "Atomistic Simulation of Si3N4 CVD from Dichlorosilane and NH3", *Predictive Simulation of Semiconductor Processing: Status and Challenges*, Eds. J. Dabrowski, E. R. Weber, Springer Series in Materials Science, **72**, pp.295-356, Springer Verlag, 2004

4. K.A. Valiev, T.M. Makhviladze, K.P. Novoselov, "Atomistic modeling of deposition processes", *Trudy FTIAN (Proceedings of IPT)*, **18,** pp.256-276, Nauka, Moscow, 2005 (*in Russian*)

5. R.A. Friesner, "*Ab initio* quantum chemistry: methodology and applications", *Proc. Nat. Acad. Sci. USA*, **102**, pp.6648-6653, PubMedCentral, NY, 2005

6. T.M. Makhviladze, M.E. Sarychev, "New results of modeling in micro- and nanoelectronics", *IC MNE-2007*, *Book of Absracts*, p.L1-06, IPT RAN, Moscow, 2007

One-dimensional Photonic Crystals on Silicon as Optical Elements for Integrated Microphotonics

V. Tolmachev[1], E. Astrova[1], T. Perova[2]

1. *Ioffe Physical Technical Institute, Russian Academy of Sciences, St. Petersburg, 194021 Russia,*
2. *Department of Electronic and Electrical Engineering, University of Dublin, Trinity College, Dublin 2, Ireland,*

E-mail address: tva@mail.ioffe.ru

Design: Optical characteristics (reflection and absorption spectra) of One-Dimensional (1D) Silicon Photonic Crystals (PCs) are calculated and presented as a gap map over the range of different filling fractions [1]. The map of forbidden Photonic Band Gaps (PBGs), calculated for over hundred of filling fractions, enables one to present the compete information on whole range of existed PBGs in the desired frequency/wavelength region on one graph. Apart of the PBG areas, the regions of the possible defect modes can also be calculated and analyzed. The results on calculations of PBGs for different angles of incidence, different polarizations of light and for different wavenumbers, corresponding to quasi-complete PBG, are presented. The design of different PCs with tunable PBGs, defect modes, extended PBGs and PBGs with additional third regular layer (three-component PC) and liquid crystal filler is demonstrated.

Fabrication: For manufacturing of the designed structures the following technologies of fabrication of photonic crystals on silicon are used: i) the anisotropic etching (AE), ii) the photo-electrochemical etching (PECE), iii) the deep reactive ion etching (DRIE) and iv) the fabrication of composite structures, using different fillers. AE process is developed for fabrication of PC structures on (110) oriented silicon with minimal losses at the interface of the PC components and with electro-tunable PBGs. PECE process is developed for fabrication of one-dimensional PCs [2], that provides the possibility to fabricate 1D and 2D PCs on one chip. DRIE process was used mainly for fabrication of the PC structures and the related elements on Si-On-Insulator (SOI) platform. Finally, the technology of fabrication of the composite photonic structures is developed by filling the air channels of photonic crystals with liquid crystal (LC) filler.

Characterisation: The reflection and transmission spectra of PCs are investigated by means of FTIR micro-spectroscopy in the range of wavelength from 1.5 to 15 μm [3] and by Optical Spectrum Analyser (OSA) in the range 1 – 1.7 μm. The obtained experimental spectra demonstrate a good agreement with the calculated ones as well as the effect of electro- and thermo-tuning of the PBG's edge, tuning the defect mode and the extended PBGs. PC-LC composite photonic structures provide the electro-tuning of the PBG edge and a complete polarisation shift of high order PBGs with response time of 30 ms in the range of the applied voltages from 2 to 10 V.

Applications: The developed photonic structures on Si are designed for utilisation as passive and active optical elements for integrated microphotonics in the middle (2-15 μm) and near-infrared (λ=1.5 μm) ranges. In particular, these structures can be used as tunable micro-polarisers, switches, filters as well as matrices for micro- and nano-biosensing.

References:

1. V. Tolmachev , T. Perova , E. Krutkova , E. Khokhlova "Elaboration of the gap-map method for the design and analysis of one-dimensional photonic crystal structures", J. Phys.E **41**, pp.1122-1126, 2009

2. E. V. Astrova, A. A. Nechitailov, V. A. Tolmachev, V. A. Melnikov, and T. S. Perova, "Photo-electrochemical etching of macro-pores in silicon with grooves as etch seeds" Phys. Status Solidi A, **206** pp.1235-1239, 2009.

3. Tolmachev, V. A., Astrova, E.V., Perova, T.S.,. Zharova, J.A, Grudinkin, S.A., Melnikov, V.A., "Electro-tunable in-plane one-dimensional photonic structure based on silicon and liquid crystal", App. Phys. Lett., **90,** pp.011908(1-3), 2007.

4. R. Soref "Towards Silicon-based Longwave Integrated Optoelectronics (LIO)"
Silicon Photonics III, edited by Joel A. Kubby, Graham T. Reed. Proc. of SPIE Vol. **6898**, pp.689809(1-13), 2008.

Reduction of noise in atomic system driven by squeezed coherent field

A. Gelman[1] , V. Mironov[1]

1. Institute of Applied Physics of Russian Academy of Sciences, Nizhny Novgorod , Russia, gelman@appl.sci-nnov.ru

Dumping plays an important role in many problems of quantum optics [1]. The development of experimental techniques to study single quantum systems (e.g. trapped ions) has stimulated the construction of theoretical methods to describe single experimental realizations conditioned on a particular observation record of the decay channel, known as quantum-jump or Monte Carlo wave function (MCWF) methods [2].

The method operates with a wave function of the system and has significant advantages over the density operator approach when we simulate the dynamics of complicated systems. The dimension of the task is N instead of N^2 elements of the density matrix. The required accuracy is obtained in stochastic simulations by making repeated runs, which can be performed in parallel on many computers. The simulation of single experimental realizations of quantum system gives one the possibility to numerically simulate ab initio many processes in the system, taking into account interaction with a reservoir, quantum noise, features of the quantized light, processes of homodyne measurement what is an up to date problem in the quantum information processing and communication science [3].

In this work the interaction of a squeezed coherent field with a medium of three-level atoms under the electromagnetically-induced transparency (EIT) conditions is investigated. We firstly investigate the problem analytically by Heisenberg-Langevin method. We study the influence of quantum properties of light on the medium in order to decrease the noise level of parameters of atomic system, which are crucial in processes of storage and transfer of quantum information. Then we investigate this problem numerically using the MCWF approach. The use of the method allowed us to analyze the dynamics of the "field + atom" system and to study the impact of relaxation processes on the system dynamics. A part of our numerical results was applied to calculate atomic spin σ_3 fluctuations spectra (Fig. 1) and outgoing field squeezing spectra. It is shown that under these condition quantum properties of light (squeezing) can be transferred to the medium, what results in suppression with $K \approx 0.7$ of the atomic operators' noise level in the EIT effect transparency window. We find a good correspondence with a theoretical research, carried out by us with the use of Heisenberg-Langevin method. In a special case of squeezed vacuum a good correspondence with experimental results is found [4]. The MCWF method allowed us to put into consideration quantum noise in the system what is crucial for full quantum investigation of the problem. The first experimental investigation of the propagation of squeezed vacuum in a medium of Λ-atoms was conducted in 2004 [4] and up to date works [e.g., 5] confirm the increasing interest in this direction.

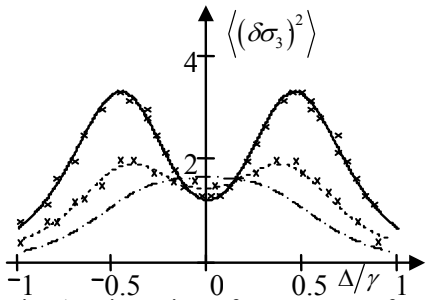

Fig. 1. Dispersion of operator σ_3 from the detuning Δ/γ. Probe field is in the coherent state (dot-dashed line), squeezed state with $r = 0.5$ (dashed line), $r = 1.5$ (solid line). Crosses – the result of numerical simulation. Parameters $\Gamma = 10^{-3}\gamma$, $g^2L/c = \gamma$, $g^2L/c = \gamma$.

The developed software implements the method for a wide class of problems in quantum optics. It has a modular construction, intuitive graphical interface, which allows the adding of new tasks and methods of calculation. It was tested on the studied problems of quantum optics, such as the spectrum of resonance fluorescence of laser-driven two-level atom and the dynamics of laser-driven three-level systems.

The research was supported by RFBR grant 09-02-97059.

1. C. W. Gardiner, P. Zoller. *Quantum noise*. Springer, Berlin, 2000

2. M. B. Plenio and P. L. Knight, "The quantum–jump approach to dissipative dynamics in quantum optics", Rev. Mod. Phys., 70, pp. 101-144, 1998

3. M. A. Nielsen and I. L. Chuang. *Quantum Computation and Quantum Information*. Cambridge University Press, Cambridge, U.K., 2000

4. D. Akamatsu et. al., "Electromagnetically Induced Transparency with Squeezed Vacuum", Phys. Rev. Lett., 92, p. 203602, 2004

5. J. Appel et. al., "Quantum Memory for Squeezed Light", Phys. Rev. Lett., 100, p. 093602, 2008

Enhancement of Optical Properties by Surface Nanostructuring

V. V. Nanumov[1] , V. A. Paporkov[2] , N. A. Rud[2] , E. I. Vaganova[1] , A. V. Prokaznikov[1]

1. Yaroslavl Division of Physico-Technological Institute RAS, Universitetskaya, 21, Yaroslavl, 150007, Russia
2. Yaroslavl State University named after Demidov P.G., Sovetskaya, 14, Yaroslavl, 150000, Russia,
E-mail: rud@uniyar.ac.ru

In the recent years attention of many scientific groups was paid to the development of photovoltaic cells of different kind. Some kinds of effects were discovered that amplify efficiency of such devices. One of such effect is connected with surface plasmon creation. Surface plasmon resonances in metallic nanoparticles are of interest for a variety of applications due to the large electromagnetic field enhancement that occur in the vicinity of the metal surface [1].

Here we report about investigations in the field of localized surface plasmon creation in order to increase absorption properties of photovoltaic devices. The system being investigated consisted of 2 microns in depth boron doped p^+ - type silicon ($p = 5 \cdot 10^{18}$ cm^{-3}) on *n*-type silicon substrate ($n = 10^{15}$ cm^{-3}). Porous silicon layer was formed by anodization in *HF* solution with pore length of the order of 120 *nm*. Then the quantum dots of *Ni* on the front side were formed by electrodeposition in corresponding solution. The average size of quantum dot was of the order of 40 *nm*. The controlled sample without *Ni* quantum dots on the upper surface was done for comparison. Aluminum (*Al*) contacts were done on the back side of *Si* samples and on the front side of the porous silicon sample without *Ni* quantum dots.

Investigations of transverse magnetooptical Kerr effect (TMOKE) which was carried out according to a method that was described in the work [2] demonstrated the anomalous behavior of angle dependence for TMOKE for devices with *Ni* quantum dots on the upper surface comparing to that with continuous *Ni* layer. These devices demonstrated very large absorption values for the angles near 75º for wave length equals 630 *nm*. This fact can be interpreted as localized surface plasmon creation (compare with results in the work [2]).

The photocurrent was measured for devices with *Ni* quantum dots on the upper surface and for controlled samples. The fill factor (FF) was nearly the same in both cases. The product of short current (I_{SC}) and open circuit voltage (V_{OC}) for devices ($I_{SC} \cdot V_{OC}$) with surface plasmon polariton effect was nearly one order higher than that for controlled devices with porous silicon and without *Ni* quantum dots. The maximum of photocurrent was observed for wave length 930 *nm*.

The results of this work can be useful by elaboration of new kind of photovoltaic devices.

1. D.M. Schaadt, B. Feng, E. T. Yu, “Enchanced semiconductor optical absorption via surface plasmon excitation in metal nanoparticles“, Appl. Phys. Lett.. 2005. V. 86. 063106
2. E. Yu. Buchin, E. I. Vaganova, V. V. Naumov, V. A. Paporkov, A. V. Prokaznikov. “Enhancement of the Transversal Magnetooptical Kerr Effect in Nanoperforated Cobalt Films”, Techn. Phys. Letters. 2009. V. 39. No 7. P. 589.

Excitation dependence of infrared emission at 1.5-1.6 μm from defect-rich Si layers

A.A. Shklyaev[1,2] , A.B. Latyshev[1,2] , M. Ichikawa[3]
1. Institute of Semiconductor Physics, SB RAS, Novosibirsk, 630090, Russia, shklyaev@thermo.isp.nsc.ru
2. Novosibirsk State University, Novosibirsk, 630090, Russia
3. Quantum-Phase Electronics Center, Department of Applied Physics, Graduate School of Engineering, The University of Tokyo, 7-3-1 Hongo, Bunkyo-ku, Tokyo 113-8656, Japan

Silicon produces infrared (IR) emission at 1.5-1.6 μm due to optical transitions via deep levels which serve as centers for radiative recombination. Deep levels can be formed by means of introduction of crystal defects, the presence of which in Si is associated with several photoluminescence (PL) peaks. We have recently developed the method for the growth of defect-rich silicon layers which produce only one PL peak located in the 1.5-1.6 μm wavelength region [1,2]. The method is based on the Si nanocrystal growth on the oxidized Si surfaces. In this work we study the dependence of the PL intensity (I_{PL}) on the excitation power density W, which was obtained at several temperatures from 5 to 230 K (Fig. 1). Approximation of the dependence by the power-law function ($I_{PL} \sim W^m$) reveals that the power exponent m depends on the interval of W. Moreover, it is found that the position of the PL peak is shifted towards the short-wavelength region with increasing W (Fig. 2). The analysis shows that the obtained dependences can be described by a model with deep levels of one type. The shift of the PL peak indicates that the occupation of deep levels decreases with increasing W that occurs in the conditions of carrier transfer between the recombination centers. Since the rate of radiative recombination is relatively low in silicon, the concentration of excited carriers is governed by the balance between the carrier generation rate and the rate of nonradiative recombination processes. In such conditions, each of the obtained values of m is associated with the mechanism of nonradiative recombination that dominates at corresponding values of W. The multiphonon recombination that prevails at relatively small W gives place to one of the possible Auger processes at high W. It should be noted that the diodes fabricated on the base of the defect-rich Si layers can produce IR emission at 1.5-1.6 μm at room temperature [3]. Carrier transfer between the recombination centers found in this work is a helpful property for the fabrication of IR emitters because it provides an additional channel for decreasing the occupation of deep levels under the injection current that leads to the increase in the radiative recombination rate.

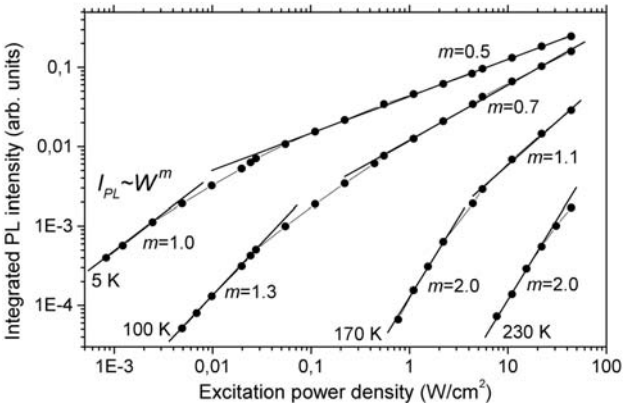

Fig. 1. Dependence of the PL peak intensity in the region from about 1.54 to 1.62 μm on the excitation power density at four temperatures marked in the figure.

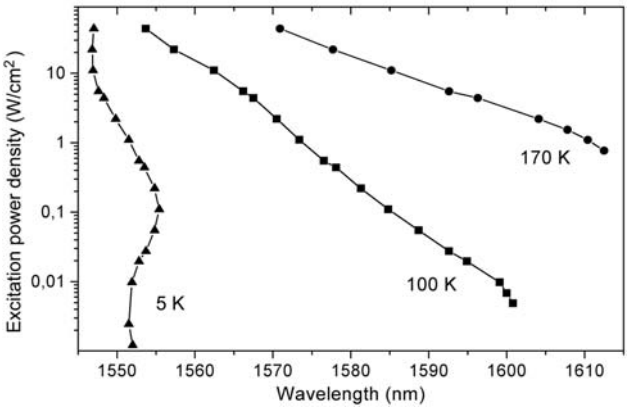

Fig. 2. Dependence of the position of the defect-related PL peak on the excitation power density at three temperatures marked in the figure.

1. A.A. Shklyaev, S. Nobuki, S. Uchida, Y. Nakamura and M. Ichikawa, "Photoluminescence of Ge/Si structures grown on oxidized Si surfaces", Appl. Phys. Lett., 88, pp.121919-1--3 (2006).
2. A.A. Shklyaev and M. Ichikawa, "Extremely dense arrays of germanium and silicon nanostructures", Physics – Uspekhi, 51, pp.133 - 161 (2008); UFN, 178, pp.139-169 (2008) (in Russian).
3. A.A. Shklyaev, Y. Nakamura, F.N. Dultsev and M. Ichikawa, "Defect-related light emission in the 1.4–1.7 μm range from Si layers at room temperature", J. Appl. Phys., 105, pp.063513-1--4 (2009).

Electronic transport in heterogeneous nanometer FET channels

V. P. Popov

Institute of Semiconductor Physics, Novosibirsk, Russia, e-mail: popov@isp.nsc.ru

To reduce unwanted short channel effects (SCE) in modern IC technology designers of new generations of CMOS ULSI used " good processing rules " which allow to receive close to ideal characteristics of field effect transistor*s* (FETs) [1]. Today, however, these requirements are far from reality. In most works (for example, [2,3]) dealing with the mobility in short channel transistors even an account of unwanted serial resistance of low dose doped (LDD) regions near the source and drain were unable to explain why reducing effective mobility μ_{eff} defined from experimental *I-V* curves happens at the reduction in the channel length [3]. On short channel transistors and particularly at reducing the length of the gates in silicon-on-insulator (SOI) μ_{eff} degradation is observed in the stressed silicon layer that were proposed be linked to the relaxation of the stress in the layers of silicon on the underlayed amorphous silicon dioxide due to its large thermal plasticity [3]. The values of mobility μ_0 in the "ideal" part of the channel can be obtained from the graph by the extrapolation of the straight line graph based on the dependence $1/\mu_{eff}$ on $1/L$ (Figure 1) according to the model [2].

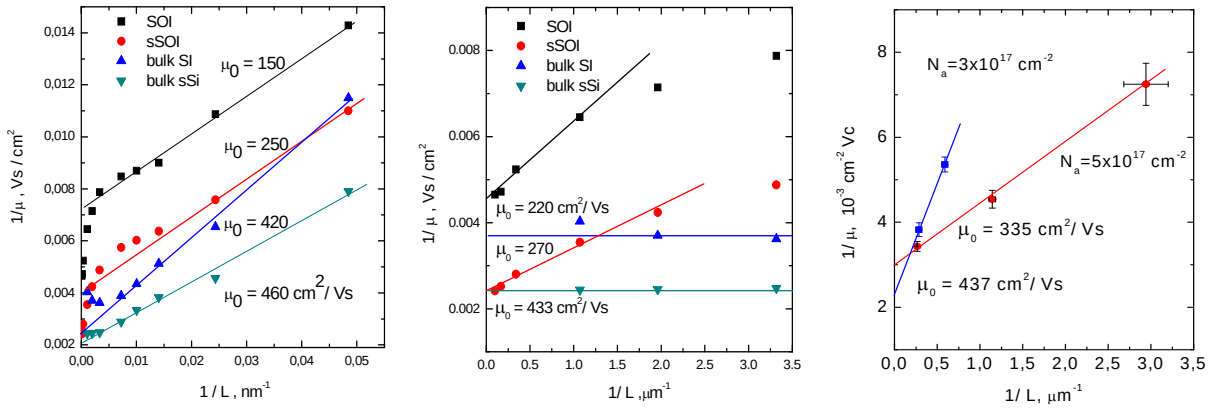

Figure 1. Changes of inverse effective mobility $(\mu_{eff})^{-1}$ depending on the $1/L$ for the bulk Si and stressed (bulk sSi) Si in comparison with similar results on SOI structures according to the data [2,3].

Thus, for the channels with L < 50 nm the values μ_0 are approximately 1.5 times less than for L > 300 nm. The reasons to reduce the mobility in nanometer channels are analyzed in the model of quasiballistic transport of charge carriers. In particular, it is shown, that instead of the value used in [3] the expression for the low field drain current with the quasi-equilibirum region with size l near the barrier takes the form:

$$I_{DS} = \frac{W}{L} C_{ox} V_{DS} (V_g - V_{th}) \left(\frac{1}{\mu_0} + \frac{1}{L} \frac{2kT}{v_{TH} q} \left(\frac{l}{\lambda_0} \right) \right)^{-1},$$

where λ_0 are the length of free electron pass in this region. The value l/λ_0 is equal to 3 and 4 for bulk and stressed silicon, respectively (Fig. 1a, bulk Si and bulk sSi curves). Moreover, an effective quasiballistic mobility μ_{qb} in the region of barrier at μ_0 = 460 cm^2/(V·s) and L = 50 nm with critical length l = 25 nm the value of μ_{qb} is μ_{qb} = 145 cm^2/(V·s), while in the case of SOI and the value of mobility μ_0 = 150 cm^2/(V·s) the value of μ_{qb} is μ_{qb} = 52 cm^2/(V·s).

1. T. Skotnicki, C. Fenouillet-Beranger, et al. Innovative materials**,** devices and CMOS technologies for low-power mobile multimedia**",** IEEE Trans. Electron Devices, 55, pp. 96-130, 2008.
2. A. A. Frantsuzov, N. I. Boyarkina, and V. P. Popov. Decrease in effective electron mobility in the channel of a metal-oxide-semiconductor transistor as the gate length is decreased. Semicond., 42, pp. 215–219, 2008.
3. C. Dupré, T. Ernst, J.-M. Hartmann, et al. Carrier mobility degradation due to high dose implantation in ultrathin unstrained and strained silicon-on-insulator films. Journ. Appl. Phys., 102, no. 10, 104505(8), 2007.

Ballistic and Pseudo-Relativistic Carrier Transport in Graphene

G. I. Zebrev

Micro- and Nanoelectronics Department, National Research Nuclear University "MEPHI", Moscow, Russia,
e-mail: gizebrev@mephi.ru

Two-dimensional single sheet of carbon, graphene, isolated first in 2004 [1], has unique properties that suggest it may have an important role to play in future nanoelectronics [2-4]. The low scattering rates in clean samples and large mean path lengths presume a possibility of ballistic transport in graphene devices. Slowly varying potential relief typical for most applications allows a use of quazi-classical approximation for not too small carrier densities. In fact, semi-classical description is rather suitable even for the neutrality point due to presence of unavoidable disorder at the Dirac point. We study the ballistic transport in graphene subject to the coordinate dependent potential $U(x)$. Motion equations for ballistic transport were derived from the variation principle via minimization of Lagrange function. It has been shown that ballistic kinetics in static potential is described for gapless extended graphene by so-called Frenet equations. Analogies between graphene electronics and optics is discussed, since the electrons in graphene behave like massless "charged photons" which have a similar dispersion [5]. Other pseudo-relativistic effects in gapless and gapped have been investigated.

1. K. S. Novoselov, A. K. Geim, et al. "Electric field effect in atomically thin carbon films," *Science*, vol. 306, pp. 666-669, 2004.
2. A. Cresti, N.Nemec et al. "Charge transport in disordered graphene-based low dimensional materials," Nano Res (2008) 1: 361-394.
3. G.I. Zebrev, "Graphene nanoelectronics: electrostatics and kinetics", Proceedings of the SPIE, Volume 7025, pp. 70250M-70250M-9 (2008).
4. G. I. Zebrev, "Electrostatics and diffusion-drift transport in graphene field effect transistors", MIEL 2008. 26th International Conference on Microelectronics 2008, pp. 159-162.
5. G.I. Zebrev, "Relativistic dynamics and optics of massless electrons in ballistic graphene", MEPHI Scientific Session Proc. http://library.mephi.ru/2/scientific-sessions?Year=2008&Volume=6 (in Russian)

Comparative studies of single- and double-nanocrystal layer NVM structures: charge accumulation and retention

V. Turchanikov[1], V. Ievtukh[1], A. Nazarov[1], V. Lysenko[1], M. Theodoropoulou[2], A.G. Nassiopoulou[2]

[1] *Lashkaryov Institute of Semiconductor Physics NASU, Prospekt Nauki 45, 03028 Kyiv, Ukraine, Nazarov@lab15.kiev.ua*
[2] *IMEL/NCSR Demokritos, P. O Box 60 228, 153 10 Athens-Greece, A.Nassiopoulou@imel.demokritos.gr*

In this paper we describe the results obtained in a course of charge accumulation and retention in single- and double-nanocrystal layer (NC layer) non-volatile memory (NVM) structures comparative studies. Both structure types were formed on p-Si and included (1) single NC layer structure: tunnel oxide 3.5 nm/ NC layer thickness 3.3 nm/ control oxide 10 nm, (2) double NC layer structure: tunnel oxide 3.5 nm/ nanocrystal layer 3.5 nm/ SiO_2 interlayer ~2nm/ nanocrystal layer 5 nm/ control oxide ~10 nm. In both cases the NC layer thickness coincided with the NC size in the z-direction. The above memory structures were prepared by LPCV deposition of amorphous silicon on the tunnel oxide, followed by solid phase crystallization and thermal oxidation [1]. This was repeated twice in the case of double layer structures. Application specific data acquisition system (DAQ), software and hardware were specially designed for window formation, relaxation and retention measurements of NC NVM cells. The flatband voltage (V_{fd}) was calculated from the HF CV characteristics (1MHz). Heterogeneity of the surface potential, which is associated with heterogeneity of charge trapping in the dielectric, was estimated on the basis of the dC/dV maximum height .
Window formation measurements under different bias conditions (symmetrical and asymmetrical program/erase pulses) demonstrated that in double layer structures there are no biasing regions in which unipolar reprogramming can be obtained [2], in contrary to the single layer structure.
Relaxation measurements of charge accumulated in NVM cell under the series of write/erase pulses reveal essential differences between single- and double-layer structures. First, under the same pulse polarity, say negative, the sign of charge accumulated in the single-layer structures was positive (associated with NC ionization), and in the double-layer cell negative (electron trapping). Second, there is a qualitative difference in a type of relaxation process. In the double-layer structure relaxation had conventional smooth character as opposed to the single-layer samples where it was of staircase type. This means that the charge accumulated under the single charging pulse and the series of pulses with the same cumulative duration will be different. In our experiments we had a possibility to make an estimation of charge heterogeneities incorporated in dielectric during write/erase processes. It turns out that the heterogeneities density is rather small in a case of negative charge buildup, rising in the direction of flat bands and then again slowly dropping as the positive charge is incorporated in NC NVM cell. The latter was true for both single- and double-layer structures. This means that heterogeneities generation took place in both structure types.
Charge retention measurements also demonstrated great differences between the two structure types. In a single-layer structure charge trapping depends mainly on the programming pulse duration but not on its amplitude. To reach an acceptable window width it must be over 1 s. At the same time in double-layer cells acceptable results were obtained with write/erase pulse width as small as 80 ms and the character of relaxation process depends rather on the height of the pulse, than on its duration. We also found that in the single-layer system the retention characteristics strongly depend on the gate potential in a course of storage. This means that retention characteristics are strongly related with the work function difference between Si substrate and gate material. The origin of this phenomenon is related to the fact that window shrinking during storage is dictated by accumulated electrons draining from dielectric into the silicon substrate.

[1]. M. Theodoropoulou and A. G. Nassiopoulou, “Multilevel charge storage in Si nanocrystals arranged in double-dot-layers within SiO2 », Microelectronic Engineering, 85 (12), pp 2362-2365, 2008.
.
[2] V.I. Turchanikov, A.N. Nazarov, V.S. Lysenko, O. Winkler, B. Spangenber and H. Kurz, «Study of the unipolar bias recharging phenomenon in the non-volatile memory cells containing silicon nanodots », Materials Science and Engineering, B124-125, pp. 517-520, 2005.

Silicon nanoballs recharging in plasma-chemical oxide of nanometric thickness

M.D.Efremov[1,2], A.Kh.Antonenko[1,2], S.A.Arzhannikova[1,2], A.V.Vishnyakov[1,2], V.A.Volodin[1,2], A.A.Gismatulin[1], G.N.Kamaev[1,2], D.V.Marin[1,2], A.A.Voschenkov[1]

1. Institute of Semiconductor Physics, Russian Academy of Sciences, Novosibirsk, Russia, efremov@isp.nsc.ru, 2. Novosibirsk State University, Novosibirsk, Russia, nsm@nsm.nsu.ru

Separate nanoballs attract science attention due to unique properties of silicon with size about several nanometers. For incrustation of nanoballs into silicon dioxide layers with thickness about several nanometers a method was chosen to prepare a suspension using silicon organic materials. Preliminary the task for preparation of very thin oxide layers was solved owing oxidation of silicon surface in pure oxygen plasma. The suspension was prepared due to placement of nanopowder into hexamethyldisiloxan representing liquid precursor for plasma-chemical formation of silicon dioxide films. The suspension was bring onto preoxidized silicon wafers using standard microelectronic method and then was oxidized in plasma of pure oxygen.

Series of nanopowder were manufactured using beam of relativistic electrons for evaporation of pure FZ-silicon in a result of silicon coagulation in gas flow of argon. 1.6MeV electron beam accelerator was used for evaporation. Size selection was as in stage of manufacturing by means of filtering, as in stage of preparation of a suspension for nanopowder. Sublayer, separating nanoballs from substrate, have a characteristic thickness about 5nm. Electrophysical properties for manufactured MOS- (in fig.1 left) and MOS:NC (in fig.2 right) – structures were investigated. There was discovered frequency dependent increasing of both differential capacity and conductivity in depletion regime, what was explained as exchange of charge between substrate and nanoballs. Instability of impedance observed for MOS:NC – structures at voltage above 7V was explained as possible variation of nanoballs electronic spectrum as influence of multi-electron effects. Increasing of frequency leads to approaching of characteristics to standard form for MOS-structures, what corresponds to retarding of charge exchange with substrate due to shortening period of voltage applied. Thus, method was realized for creation of MOS:NC-structures with nanoballs in dielectric layer and researching of its electronic properties was provided.

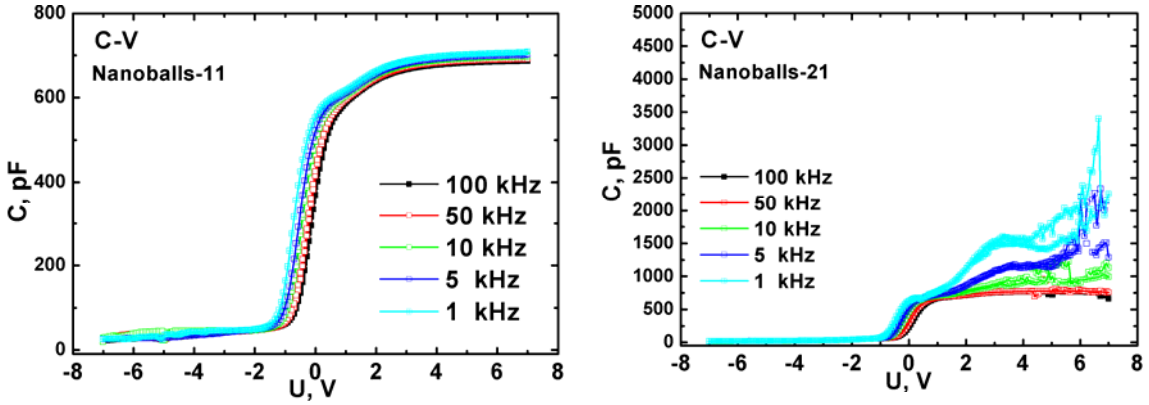

Fig.1. CV(up) characteristics for MOS–structures with nanoballs (right) and without ones (left)

Charges and states in nitrided buried dielectrics of SOI structures

V.P. Popov, I.E. Tyschenko
Institute of Semiconductor Physics, Novosibirsk, Russia; e-mail: popov@isp.nsc.ru

As known nitrided silicon dioxide SiON is a common material for gate dielectric in modern CMOS technology. But the nitrogen content in SiON should be lower than 10% to avoid DIBL and NBTI effects [1]. Another interesting property for SiON is a reduced rate of positive charge accumulation during irradiation. The goal of our efforts was to introduce nitrogen atoms in buried oxide to improve a radiation tolerance of SOI fully depleted CMOS transistors with undoped channels on thin (30 nm) silicon film. Compound buried oxide (BOX) layers may be obtained by direct bonding of silicon wafers covered by Si_3N_4 and SiO_2 respectively [2]. But due to initial hydrophobity and hydrophility of such films high strength of bonding is possible only after plasma treatment of the surfaces [3].

An effective method of interface mediated endotaxy (IME) using ordinary DeleCut method for SOI formation to produce semiconductor heterostructures on insulator was suggested by us using implantation of respective ions in thermally grown dioxide on silicon substrate before wafer bonding and Si layer transfer from another (donor) wafer by implanted hydrogen [4]. In this work we used the same operations as described in [4,5] to produce a SiON layer at the bonding interface between silicon layer and buried dioxide with 300 nm thickness in SOI structure. Different doses of 40 keV N^+ ions were used: $1x10^{15}$, $3x10^{15}$, $6x10^{15}$, $1x10^{16}cm^{-2}$. SOI structures with buried silicon oxinitride layer are labelled next as SOIBON.

Test MOS mesa structures were produced by standard CMOS technique, which were irradiated then by ^{60}Co γ-rays up to total irradiation dose (TID) 10 Mrad. All MOS structure contacts during irradiation were grounded. The mesa structures were used for CV low-high frequency (10 Hz - 1 MHz) measurements. The voltage shift ΔV_{th} at the upper interface was about 10 times less than for botom one after irradiation as a result of nitridation of the upper SOI / BOX interface. The breaks in the curves near O V and the increase in MOS capacity near +20 V almost disappear for the square of the MOS structures 1000×1000 μm^2 following the decrease in the contribution of square angles and volume BOX states in the total capacity of mesa structures.

The radiation induced effective charge ΔQ is equal to the sum of interface and volume charges and is reduced to the respective interface according to the estimation by $\Delta Q = \Delta V_{th} \cdot C_{ox}$, where C_{ox} is the buried oxide capacity, which is the same for both interfaces. The effective charge accumulation was observed at about five time lower rates for all nitrided interfaces of SOIBON structures. Effective negative charge accumulation was obtained at the upper interface for more heavily nitrided BOX at the total irradiation dose lower than 1 Mrad. Relatively weak dependence on nitrogen content coincides with the HREM analysis, according to which the interface SiON layer thickness is approximately constant.

It is interesting to compare the values of effective charges accumulated in different SOI structures after TID equal to 1 and 10 Mrad. The lowest value after 1 Mrad is equal to $3x10^{10}cm^{-2}$ for SOIBON structure with optimal nitrogen content, the highest value is equal to $1.4x10^{12}cm^{-2}$ for SIMOX structure. For 10 Mrad TID the differences between DeleCut and SOIBON are lower: $3x10^{11}cm^{-2}$ for SOIBON structure and $1.3x10^{12}cm^{-2}$ for DeleCut SOI wafers.

The obtained results give the evidence that suggested in [4,5] IME process is acceptable not only for semiconductor heterostructure-on-insulator, but also for compound buried dielectrics like in SOIBON, providing excellent radiation tolerance for SOI structures in radiation harsh environment.

References

[1] M.L.Green et al. J. Appl. Phys., **90**, pp.2057-2121, 2001.
[2] Q.Tong, U. Goesele. Semic. Wafer Bonding, Wiley, 1999.
[3] P. Patruno et al. IEEE SOI Conf. pp.51-52, 2007.
[4] V.P. Popov et al. ECS Trans. **6**, (1) 87 (2007).
[5] V.Popov et al., In Nanoscaled SOI Structures and Devices, S Hall et all (eds), Springer, pp.59-72, 2007.

DC SQUID modulation electronics for operation with HTS DC SQUID magnetometers in the unshielded environment

E. V. Burmistrov, V. Yu. Slobodchikov, V.V. Khanin, Yu.V. Maslennikov

Kotel'nikov Institute of Radio Engineering and Electronics of RAS

Uses of HTS DC SQUIDs in extra sensitive magnetic measurements are still very prospective. Ultra sensitive HTS dc SQUID-magnetometers with magnetic field resolution of about 15 fT/√Hz were developed recently [1]. Moreover these detectors were improved to commercially available samples, HTM-8 type magnetometers. These sensors already have sensitivity close to LTS dc SQUID based magnetometers. But still two serious problems appear when one tries to operate HTM-8 type magnetometers in an open space. First of all, SQUIDs should be operated with FLL electronics with huge dynamic range. Secondly, there is no capability to use HTS external gradiometric input coils in contrast to LTS dc SQUID-magnetometers due to absence of available HTS soldering technology.

The main task of our work was to develop the modulation electronics capable to operate with new ultra sensitive HTS dc SQUID based detectors in unshielded environment.

The new variant of DC SQUID modulation electronics for functioning with HTS DC SQUID magnetometers in the unshielded environment, was designed, manufactured and tested. The electronics was optimized for operation with new ultrasensitive HTS DC SQUID magnetometer providing magnetic field resolution of about 15 fT/√Hz at frequencies above 10 Hz and 30 fT/√Hz at 1 Hz. The central commutation core of electronics was based on a complex programmable logic device (CPLD). It has allowed to include into the SQUID-electronics the flexible system of a bias reversal which provides a stable magnetometer operation for various configurations of wiring in the cryostat and various HTS DC SQUID topologies. The electronics was manufactured in one compact box with size 110 mm x 60 mm x 15 mm. The channel has standard bandwidth of about 100 kHz with greatly increased dynamic range due to high coupling ($8\ \mathrm{mV}/\Phi_0$) of feedback signal with main SQUID's loop.

1. M.I. Faley, U. Poppe, K. Urban, D. Paulson and R. Fagaly, "A New Generation of the HTS Multilayer DC-SQUID Magnetometers and Gradiometers", *Journal of Physics: Conference Series*, vol. 43**,** pp. 1199–1202, 2006.

Properties of planar Nb/α-Si/Nb Josephson junctions with various doped degree of α-Si interlayers

A.L. Gudkov, A.A. Gogin, A.I. Kozlov, A.N. Samys
CJSC "Compelst", FSUE "SRIPP n. F.V. Lykin", Moscow, Zelenograd, Russia, E-mail: gudkov@niifp.ru

Josephson junctions with direct conductivity are the most perspective superconducting electronic element base. In helium temperature area the best characteristics have been reached on edge Nb/α-Si/Nb Josephson junctions [1]. In these junctions α-Si interlayers was doped by Nb atoms by diffusion method until full degeneration of the semiconductor. Edge junctions showed high critical current density to 10^5 A/см^2 and above. However, the small areas of edge junctions (less than 1 мкм^2) and accordingly small values of critical currents ($I_c \leq 1$ мА) have limited application areas of these junctions [2]. Josephson junctions with great values I_c for high-frequency applications and for schemes of Volt standards are especially important.

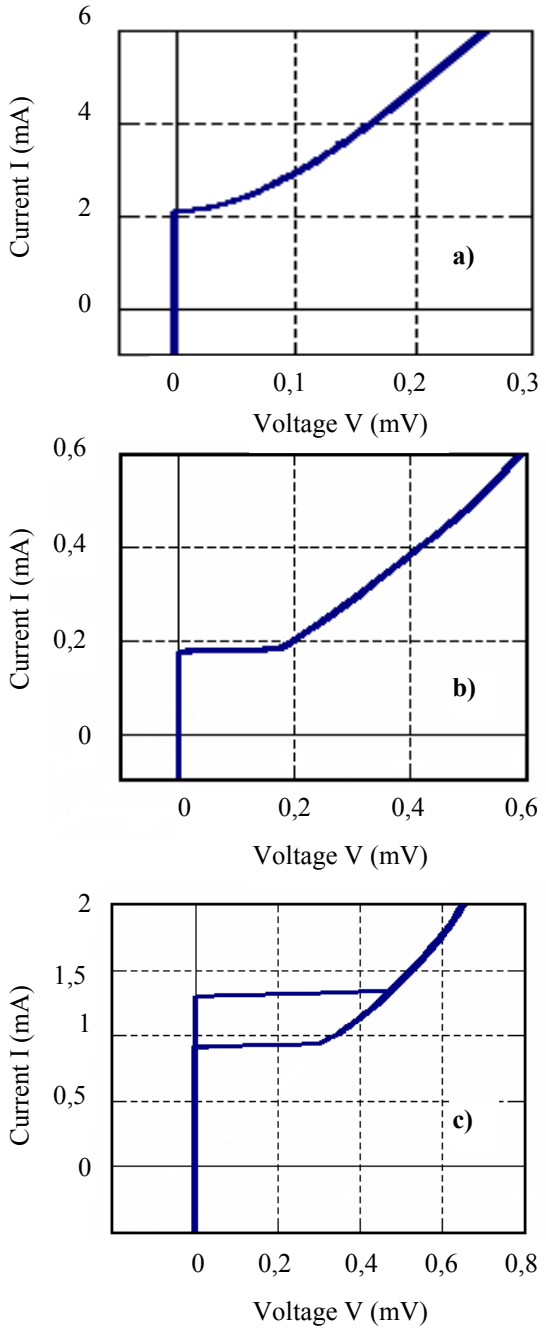

Fig 1. Current-voltage characteristics of Nb/α-Si/Nb Josephson junction with various doped degree of α-Si – interlayer: a) $\beta < 1$; b) $\beta \approx 1$; c) $\beta > 1$.

Electrophysical characteristic researches of planar Nb/α-Si/Nb Josephson junctions with the sizes 6 x 6 μm^2 and 9 x 9 μm^2 are carried out in the present work. The three-layer structure of Nb/α-Si/Nb junctions was made by magnetron sputtered method. The doping of α-Si interlayer was made in the process of its formation by co-sputtered method of Si and W. With increase in the area of junction its normal resistance (R_n) decreases and the resistance increase is possible only at the expense of reduced doped degree of α-Si interlayer. Change of interlayer conductivity leads to change of capacitance parameter: $\beta = (2e/\hbar)I_cR_n^2C$, where C is geometrical capacitance of junction. Researches of current-voltage characteristics of junctions with various doped degree of α-Si interlayers have been made in the given work (fig. 1). It has been shown, that at $\beta < 1$ current-voltage characteristic behaviour is described by resistive model for SNS junctions with excessive current. In a case $\beta \geq 1$ current-voltage characteristic form varies and described by a cubic hyperbole. There is capacitor hysteresis on the current-voltage characteristics, and its range depends on value of a critical current. High-frequency properties of junctions vary. At junctions with $\beta \geq 1$ the amplitude of the first step exceeds size of a critical current. Temperature dependences I_c and R_n are investigated. At $\beta \geq 1$ R_n strongly depends on temperature. The results of investigation of Josephson junction stack characteristics (Nb/α-Si/Nb/α-Si/Nb) are presented. In case of equality of α-Si interlayer thickness the critical currents of junctions in a stack also are equal.

1. A.L. Gudkov, M.Yu. Kupriyanov, and K.K. Likharev "Properties of Josephson junctions with amorphous-silicon interlayers". Sov. Phys. JETP, V. 68(1). P. 1478-1485. 1988.
2. A.L. Gudkov "Josephson junctions and areas of their applications". Electronic industry. №3. P. 77-87. 2004.

The theoretical analysis of the new microwave detector based on a Josephson heterostructure

I.A. Devyatov[1], M.Yu. Kupriyanov[1]
1. Lomonosov Moscow State University Skobeltsyn Institute of Nuclear Physics, 119991 Moscow, Russia,
igor-devyatov@yandex.ru.

High-sensitivity superconducting microwave detectors of various types are widely used now in a number of applications [1]. Among the most important theoretical results achieved in this field in the last few years was the creation of theories [2,3], taking into account the quantum nature of microwave radiation absorption in these detectors as well as excited quasiparticles relaxation and multiplication. These theories have obtained the limits of sensitivity of such popular microwave detectors, as CEB (cold electron bolometer) detector and KID (kinetic inductance bolometer) detector. The results of [2,3] clearly demonstrate, that principles of operation of CEB and KID do not permit to achieve the values of sensitivity, relevant for the present radio-astronomy applications. On the other hand, recent calculations of non-equilibrium fluctuations, arising in normal diffuse metal strip under microwave irradiation [4], and the response of Josephson S-I-N-I-S (superconductor-insulator-normal metal-insulator-superconductor) heterostructure on microwave power [5], allow us to hope that THZ frequency range microwave detector, having the sensitivity, suitable for the radio-astronomy applications, can be created.

In this work, we consider theoretically signal and noise properties of the new type of a high-sensitivity detector, based on a S-I-N-I-S Josephson junction, in which the electron energy distribution function $f(\varepsilon)$ in the nanoscale normal metal N_region is nonequilibrium due to the capacitive coupling of this region with a receiving antenna [5]. The deviation of $f(\varepsilon)$ from the equilibrium distribution function leads to a change in the critical current I_c of the junction, i.e., in fact, to its inductance $L = \Phi_0/2\pi I_c$ ($\Phi_0 \approx 2.07*10^{-15}$ Wb is the magnetic flux quantum), which is the output signal of this device. We also show that this device has a number of advantages as compared to the recently proposed bolometer based on a long S-N-S (superconductor–normal metal–superconductor) Josephson junction [6] and is free from a number of inherent drawbacks of the S-N-S bolometers. Up to now there was no calculation of the noise properties of S-I-N-I-S Josephson junction bolometer, taking into account non-equilibrium form of electron distribution function $f(\varepsilon)$ in the normal metal absorber of this detector. Based on results of [4,5], we make this calculations and demonstrate, that noise parameter NEP of this detector is lower, than in others modern microwave detectors.

The work is supported by RFBR grants 09-02-01351-a, 09-02-12351-офи_м.

1. F. Giazotto, T. Heikkila, A. Luukanen, A.M. Savin and J.P. Pekola, “Opportunities for mesoscopics in thermometry and refrigeration: Physics and applications”, Rev. Mod. Phys., **78**, pp. 217-275, 2006
2. I.A. Devyatov, P. A. Krutitskii, M.Yu. Kupriyanov, “Investigation of Various Operation Modes of a Miniature Superconducting Detector of Microwave Radiation”, JETP Letters, **84**, pp. 57–61, 2006
3. A. V. Semenov, I.A. Devyatov, M.Yu. Kupriyanov, “Theoretical Analysis of the Operation of the Kinetic Inductance-Based Superconducting Microwave Detector”, JETP Letters, **88**, pp. 441–447, 2008
4. I.A. Devyatov, P. A. Krutitskii, A. V. Semenov, D. V. Goncharov, “Nonequilibrium Fluctuations of a Thin Metal Diffuse Film Exposed to Microwave Radiation”, JETP Letters, **88**, pp. 254–258, 2008
5. I.A. Devyatov, M.Yu. Kupriyanov, “High_Sensitivity Microwave Detector Based on a Josephson Heterostructure”, JETP Letters, **89**, pp. 451-456, 2009
6. F. Giazotto, T. Heikkila, G.P.Pepe, P. Helisto, A. Luukanen, J. Pekola, “Ultrasensitive proximity Josephson sensor with kinetic inductance readout”, Appl. Phys. Lett., **92**, pp. 162507-1-162507-3, 2008

«Conventional» SQUIDs and quantum interferometers on matter waves in superfluid helium

A. Golovashkin[1], G. Izmaïlov[2], G Kuleshova[3], A. Tshovrebov[1], L. Zherikhina[1],
1. Lebedev Physical Institute, Russian Academy of Science, Moscow 119991, Russia; e-mail: tshovrebov@rambler.ru,
2. Moscow Aviation Institute (State Technical University), Moscow 125993, Russia
3. Moscow Engineering Physics Institute (State University) , Moscow 115409, Russia

Research of Josephson effect in superfluid He allowed to approach to the problem of creation of quantum interferometer on matter waves. This device is analogue «conventional» superconducting quantum interferometer of direct current (DC-SQUID) and in accordance with the above analogy, whom is illustrated by the figure, may be called by the SHeQUID [1]. If «conventional» DC-SQUID is superhigh sensitive probe, registering the flux of magnetic field, then SHeQUID is intended for high-accuracy measurements of mechanical angular momentum. In DC-SQUID the quantum interference arises owing to presence two Josephson tunnel junctions (the crosses in the picture), inclusing to the superconducting coil, the role of whom in SHeQUID carry on two nano throttle (microscopic narrowing 1,2 in toroidal circuit). In consequence of quantum interference the magnetic flux operates resulting crit.current of DC-SQUID, what in case of fixed exterior current causes a change of potential difference, him registered electronics. In SHeQUID the analogous changes of pressure either temperature differential are controlled by the mechanical turning moment. The consideration of quantum fluctuations, performed of by us, made it possible to determines limiting values of sensitivity of quantum interferometers and to estimate their the geometrical dimensions. 1.The mode of, when to the single Cooper-pair in DC-SQUID either to the single atom ^{4}He in SHeQUID has to quantum of action $2\pi\hbar$, leads to sensitivity restriction of DC-SQUID at the level of $\sqrt{<\delta\Phi^2>/1Hz} = \sqrt{2\pi\hbar L} \approx (2\times10^{-8} \div 6\times10^{-7})\Phi_0/\sqrt{Hz} << \Phi_0/\sqrt{Hz}$ (L - the coil inductance, $\Phi_O=\pi\hbar/e\approx2{,}07\times10^{-15}Wb$ - the quantum of magnetic flux) and to analogous restriction for SHeQUID $\sqrt{<\delta\Lambda^2>/1Hz} = \sqrt{2\pi\hbar J} < N_{He}\hbar/\sqrt{Hz}$, where the moment of inertia is expressed as the atoms number of ^{4}He in ring as $J=r^2 m_{He} N_{He}$. For $N_{He}=10^{15}$ (nearly 4 nanograms ^{4}He), circulating in torus by the diameter 100 micrometres with section of canal 100mkm^2, obtain $\sqrt{<\delta\Lambda^2>/1Hz} \approx 6\times10^7\,\hbar/\sqrt{Hz}$, i.e. 6×10^{-8} from fundamental period, equal $N_{He}\hbar/\sqrt{Hz} \approx 10^{-19}(kg\,m^2/s)/\sqrt{Hz}$. 2.Another mode of, when the interference period is responsible for transmission of single action quantum $2\pi\hbar$ of whole dissipationless macroquantum system, as a single whole, is reduced for SHeQUID to term $2\pi\hbar > \sqrt{J\hbar/(2s)}$. Whence it follows that the significance of total moment of inertia of superfluid ^{4}He in SHeQUID ring nor must exceed $8\pi^2\hbar/s \approx 8\times10^{-33}m^2kg$, that taking into account of density liquid helium $120kg/m^3$ is performed for circular channel with $Ø\approx0{,}3mkm$ and total cross-section $50\times50nm^2$. Realization of this mode of DC-SQUID would require condition satisfactions $\pi\hbar/(eN_{2e}) > \sqrt{L\hbar/(2s)}$. From superconductor with density of Cooper condensate of $10^{22}sm^{-3}$ this condition is performed for DC-SQUID coil $Ø\approx1mkm$, having the total cross-section $150\times150nm^2$. By that of coil L appears to be at the level of $0{,}5pH$, and the number of Cooper pairs of N_{2e} nor should exceed 4×10^8. Of course the process of manufacturing of channels and coils of submicrometer size of SHeQUID and SQUID would require methods co-operations of nanotechnology. However the technical difficulties in many respects «pay out» possibility to measure of magnetic flux with precision $2{,}5\times10^{-9}\Phi_0/\sqrt{Hz}$, either possibility to register transmitted the mechanical turning moment in terms of $\hbar$ [2].

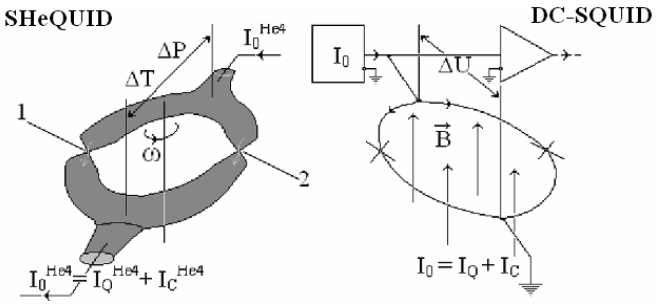

1. Y. Sato, E. Hoskinson, and R. E. Packard. Phys. Rev. B 74, p.144502, 2006
2. A. I. Golovashkin, G. N.Izmailov, V. V.Ozolin, A. M.Tskhovrebov, L. N.Zherikhina. Journal Gravitation and Cosmology. №2 (58) (June 2008)

The thermodynamic theory of interfacial adhesion between materials containing point defects

R. Goldstein[1], T. Makhviladze[2], M. Sarychev[2]
1. Institute for Problems in Mechanics, Russian Academy of Sciences, Russia, goldst@ipmnet.ru 2. Institute of Physics and Technology, Russian Academy of Sciences, Russia, tarielmakh@mail.ru

Adhesion forces play a decisive role in the strength characteristics of layered structures. The adhesive strength may have a profound effect on the reliability and lifetime of nano- and microelectronics elements. According to the commonly accepted view the interlayer adhesion consists in an attraction between the contacting surfaces of the layers. Therefore the adhesion results in decrease of the surface free energies of the layers. This decrease per unit surface f_A is considered as the measure of adhesion and can be given by the expression:

$$f_A = \gamma_1 + \gamma_2 - \gamma_{12} \quad , \qquad (1)$$

where γ_1 and γ_2 are the surface tensions of the free layer surfaces of materials forming the interface, and γ_{12} is the interfacial surface tension. The quantities γ_1 and γ_2 involved in (1) are studied much better than γ_{12}, both experimentally and theoretically. At the same time the quantity γ_{12} determines significantly the adhesive power of an interface. It should be particularly emphasized also that the influence of structural defects on adhesion properties of interfaces, that is on the quantity γ_{12}, is of great practical importance for many applications of multilayered coatings and structures in modern technologies, in particular in micro- and nanoelectronics. Therefore there is acute necessity for understanding these properties. Meanwhile the theory of these effects is not sufficiently advanced to permit adequate description of the matter.

We develop here the general approach and the thermodynamic theory of interfacial adhesion between materials which may contain various point defects [1]. It allows specifically to describe, to understand, to calculate and/or to estimate interfacial surface tension and interfacial separation work as functions of the point defect concentrations in the materials forming the interface. The proposed approach goes back to the work by B.S. Bockstein, Ch.V. Kopetzki, P.S. Schwindlerman [2]. The authors considered there the boundaries between grains of the same material (grain boundaries) in a polycrystalline structure. They used the Gibbs equation describing the thermodynamics of boundaries and the conception that a grainboundary can be considered as the absorber of the defects containing in grain bulks.

On the basis that the Gibbs equation is true for boundaries of any types, in the present work we have proposed the generalized approach to describe the interfaces between two different materials. We have also developed a reasonably general model in order to describe the kinetics of defect adsorption and desorption by the interface. The theory has been applied to the cases when lattice defects are vacancies, vacancy clusters, and impurity atoms (both substitutional and interstitial ones). For all types of defects we have obtained and analyzed the dependences of the interfacial surface tension and separation work on the defect concentrations.

Specifically, we have shown that the interfacial adhesion characteristics such as surface tension and separation work essentially depend on the parameters h_i, that specify the relative ability of the interface to adsorb defects. In particular, if defects are vacancies or substitutional impurity atoms and $h_i > 1$, i.e. the interface is a good absorber of the defects, the surface tension coefficient can vanish and even become negative at sufficiently low defect concentrations. In the case of interstitial impurity atoms the same behavior is possible if $h_i < 1$. The interfacial separation work can also become equal to zero and even negative as a function of non-equilibrium vacancy or impurity concentrations in the adjoint materials. The latter result means that at certain defect concentrations the interface may fall into to the state, for that spontaneous separation of layers is thermodynamically preferable. This effect could be used in different practical applications.

1. R.V. Goldstein, T.M. Makhviladze, M.E. Sarychev, “Influence of impurities on the interfacial separation work for conjugate materials”, Poverkhnost (Journal of Surface Investigation), №12, 2009 (to be published) (in Russian)
2. B.S. Bockstein, Ch.V. Kopetzki, P.S. Schwindlerman. *Thermodynamics and kinetics of grain boundaries in metals*. Moscow, Metallurgiya: 1986 (in Russian)

The thickness-dependence of the polariton effect in the single quantum well

Yu. V. Moskalev[1], S. B. Moskovski[2]
1. Yaroslavl State Pedagogical University, Yaroslavl, Russia, E-mail address: moscalev@ya.ru
2. Yaroslavl State University, Yaroslavl, Russia, E-mail address: moskov@zavolga.net

The exciton-polariton interaction in the vicinity of isolated absorption line under the finite translation mass of exciton leads to the decreasing of total absorption coefficient under a weak bonding with dissipative subsystem and to violation of Kramers-Kronig dispersion relations in the transmission spectra [1-3] (polariton effects). The theoretical explanation of these nonclassical integral effects for the thin plane crystal layer (single quantum well) is presented in the works [4,5].

In this study, we consider the theoretical model and the results of numerical calculations the polariton effect dependence on the crystal layer thickness in the range 100-2000 nm. The transition to the large thickness quantum well limit leads to the description of the polariton effect in the model of a semi-infinite crystal [6]. These results are generalized to the case of the oblique incidence of light.

In present work the interference of both ordinary and additional exciton-polariton waves is considered in the entire region of their overlapping. As the additional boundary conditions we used the Pekar conditions [7] (the exciton polarization is equal to zero on the crystal surface). This approach is equivalent to the consideration of the interaction between the electromagnetic field and the spatially quantified exciton state in the infinite rectangular quantum well [8] which differ from the model [6] in which the polariton wave with the least amplitude is not taken into account.

The description of the integral polariton effect is based on consideration of the complex transmission coefficient analytical properties, following from the causality principle. Only the transmission zeros caused by the interference of ordinary and additional exciton-polariton waves can be the singularities of the complex logarithm of a transmission coefficient in the upper half-plane of the complex frequency. The transmission coefficient zeros can appear in the case of nonzero absorption at small values of exciton decay constant under a certain critical value. The account of these isolated singularities contribution allow to describe both of the nonclassical integral effects within the general approach.

The exploration of dependence of the transmission zeros coordinates on the complex plane and the magnitude of their polariton effect on the thickness of crystal layer was performed by the numerical methods, using the approximate analytic solutions. Analysis of this dependence has revealed the existence of the minimum limit thickness of the layer below which the polariton effect is impossible. This minimum thickness has proved to be close to the limit of applicability of the three-dimensional model of exciton.

For thick crystal layers the number of transmission zeros is rapidly increasing and the sum of the contributions of discrete zeros can be replaced by integration using a quasi-continuous distribution function. In this case the obtained results coincides with the results of the model [6] both for the integral absorption and the dispersion relations.

The calculations were carried out for parameters of the leading exciton line of CdSe crystal corresponding observation conditions within liquid helium temperature.

1. J. Voigt, Phys. Status Solidi B, 64, pp.549-556, 1974
2. A. Bosacchi, B. Bosacchi, S. Franchi, Phys. Rev. Lett., 36, pp.1086-1089, 1976
3. M.S. Brodin, N.A. Davydova, M.I. Strashnikova, Phys. Stat. Sol. B, 70, pp. 365-371, 1975
4. S.B. Moskovskii, A.B. Novikov, L.E. Solov'ev, Sov. Phys. JETP, 78, pp.533-538, 1994
5. S.B. Arkadova, Yu.V. Moskalev, S.B. Moskovskii, L.E. Solov'ev, Opt. Spectrosc., 96, pp.538-548, 2004
6. N.N. Akhmediev, Sov. Phys. JETP, 52, pp.773-778, 1980
7. S.I. Pekar, Sov. Phys. JETP, 6, pp.785-793, 1958
8. V.A. Kiselev, I.V. Makarenko, B.S. Razbirin, I.N. Uraltsev, Sov. Phys. Solid State, 18, pp.782-786, 1977

$CoSi_2/TiO_2/SiO_2/Si$ gate structure formation

Rogozhin A.E.[1],Khorin A.I.[1,2], Naumov V.V.[1], Orlikovsky A.A.[1],
Ovcharov V.V.[1], Rudakov V.I.[1], Vasiliev A.G.[1,3]

1. *Institute of Physics and Technology, Russian Academy of Sciences, Moscow, Russia, ellipsoid@yandex.ru*
2. *Moscow State Institute of Radio-engineering, Electronics and Automation, Moscow, Russia, horin@ftian.ru*
3. *Federal State Unitary Enterprise "Scientific & Product Enterprise "Pulsar", Moscow , Russia*

Recently investigations of the technologies using self-organization and phase layering occur more and more frequently. Considerable simplifications of processes, self-alignment of elements and reduction of stage quantity are the reason of that. In this work we present results of computer simulation and experimental study of $CoSi_2/TiO_2/SiO_2/Si$ gate structure formation technology which uses solid-phase diffusion and phase-layering. The bilayer of TiO_2 and SiO_2 was chosen as gate dielectric because titanium dioxide is possessed of extremely high dielectric permittivity and silicon dioxide has large band gap and high quality interface with Si. Because of its low resistivity $CoSi_2$ is considered now as one of the most prospective material for metal gate electrodes. The technology which was simulated in this work allows to form such a gate structure during the sole annealing process. To compute the technology parameters the program, which take into account diffusion properties of Co, Ti, Si and O in different materials, Gibbs free energies of cobalt and titanium silicides, oxides and silicon dioxide, was realized. Simulation results show that the technology can be used for gate structure formation.

In the first stage of tech the layer of SiO_2 is formed on the Si substrates. Thermal oxidation was used in this work because it secures the best quality of SiO_2/Si interface. Then the multilayer Ti-Co structure (10 alternate 2 nm-Ti and 2 nm-Co layers) or Ti-Co alloy layer is formed by magnetron sputtering or electron beam evaporation. After that the layer of Si should be formed (~10 nm). During the annealing at 650-900ºC for 2-5 s Ti atoms penetrate into SiO_2 and form TiO_2. Diffusion of Si atoms from SiO_2 and upper Si layer to the Co-Ti layer leads to the formation of cobalt silicide. In this work magnetron sputtering was used for multilayer Ti-Co structure and Si layer formation. The thickness of SiO_2 was approximately 10 nm. TOF SIMS was used to evaluate profile of the structure during the formation process.

Local performances of PZT films with a thickness less than 100 nanometers

V. M Roshchin, M.V. Silibin
Moscow Institute of Electronic Technologies (Technical University), E-mail:rvm@miee.ru

Development and setting of measurement procedures of local electrophysical characteristics of ferroelectric films with a thickness less than 100 nanometers is the actual application task. For comprehensive investigation of such objects creation of test structures that can be not always realised due to small thickness of a ferroelectric film (5-100 nanometers) is required. One of possible variants of research of electrophysical parametres of nanoscale ferroelectric films is application of scanning probe microscope in Kelvin probe mode. On a sample with structure the dielectric wafer (sapphire)/bottom electrode/PZT film the scanning of the given part of the surface of the sample in Kelvin probe mode was performed. It represented two-pass AFM procedure. On the first pass the topography of the sample in a semicontact mode is filmed, on the second pass the probe moves the given distance from the surface, iterating its relief and registering allocation of the surface potentials. In this experiment probe motion speed, the given potential and dwell time on the sample in one point. The given procedure is of practical interest for local testing of nanoscale elements and coatings of ferroelectric materials in mechanotronics and sensor products.

In case of polarisation and repolarisation a surface area of a film with size 8×8 μm^2 was originally selected and its topology was registered. Further under the given program at positive potential on a cantilever tip the surface area of 4×4 μm^2 size was scanned in a contact mode, located in centre of initial scan 8×8 μm^2. Repeated contact scanning at a negative bias on a cantilever tip was made on 2×2 μm^2 area which was located inside 4×4 μm^2 area with the positive polarization. Final scanning of a surface was made in a mode Calvin-modes for registration of polarized fields in a film. Results of final scanning are given where lighter field is gained after polarization at the positive potential on a cantilever tip +10 V, and dark field inside light - at negative potential on a cantilever tip-10 V. In process of polarization on the lower electrode zero potential was given. A cross-section profile of remanent polarization on a line is presented, and - 3D image of a polarized area of a film surface is given. The value of remanent polarization for these areas has amounted to accordingly +200 mV and -500 mV.

Repeated research of a polarized surface in a mode Calvin-modes in 48 hours of endurance on air has not revealed essential changes of polarized areas and the value of remanent polarization.

Results of research of resolving ability of local polarisation are presented at positive potential on a cantilever needle +10 V, and time of polarisation 250-300 msec. In the process of polarisation zero potential was sent on bottom electrode. 3D image of a polarised area of a film surface is given, and the cross-section profile of remanent polarisation on a line is presented. The value of remainder polarisation for the given fields has made accordingly from +60 to +200 mV.

All SPM measurements on local polarisation were carried out on air. At the same time resolving ability of local polarisation greatly depends on presence of sorbate on a surface which can lead to contortion of allocation of an electrostatic field of a microscope probe and, thereby, increment the size of polarised areas. For detailed and more exact research it is necessary to carry out measurements in vacuum.

In this research results on local polarisation and repolarisation with application of AFM are presented and stability of piezoelectric properties of $PbTi_{0,52}Zr_{0,48}O_3$ films is confirmed.

Polysilicon Inductive Elements for IC's

Pashayev A.M.,*Kasimov F.D., Ibragimov R.A.
National Academy of Aviation, Baku, Azerbaijan
e-mail: fredkasimi@mail.ru

Recently disordered structures have received much attention from designers of active devices as they offer an increase in functional possibilities per unit volume of electronic devices without an increase in the packing density of integrated circuits.

In such materials a phase transition takes place under influence of different modes of excitation.

The particular interest is the investigation of such phenomena in polycrystalline silicon (poly-Si) films, because silicon is the basic semiconductor material in microelectronics. Use of the technique of local growth of poly-Si films during the epitaxial formation of monocrystalline silicon [1] makes it possible to form elements with data processing circuits on the same chip. As shown in [2], locally grown poly-Si films exhibit a memory switching effect.

In this paper we report some inductive phenomena which were first observed in switching poly-Si films during capacitance-voltage measurements.

The poly-Si films (200 μm x 20 μm) were formed on locally oxidized silicon-substrates of p-type conductivity with a resistivity of 10 Ω-cm during the process of epitaxial growth of a 5 μm monocrystalline film of n-type conductivity with a dopant concentration (phosphorus) of 10^{16} cm^{-3}

Epitaxial growth was performed in a heated (by high frequency power) vertical-type reactor using the high temperature (l200º C)chloride process.

The capacitance-voltage (C-V) characteristics were measured with an L2-7 impedance bridge at room temperature over the frequency range 0.465-10 MHz using an ac signal of low voltage (25 mV).

Typical C-V characteristics of poly-Si films in the OFF state at different frequencies of the ac signal are presented in Fig. 1. As can be seen, at definite voltage values for both bias polarities the capacitance changes from positive to negative, the phenomenon showing a purely inductive behavior. With increasing frequency of the ac signal the voltage corresponding to this inversion of sign also increased. The capacitance of poly-Si films in the ON state was negative over the full frequency range. The current-voltage (I -V) characteristics of poly-Si films were measured on the wafers by probes. When a microscope lamp with a power of 20 W was switched on, the negative resistance region disappeared from the I-V curve while the rest of the curve was almost unchanged. C-V measurements performed with and without illumination showed that under illumination the capacitance changed from negative to positive values simultaneously with the disappearance of the negative resistance region from the I-V curve.

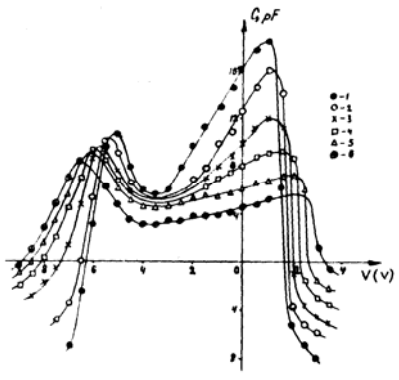

Fig. 1. Capacitance-voltage characteristics of a poly-Si film at various frequentcies: (a) OFF state curve 1- 0.465 MHz; curve 2- 1 MHz; 3- 3MHz; 4-5MHz; 5-7MHz;6-10 MHz.

From the investigations carried out we concluded that a locally grown poly-Si film is a functional element with non-linear C-V-characteristics, having two stable conduction states with voltage- and light-controlled parameters.

1. A.G. Abdullaev, F.D.Kasimov. «The simultaneous growth of mono and poly-crystalline silicon films»,Thin Solid Fi1ms, v.115, №3, pp. 237-243,1984.

2. F.D.Kasimov, A.G. Abdullaev and V.A.Vetkhov. «Memory switching effects in locally grown polysilicon films»,Thin Solid Fi1ms, v.112, №2, pp.121-125,1984.

SiGe and GaN heterostructure microwave devices

A.G. Vasiliev, Y.V. Kolkovsky, S.V. Korneev, A.A. Dorofeev, V.M. Minnebaev
FSUE "Science and Production Enterprise "Pulsar" Moscow, Russia, pulsar@dol.ru

Nowadays and in the nearest future the main requirements to microwave semiconductor electronics are the increase of output power in microwave devices and the enhancement of functional capability providing downsizing and decreasing power consumption.

In this work are discussed a comparative experimental analysis of microwave devices in different semiconductor materials to specify microwave electronic components of transmit/receive modules for active phased array radars.

It was found out, that:

- phase error of SiGe phase shifters is about ≈±3° that is comparable to GaAs phase shifters and even go beyond them in power consumption and scale of integration;
- GaAs low noise amplifier's (LNA) minimal noise figure is 0.4 dB (NF≈0.4 dB), however considering the hardness to microwave power, the most available for active phased array radars is GaN LNA that have NF≈2.0 dB with the destruction input power ≈25 watt;
- SiGe amplifiers have minimal level of low-frequency noise (160 dBV/√Hz at 1 kHz offset), which makes them superior in comparison with other devices while designing the solid-state synthesized signal generator of C-band.
- because of high drain-source voltage (Vds = +45V) of GaN power amplifiers produce 4 times more microwave output power than GaAs power amplifiers.

Obtained results let us make a conclusion, that GaN and SiGe technology is optimal for creating the electronic components of transmit/receive modules for active phased array radars, where analog-digital SiGe MMIC form an intelligent microwave module, IC based on GaN form input and output devices of transmit/receive modules, that provide the level of output power and low-noise receiving of probing signal.

Methods of cache memory optimization for multimedia applications

A. Kravtsov

- *JSC Mikron, Moskow, Zelenograd, Russia, kravtsov@mikron.ru*

1. Introduction

Critical issues in parallel processor systems are communication between processors, communication between processors and memory as well as synchronization. Caches are often implemented between fast on-chip processors and slow off-chip memory.

2. Cache memory

Cache memory is intended to give memory speed approaching that of the fastest memories available, and at the same time provide a large memory size at the price of less expensive types of memories. The architecture of cache subsystems is defined by a number of options and parameters which determine performance, power consumption and area.

2.1 Elements of Cache Design

- Number of cache levels: The most common organization of cache systems is known as a two-level cache, with the internal cache designated as level 1 (L1) and the external cache designated as level 2 (L2).

- Size: Increasing the cache capacity leads to increased power consumption, delay and therefore reduces clock frequency of cache and processor. On the other hand minimization of cache size increases cache misses and the cache performance strongly depends on the number of misses.

- Set-associativity: If some memory block can be situated on limited multitude in cache then it is a set associative cache.

- Write through/ write back: In a write through cache new data is immediately written to the memory. In a write-back cache, the cache line is marked as dirty, which means that it contains data values which are more up-to-date than those in memory.

- Read allocate/ write allocate: In a read-allocate cache, cache lines are only allocated to memory location in cases of read miss. In a write-allocate cache, a write always update data in the cache.

- Replacement strategy: When a new block is brought into the cache, one of the existing blocks must be closing for replacement. The most common policies are the following:

- *LRU* replacement picks the line which was *least recently used*.
- *Random* replacement picks a random line of the set and therefore manages without cache history.
- *FIFO:* It replaces that block in the set that has been in the cache longest.
- *Round-robin replacement:* The cache control logic contains the counter which is used to select the cache line to be re-allocated.

- Prefetching: So called methods of prefetching are used in these cases to optimize the memory sub-system.

- Partitioning: By working with frequently changing data streams such as MPEG video the data cache can "trash" with data reload. In such a case, a mini data cache (or tiny cache) can be used.

- Line location: In case when the same data is used many times (or always) without changing, the cache line with this data may be locked in order to prevent eventually replacements by rarery used data. This line will be inaccessible for rewrite.

- Parallel data processing: Parallel data processing implements the idea of simultaneous actions and has two varieties: pipeline and the parallel in essence. Both varieties are intuitively clear.

- Summarizing the methods of cache memory optimization: Formula for average time of access to memory in cache memory systems is as follows:

Average access time = Reference time at hit + Share of misses x Losses at a miss (1)

This formula shows ways of optimization or cache memory work: reduction of miss share, reduction of losses at a miss, and reduction of reference time to memory at a hit.

1. J. Hennessy, D. A Patterson, "*Computer architecture a quantitative approach"*, Morgan Kaufmann Publishers, INC. 1996

2. J. Smith, "*Cache memories*" ACM Comput. Surveys, vol. 14, Sept. 1982

3. N. P. Jouppi, "*Improving direct-mapped cache performance by the addition of a small fully-associative cache and prefetch buffers*" in Proc. 17th Annu. Int. Sympo. Computer Architecture, May 1990

4. J. W. C. Fu and J. H. Patel, "*Data prefetching in multiprocessor vector cache memories"*, in Proc. 18th Annu. Int. Symp. Computer Architecture, May 1991

Integrated Injection Laser with Amplitude Modulation in Terahertz Band

B. Konoplev[1,2], E. Ryndin[2], M. Denisenko[1]
1. Taganrog Institute of Technology - Southern Federal University, Taganrog, Russia, kbg@tsure.ru.
2. Southern Scientific Center of Russian Academy of Sciences, Rostov-on-Don, Russia, ryn@fep.tsure.ru

Laser diodes are very important elements of optoelectronic circuits [1]. Proposed laser diode contains a functionally integrated amplitude modulator of laser beam intensity. This modulator may be fabricated in a single technological process simultaneously with the structure of integrated laser element.
Development of the wave-function-rearrangement (WFR) quantum devices is an important direction of nanoelectronics [2]. In [3], [4] results of development and modeling of integrated logic elements and high-speed integrated WFR-switchboards based on both electrons and holes wave-function-rearrangement in quantum wells were presented and discussed. Adaptation of the principles of wave-function-rearrangement for decreasing of delay of optoelectronic nanostructures is a main purpose of this investigation.
Functionally integrated amplitude modulator of proposed injection laser includes two partially aligned quantum wells (one in conduction band and one in valence band) and two controlling junctions (Schottky gate and p-n-junction). Fig. 1 illustrates diagrams of amplitude modulator in active region of integrated injection laser. Suppose that injection current density is high enough for laser generation. Under the direct polarity of the controlling voltage maximums of amplitude of wave functions of electrons and holes are spatially superposed (Fig. 1,a) and under the inverse polarity of the controlling voltage maximums of amplitude of wave functions are spatially disposed (Fig. 1,b) which allows modulate the intensity of laser beam under the constant density of injection current.

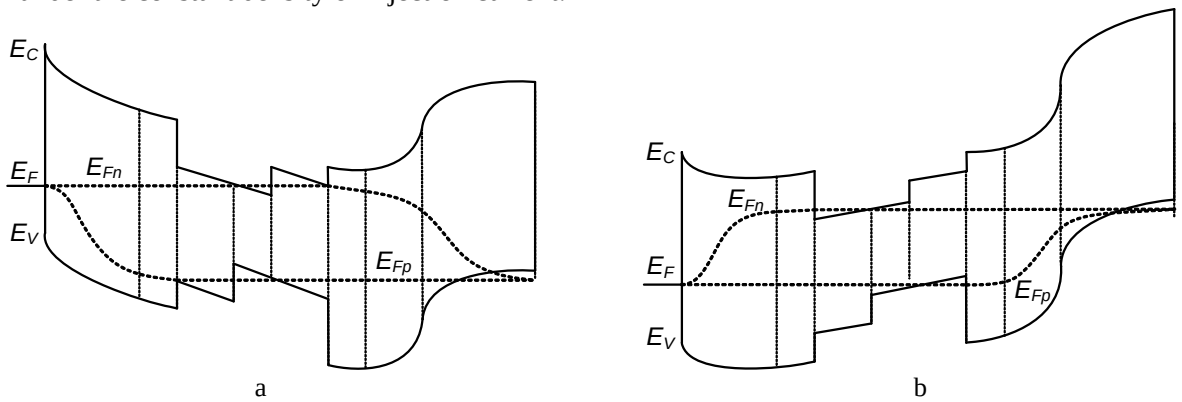

Fig. 1. Diagrams of amplitude modulator in active region of integrated injection laser in high-level generation mode (a) and low-level generation mode (b)

According to the results of analysis speed of switching for this quantum device defined by a time of carriers wave-function-rearrangement. It is not limited by time of accumulation and recombination of carriers in active region of laser. According to the results of numerical modeling time of switching is less than 0,1 ps for 40 – 65 nm quantum wells and frequency of amplitude modulation of laser beam intensity conforms to terahertz band.
The research is executed under financial support of Ministry of education and science of Russia, project No. 2.1.2/3775.

1. G.I.Alferov. “Double Heterostructures: Conception and Using in Physics, Electronics and Technology”, *Uspekhi Fizicheskih Nauk*, Vol. 172, No. 9, 1068 – 1086, 2002.
2. A.A.Gorbatsevich, V.V.Kapaev, Yu.V.Kopaev, V.Ya.Kremlev. “Wave-function-rearrangement Quantum Devices”, *Phys. Low-Dim. Struct.*, No. 4/5, pp. 57 – 62, 1994.
3. B.G.Konoplev, E.A.Ryndin. “A Study of the Transport of Charge Carriers in Coupled Quantum Regions”, *Semiconductors*, Vol. 42, No. 13, pp. 1462–1468, 2008.
4. E.A.Ryndin. “High-Speed Integrated Switchboards on the Basis of Control Rearrangement of Carrier Wave Function Maximum”, *Jornal of Southern Scientific Center of RAS*, Vol. 2, No. 2, pp. 8 – 16, 2006.

Gas medium influence on characteristics stability of electroformed structures Si-SiO_2-W and reliability of switching processes of memory elements on the basis of these structures

V. M. Mordvintsev, S. E. Kudryavtsev, V. L. Levin, L. A. Tsvetkova
Yaroslavl Branch of the Institute of Physics and Technology, Institution of Russian Academy of Sciences, Russia,
E-mail: Mordvintsev-Viktor@yandex.ru

Electroformed open sandwich-structures Si-SiO_2-W are perspective elements for the construction of non-volatile electrically reprogrammable memory [1]. The information in them is coded by means of the self-formed conducting nanostructures generated in an insulating slit at an electroforming. The slit is carried out in the form of a free end-surface of a silicon dioxide film by thickness about 20 nm which should be opened in vacuum, i.e. gas medium with low pressure.

Operation of an electroforming of sandwich-structures represents an exposition at voltage in a range from 3 to 10 V during about several seconds. Thus in the insulating slit there is a formation of conductive phase particles and for the account of their accumulation a conductive medium is created in which then the nanometer insulating gap is self-formed already. The base material for conducting nanostructures are surface layers of the silicon dioxide the destruction of which under the influence of electron flow leads to oxygen removal in a gas phase and to enrichment of the slit surface by silicon atoms which is carrying out a function of a conductive phase particles.

Critical component of gas medium for execution of the electroforming and the subsequent switches of the memory element is oxygen. So for the electroforming process it is necessary, that the residual pressure in the chamber did not exceed 1 Pa, differently the process of the conductive phase particles accumulation does not go because of their intensive oxidation. If the measurement of static current-voltage characteristic (I-V-characteristic) after the electroforming (it has the N-shaped form with a maximum near 4 V) is carried out by applying of the slowly varying (0.5 V/s) voltage in a range from 0 to 10 V and reverse, the amplitude of curves starts to decrease gradually when pressure of air in the chamber exceeds 50 Pa, i.e. the state of conductive medium varies irreversibly for the account of its oxidation by oxygen of a gas phase. At the same time, drift of I-V-characteristics at pressure less than 10 Pa is not appreciable.

Processes of pulse switching of memory elements from high- to a low-conducting state and reverse (i.e. a change of the nanometer insulating gap width is occurring) were investigated by means of two techniques. In the first technique impulses of the triangular form voltage with amplitude 8 V and duration about hundreds microseconds were applied on samples and oscillograms of the switching process were registered. In the second technique rectangular impulses of voltage by amplitude 4 - 6 V with duration 1 - 1000 μs - for "switching-on" (switching from low- to a high-conducting state) and amplitude 6 - 10 V with duration 0.3 - 1 μs - for "switching-off" (switching from high- to a low-conducting state) were used. State reading was carried out by current measurement at voltage 1.5 V with duration of the reading impulse near 1 ms and the quantity of rewriting cycles was counted up. Reading at voltage up to approximately 3 V is nondestructive.

For memory elements placed in high vacuum (pressure near 10^{-2} Pa) containing oil vapour, the quantity of rewriting cycles achieved about 10^4, after that a state with very high conductivity has arisen which cannot be "switched-off" that it is possible to consider as breakdown of the memory element. In case of an inflow of air to pressure near 100 Pa, the quantity of rewriting cycles achieved about 10^6. Experiments at atmospheric pressure quickly led to appearance of a low-conductive state which could not be "switched-on" in the usual way. For this purpose the repeated execution of an electroforming was required. These results show an existence of optimum pressure of oxygen in a gas phase for achievement of maximum reliability of switching of the memory element.

From the analysis of data received in our experiments it follows, that at "switching-on" of the memory element, there is a local removal of oxygen from surface molecules SiO_2 in a gas phase and enrichment of a surface by atoms of silicon, and at "switching-off" - oxidation of atoms of silicon by the oxygen adsorbed from a gas phase. Thus, at the electroforming and switching of the memory element on the basis of structure Si-SiO_2-W we reversibly control an oxygen balance in the surface layer of the insulating slit dielectric, in the adsorbed layer and in gas medium.

1. Mordvintsev V. M., Kudryavtsev S. E., Levin V. L., “High-stable nonvolatile electrically reprogrammable memory on self-formed conducting nanostructures”, Nanotechnologies in Russia, 4, pp. 129-136, 2009.

Low-resistance Ge/Au/Ni/Ti/Au based ohmic contact to *n*-GaAs

E. Erofeev[1], V. Kagadei[2]
1. Scientific Research Institute of Electrical Communication Systems, Tomsk, Russia, erofeev@sibmail.com
2. Research and production company "Micran", Tomsk, Russia, vak@micran.ru

Ohmic contacts to III-IV semiconductors are often limiting factors in the performance of high speed digital and microwave analog nanoscale devices, or devices used for optoelectronic applications [1]. Since new generation GaAs semiconductors nanoscale devices demand better performance and shallow penetration during formation, improved ohmic contacts are very important. The most commonly used contact to *n*-GaAs with reasonable stability, low specific contact resistance, corrosion resistance, and low residual stress is the AuGeNi alloyed system. Limiting characteristics of the AuGeNi ohmic contact in many cases are defined by the metal layers thickness and composition and the processes occurring during thermal annealing, in particular: i) by the formation of intermetallic unstable high-resistance phases on the interface; ii) by the mixing of the metal films and GaAs leading to increasing of the transition layer thickness and compensation of the charge carriers; iii) by the formation of thick melting region [2]. The some disadvantages could be eliminate by the introduction to the multilayer ohmic contact of the diffusion barrier film based on thermally stable refractory metal, for example, Ti.

The work purpose is investigation of the opportunities of the Ge/Au/Ni ohmic contacts improvement by incorporation in multilayer metal film of the Ti diffusion barrier deposited at special conditions.

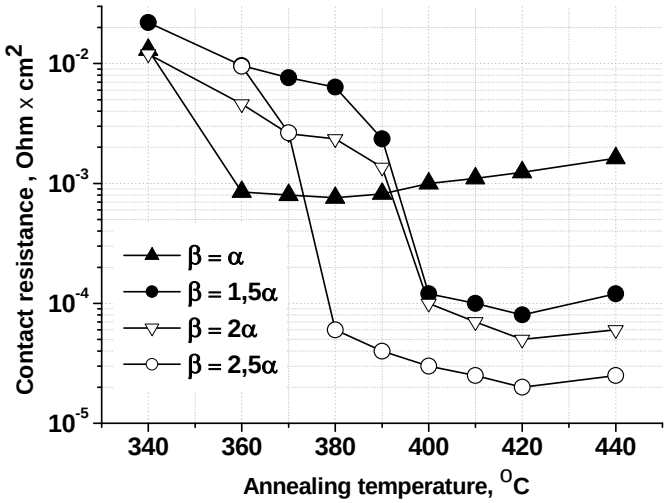

Fig.1. Dependence of the specific contact resistance of Ge/Au/Ni/Ti/Au ohmic contacts versus the annealing temperature for different Ti atoms angles β.

The Si-doped samples *n-i*-GaAs ($n \cong 2\times10^{17}$ cm^{-3}, d = 0.12 μm) were used in experiments. The two-layer resist mask with TLM patterns was formed by standard photolithographic techniques. For the GaAs native oxides removal the samples were processed in H_2SO_4 (1:10) water solution within 3 min. Metal films Ge/Au with eutectic ratio (Au at. 88% / Ge at 12%) and Ni film were deposited by the electron beam or the thermal evaporation methods in a vacuum with a base pressure 10^{-6}–10^{-7} torr. Thickness of Ge/Au layers varied in a range from 50 up to 300 nm and Ni layer varied in a range from 10 up to 100 nm. During evaporation of Ge, Au, Ni the atoms were deposited to the GaAs substrate with angles α_1, α_2, и α_3 in the range $\alpha_{1\text{-}3}$ = 0–2° relatively to the normal to the wafer surface. Then Ti film of the diffusion barrier was deposited to substrate with atoms angle $\beta = n \times \alpha$ (n = 2–10). After that top Au layer (20-1000 nm) was deposited with atoms angle $\alpha_5 = \alpha$. The control of the atom angles was realized by changing of the evaporation area (e-beam power or liner area in the cause of e-beam and thermal evaporation methods, respectively). The control of the deposition rate and layers thickness was carried out *in situ* by the quartz monitor. The topology of the contact pads was formed by the lift-off process. Samples were annealed in inert gas environment by the rapid thermal annealing (T = 320–460 °C, t = 30-300 s). Specific contact resistance ρ was measured by the TLM method.

That have been shown, that incorporation of the Ti diffusion barrier film in multilayer metal film of the ohmic contact with optimized deposition atom angle β allows to reduce the minimal value of the specific contact resistance by factor 8–30 (fig.1), and also to achieve the smoother morphology of the contact pads surface. The mechanism responsible for discovered phenomenon has been discussed.

1. M. Shur. *GaAs Devices and Circuits*. Plenum, New York, 1987
2. Blank T. V., Goldberg Y. A., "The current flow mechanism in metal-semiconductor ohmic contacts", Semiconductors physics and technique, **41**, 11, pp. 1281 – 1308, 2007

Manipulating superconductivity with magnetism: from unconventional physical effects to cryogenic spintronics

L.R. Tagirov
Solid State Physics Department, Kazan State University, 420008 Kazan, Russia, E-mail: ltagirov@mail.ru

A Fulde-Ferrell and Larkin-Ovchinnikov (FFLO) like state [1, 2], in which a superconducting pairing function is spatially oscillating, can be induced in a superconducting layer being in a proximity contact with a ferromagnetic metal (see recent review [3] and references therein). If two ferromagnetic (F) layers sandwich the superconducting (S) layer, the supercurrent in the middle layer can be controlled by a mutual alignment of magnetizations in the ferromagnetic layers [4,5]. The magnetic field to control superconductivity is the coercive field of a soft magnetic layer of the two. It can be small as a few oersted for a magnetically soft material like permalloy. The resulting spin-valve has 100% efficiency (infinite magnetoresistance) if the re-entrant behavior of superconducting T_C as a function of F-layer thickness is realized in an S/F bilayer, a building block of the superconducting spin-valve. The core structure described above is not a sole design of a superconducting switching structure manipulated by magnetism. The role of the triplet component of the superconducting wave function in the switching characteristics of the superconducting spin-valves is discussed.

In cooperation of the groups from Kishinev, Chernogolovka, Moscow and Augsburg we have made a certain progress towards realization of the superconducting spin-valve. With careful adjustment of the layer thickness as well as improved technique for deposition of thin, 5-10 nm in thickness, qualitative niobium films we succeeded in observation of very deep oscillations of T_C and pronounced re-entrant behavior of superconductivity as a function of the ferromagnetic layer thickness d_F [6]. The $Cu_{1-x}Ni_x$ alloy with x=0.59 has been used as a material to deposit the ferromagnetic layer. The wedge-layer design of the ferromagnetic layer allowed us to prepare a set of 36 stripes with variable d_F in a single run. The layers thickness, as well as their composition, has been intensively controlled with Rutherford backscattering measurements. The superconducting transitions have been measured by observing the resistance drop at temperatures down to 40 mK. In the sample with d_{Nb}=7.3 nm ten of the measured d_F thickness points fall into the re-entrance region where the superconducting T_C has been experimentally established as a zero value below the 40 mK threshold [5]. For the sample with the Nb layer thickness of d_{Nb}=6.2 nm the second region of suppressed T_C appears after the superconductivity revival in the certain range of the smaller ferromagnetic alloy thickness [7,8]. The S/F proximity-effect theory satisfactorily describes the spectacular re-entrant superconductivity observed in our experiments. Having obtained the physical parameters from fitting the experiment we calculated the temperature range for switching and the thicknesses of the functional layers to maximize the effect. Implications of the experiments to the superconducting spintronics are discussed.

A cooperation with V.I. Zdravkov, A.S. Sidorenko, R. Morari, J. Kehrle, G. Obermeier, S. Gsell, M. Schreck, C. Müller, H.-A. Krug von Nidda, J. Lindner, J. Moosburger-Will, R. Tidecks, S. Horn, E. Nold, I.A. Garifullin, V.V. Ryazanov, M.Yu. Kupriyanov, Ya.V. Fominov, B.P. Vodopyanov and R.G. Deminov is gratefully acknowledged. The work is supported by RFBR grants Nos 07-02-00963-a, 08-02-90105-Mol_a, and 09-02-12260-ofi_m.

1. P. Fulde and R. Ferrell, Phys. Rev. **135**, p. A550, 1964.
2. A. I. Larkin and Yu. N. Ovchinnikov, Sov. Phys. JETP **20**, p. 762, 1965.
3. A. I. Buzdin, Rev. Mod. Phys. **77**, p. 935, 2005.
4. L. R. Tagirov, Phys. Rev. Lett. **83**, p. 2058, 1999.
5. A. I. Buzdin, A. V. Vedyayev, and N. V. Ryzhanova, Europhys. Lett. **48**, p. 686, 1999.
6. V.I. Zdravkov, A.S. Sidorenko, G. Obermeier, *et al.*, Phys. Rev. Lett. **97**, p. 057004, 2006.
7. A.S. Sidorenko, V.I. Zdravkov, J. Kehrle, *et al.*, Pis'ma v ZhETF **90**, p. 149, 2009.
8. V.I. Zdravkov, J. Kehrle, G. Obermeier, *et al.*, Phys. Rev. B (accepted).

Magnetic field-tuned superconductor-insulator transition in PbTe/PbS heterostructures with superconducting interface

O. Yuzephovich[1,2], S. Bengus[1,2], M. Mikhailov[1], A. Sipatov[3], E. Buchstab[4], N. Fogel[4]

1. Institute for Low Temperature Physics and Engineering, 61103 Kharkov, Ukraine, yuzephovich@ilt.kharkov.ua
2. International Laboratory of High Magnetic Fields and Low Temperatures, 53-421 Wroclaw, Poland
3. National Technical University "Kharkov Polytechnical Institute" Kharkov 61002, Ukraine
4. Solid State Institute, Technion, 32100 Haifa, Israel

Here we report on observation of the magnetic field-tuned superconductor-insulator transition (SIT) found in a new type of superconductors. Recently a new kind of intrinsically 2D superconductors arising on the interface of epitaxially grown semiconducting $A^{IV}B^{VI}$ heterostructures has been discovered [1]. Superconductivity is inherent only to the layered systems, while individual films constituting them are not superconducting. The metallic-type conducting (and correspondingly, superconducting) layers are adjacent to the interfaces.

We present results of experimental studies of the SIT transition in two-layer PbTe/PbS heterostructures in magnetic fields *H* up to 14T. For these samples all typical features of the SIT have been observed: the fan-like set of *R(T)* dependences (see fig. 1, sample A), the crossing of *R(H)* curves in a single point obtained at different *T* for both perpendicular and parallel to the interface magnetic fields (see Fig.2, sample B, in parallel magnetic field) and the negative magnetoresistance. The resistance increase is usually in a limit of about 10% in a magnetic field 14T at temperatures about 1.7K.

As was shown earlier [2], in a case of heterostructures studied we deal with dislocation-induced superconductivity. Due to such origin, the superconducting layers have periodical nano-net structure.

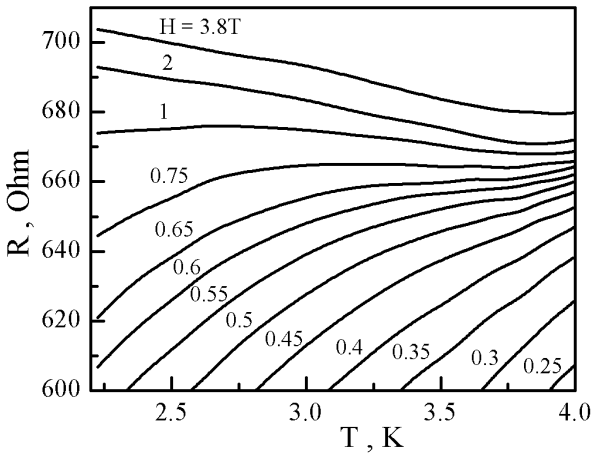

Fig.1.

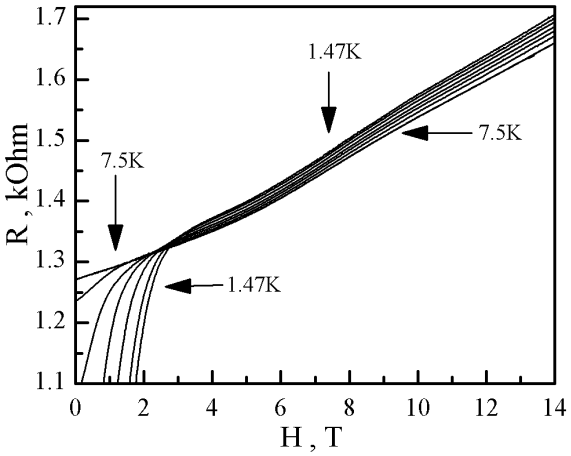

Fig.2.

We found that the presence of defects in superconducting interfacial nano-nets, which are due to the defects in dislocation grids, essentially influences features of SIT in these systems. As follows from the TEM study [1, 3], such defects are always present in the samples with thin semiconducting layers (at the layer thickness *d* less than 80nm). For heterostructures with more perfect nano-nets (values of $d > 100$nm), SIT is not observed. The nature of the SIT in studied systems is most probably associated with percolation phenomenon, but its detailed interpretation requires additional experiments at the lower temperatures. This work was supported by the grant for young scientists of NAS of Ukraine "Magnetic field induced phase transitions in magnetic and nonmagnetic nanostructures" (N15-2009).

1. N.Ya. Fogel et al., Phys. Rev. **B 73**, RC161306 (2006)
2. N.Ya. Fogel et al., Phys. Rev. Lett. **86**, 512 (2001)
3. O.I. Yuzephovich et al., Low Temp. Phys. **34,** 985 (2008)

Could equilibrium noise be detected with help of series-connected asymmetric superconducting rings?

V.L. Gurtovoi, A.I. Ilin, A.V. Nikulov, and V.A. Tulin
Institute of Microelectronics Technology, Russian Academy of Sciences, 142432 Chernogolovka, Moscow District, Russia. E-mail: nikulov@ipmt-hpm.ac.ru

It was discovered [1,2] that asymmetric Al ring can rectify an electric noise in a critical temperature region $T \approx T_c$ of superconducting transition $T_c \approx 1.3$ K. Sign and value of the rectified voltage V_p change periodically $V_p(BS/\Phi_0)$ with magnetic field B with period $B_0 = \Phi_0/S$ corresponding to flux quantum $\Phi_0 = \pi\hbar/e$ inside the ring area [2] like sign and value of the persistent current $I_p(BS/\Phi_0)$ circulating in the superconductor ring [3]. Therefore it is obvious that this rectification effect is a consequence of this equilibrium quantum phenomenon. The Little-Parks experiment [4] and the magnetization measurements [5] give experimental evidence of the persistent current $I_p \neq 0$ observed in the critical temperature region $T \approx T_c$, where the resistance is not zero $R > 0$. The observations of both the dc voltage $V_p(BS/\Phi_0)$ on a ring segment [1,2] and the persistent current $I_p(BS/\Phi_0)$ [4,5] circulating along the ring at $R > 0$ mean that a ring segment is a power $W_p = \langle V_p I_p \rangle = V_p^2/R$ source of direct current [2]. This power results from a power $W_{noise} = \langle RI_{noise}^2 \rangle$ of a chaotic ac currents or noise which switches ring segments between superconducting and normal states [6,7]. The power of series-connected N dc power sources $W_{p,N} = (NV_{p,1})^2/NR_1 = NV_{p,1}^2/R_1 = NW_{p,1}$ increases with their number N in contrast to the chaotic power W_{noise}. Therefore a weak noise with an amplitude $\langle I_{noise}^2 \rangle^{1/2} \approx \Delta V_{err}/NR_{n1}Eff_{Re}$ decreasing with the N increase can be detected with help of the rectification effect discovered in [1,2] at a finite value of an voltage measurement error ΔV_{err} and non-zero value of rectification efficiency $Eff_{Re} = (W_{p,max}/W_{noise})^{1/2} = V_{A,max}/R_{n,1}\langle I_{noise}^2 \rangle^{1/2}$. In order to confirm that the maximum amplitude $V_{A,max}$ of the $V_p(BS/\Phi_0)$ oscillations induced by an ac current with a weak amplitude $\langle I_{noise}^2 \rangle^{1/2} < 1$ μA can indeed increase with the number N of series-connected asymmetric superconducting rings we have measured the rectified voltage oscillations $V_p(BS/\Phi_0)$ observed on systems of N = 20, N = 110 and N = 1080 series-connected asymmetric Al rings with radius $r \approx 2$ μm and $r \approx 1$ μm and half-ring width $w_w \approx 0.4$ μm, $w_n \approx 0.2 \div 0.3$ μm. Our measurements have confirmed that the amplitude $V_{A,max}$ increases approximately proportional N and the amplitude $\langle I_{noise}^2 \rangle^{1/2}$ of the detectable noise current, determining with the relation $V_{A,max} > \Delta V_{err}$, decreases with N increase. A weak noise with the amplitude $\langle I_{noise}^2 \rangle^{1/2} \approx 20$ nA was detected with help of the 1080 ring system at $V_{A,max} \approx 100$ nV, $\Delta V_{err} \approx 20$ nV, $R_{n1} \approx 7$ Ω and $Eff_{Re} \approx 0.001$. These results will be considered in the present work from the point of view subsequent improvement of the noise detection and a possibility of an equilibrium noise detection, assumed by some theoretical results [6-8].

1. S.V. Dubonos, V.I. Kuznetsov, A.V. Nikulov, and V. A. Tulin, “Observation of a dc voltage on segments of inhomogeneous superconducting ring oscillated in a function of the magnetic field”, in *Abstracts of All-Russian Scientific and Technical Conference on Microelectronics and Nanoelectronics*, Vol. 2, P2-25, “Lipki”, Zvenigorod, 2001.
2. S.V.Dubonos, V.I.Kuznetsov, and A.V.Nikulov, "Segment of an Inhomogeneous Mesoscopic Loop as a DC Power Source", in *Proceedings of 10th International Symposium "NANOSTRUCTURES: Physics and Technology"*, p. 350-353, St Petersburg: Ioffe Institute, 2002
3. M.Tinkham, *Introduction to Superconductivity*. McGraw-Hill Book Company, 1975.
4. W. A. Little and R. D. Parks, “Observation of Quantum Periodicity in the Transition Temperature of a Superconducting Cylinder”, Phys. Rev. Lett., 9, pp. 9–12, 1962.
5. N.C. Koshnick, H. Bluhm, M.E. Huber, K.A. Moler, “Fluctuation Superconductivity in Mesoscopic Aluminum Rings”, Science 318, pp. 1440 – 1443, 2007.
6. A.V. Nikulov and I.N.Zhilyaev, “The Little-Parks Effect in an Inhomogeneous Superconducting Ring”, J. Low Temp.Phys. 112, pp.227-236, (1998)
7. A. V. Nikulov, “Quantum Force in Superconductor”, Phys.Rev. B 64, 012505 (2001).
8. J. Berger, “The Chernogolovka experiment“, Physica E 29, pp. 100-103 (2005)

Superconductivity of polymers with charge injection doping

A. N. Ionov [1] and R. Rentzsch [2]

1. *A.F. Ioffe Physico-Technical Institute, 194021 St. Petersburg, Russia, ionov@tuch.ioffe.ru.*
2. *Institut für Experimentalphysik, Freie Universität Berlin, 14195 Berlin, Germany, rolf.rentzsch@fu-berlin.de*

It is well known that conductive polymer demand is growing annually in the industry of many countries. The importance of conductive polymers is based on such properties as their high conductivity, near to metallic conductivity at room temperature, plasticity, light weight, low energy expense for their production, simple processing technology, and low cost. Overall advances will result from more intensive use of conductive polymers in electronics, cars, ships and the aero-spatial industry. At the moment, the main technological process by to which conjugated polymers acquire high conductivity is chemical and/or electrochemical doping. The induced electrical conductivity is permanent, until the carriers are chemically compensated or until the carriers are purposely removed by ‘‘undoping ’’ [1]. At first sight, there is every reason to be optimistic that have metallic conductivity; (ii) Upon doping, the bond lengths change so that charge is stored in solitons, polarons, and bipolarons. Thus the electron-phonon interaction that is responsible for superconductivity in conventional metals leads to important effects in metallic polymers. In this context, doubly charged bipolarons can be thought of as analogous to real-space Cooper pairs [1,2]. However, superconductivity has not yet been observed in doped conjugated polymers. The reason for this may be connected with the strong disorder of the polymer macromolecules due to chemical self-doping and/or electrochemical doping. High doping levels play a destructive role by spatial segregation of polymer chains. As a result, the metallic islands can be surrounded by a dielectric matrix. However there is an additional possibility of doping which is connected with charge injection from metallic electrodes into the polymer. In the case of an ideal polymer structure, electrons reside in the π^* band and/or holes reside in the π band only, as long as a biasing voltage is applied. Here, we focus on charge injection into polymers due to the electrification process, which leads to metallic conductivity in a weak external electrical field. The advantage of charge-injection doping is that the polymer acquires a much higher conductivity then with chemical and/or electrochemical doping. Moreover, a super-conducting current flows through polymers with thicknesses up to some tens of microns in Superconductor–Polymer–Superconductor structures [3]. There are three principal alternatives for explanation of the supercurrent: (i) proximity effect; (ii) ballistic transport; (iii) intrinsic superconductivity. We describe experiments which eliminate the proximity effect and ballistic transport mechanisms. It is intrinsic superconductivity that must be the main source of supercurrents. We also discuss the technology of preparation for polymers which would have superconducting properties and some related phenomena for practical applications.

1. Alan J. Heeger. *Rev. Mod. Phys*., vol. 73, No.3, 2001.
2. D.M.Eagles. *Phil. Mag.* Vol. 85, 1931, 2005.
3. V.M.Arkhangorodskii, A.N.Ionov, V.M.Tuchkevich, I.S.Shlimak, *Pis’ma Zh. Eksp. Teor. Fiz.* 51, 56, 1990; *JETP Lett.*, 51, 67 1990.

CMOS color image sensors. Current state and aspects

V.A. Gergel[1], I.V. Vanyushin[2]

1. Institute of Radio Engineering and Electronics, Russian Academy of Sciences, Moscow, Russia.
2. LCC "SensorIC", Moscow, Russia, E-mail address: vgergel@mail.ru

As it is widely known, in the first multi-element photosensitive devices designed for image capturing the main principals of charge-coupled devices (CCD) charge transfer were used. Corresponding structures were organized as an assembly of some number of CCD raws, and this solution inherited all advantages and disadvantages of CCD technology. It is clear that the main difficulty, which restrains a mass production and a commercial application of CCD image sensors, is arrived from the necessity to provide high-efficient charge transfer to the reading analog amplification circuits.

Some time later an alternative "matrix"-structure solution with a possibility of signal readout from large photosensitive arrays was introduced, which is closer to semiconductor random access memory (RAM) functionality. The unity cell of CMOS image sensor works as an active CMOS photo-element (pixel), which consists of not only a photodiode, but three or four transistors for preset and signal reading. A generalized scheme of such active CMOS pixel has a photodiode, which is connected through the charge transferring channel of the first transistor to a floating-gate storage. This floating-gate storage, in turn, consists of an active transistor's gate and source-drain n+ area between signal transferring and preset transistors.

Nevertheless, contrary to RAM, analog (not digital) signals are being read, that's why some certain schematic difficulties arise, because an acceptable time-delay level of transfer characteristics should be achieved in order to minimize a distortion of light-to-signal (optoelectronic) conversion function.

In the most of well known CMOS color image sensors a "color" is being detected with the aid of external band color filters, whose selectiveness is defined by appropriate spectral transmittances; corresponding mosaic of polymeric filters (for example, Bayer Color Filter Array - BCFA) is placed over a matrix of non-selective photodiodes. Such "hybrid" solutions presume a specific image processing with an interpolation of absent color components in the current pixel position with the use of color information from the nearest pixels. It is clear that, along with high expenses for necessary interpolation processing, such structures are not free of perceptible distortions (artifacts), which take place on color boundaries in the captured image.

More perspective way for image sensors' improvements is to provide full color detection inside each pixel structure. As it is well known, the light absorption (and electron-hole pairs' photogeneration) depth in a semiconductor wafer depends on the wavelength of the incident light. Thus, if the photogenerated charge flows are being separated according to their depths in the wafer, a single pixel structure with three color components can be created. Contrary to BCFA, such image sensor is free of interpolation problems, it has better color resolution, utilize full light flux and has no temperature limitations of polymeric color filers. Besides, the very important advantage of this kind of pixel structure is a possibility to get "black-and-white" image by summarizing all color components in a single pixel. In this case 100% of luminous flux is used, so higher sensitivity and better spatial resolution can be achieved.

Lately color CMOS image sensors are being used in a growing number of mobile applications, that's why image sensors with color detection in a single pixel without polymeric color filters can conquer this field of market due to their lower cost, better sensitivity and resolution, lower power consumption and comparable simplicity of integration with digital processing circuits in a single chip.

1. S.Mendis, S. Kemeny, E. Fossum "CMOS active pixel image sensor", IEEE Trans. Electron Devices, vol. 41, pp.452-453, 1994

Monolithic photodetector 32×32

A.V. Sorochkin, M.V. Yakushev, S.A. Dvoretsky, A.I. Kozlov, I.V. Sabinina, Y.G. Sidorov, B.I. Fomin, A.L. Aseev

Institute of Semiconductor Physics, Russian Academy of Sciences, Novosibirsk, Russia, alexandersm@mail.ru

The current baseline for infrared focal plane arrays (IRFPAs) is a hybrid technology wherein the HgCdTe (MCT) detector array and the Si readout integrated circuit (ROIC) chips are fabricated separately and connected element by element with indium. The number of pixels, as well as mechanical and thermal capability, is limited. A technology for which HgCdTe detector arrays are monolithically integrated with Si ROICs would obviate these deficiencies.

We have investigated issues concerning the development of the monolithic technology based on HgCdTe photosensitive elements grown on Si multiplexer.

We have analyzed processes of growth of CdTe and HgCdTe on Si(310) with SiO_2 layer in which growth windows were opened. The windows represent squares with the side from 30 μm to 100 μm. The influence of preepitaxial annealing on the parameters of CMOS transistors of 128×128 MX-4 multiplexer have been investigated. It was demonstrated that p- and n-channel transistors save their characteristics during annealing till 580^0C and 520^0C respectively. The decreasing of preepitaxial annealing temperature from 600^0C to 450^0C – 500^0C have no influence on the structural quality of MCT layers.

"MCT-32" crystal has been developed. It consists of 32×32 photosensitive cells. Each cell includes MCT photodiode and n-MOS transistor. The size of the single cell is 100×100 μm^2. Multiplexer contains test electronic components for the process checking being able. The size of the crystal is 7.1×7.8 mm^2. The crystal is assembled by the n-MOS technology with polysilicon gates and metal interconnections on Si(310) substrate.

The developed multiplexers provide free access to the elements of photodetector array, high uniformity of photodiode bias and opportunity to operate with the dark and background high-degree currents. The selected photodiode connects to readout common bus. Photodiode bias is specified by external precision low-noise read-out circuit which averages and transforms photocurrent into output voltage. Multiplexer provides a read-out in the range of frequencies from 4 to 40 frames per second.

"MCT-32" multiplexer has been fabricated, and its characteristics have been measured. The technology of preepitaxial preparation which does not destroy multiplexer elements has been developed. MCT layers have been grown on a substrate with the multiplexer. The operations for the development of the monolithic infrared photodetector based on "MCT-32" multiplexer have been performed. These operations are listed further: 1) Annealing in inert atmosphere for obtaining the p-type conductivity; 2) Obtaining n-p junctions in the process of ion implantation of boron; 3) Selective etching of polycrystal; 4) Deposition of protective dielectric; 5) Formation interconnections between MCT photodiodes and multiplexer elements.

Measuring results of electrooptical parameters of monolithic photodetector are presented.

Improvement of Radiation Resistance of Multijunction Solar Cells by Application of Bragg Reflectors

V. Emelyanov, N. Kaluzhniy, S. Mintairov, M. Shvarts, V. Lantratov
Ioffe Physico-Technical Institute of RAS, St.-Petersburg, Russia, E-mail: resso2003@bk.ru

Nowadays, solar cells (SCs) are the main power sources for spacecrafts operating on the near-earth orbits. For a long time, the bulk of space power installations were solar arrays based on single-junction silicon and gallium arsenide SCs. For GaAs SCs, the sunlight (AM0) conversion efficiencies of 22% (1x) and 24% (100x) have been achieved. In recent years, the single-junction GaAs SCs started to be actively supplied by the multijunction ones based on GaInP/Ga(In)As/Ge monolithic structures fabricated by the MOCVD technique. The highest obtained conversion efficiency of such space cells is 31% (AM0, 1 sun) [1].

Besides conversion efficiency, another important space SC operation parameter is the resistance to the action of high-energy particles of the near-earth space. A way to increase the radiation resistance of the single-junction SCs by integrating the Bragg reflector (BR) multilayer structures into them has been considered in [2]. A similar approach can be applied for rising the radiation resistance of the multijunction GaInP/Ga(In)As/Ge SCs, the rate of the radiation degradation in which is determined by the Ga(In)As subcell. This is expressed in an essential drop of its photocurrent at radiation.

In the present work, feasibilities to increase the radiation resistance of multijunction SCs with using BRs have been shown, and also the SC structure optimum parameters and the optical reflector design have been chosen.

Spectral characteristics and photocurrent values of single- and multi-junction SCs with and without BRs at different Ga(In)As subcell thicknesses have been calculated. For these simulations the method presented in [3] has been used. Calculation of the light wave propagation in a SC multilayer structure was performed by means of the Abeles matrix method. The efficiency of collecting photogenerated charge carriers was determined by approximate analytical solving the basic equations of the photovoltaic effect with use of the small parameter method. The dependencies of the SC photocurrent on the minority charge carrier diffusion length in the Ga(In)As subcell base at different subcell thicknesses have been investigated for structures both with and without BRs. A good fit of the calculated dependencies to the experimental ones have been obtained.

As a result of simulation, a design of a multijunction SC with a BR has been found, which allows ensuring in the Ga(In)As subcell base an effective collection of minority charge carriers at the decrease of their diffusion length more than in two times. As consequence, the Ga(In)As subcell photocurrent degradation rate has been reduced essentially at radiation, and a way to increase the radiation resistance of multijunction GaInP/Ga(In)As/Ge SCs has been demonstrated.

1. M. Meusel, C. Baur, W. Guter et al. “Development status of European multi-junction space solar cells with high radiation hardness”, *Proc. of the 20th EPSEC*, pp. 20-25, Barcelona, 2005.
2. M.Z. Shvarts, O.I. Chosta, I.V. Kochnev, V.M. Lantratov, V.M. Andreev “Radiation resistant AlGaAs/GaAs concentrator solar cells with internal Bragg reflector”, Solar Energy Materials and Solar Cells, **68**, pp.105-122, 2001.
3. V.M.Andreev, V.M. Emelyanov, N.A. Kalyuzhnyy, V.M. Lantratov, S.A. Mintairov, M.Z. Shvarts, N.K. Timoshina “Rated Exterbal Quantum Efficiency of III-V Multijunction Solar Cells”, *Proc. of the 23rd EPSEC*, pp. 375-381, Valencia, 2008.

Polycrystalline Silicon Short Wave Photodetectors

Kasimov F.D., Javadov N.G.
National Academy of Aviation, Baku, Azerbaijan
e-mail: fredkasimi@mail.ru

During recent years an increasing interest is being towards high-speed short wave photo detectors. It is known that sensitivity in this region of spectrum is obtained by the use of extremely shallow p-n junction the formation of which presents some difficulties from the technological point view. For this reason the lightly doped poly-Si films are of interest due to the presence of deep traps at the grain boundaries which conditioned the formation of space charge regions the r-parameters of which can be controlled at a given concentration by changing the grain size [1]. Taking into account the grain
(size and the doping concentration level ratio in polycrystalline semiconductors the following cases can be realized [2].The grain conductivity type corresponds to that of impurity (high concentration, large grain size), either the depleted Shottky layers or the regions with the opposite conductivity types are formed at the grain boundaries (average concentration and grain size). At last, at a low impurity level and a small grain size the space charge region can spread over the whole grain and condition is realized through intergrain spaces. The lightly doped space charge regions with small grain sizes can act as shallow p-n junctions at the grain boundaries of poly-Si films enabling their use as photodetectors and thus omitting the diffusion and ion doping steps.

The films with average grain sizes of 0.5 and 5 μm and linear sizes 200x20, 400x40 and 600x60μm^2 were investigated. The measurements of poly-Si films under influence of illuminated showed that for both fine and large grain sized films the open circuit voltage U(l) was in proportion with film length. The short circuit current didn't depend on the film length and was defined by its width and the grain size within the film.

The electrically formed poly-Si was measured in a light irradiation pulse mode. The light pulses were supplied by the light-emitted diode (LED) AL106 with the wavelength radiation and power being 0.9uro and 2 mW, respectively. The LED was fed by the generator G5-54. The reading from the oscilloscope Cl-65 showed the value of the output pulse height from the poly-Si film being 150mV. The form of the output pulses from the poly-Si film was similar to that of the rectangular pulses supplied by the generator to LED up to maximum frequency being in the order of 90kHz.

The absolute sensitivity spectral dependencies for the fine (curve 1) and large (curve2) grain sized electrically formed poly-Si films are presented on Fig. As could be seen from the figure with the increase of grain size the pick of sensitivity is biased towards the longer waves. For the fine grain sized films the absolute sensitivity is 3,2mA/W at the wavelength being 0,5μm and its maximum rating of 10 mA/W is observed at λ=0,7μm.

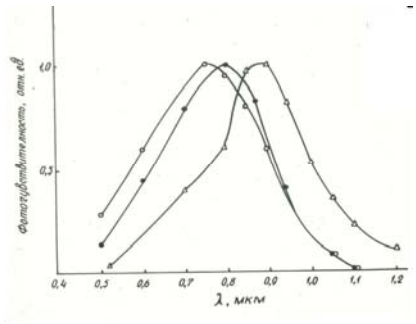

Spectral dependence absolute sensitivity electrical formed Poly-Si films. Curve o-fine grain sized; curve •-large grain sized; Δ-mono-Si.

For the large grain sized films at 0.5um the sensitivity is 12mA/W and its maximum rating of 11mA/W is reached at the wavelength being 0.84μm . The integral sensitivity of poly-Si films was measured in a photo-resistive mode and for the fine grain sized film increases from 15 to300 nA/lx.

1. A.G.Abdullayev and F.D.Kasimov. «The simultaneous growth of mono and polycrystalline silicon films», Thin Solid Films, v.115, №3, pp. 237-243,1984.
2. F.D. Kasimov, E.V.Kuchis and Kh.A. Asadov. «The switching mechanism in polycrystalline silicon films», Litovskii Fizicheskii Sbornik. v.30, №1, pp.67-70, 1990.

Carbon nanostructures as a new material for emission electronics

Yu.V. Gulyaev

Institute of Radio Engineering and Electronics,Russian academy of sciences, Moscow, Russia

Evolution of Ion Implantation Technology Towards sub-45 nm Device Fabrication

S. I. Kondratenko, R. N. Reece, M. S. Ameen, M. A. Harris, and L. M. Rubin
Axcelis Technologies, 108 Cherry Hill Drive, Beverly, MA 01915 USA
Email: serguei.kondratenko@axcelis.com

The scaling of CMOS transistor technology from the 110-130 nm nodes to the 45 nm node and beyond has created challenges for the process and equipment aspects of ion implantation technology. For high current and high-energy implanters, major transitions were made from multi-wafer to single wafer systems around the 65nm (high current) and 32nm (high-energy) nodes, respectively. This was driven by several process control requirements. The single wafer architecture allows better process control in angle for high current implantation, but revealed a significant difference in damage layer formation affecting junction properties and device parameters. Process and equipment optimization of the multi-wafer implanter architecture has proven them capable down to at least the 65 nm node. The remaining challenges for high current implantation include low energy ion beam transport in both drift and deceleration modes, and the implantation of molecular ions. For the high-energy and medium current systems, requirements for precise angle and energy accuracy and control have increased. Recently the widespread manufacturing of CMOS image sensors and CCD devices have significantly tightened requirements for metallic contamination control on all implanter designs.

In addition to the equipment challenges, advanced transistors require ultra shallow junctions (USJ) with low parasitic resistance and low leakage. Dynamic damage accumulation and amorphous layer formation during implantation plays a fundamental role in the device fabrication process affecting the annealing requirements, dose retention, dopant activation, defect morphology, and ultimately device performance. We report an investigation of various process parameters on the damage induced during amorphizing implants for 65nm and sub-45nm devices. We define an "effective" dose rate on the wafer as a combination of beam current, beam density, and implanter duty cycle, and show that these implanter architecture-specific parameters significantly affect the damage profile from the ion beam. It is well known that wafer temperature plays a critical role in damage annihilation during implant. We demonstrate that the use of both cooled and heated implants implemented in a simple fashion can be used to control the thickness of the amorphous layer and extended defect formation during subsequent annealing. The damage rate and the resulting thickness of the amorphous layer can be influenced through control of these variables. This affects the amount of residual damage in the substrate after implantation and can be used to fine tune device characteristics such as Vt, overlay capacitance, active Rs, and effective channel length. For example, implanting below 0^{o}C increases the thickness of the amorphous layer by 10-30 Å and reduces the concentration of residual damage by over an order of magnitude.

The shallower the implanted layer, the more the structural and chemical properties at the surface affect the junction formation and device behavior. Controlling surface oxidation and residual contamination from ion beam sputtering and the byproducts of photoresist outgassing during ion implantation is important to achieve characteristics such as dopant retention, dopant activation, silicide contact resistance and leakage current. Additionally, control of the substrate loss during photoresist ashing is important to for similar reasons.

There are several applications under investigation for junction formation in sub-45 nm devices using molecular implantation. Molecular ions such as $B_{18}H_{22,}$ or $C_{16}H_{10}$ provide self-amorphization and can further improve junction residual damage and leakage current. $B_{18}H_{22}$ and $(B_{18}H_{22})_2$ are viable substitutes for ultra low energy boron implantation. $C_{16}H_{10}$ is being investigated in PMOS junction engineering for replacing germanium pre-amorphization and control of boron diffusion. Molecular carbon can be implemented on NMOS transistors as well for lattice strain engineering and drive current enhancement.

Challenges and future prospects in plasma etching processes

O.Joubert[1], E. Pargon[1], T. Chevolleau[1], G.Cunge[1], L. Vallier[1], T. David[2], S. Barnola[2], T. Lill[3]

[1] *LTM (CNRS-UJF-INPG),17 avenue des martyrs (CEA-LETI-MINATEC), 38054 Grenoble cedex 09, France*
[2] *CEA-LETI,17 avenue des martyrs , 38054 Grenoble cedex 09, France*
[3] Applied Materials Inc., Santa Clara, CA 95054, USA

Plasma etching is the universal tool to define high-resolution patterns in integrated chip manufacturing [1]. To create structures in a chip, a pattern is formed in a photoresist by lithography and then transferred into the device materials by plasma etching. As the industry approaches the ability to create microcircuit structures on the order of 20 nm, this technology faces fresh challenges. To make progress, we need to go back to the basic science of how plasmas interact with surfaces.

Several trends are at work: First, circuit patterns need to be accurate to within 1 nm and below, within a single wafer and across several wafers. Second, plasma etching is becoming an integral part of pattern generation (using lateral erosion of the lithographic photoresist to improve resolution, for example). Third, aspect ratios of the final structures (that is, the ratio of length to width) are increasing dramatically. Finally, the number of potential new material candidates and their possible combinations in future structures is exploding.

To meet these challenges, the range of plasma densities and chemistries and the ion energies that can be generated must be continuously increased. State-of-the-art etch reactors must allow for perfect center-to-edge uniformity of neutral atoms and ions in the plasma, and uniform wafer surface temperature for any plasma regime that can be generated. The other frontier of advanced etch reactor development is the extension of the range of usable ion energies. At one extreme, ion energies are being extended to very low values— for instance, tens of electron volts for high-k (dielectric constant) materials etching. On the other end of the ion energy spectrum, high–aspect ratio oxide etching requires extremely high ion energies (thousands of electron volts). The introduction of novel materials such as high-k dielectrics is also driving the development of plasma etching at elevated wafer temperatures.

In this context, understanding the fundamentals of the etch mechanisms and their correlations to key process parameters is crucial. Each etch step must be characterized not only by etch rate and uniformity, but also by more fundamental properties such as the composition, thickness, and line-edge roughness of the sidewall layers of the structure, the chemical nature of etch by-products deposited on the chamber walls (which affects process stability and reproducibility), the thickness of the etch-front mixing layer (correlated to etch rate and selectivities between layers), and the impact of aspect ratio–dependent etching phenomena. Obtaining process repeatability is quickly becoming the biggest challenge for plasma etching. Because complex microstructures contain a larger number of thinner layers, the etch recipes contain multiple short etch steps. Advanced etch recipes to pattern a transistor electrode contain 5 to 10 steps with a total of 100 to 150 steps. In addition, chamber walls have an effect on complex recipes with multiple steps and chemistries. A deep knowledge of the coatings formed on the chamber walls during the process and the capability to modify them is needed to master this challenge.

In this talk, we will show that *in situ* and *ex situ* characterization techniques can contribute to get a better understanding of plasma processes and discuss how some intrinsic properties of the plasma (difference in directionality between ions and electrons or ion penetration depth in thin layers) can generate some fundamental limitations in performance. These limitations are particularly important when very thin material layers must be etched selectively and when high aspect ratio structures are formed in dielectric materials. More specifically, we will discuss resist line edge roughness issues and how they can be minimized to achieve the appropriate critical dimension control requirements. We will also show that quasi in situ XPS can be used to monitor the passivation layer formation on pattern sidewalls and the coatings formed on chamber walls during processes. Finally, we will introduce the potential evolution of etching technologies for the next decade showing the current limitation of cold plasmas for new device concepts and discuss how the "so-called" atomic layer etching technologies could eventually be implemented in the future.

1. T. Lill, O. Joubert, the cutting edge of plasma etching, Science, Volume 319 ,issue 5866, 1050, (2008)

Linear-chain carbon films for micro- and nanoelectronics

N.D. Novikov, A.F. Alexandrov, M.B. Guseva, V.V. Khvostov, N.F. Savchenko, Yu.V. Korneeva
Physics Department, M.V. Lomonosov Moscow State University, Leninskie Gory, Moscow State University, Physics Dept., Moscow, 119899 Russia, E-mail: nick.d.nov@mail.ru

Linear-Chain Carbon (LCC) (sp^1–carbon) can be obtained as film material by pulsed arc-discharge condensation in vacuum. The structure of the film of two-dimensionally ordered linear-chain carbon (2DLCC) represents by itself parallel chains of carbon atoms in sp^1-state, densely packed in layers that are randomly shifted. These carbon chains are oriented normally to the substrate and to the surface of the film [1].

By the crystal lattice, interatomic distances and the atomic structure, the 2DLCC film material radically differs from all known carbon materials. In certain aspects 2DLCC strongly resembles films of tubulenes and can be considered as a limiting case of the tubulene film, consisting of nanotubes with diameters equal to the diameter of a carbon atom. Particularly, this shows itself in the fact that band structure of tubulene consists of several one-dimensional subzones. In the specified limiting case what is left is only a single one-dimensional subzone. The chemical bond between carbon atoms changes from sp^2 to sp^1, and we obtain fundamentally new one-dimensional modification of carbon with single one-dimensional electronic zone, while the tubulene film is the quasi-one-dimensional material in which the quantity of one-dimensional zones increases with increase in the nanotube's diameter.

Strong anisotropy of electrical conductivity is the unique characteristic of 2DLCC that is associated with its regular structure: the electrical conductivity along chains is by six orders of magnitude higher than in the other directions. The special features of the LCC structure allow to lower the work function of electron escape and, by that, ensure high emissive properties of the material and, correspondingly, solve a problem of creation of highly effective emitter.

Such films, in essence, represent by themselves the system of quantum strings and they open prospects of creation of the new solid-state electronics – electronics of one-dimensional systems. A unique property of such 2DLCC films is the anisotropy of their physical properties. The quantum conductivity takes place along the chains – electron motion is ballistic, without dispersion, as in vacuum. Resistance of the film across chains is by 6 orders of magnitude higher. This opens prospects of creation of ballistic solid-state electronics, in which physical principles correspond to vacuum emission electronics, where the 2DLCC film is the analogue of vacuum medium. Ballistic solid-state electronics will retain in itself advantages of the vacuum electronics, such as high speed and absence of noise, and further improve valuable qualities of the solid-state microelectronics, such as capability of miniaturization (practically boundless - up to atomic level) and integration.

2DLCC could be doped or intercalated to attain a change of its electrical, mechanical and optical properties, and in that case a one-dimensional semiconductor or metal dependence of conductivity on temperature appears. On the basis of the LCC chains it is possible to create active and passive electronic components, such as diodes and transistors. In this report, ballistic and semiconductive prototypes of the devices are considered that have been developed on the basis of 2DLCC.

Anisotropy of 2DLCC films and their quantum conductivity along the chains lead to another unique property – abnormally high, oriented emission of secondary electrons, which allows to design such electronic devices as nanochannel electron multipliers, secondary emission cathodes, etc.

1. V.G. Babaev, M.B. Guseva, N.D. Novikov, V.V. Khvostov, P. Flood, "Carbon material with a Highly Ordered Linear-Chain Structure", *Polyynes Synthesis, Properties, and Applications* edited by Franco Cataldo, Taylor & Francis, Boca Raton London, New York., 2006

Fabrication of device structures from single-walled carbon nanotubes selectively grown on patterned catalytic layers

O.V. Kononenko [1] , V.N. Matveev [1] , Yu.A. Kasumov[1], I.I. Khodos[1], D.V. Matveev[2], V.T. Volkov[1], A.I. Il'in[1], M.A. Knyazev[1]

1. Institute of Microelectronics Technology and High Purity Materials, Russian Academy of Sciences, Chernogolovka, Russia, E-mail adderss: oleg@iptm.ru. 2. Institute of Solid State Physics Russian Academy of Sciences, Chernogolovka, Russia

Single-walled carbon nanotubes (SWCNT's) have attractive properties for using as a building blocks for future nanoelectronics devices due to the outstanding electrical, mechanical, physical, and optical properties of the typical one-dimensional (1D) materials. In recent years, many studies have been performed on single-walled carbon nanotubes for their promising applications in future nanoelectronics and nanodevices such as SWCNT field effect transistors (FET's), logic devices, resonators, field emitters and sensors.

It is known that electronic properties of carbon nanotubes depend on their structure. In order to use nanotubes to create electronic devices, it is necessary to control their structural parameters. Diameter of nanotubes is one of the important parameters. It depends on diameter of a catalytic particle on which the nanotube grows. By means of various methods of deposition (electron beam evaporation, rf-sputtering, laser beam evaporation) and processing (for example, annealing) of the catalytic particles it is possible to vary the diameter distribution of catalytic particles, and thus control the diameters of produced nanotubes.

Using the optimized catalyst the single-walled carbon nanotubes were grown selectively on oxidized silicon subtrates (fig.1). The catalyst layers for nanotube growth of various sizes were patterned on resist-covered substrates using electron beam lithography. 10 nm Al/0.5 nm Fe bi-layer catalyst was deposited by electron beam evaporation onto substrates and then selectively removed using a lift-off procedures. After that the substrates with deposited bi-layer catalyst were heated in a furnace for 2 min in order to form Fe nanoparticles.

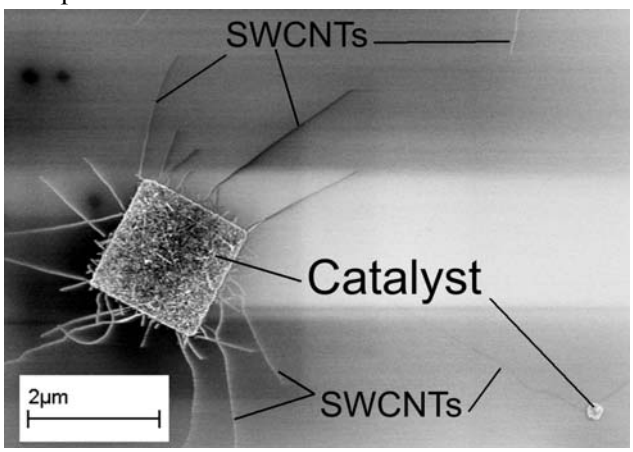

Fig.1 SEM image of single-walled carbon nanotubes selectively grown on oxidized silicon subtrates.

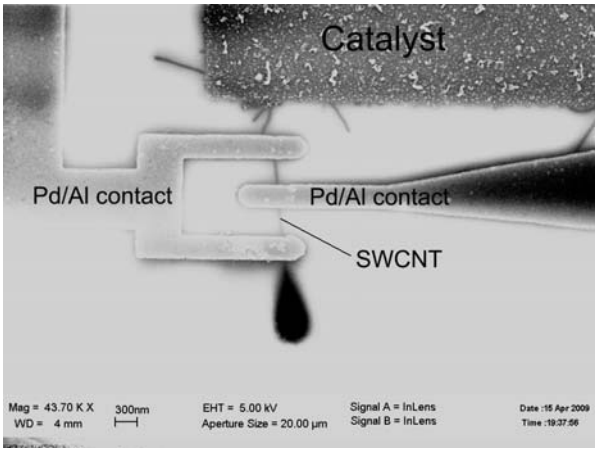

Fig.2 SEM image of device structure fabricated from SWCNT by electron beam lithography.

Growth of nanotubes was carried out by a method of single injection of acetylene [1] at pressure of 2.5 mbar at temperature 950°C. Grown nanotubes and catalytic nanoparticles were characterized by transmission and scanning electron microscopy. E-beam lithography and a lift-off process were used to pattern e-beam evaporation deposited palladium electrodes contacting nanotubes. Two-terminal structures were fabricated for measurements of electrical properties of SWCNTs.

This work has been supported by the International Science and Technology Center, Grant no. 3836

1. Y.A. Kasumov, A. Shailos, I.I. Khodos, V.T. Volkov, V.I. Levashov, V.N. Matveev, S. Gueron, M. Kobylko, M. Kociak, H. Bouchiat, V. Agache, A.S. Rollier, L. Buchaillot, A.M. Bonnot, A.Y. Kasumov, "CVD growth of carbon nanotubes at very low pressure of acetylene" Appl. Phys., A 88, pp. 687-691, 2007.

CNS catalyst growth from carbonaceous substrate

E. Ilyichev, V. Inkin, D. Migunov, G. Petruhin, E. Poltoratskii, G. Rychkov, D. Shkodin
FSUE "Res. Inst. of Phys. Problems named after F.V. Lukin", Zelenograd, polt@niifp.ru

The research results of carbon nanostructures (CNS) grown directly from carbonaceous substrate (carbon diamond-like films - DLF), in contrast to traditional methods [1], are presented.

The probability of successful realization of CNS by proposed methods is estimated. In particular, at T ~ 820 K, the typical CNS nucleation time value (~ 30 min) has been obtained for the following parameters: activation energy of diffusion process of carbon atoms in nickel catalyst ($E_{act} \approx 1.55$ eV); frequency factor ($\nu \approx 10^{12}$ Hz); concentration of diffusing atoms at the interface ($n_C \approx 1.5 \cdot 10^{15}$ cm^{-2}); lateral dimension of initial catalyst drops is ~ 0.3 μm and their height is ~ 0.1 μm.

Si(substrate)/Cr/DLF/Ni experimental structure was used in this work. The diamond-like film was obtained in the arc-discharge (graphite) process combined with carbon ions separation in magnetic field.

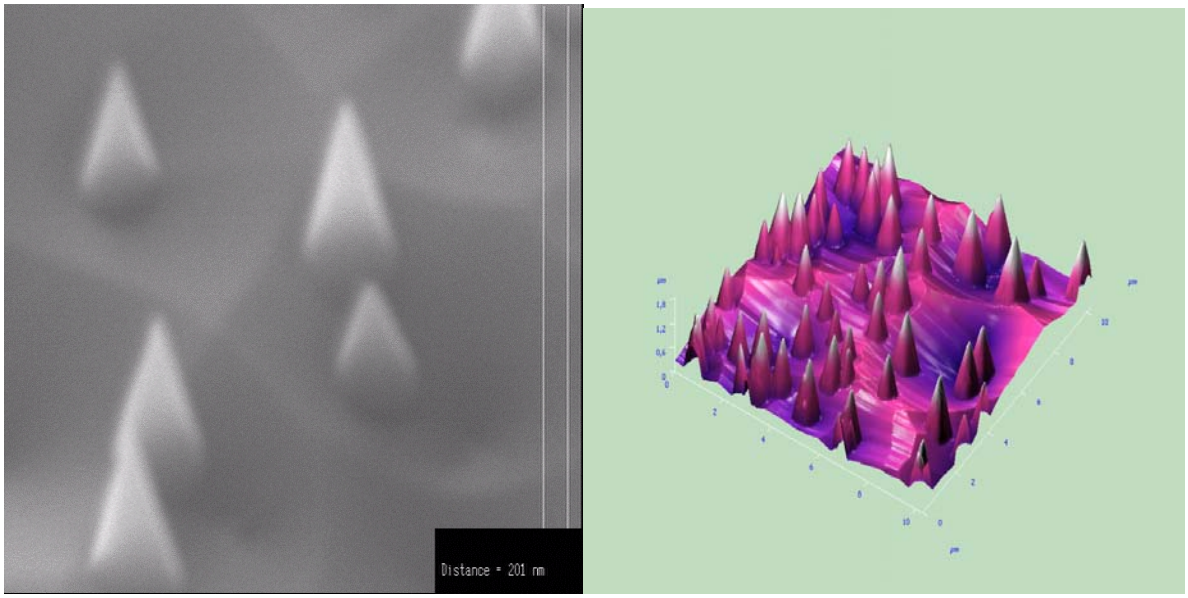

Fig. 1. Typical picture of CNS SEM and SPM image

Carbon nanostructures' forms are cone-like and hollow under the tip. Curvature of the cones tips is ~ 20 nm. Dispersion of CNS geometrical parameters corresponds to dispersion of catalyst particles' diameters. The cones typical height is ~ 1 μm and typical diameters of the cones base are ~ 0.3 - 0.5 μm.

The SEM and SPM results of CNS (fig. 1) and field emission characteristics of such structures are presented. The growth model of CNS perfect forms is offered.

1. A. Huczko, "Synthesis of aligned carbon nanotubes", J. Appl. Phys. A, **v.74**, pp.617-638, 2002.

Dry Etch Solutions for 3D Integration Technology

N. Tutunjyan, M. Van Cauwenberghe, P. Verdonck, B. Majeed, T. Buisson, Y. Civale, W. Boullart
IMEC, Kapeldreef 75, 3001 Leuven, Belgium
Nina.Tutunjyan@imec.be

3D Packaging and Interconnect Technologies play nowadays an important role in the overall performance of microelectronic devices. The limitations of the traditional 2D packaging systems can be successfully overcome by the advanced 3D Integration Technologies.

Our study covers a variety of dry etch tasks within the frames of 3D – WLP (Wafer Level Packaging) Technology, which is realized by 3D – Through Silicon Vias (TSVs) connections, followed by staking with a method similar to flip – chip mounting [1]. TSV formation is a key component in 3D interconnects. Via contacts through silicon can improve electrical performance, reduce power consumption and miniaturize the device sizes. TSVs formed on the backside of the silicon wafer are called "last vias" since they are integrated after BEOL (back-end-of-line) modules and after the wafer thinning step.

A modified Bosch process well known as a pulsed or time-multiplexed etching as well as conventional chemistry SF_6/O_2 have been investigated to create vias with the specified depth and profile.

DRIE based on the Bosch process is the most popular method for TSV formation since it provides etching with vertical sidewalls. But the process is rather limited from the point of view of creating tapered/sloped via profiles. The requirement for a sloped profile is triggered by the boundary condition of conformal filling of TSVs in the subsequent insulation liner and the Cu metallization process steps.

We demonstrate a novel method of TSV fabrication comprising three different etching steps. For the first etching step we have investigated $SF_6/C_4F_8/O_2$ chemistry to form sloped profiles with an angle of 60^o and a depth of 30µm. For the second step the standard Bosch process including the etch (SF_6) and the passivation (C_4F_8) steps has been studied. The process has been optimized by tuning the process parameters: LF pulsed bias - 20% and temperature - 0^0C, to form "grass" – free vertical vias with a depth of around 70µm. For the third step - a soft landing with a longer passivation phase of C_4F_8 has been investigated to avoid notching at the dielectric interface. The soft landing step is implemented now as a desired step for the majority of applications with a dielectric stop layer. The final depth of the vias is 100µm. The profile of TSV has been named "chamfered" and demonstrates the conformal filling with the Cu (Fig.1).

Our work has also focused on the problem related to the cyclical nature of the Bosch process - scallops formation. For the "chamfered" via profile the presence of scallops is not as critical as for the vertical TSVs. We have investigated the possibilities to reduce the scallop's formation by shortening the cycle times of etch and passivation. This allows us to fill vertical TSVs with the LTO (low-temperature oxide) (Fig. 2).

The next task in our study is the Teflon-type polymer removal which is produced in C_4F_8 based passivation step of the Bosch process. The residues of the fluorocarbon polymer inside the vias can reduce the yield of the TSV technology. For the polymer removal we have developed two types of the strip process in an ICP type reactor using pure O_2 and O_2 with SF_6 addition.

The final etch process in TSV technology is SiO_2 or PMD (pre-metal deposition stack) etch at the bottom of the vias to allow contacting the landing pads on the front side of the wafer. Realization of this task as well as solutions of all the above mentioned issues contributes to the improvement of quality and yield of the TSV technology.

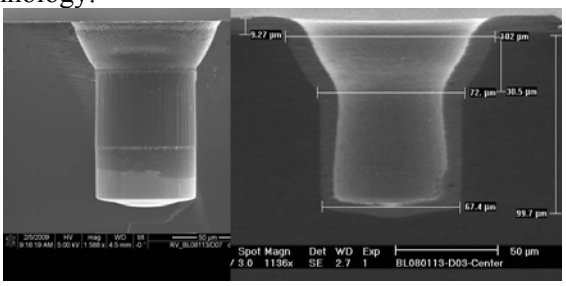

Fig.1 "Chamfered" TSV with the Cu conformal filling

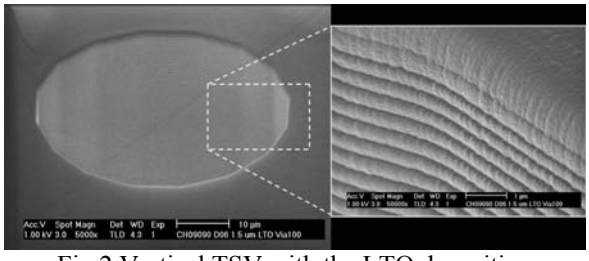
Fig.2 Vertical TSV with the LTO deposition

1. E. Beyne, "3D Integration Technologies at IMEC", *Handbook of 3D Integration,* P.Garrou *et al.,* vol. 2, pp.413-430, WILEY-VCH Verlag GmbH&Co.KGaA, Weinheim, 2008

Impact of plasma exposure on organic low-k materials

E. Smirnov[1,2], A. K. Ferchichi[1], C. Huffman[1], M. R. Baklanov[1]
1. *IMEC vzw, Heverlee, Belgium, E-mail: baklanov@imec.be*
2. *Moscow Institute of Electronic Technology, Moscow, Russia, E-mail: smirnovevgenyandreevich@gmail.com.*

Interconnect technology becomes determining factor for signal delay in nowadays VLSI technology where channel length reaches few tens of nanometers. The propagation velocity of electromagnetic waves becomes increasingly important due to their unyielding constraints of interconnect delay. The introduction of Cu and low-κ dielectrics has incrementally improved the situation as compared to the conventional Al/SiO_2 technology by reducing both resistivity of and capacitance between wires. Since copper has become the common metallization material, lowering signal delay by introducing low-κ dielectrics is one of the main objectives today. The impact of dielectric constant on system performance has triggered all the research on new dielectrics. The chemical industry has been very active in bringing new materials to the market with ever decreasing κ-values, attempting to comply with the performance specifications provided by microelectronics industry.

The most important challenges in the integration of low-κ materials are related to damages during plasma and thermal treatment. The problem is determined by the hybrid nature of these materials which means both inorganic and organic parts, having completely different chemical reactivity. For these materials, a strip in O_2 or H_2 based plasmas, removes organic components, increases their hydrophilic properties and adsorbed moisture increases their κ-value. The latter reveals clear advantage of mono-component organic polymers. However, early generations of organic low-κ materials for several reasons were rejected by technology: they didn't have sufficiently low-κ value, high non-uniformity, complicated pore shape and poor mechanical properties. The new advanced organic low-κ material "Polymer M" exhibits several advantages comparing to predecessors. Apart from its low κ-value (2.2), this material has low coefficient of thermal expansion (CTE=25), good mechanical properties and no damage effect after plasma exposure and CMP. Consequently, determination of proper plasma treatment conditions is of great importance for low-κ application.

This work continues a set of studies on a new advanced organic low-κ material and dedicated to investigation of the following properties: κ-value, porosity, pore size, density, hydrophobicity and refractive index. Plasma treatment processes were performed in the various types of chambers: CCP, ICP, μWave. Different types of plasmas have been applied: Cl/HBr/Ar, O2/Cl2, He/H2, C4F8/CH2F2/O2/Ar/N2, C4F8/CH2F2/Ar/N2, CF4/CH2F2/Ar/O2, μWave He/H2 including treatment time variation (20 and 30 sec). These plasmas are considered as candidates for the etching of low-κ material itself and hard masks deposited on top of low-κ film. Therefore, the purpose of this study was to determine the etch selectivity and also to evaluate possible degradation of low-κ films after exposure in these plasmas.

The thickness determination experiments revealed that the highest etch rate of "Polymer-m" is obtained in O2/Cl2 plasma (5.5 nm/s) and H2/N2 (3 nm/s) in the ICP and CCP chambers respectively. These processes thus can be used for the etch purpose. In the mean time He/H2, C4F8/CH2F2/O2/Ar/N2, CF4/CH2F2 plasmas provides partial pore sealing because of deposition of fluorocarbon polymers. The surface hydrophobicity measured by WCA : 27 º, 82 º, 55 º respectively. C4F8 / CH2F2 / Ar/N2 plasma completely seals "Polymer-m" pores, exhibiting high hydrophobicity (surface contact angle 88º). These results are in agreement with the results of evaluation of bulk hydrophilicity carried out by water based ellipsometric porosimetry. FTIR spectroscopy found no significant change of composition. However, O2/Cl2 treatment shows a tendency of C=O groups formation which may act as further centers of moisture adsorption. Results of evaluation of refractive indices and dielectric constant will also be reported.

1. M.Baklanov, M.Green, K.Maex (Editors). *Dielectric Films for Advanced Microelectronics*. John Wiley & Sons, London 2007.
2. K.Maex, M.R.Baklanov, D.Shamiryan, F.Iacopi, S.H.Brongersma and Z.S.Yanovitskaya. Low dielectric constant materials for microelectronics. J.Appl.Phys. 93, 11, pp. 8793-8841 (2003).
3. A.K.Ferchichi, Y. Travaly, G. Beyer, M.R. Baklanov. Evaluation of an advanced organic ultra-low-k material. Proceedings of Advanced Metallization Conference in 2008 AMC XXIV, MRS, p. 587, 2009.

Application of Langmuir probe technique in depositing plasmas for monitoring of etch process robustness and for end-point detection

A.V. Miakonkikh, K.V. Rudenko
Institute of Physics and Technology, Russian Academy of Sciences, Moscow, Russia, rudenko@ftian.ru

In our recent paper [1] we have proposed Dynamic Langmuir probe (DLP) technique that allows correct measurements of electron temperature, densities of charged particles and plasma potential in processing film-depositing plasmas. The purpose of the present paper is to examine DLP method as a tool of *in situ* measurement of process robustness and monitoring of end-point detection in adverse conditions. The method was compared with optical emission spectroscopy (OES) technique of end point detection.

Experiment was carried out in dense ICP plasma of mixture CF_4 (95%) and O_2 (5%) which polymerizing properties widely used for anisotropic plasma etching of dielectrics/silicon structures. The following parameters in ICP-etcher chamber were set up as: P = 3.0 mTorr, f= 40 sccm, W_{RF} = 800 Watt, (13.56 MHz), and RF_{bias} = 20 - 50 V. Probe analytical signal choice procedure was described in details in [2]. In this research whole set of probe data was used for real time analysis. Examples of traces of probe current at fixed potential (+5 V) as DLP monitoring signal and the intensity of a spectral line of F* (703.7 nm) from plasma as OES end point signal are demonstrated at Fig.1 and Fig.2.

In order to compare abilities of DLP and OES signals on responding to fast changes of plasma parameters, we examined their responses to abrupt shocks in gas inflow (up to 10%). Fig. 1 shows that DLP signal traces variations of plasma parameters as quickly as OES signal.

To account for possible practical obstacles of end-point diagnostics in etch process, the experimental conditions were chosen to be quite complicate. The etch windows was shrunk to 35% of total area (Ø150 mm). Helium inflow under the wafer was reduced to artificially increase temperature instabilities during plasma etching. Process selectivity also was very bad: it is about 3 at SiO_2/Si and close to 1 at Si_3N_4/SiO_2 interfaces. Under those conditions, the end-point detection between two dielectric layers should be extremely difficult by probe technique. Fig. 2 compares probe current at potential +5 V with OES signal during etching. At OES trace the graphs is sloped downward due to increasing of etching rate caused by uncontrolled heating the wafer [3].

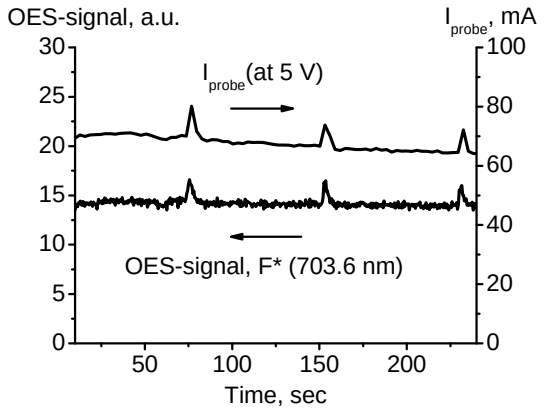

Fig. 1. Respond of probe current (at V_{probe}= +5V) and intensity of F* line (703.6 nm) to sharp gas inflow shocks

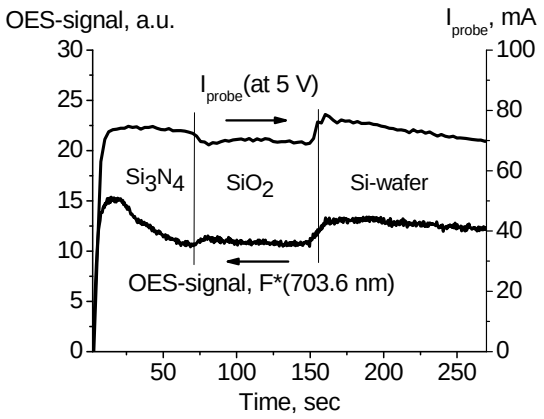

Fig. 2. DLP end-point signal (probe current at V_{probe}= +5V) and OES end point signal measured in situ during etching of Si_3N_4/SiO_2/Si-structure

The analysis of probe data shows that corresponding responses in probe signal (not only on ion current) reveals enough sensitivity the DLP technique to etch parameters drift and its applicability for end point detection during etching of dielectric layers in deteriorated conditions. Then DLP method could be a simple good choice for monitoring of plasma etching even in polymerizing plasmas if the pressure in chamber not exceeds 10-20 мTorr.

1. K.V. Rudenko *et al.*, “New Method for the Langmuir Probe Diagnostics of Polymerizing Plasmas”, Russian Microelectronics, **36**, issue 1, 14–26, 2007.
2. K.V. Rudenko *et al.*, “Plasma Etching of poly-Si/SiO_2/Si Structures: Langmuir-Probe and Optical-Emission-Spectroscopy Monitoring”, Russian Microelectronics, **36**, issue 3, 179–192, 2007.
3. K.V. Rudenko, “Diagnostics of Plasma Processes in Micro- and Nanoelectronics”, High Energy Chemistry, **43**, issue 3, 196–203, 2009.

Mathematical modeling of a fast neutrals beam source neutralization channel

A.V. Degtyarev, V.P. Kudrya, Yu.P. Maishev
Institute of Physics and Technology, Russian Academy of Sciences, Moscow, Russia, E-mail address kvp@ftian.ru

Now plasma and ion beam processing are successfully used in 45-nm IC technology. However, such intrinsic drawbacks of plasma and ion beam processing as charged particle bombardment and VUV exposure of substrates treated resulting in geometry distortion of nanoelement topology and defect generation within thin films became critical for further progress. It was established in Ref. 1 that a transition to sub-32-nm technology will demands using the fast neutral beam (FNB) technology for structuring.

A key problem of the FNB technology is to develop high-performance and stable sources providing uniform flows of fast neutral particles (atoms and/or radicals). Such sources can be constructed basing on the Radical type source of ring or band (for example, racetrack) ion beams with a cold cathode, crossed electric and magnetic fields, and a closed electron drift (see, for example, Ref. 2). Due to a large number of geometrical and physical parameters characterizing such a FNB source, its design and optimization should be supported by comprehensive modeling and simulation.

A full description of a neutralization channel model of such a FNB source is presented. The model takes into account the charge exchange and elastic scattering of fast heavy particles in gas phase, as well fast ion neutralization due to grazing scattering by channel walls. The physical processes occurring into the neutralization channel are considered in detail. The computational model of the neutralization channel is based on the Monte Carlo method. The Monte Carlo procedures are described with necessary formulas for random values sampling.

The simulation results of FNB source output characteristics for three different channel designs are presented. The energy and angle characteristics and spatial distributions of output FNBs as well dependencies of neutrality degree and neutralization efficiency on the channel geometry, pressure, and angle width of the initial ion beam are considered in detail. Firstly, a direct neutralization channel was studied which exhibits a considerable aperture effect for both neutrals and ions. Contributions of the two neutralization mechanisms to the neutrality degree are analyzed.

Then, studying the inclined neutralization channel, we found a strong effect of an angle separation of ions and fast neutrals (see also Ref. 3). With an angle restriction of the output beam this effect provides an effective elimination of the most part of ions resulting in significant increasing the beam neutrality degree.

Finally, for a channel with additional reflected surfaces a FNB focusing effect was founded. This effect provides a high neutrals density in beams overlapping. It can be effectively used with ion sources both band and ring output beam.

The results presented show that the neutralization channel model proposed allows to make a comprehensive analysis of the channel geometry and ion beam parameters influence on energy and angle characteristics of the output FNB. In turn, such results can be used to optimize the design and working mode of FNB sources.

This work was supported by the Russian Foundation for Basic Research, project no. 07-07-00120.

1. S. Samukawa, "Recent Development in Neutral Beam Processes (Editorial)", J. Phys. D, 41, p.1, 2008.
2. K.L. Enisherlova, Yu.A. Kontsevoi., E.N. Chervyakova, E.A. Mitrofanov., Yu.P. Maishev, "Investigations of diamond-like carbon films produced directly from an ion beam of industrial ion source with a cold cathode", Mater. Sci. Eng. B, 46, p.137, 1997.
3. A.V. Degtyarev, V.P. Kudrya, Yu.P. Maishev, "Mathematical Simulation of an Inclined Neutralization Channel for a Plasma Source of Neutral Beams", Russian Microelectr., 2009, v.38, p.171, 2009.

TCAD technique to simulate total dose effects in SOI MOSFETs

K. Petrosjanc, I. Kharitonov, E. Orekhov
Moscow State Institute of Electronics and Mathematics (Technical University), 3, B. Tryokhsvyatitelskiy side-street, Moscow 109028, Russia, e-mail: eande@miem.edu.ru

The use of TCAD simulation to investigate device characteristics degradation due to radiation can reduce time and cost of design process. The mobility degradation and interface traps charge due to radiation is not accounted by Sentaurus TCAD total dose model [1]. We modified TCAD total dose model to account carrier mobility degradation and interface traps charge. The mobility degradation due to dose of irradiation calculated as:

$$\mu(D)= \mu_0 (1+\alpha \cdot N_{it}(D))^{-1}, \quad (1)$$

where μ_0 is the mobility of unirradiated device ($cm^2/(V \cdot s)$), α is a constant, $N_{it}(D)$ is the interface traps density (cm^{-2}) defined by following equation:

$$N_{it}(D)=a_{it} \cdot D^{bit}, \quad (2)$$

where D is the dose of irradiation (rad), a_{it} and b_{it} are fitting parameters.
Equations (1) and (2) were implemented in device simulation flow via TCAD PMI (physical model interface). Additionally the interface traps charge (Q_{it}) was modeled as:

$$Q_{it}(D)=q_e N_{it}(D), \quad (3)$$

where q_e is the electron charge.
Sidewall leakage current cannot be accounted in 2D TCAD simulation of irradiated MOSFET and it is necessary to use the complex 3D simulation procedures which consume too much time and hardware resources. However it is possible to use the quasi-3D simulaton that provides acceptable accuracy and saves time [2, 3]. For calculation of sidewall leakage current we developed a quasi-3D modeling technique which consisted from three stages:
1. For defined set of gate voltages 2D simulations of both A-A and B-B cross sections (Fig. 1) and Id-Vg dependence of MOSFET before irradiation were performed.
2. For the same set of gate voltages 2D simulations of B-B cross section of irradiated MOSFET with different radiation induced charge densities at the silicon/oxide interface were performed.
3. Simulation results of B-B cross section of MOSFETs with interface charge and without interface charge were analyzed to correct the initial Id-Vg dependence obtained from A-A cross section at first stage.
N-channel partially depleted SOI MOSFET with 1.5/0.5 um gate size, gate oxide and buried oxide thickness of 12 nm and 150 nm respectively and 200 nm thickness of active silicon layer was modeled following proposed technique. Fig. 2 shows that 2D simulation in comparison with quasi 3D simulation doesn't provide necessary accuracy for radiation hardness modeling.

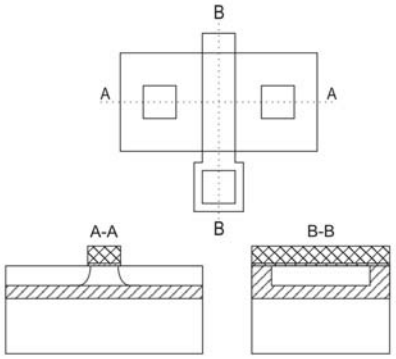

Fig. 1. SOI MOSFET layout with A-A and B-B cross sections

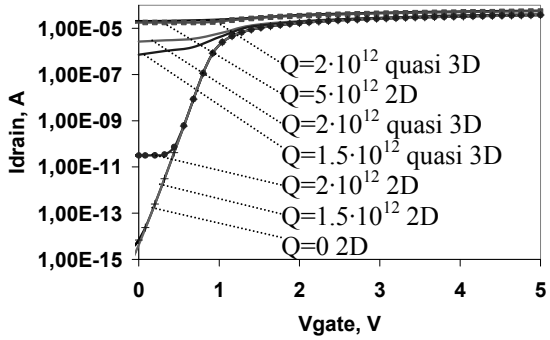

Fig. 2. Comparison of 2D and quasi 3D simulated Id-Vg characteristics of 0.5 um SOI nMOS for different doses

1. Synopsys Sentaurus TCAD v.2008.9, User's manual
2. H. Barnaby, I. Sanchez, "Modeling and Analysis of Ra-diation-Induced Off-State Leakage in Deep Submicron CMOS Technologies", Proc. of 2004 Microelectrinics Reliability & Qualification Workshop, 2004, www.aero.org/conferences/mrqw/2004-papers/Barnaby.pdf
3. C. Brisset, V. Ferlet-Cavrois, O. Flament, "Two-Dimensional simulation of Total Dose Effects on MOSFET with Lateral Parasitic Transistor", IEEE Trans. Nucl. Sci., **Vol. 43**, N 6, pp. 2651-2657, 1996.

Optimization of near-surficial annealing for decreasing of depth of *p-n*-junction in semiconductor heterostructure

E.L. Pankratov

The Mathematical Department, Nizhny Novgorod State University of Architecture and Civil Engineering, 65 Il'insky street, Nizhny Novgorod, 603950, Russia, elp2004@mail.ru

In this paper we consider a heterostructure, which consists of an epitaxial layer and a substrate (see Fig.1). A dopant has been infused or implanted through the boundary $x = 0$. We assume, that type of conductivity of the substrate is known (*n* or *p*). The dopant produces another type of conductivities (*p* or *n*) in the epitaxial layer. Therefore, one can obtain diffusive-junction or implanted-junction rectifiers between layers of the heterostructure. At the moment of time $t = 0$ annealing of dopant (for infused dopant) or radiation defects (for implanted dopant) is started. It has been recently shown (see, for example, [1-3]), that one can obtain increasing of the homogeneity of dopant distribution in epitaxial layer and at one time increasing of the sharpness of the *p-n*-junction near the interface between layers of the heterostructure after appropriate choosing of annealing time, diffusion coefficient $D(x)$ and limits of solubility $P(x)$ of dopant (see [1-3]). Figs. 2 and 3 have illustrated the effect for volumetric annealing. In this paper we optimized characteristics of near-surficial types of annealing (microwave [4] and laser ones) to increase the effect of simultaneously increasing of homogeneity of dopant distribution in doped area and sharpness of *p-n*-junction. For example, it have been optimized thickness of scin-layer, power and pulse width of pulse laser annealing.

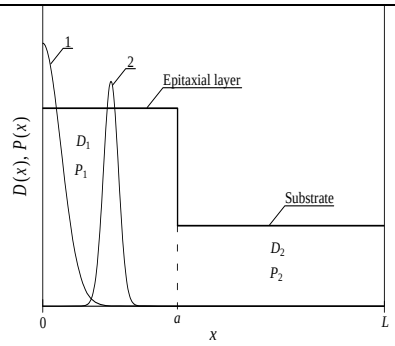

Fig. 1. Heterostructure with an epitaxial layer and a substrate. Curves 1 and 2 are distributions of infused and implanted dopants before annealing.

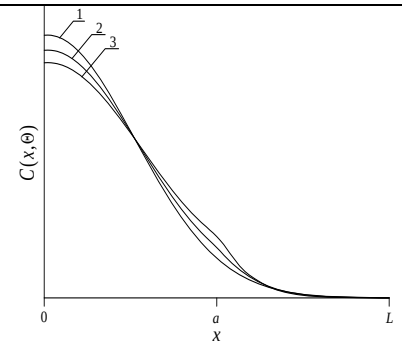

Fig. 2. Calculated spatial distributions of dopant in infused-junction rectifier after annealing with time $\Theta = 0.1L^2/(D_1+D_2)$. Curves 1-3 correspond to following relations $D_1/D_2 = 1$, $D_1/D_2 = 1.5$ and $D_1/D_2 = 2.3$.

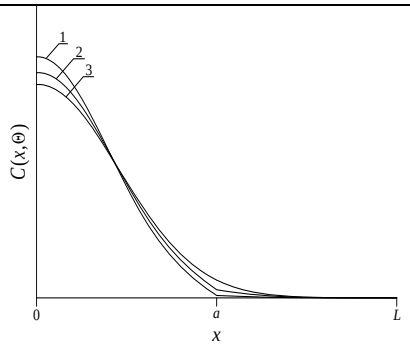

Fig. 3. Calculated spatial distributions of dopant in infused-junction rectifier after annealing with time $\Theta = 0.1L^2/(D_1+D_2)$. Curves 1-3 correspond to following relations $P_1/P_2 = 1$, $P_1/P_2 = 3$ and $P_1/P_2 = 10$.

This work has been supported by grant of Nizhny Novgorod State University of Architecture and Civil Engineering (project 241).

1. E.L. Pankratov, "Influence of the spatial, temporal, and concentrational dependence of the diffusion coefficient on dopant dynamics: optimization of annealing time", Phys. Rev. B, 72, pp.075201-075208, 2005
2. E.L. Pankratov, "Dopant Diffusion Dynamics and Optimal Diffusion Time as Influenced by Diffusion-Coefficient Nonuniformity", Russian Microelectronics, 36, pp. 33–39, 2007
3. E.L. Pankratov, "Redistribution of dopant, implanted in a multilayer structure for production of a *p–n*-junction, during annealing radiative defects", Phys. Lett. A, 372, pp. 1897–1903, 2008
4. E.L. Pankratov, "Redistribution of dopant during microwave annealing of a multilayerstructure for production *p-n*-junction", J. Appl. Phys., 103, pp.064320-064330, 2008
172113, 2006

Research of current injection process in to the substrate during digital gate switching

T. Krupkina, D. Rodionov.
Moscow Institute of Electronic Technology (Technical University), Russia, Moscow, E-mail: ieem@miee.ru

Today one of the most important area in the microelectronics industry is develop and design of *system-on-chip* – mixed signal very large scale integration circuits (VLSI IC) that contain hight speed digital and hight precision analog IP-blocks. Combination of digital and analog circuits in such VLSI and fast design rules miniaturization are cause to increase substrate role that can conduct noise injected by digital blocks. Current injection process is showed on pic 1.

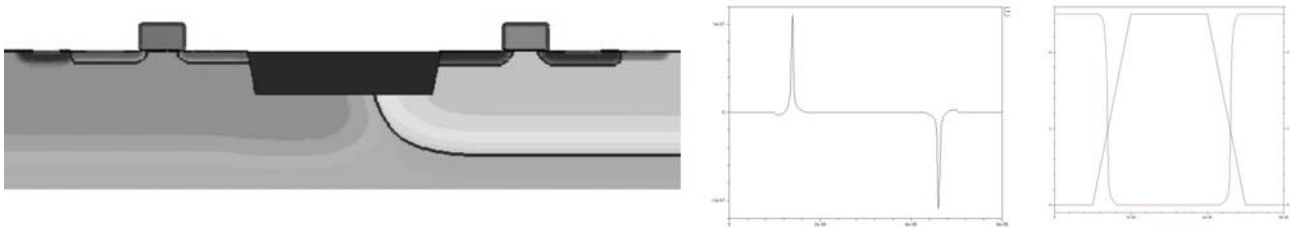

a) b) c)

Pic 1. CMOS structire (a), current via substrate contact (b), input, output signals (c)

For more detailed understanding of researched process there is physical condition of one transistor in CMOS structure with maximum current via substrate contact is showed on the pic 2a. There is nonlinear equivalent circuit is showed on pic 2b. This equivalent circuit contains additional elements that model interactions between device and substrate.

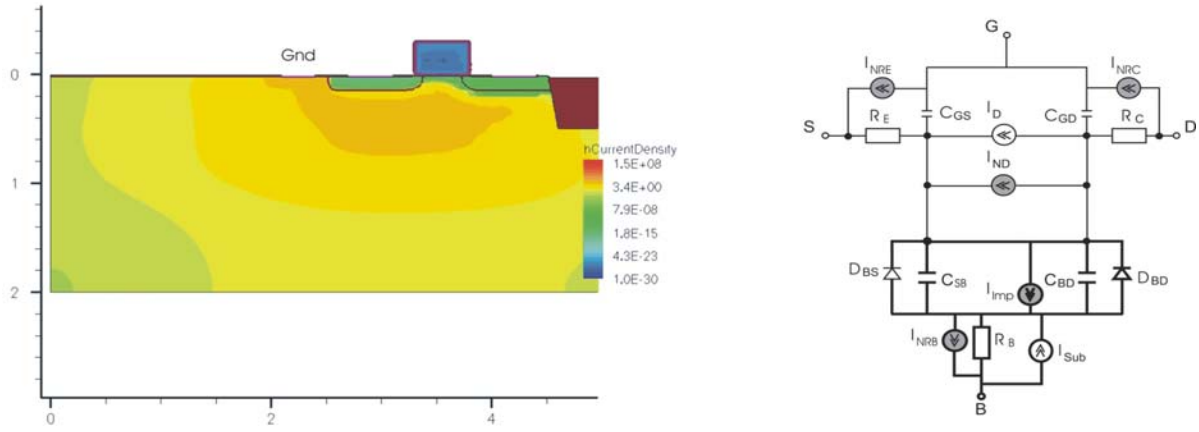

a) b)

Pic 2. Physical condition of nMOS (a), nonlinear equivalent circuit (b)

In the mentioned equivalent circuit current source Iimp models current that generated by avalanche generation effect in transistor channel, that cause current injection in to the substrate. This cause to occur overconcentration region under the device-source (Pic 2a). This region picked by substrate contact (low-resistive region).

Device modeling of CMOS structure, electrical characteristics and carrier redistribute process was performed with technology CAD – Synopsys Sentaurus using drift-diffusion model.

Extrinsic Compact MOSFET Model with Correct Account of Positive Differential Conductivity after Saturation

V.O. Turin[1], A.V. Sedov[1], G.I. Zebrev[2], B. Iñiguez[3], and M.S. Shur[4]
[1] *Orel State Technical University, Orel, Russia, e-mail:* voturin@ostu.ru
[2] *National Research Nuclear University "MEPHI", Moscow, Russia, e-mail:* gizebrev@mephi.ru
[3] *Rovira i Virgili University, Tarragona, Spain, e-mail:*benjamin.iniguez@urv.cat
[4] *Rensselaer Polytechnic Institute, Troy, NY, USA, e-mail:*shurm@rpi.edu

We have developed the improved compact MOSFET model based on the simple Charge-Sheet Model (CSM) [1] that is the base of the most MOSFETs models used in modern SPICE-type simulators. The developed model has its origin in the work under improvements of α-Si RPI-TFT compact model that is used, for example, in modern Cadence PSPICE and Synopsys HSPICE circuit simulators. Entry level models (including the RPI TFT model [2]) use channel-length modulation parameter λ to account for positive differential conductivity after saturation due to Channel Length Modulation (CLM) and Drain Induced Barrier Lowering (DIBL) effects. This is done by multiplying the expression for the drain current by the $1+\lambda_0 V_{DS}$ factor, where V_{DS} is the drain-to-source bias. In more advanced models (for example BSIM4), a more sophisticated expression is used. However, all these traditional approaches suffer from non-monotonic behavior of the differential conductivity with increasing drain-to-source bias. In the improved model, we offer a new approach that gives smooth transition between current before and after saturation with the correct monotonic decrease of the differential conductivity. The new model equation for drain current is infinitely continuous. This is done by first introducing a new asymptotic "after saturation" equation I_2* for the dependence of the drain current on V_{DS}:

$$I_2^* = I^* + \lambda_0 I_{SAT} (V_{DS} - V^*), \quad (1)$$

instead of $I_2 = I_{SAT}(1+\lambda_0 V_{DS})$ in the RPI-TFT model. Parameters I^* and V^* are derived from the condition, that this asymptote should be tangential to the quadratic part of the output characteristic given by CSM. Second, we use a generalized mean (also known as Hölder or power mean) with exponent $-m$ of CSM equation I_{1L} for the linear part of the output characteristic and the "modified after saturation" equation I_2**:

$$I = I_{1L} I_2^{**} / [I_{1L}^m + I_2^{**m}]^{1/m} \quad (2)$$

(note that instead of use of the "after saturation" asymptote I_2* in (2) it is necessary to use "modified after saturation" equation I_2** as discussed in detail in our presentation). In addition, we have transformed the developed intrinsic model into extrinsic that accounts for the source and drain series resistances analytically. To obtain the equations of the extrinsic model we have followed the approach suggested in [3]. For the saturation current in the extrinsic model, we have used the equation from the MOS saturation model adapted to α-Si TFTs [4]. The extrinsic compact model is useful to analyze and predict the behaviour of different types of MOSFETs (including α-Si TFTs) and for the computer-aided design of integrated circuits, since it can improve convergence and speed of SPICE modeling.

1. S.M. Sze and Kwok K. Ng. *Physics of Semiconductor Devices.* John Willey and Sons, New Jersey, 2007
2. G.I. Zebrev. *Physical Basics of Silicon Nanoelectronics*. MEPHI, Moscow, 2008 (in Russian).
3. M.S. Shur, V.O. Turin, D. Veksler, T. Ytterdal, B. Iñiguez, and W. Jackson, "Compact Iterative Field Effect Transistor Model", NSTI-Nanotech 2006, ISBN 0-9767985-8-1, **3**, pp. 648-651, 2006
4. T. Fjeldly, T. Ytterdal, and M.S. Shur. *Introduction to Device and Circuit Modeling for VLSI*, John Wiley and Sons, New York, 1998

Informational charge readout dynamics and non-linearity of photosignal characteristics of active pixels in CMOS image sensors

A.V. Verhovtseva, V.A. Gergel', V.A. Zimoglyad
LLC RPC «SensorIS», Moscow, Russia, E-mail address: alevteena@gmail.com

At present, CMOS image sensors are becoming more and more applicable in mobile devices a because of their cheapness, low power consumption and easy integration with on-chip photosignal processing digital circuits [1, 2].

The base element for these devices is the so-called active CMOS pixel, which is produced by diode photosensor with reset and read transistors. Investigating pixel's quasi-cylindrical model structure, we've developed the iterative procedure to calculate the relaxation of photocharge and numerically created the corresponding time curve. The universal curve of relaxation of photocharge we've got allows us to model it's behavior in time at setting reset, exposition and result readout stages, to build photosignal characteristics we need in wide range of process parameter variance like exposition time to full frame ratio and setting resets and signal readout durations.

In a fig. 1 the resulting pixel photosignal characteristic is presented with an anomalously high value of photosensitivity on small signals that completely coincides with experimental data.

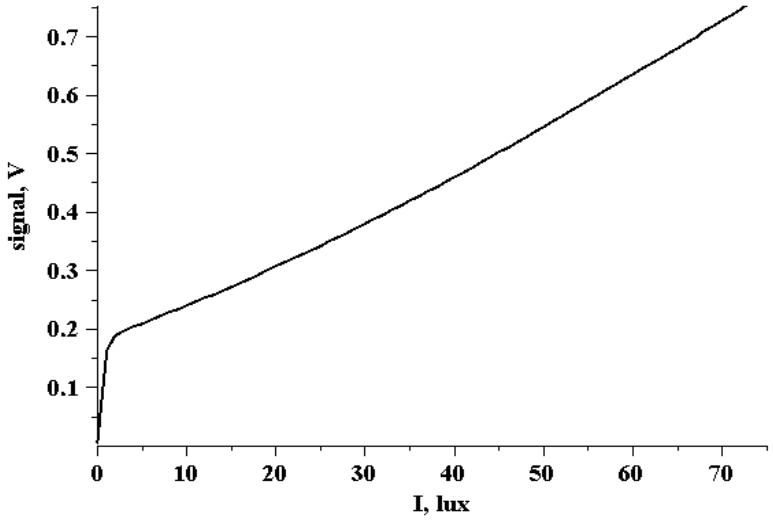

Fig. 1. The calculated photosignal characteristic of a pixel

The constructed mathematical model explains such behavior by the nonlinearity of charge transport speed. The big charges quickly (approximately for 10 ns) flow down almost completely at an open operating mode of transistor TX while at flowing down of small portions of a charge, transistor TX is in a subthreshold mode that causes slow (logarithmic) form of a charge relaxation. Therefore at small illuminations "the tail" of the photocharge that has remained in photodiode element at the first adjustment readout, appears much more than the additive of a charge during an exposition, and dominates at the second signal readout.

In the conclusion we emphasize that the carried out mathematical analysis has revealed the fundamental nature of CMOS photosensor signal characteristics nonlinearity. The understanding of it will undoubtedly facilitate for developers the overcoming of corresponding difficulties in the organization of a correct color rendering in wide range illumination intensities.

1. S. Mendis, S. E. Kemeny, E. R. Fossum., "A 128x128 CMOS active pixel image sensor for highly integrated imaging systems", Pros. IEEE IEDM Tech.Dig., pp. 583-586Dec. 1993.
2. S. Mendis, S.E. Kemeny and E.R. Fossum, "CMOS Active Pixel Image Sensor," IEEE Trans. Electron Devices, vol. 41(3), pp 452-453, 1994.

Quantum Mechanics as Emergent Phenomenon

Andrei Khrennikov
International center for mathematical modeling in physics, engineering and cognitive science, University of Vaxjo, Sweden

We show that, inspite the general opinion, one can obtain QM formalism as an approximative description of a classical statistical model. One of the crucial differences between mathematical models of classical and quantum mechanics is the use of the tensor product of the state spaces of subsystems as the state space of the corresponding composite system. To describe an ensemble of classical composite systems one uses random variables taking values in the Cartesian product of the state spaces of subsystems.
We show that, nevertheless, it is possible to establish a natural correspondence between the classical and quantum probabilistic descriptions of composite systems. Quantum averages for composite systems (including entangled) can be represented as averages with respect to classical random fields. It is essentially what Albert Einstein was dreamed of.
Quantum mechanics is represented as classical statistical mechanics with infinite-dimensional phase space. While the mathematical construction is completely rigorous, its physical interpretation is a complicated problem (which will not be discussed in this paper).

Dynamical Decoupling Pushed to the Extreme

V.M. Akulin

Laboratoire Aime Cotton CNRS ,Orsay, France

We propose a bang-bang technique for the universal control of evolution of an arbitrary n-level quantum system with simultaneous compensation for an arbitrary (unknown) static Hermitian noise up to a desired order of the perturbation theory. We show that a three-valued bang-bang Hamiltonian is necessary and sufficient for such a protection. Moreover, we present an explicit numerical algorithm how to compute the appropriate control signal, which is illustrated at the example of totally protected two-qubit gate.

Tunneling without tunneling: wavefunction reduction in a mesoscopic qubit

James A. Nesteroff and Dmitri V. Averin
Department of Physics and Astronomy, Stony Brook University, SUNY, Stony Brook, NY 11794-3800, U.S.A.

We consider a transformation cycle and associated inequality that provide the most basic demonstration of the wavefunction reduction in a mesoscopic qubit. In the evolution according to Schrödinger equation, the probability amplitudes c_j for the qubit to be in one of its two basis states $|j\rangle$ separated by a tunnel barrier, $j=0,1$, change their magnitude, i.e. the qubit tunnels between the basis states, only if the corresponding tunnel amplitude Δ (Fig. 1) is non-vanishing. The tunneling is suppressed exponentially by sufficiently large tunnel barrier. By contrast, in the process of the wavefunction reduction due to interaction with a quantum-limited detector which measures the σ_z operator with the eigenstates $|j\rangle$, the amplitudes evolve as follows: Equations must be centered and numbered on the right as the following one:

$$c_j \rightarrow c_j(q) = c_j \, [w_j(q)/(w_0(q)\,|c_0|^2 + w_1(q)\,|c_1|^2)]^{1/2} \qquad (1)$$

Here $w_j(q)$ is the probability of obtaining the detector output q when the qubit is in the jth basis state. This evolution implies that the probability amplitudes can be transferred even across the infinitely large barrier with vanishing tunnel amplitude.

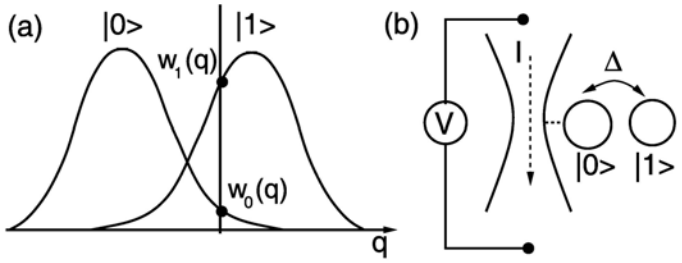

Fig. 1. Illustration of the qubit measurement process. (a) Typical probability distributions $w_j(q)$ of a detector output q for the qubit in the state $|j\rangle$, $j=0,1$. (b) Schematics of the particular measurement setup based on the quantum-point-contact (QPC) detector measuring mesoscopic ``charge" qubit. In this case, the qubit states $|j\rangle$ differ by position of some elementary charge which, through electrostatic interaction with electrons in the contact, controls the QPC transmission properties, and therefore the current I in the contact driven by the applied voltage V.

The purpose of the transformation cycle developed in this work is to demonstrate that the evolution of the wavefunction in the measurement process is ``real" to the same extent as the dynamics of wavefunction governed by the Scrödinger equation, i.e., it describes evolution of the physical quantities, e.g. electric charge or magnetic flux in typical solid-state qubits, and not only the information about them, even if the specific form of this evolution is qualitatively different. This is accomplished by combining the two types of evolution in one cycle which can be arranges so that they completely compensate each other, leaving the initial qubit state unchanged. The first part of the cycle is the partial wavefunction reduction in weak quantum-limited measurement which coherently changes the amplitudes c_j, mimicking the tunneling between the qubit states $|j\rangle$ in the situation, when Δ. The second part is the regular tunneling between the states $|j\rangle$ with nonvanishing $\Delta \neq 0$. In the ideal case, the cycle can be closed precisely, i.e., the qubit returns at the end precisely to the initial state. This implies that no charge or flux is transferred through the tunneling barrier in the whole cycle, and therefore, that the wave-function reduction induces tunneling even without the corresponding tunneling amplitude.

In the presence of the finite noise and detector non-ideality, the error probability p of qubit not returning to its initial state is non-vanishing, $p \neq 0$. Still, the probability $1-p$ with which the cycle is closed can be larger in this case than the classical value $1-p^{(cl)}$ explainable within the classical description of the measurement process. In this description, the state of the qubit before the measurement is well-defined classically and coincides with one of the two basis states localized on the opposite sides of the tunnel barrier, and the measurement provides information about this unknown state, i.e., changes only the probabilities assigned to this states. Experimental observation of the error probability smaller than the classical value: $p < p^{(cl)}$, would demonstrate that the actual qubit evolution in measurement is governed by the counterintuitive relations of the wavefunction reduction implying charge or flux tunneling through infinitely large barrier.

Superconducting Qubits

E. Il'ichev
Institute of Photonic Technology, P.O. Box 100239, D-07702 Jena, Germany

We review the recent results of experimental study of superconducting qubits. Instead of strong projective measurements, well known in quantum mechanics, we have proposed and realized weak continuous measurements which belong to class of quantum nondemolition measurements. In this scheme, which is widely used nowadays, the superconducting oscillator coupled to the superconducting qubit is used as a detector of the qubit's state.

Sisyphus mechanism of exchange energy between tank circuits and flux qubit is demonstrated. Consistency between ground state and spectroscopic measurements is convincingly shown. A fixed ferromagnetic, antiferromagnetic as well as tuneable qubit-qubit coupling is realized. We argue that the ground state measurements can be used for characterization of N coupled flux qubits.

Quantum Measurement of Open Systems

L. Fedichkin
Michigan State University, East Lansing, MI 48824, USA

Quantum measurements are often performed on open systems. Such measurements are of interest for various proposed realizations of a quantum computer where the qubit-qubit or qubit-environment coupling may not be completely turned off. Because of the coupling, the stationary state of system cannot be described by wavefunction, which is fully localized on individual system. As a result, an instantaneous projective single-qubit measurement gives the state population with an error.

We show that the highly precise measurement of open system is still feasible. The measuring detector can be much more sensitive to the individual quantum state than it seems from the rough estimate. Measurement error may be significantly reduced. The results bear on the scalability of uantum computers with qubits.

Simulation of entangled nuclei in two-atom association

B. Aksenov, Yu. Ozhigov

Lomonosov Moscow State University, Russia

We show how the heuristic of collective behavior can be used for the computer simulation of two-atom association in chemical reactions. It is shown how the choice of quantum world recombination during the reaction is fulfilled by means of the principle of minimal action. This method is scalable to more complex reactions, when the lack of classical memory serves as the absolute model of decoherence. We show the results of computer simulation of such reactions and compare the results with and without the entanglement selection.

Could the Schrodinger's Cat be used as Quantum Bit?

V.V. Aristov and A.V. Nikulov

Institute of Microelectronics Technology, Russian Academy of Sciences, 142432 Chernogolovka, Moscow District, Russia. E-mail: nikulov@ipmt-hpm.ac.ru

The idea of the quantum computation is based on the most paradoxical quantum principle – entanglement of states. The term "entanglement" was coined in 1935 by Erwin Schrodinger [1] who was motivated by the famous paper [2] of Einstein, Podolsky and Rosen (EPR). Schrodinger consider the "entanglement of our knowledge" as the essence of quantum mechanics [3]. He wrote in [4]: "Maximal knowledge of a total system does not necessarily include total knowledge of all its parts, not even when these are fully separated from each other and at the moment are not influencing each other at all". In order to elucidate the essence of the "entanglement of our knowledge" Schrodinger has proposed in [1] the paradox with a cat in which he has entangled states of atom and cat. Both paradoxes proposed in 1935, EPR [2] and Schrodinger's cat [1], demonstrate that quantum mechanics is not a complete theory in the sense, that it does not describe an objective reality in which each effect has a cause. Niels Bohr and Verner Heisenberg did not contest that quantum mechanics does not describe a reality. Bohr stated: "*There is no quantum world. There is only an abstract quantum physical description*", see [5] and Heisenberg realized [6] that quantum mechanics can not describe what happens between measurements. The controversy between the founders of quantum mechanics concerned the object of physics. Einstein and Shhrodinger insisted that physics should investigate a reality whereas adherents of the Copenhagen interpretation proposed by Bohr and Heisenberg stated that a reality is only metaphysical prejudice and the object of physics is a description of phenomena which we observe. Most physicists studied during many decades quantum mechanics in its Copenhagen interpretation since it turned out, that it is impossible to describe some quantum phenomena as manifestation of real processes. According to the positivism point of view of the adherents of the Copenhagen interpretation such description is not needed. But how can we make a real equipment without a description of a reality? This question is especially urgent for quantum computer since quantum computation assumed to be between measurements and consequently quantum mechanics can not describe the process of the quantum computation. This paradoxical situation will be considered in the present work. Combining the two paradox [1,2] of two opponents of positivism, Einstein and Schrodinger, we will show that Schrodinger cats can be used as quantum bits according to the positivism point of view.

1. E. Schrodinger, "Discussion of probability relations between separated systems," Proc. Cambridge Phil. Soc, 31, pp. 555-563, 1935.
2. A. Einstein, B. Podolsky, and N. Rosen "Can Quantum - Mechanical Description of Physical Reality Be Considered Complete?" Phys. Rev. 47, pp. 777-780, 1935.
3. C. Brukner, M. Zukowski, A. Zeilinger, «The essence of entanglement», E-print arXiv: quant-ph/0106119.
4. E. Schrodinger, "Die gegenwartige Situation in der Quantenmechanik," Naturwissenschaften 23, pp. 807-812; pp. 823- 828; pp. 844-849, 1935. Translation published in Quantum Theory and Measurement edited by J. A. Wheeler and W. H. Zurek(Princeton University Press, Princeton), pp. 152-167, 1981.
5. C. Brukner, A. Zeilinger, "Information and fundamental elements of the structure of quantum theory", *Contribution to the Festschrift for C. F. v. Weizsaecker on the occasion of his 90th birthday*; E-print arXiv: quant-ph/0212084
6. Werner Heisenberg, *Physics and philosophy: the revolution in modern science*, Princeton University Press, 1999.

Unified Statistical Method for Tomography of Quantum States by Purification

Yu.I. Bogdanov

Institute of Physics and Technology, Russian Academy of Sciences, Moscow, Russia

Mixed state purification is used as a basis to formulate a general method for statistical reconstruction of density matrix of an arbitrary quantum state. A universal statistical distribution is obtained for the accuracy of the reconstructed quantum state. The proposed theory is confirmed by results of numerical simulations.

Information aspects of «which way» experiments with microparticles

Yu.I. Bogdanov*, K.A. Valiev*, S.A. Nuyanzin**, A.K. Gavrichenko*

**Institute of Physics and Technology, Russian Academy of Sciences, Moscow, Russia*
***Moscow Institute of Electronic Technology (Technical University),Zelenograd, Russia*

In present work we study informational measures for the problem of interference of quantum particles. We demonstrate that diffraction picture in the far field, which is given by probability density of particle momentum distribution, represents a mixture of probability densities of corresponding Schmidt modes, while the number of modes is equal to the number of slits in the screen.

The paper analyses the phenomenon of optical coherence by means of completing a mixed state to a pure state by purification procedure. It proposes several informational characteristics describing the quality of interference picture and explains the relation between visibility of the interference picture and its Schmidt number. The analysis is provided for different settings of "which way" experiments. Finally, results of numerical calculations of two and three-slit interference of Rydberg atoms obstructed by trajectory-tracking resonators are described in detail.

Simulation of electron jumps in the collision of two hydrogen atoms

K. Burtniy[1], Yu. Ozhigov[1,2]

1. Institute of physics and technology, RAS, Moscow, Russia
2. Lomonosov Moscow State University, Russia

We describe the simple method of the computer simulation of electron dynamics in the collision of a hydrogen atom and a proton. We show the computation of the relative probability of two possible channels: recharge and complete dissociation; the forming of the molecular ion of hydrogen turns to be negligible and happens for extremely small speeds of reagents. For the computer simulation, we used the heuristic of collective behavior and the scenario at the sparse grid corresponding to the nuclei. We obtained the good visual pictures of the dynamics of protons and electron in the association for the considered channels.

Quantum Entanglement and its Observation at Measurement of Magnetic Succeptibility and in Multiple Quantum NMR Experiments

E.B. Fel'dman

Institute of Problems of Chemical Physics of Russian Academy of Sciences, Chernogolovka, Moscow Region, 142432, Russia; e-mail: efeldman@icp.ac.ru

The choice of chemical compounds for quantum registers is an important problem for creating quantum computers. Chains of electron and nuclear spins are appropriate systems if all spin pairs are in the entangled states. We work out methods for experimental study of the entanglement with the measurement of the magnetic susceptibility [1,2] and with multiple quantum (MQ) NMR spectroscopy [3]. We show that quantum-mechanical entanglement of the spin degrees of freedom exists in binuclear nitrosyl iron complexes [1]. Our conclusions are based on the analysis of the experimental data which was obtained from the measurement of the magnetic susceptibility of polycrystalline samples of these complexes [2]. The entanglement exists below 90^0 K in binuclear nitrosyl iron complexes. The temperature dependence of the entanglement of these complexes can be found using an expression of the entanglement in terms of the magnetic susceptibility for a Heisenberg dimer. It is shown that the entanglement measure monotonically increases when the temperature decreases. Decoherence times are significant for quantum registers with electron spins. These times restrict possibilities of using such registers. The decoherence times of nuclear spins exceed the corresponding times of electron spins by several orders. We investigate the evolution of the entanglement in MQ NMR experiments in crystals with pairs of close nuclear ½-spins [3]. The initial thermodynamic equilibrium state of the system in a strong external magnetic field evolves under the non-secular part of the dipolar Hamiltonian. As a result, MQ NMR coherences of the zeroth and plus/minus second orders emerge. A simple condition for the emergence of the entanglement is obtained. We show that the measure of the spin pair entanglement (concurrence) coincides qualitatively with the intensity of MQ NMR coherence of the plus/minus second order and, hence, entanglement can be studied with MQ NMR methods. We find the threshold between separable and entangled states of the spin pair which depends on the temperature and the external magnetic field. The entangled states of the pair of nuclear spins emerge at millikelvin temperatures [3]. We introduce an entanglement witness using MQ NMR coherences of the plus/minus second order.

1. S.M.Aldoshin, E.B.Fel'dman, M.A.Yurishchev, JETP, **107**, No.5, pp.804 -811 (2008).
2. N. A. Sanina, S. M. Aldoshin, T. N. Rudneva, et al., J. Mol. Struct. **752**, 110 (2005).
3. E.B.Fel'dman, Pyrkov A.N., JETP Letters **88**, No.6, pp.398-401 (2008).

[1]The work is supported by the Russian Foundation for Basic Research (project no. 07-07-00048)

The qubit states decoherence in antiferromagnet-based nuclear spin model of quantum register

Alexander A.Kokin[a], Vladimir A.Kokin[b]
[a]*Institute of Physics and Technology of RAS, 34, Nakhimovskii pr., 117218, Moscow, Russia*
[b]*Institute of Radioengineering and Electronics of RAS, 11,Mokhovaya str, 103907, Moscow Russia*

This study deals with the further development of nuclear spin model of scalable quantum register, which presents the one-dimensional chain of the magnetic atoms with nuclear spins 1/2, substituting the basic atoms in the plate of nuclear spin free easy-axis 3D antiferromagnet.[1]. The decoherence rates of one qubit state and entanglement state of two removed qubits are caused by the interaction of nuclear spins-qubits with virtual spin waves in antiferromagnet ground state were calculated. We have considered also decoherence of encoded DFS (Decoherence-Free Subspaces)-states of logical qubits are constructed on clusters of the four-physical qubits, given by the two states with zeroth total angular momentum.

[1] A.A. Kokin and V.A. Kokin, Proc. SPIE Vol. 7023, 70230B (2008); LANL arXive: quant-ph/ 0812.9135.

Quantum Double Helix

A.Yu.Okulov[1]
General Physics Institute of Russian Academy of Sciences
Vavilova str. 38, 119991, Moscow, Russia, okulov@kapella.gpi.ru

The double helix is an intrinsic geometry of proteins [1]. The analogous double helix structures were reported recently for dusty plasmas [2] and for the interference of the phase-conjugated speckle fields in Brillouin scattering [3]. The helical wavefronts around phase singularities [4] of the optical speckle fields were shown to form the spiral structures in Brillouin medium. This process is not accompanied by change of photon's *helicity* [5] but orbital component of the angular momentum (OAM) $L_z = \hbar$ is reversed. The conservation of angular momentum requires as a must an excitation of a spiral acoustical phonon [6] with doubled vorticity and doubled OAM $L_z^{ac} = 2 \cdot \hbar$ [3]. In classical picture spiral acoustical phonons form the circular flow around phase singularity. The whole picture in inhomogeneous speckle field is composed of randomly spaced optical vortex-antivortex pairs with collocated acoustical vortices [7]. The reflection of light beams via nondegenerate four-wave mixing from ultracold atomic cloud had been reported to form corkscrew interference pattern in cloud and rotational motion of cold matter around phase singularity [8]. The goal of present communication is in consideration of the disordered bosonic cloud with coherent backscattering from random medium[9]. We will discuss the BEC trapping in helical optical dipole traps which might extend the set of controllable quantum dynamics system [10].

The "envelope" complex amplitudes of Heisenberg annihilation operators [5] for optical pump wave $\Psi_f(z,r,\theta,t)$ moving in positive direction of z-axis and Stockes wave $\Psi_b(z,r,\theta,t)$ moving in negative direction of z-axis are described by the following system of equations:

$$\frac{\partial \hat{\Psi}_f(z,r,\theta,t)}{\partial z} + \frac{\partial \hat{\Psi}_f(z,r,\theta,t)}{c \quad \partial t} + \frac{i}{2k_f}\Delta_\perp \hat{\Psi}_f = -\frac{i\gamma\omega_f}{4\rho_0 nc}\hat{\Psi}_b\hat{\Phi}$$

$$\frac{\partial \hat{\Psi}_b(z,r,\theta,t)}{\partial z} - \frac{\partial \hat{\Psi}_b(z,r,\theta,t)}{c \quad \partial t} - \frac{i}{2k_b}\Delta_\perp \hat{\Psi}_b = \frac{i\gamma\omega_b}{4\rho_0 nc}\hat{\Psi}_f\hat{\Phi}^*$$

The "envelope" annihilation operator $\Phi(z,r,\theta,t)$ for bosonic matter-wave moving in positive direction of z -axis obeys to:

$$v_{ac}\frac{\partial \hat{\Phi}(z,r,\theta,t)}{\partial z} + \frac{\partial \hat{\Phi}(z,r,\theta,t)}{\partial t} + \frac{\Gamma}{2}\hat{\Phi} = \frac{i\gamma k_{ac}^2}{16\pi\omega_{ac}}\hat{\Psi}_f\Psi_b^*$$

The expectation value of matter-wave annihilation operator near phase singularity $\Phi_{helical}(z,r,\theta,t)$ is obtained as follows [3]:

$$\left\langle \hat{\Phi}_{helical}(z,r,\theta,t)\right\rangle \approx \left\langle \hat{\Psi}_f\Psi_b^*\right\rangle \approx exp[i2\ell\varphi]r^{2\ell}\,exp\left(-\frac{2r^2}{D^2(1+z^2/k_P^4 D^4)}\right)$$

References.
1. Watson J.D. and Crick F.H.C., Nature, 171, pp. 241-257, 2008.
2. V.N.Tsytovich, Phys.Usp., 177, p. 428, 2007.
3. A.Yu.Okulov, J.Phys.B., 41, 101001, 2008.
4. J.F.Nye and M.V.Berry, Proc. R. Soc. London, A336, 165, 1974.
5. E.M.Lifshitz, L.P.Pitaevskii, and V.B.Berestetskii, "Quantum Electrodynamics", (Landau and Lifshitz Course of Theoretical Physics,Oxford, Vol.4,1982.
6. R.Marchiano,F.Coulouvrat,L.Ganjehi,J-L.Thomas, Phys.Rev., E 77, 016605, 2008.
7. A.Yu.Okulov, JETP Lett. 88 ,561, 2008.
8. D.V.Petrov and J.W.R.Tabosa, Phys. Rev. Lett., 83, 4967, 1999.
9. V.S.Letokhov, JETP, 7 ,n.9, p.272, 1968.
10. K.A.Valiev, Phys. Usp., v.48, p.1, 2005.

Time-optimal control of quantum dynamics of a quadrupole nucleus by NMR techniques

V. P. Shauro, V. E. Zobov
L.V.Kirensky Institute of Physics, Siberian Branch, Russian Academy of Sciences, Krasnoyarsk, Russia, rsa@iph.krasn.ru

Recently the problem of quantum system control is of great interest. Particularly the time-optimal control of spin systems plays an important role in the realization of quantum computation by nuclear magnetic resonance (NMR) techniques. In this work we consider the problem of time-optimal control in order to implement the selective rotation on a multi-level quantum system (qudit). The quantum computation on qudits has a number of advantages compared to qubits, but there are very few paper devoted to the qudit control. As a quantum system we have chosen a quadrupole nucleus with spin $I > ½$ placed in a static magnetic field and controlled by an external radiofrequency (rf) magnetic field. In a reference frame rotating with rf frequency which equal to the Larmor frequency, the Hamiltonian of this system is

$$H = q\left(I_z^2 - I(I+1)\right) + u_x(t)I_x + u_y(t)I_y,$$

where I_α is the spin projection operator onto the α axis, q is the constant of quadrupole interaction with the axially symmetric electric field gradient and $u_\alpha(t)$ is the amplitude of control rf field along the α axis. As a computational basis of qudit we take the states with different spin projection onto the z axis, e.g. $I_z = -1, 0, +1$ corresponds to the $|-1\rangle$, $|0\rangle$ and $|+1\rangle$ basis states for I=1.

For the NMR implementation of selective rotation the time dependence of control field amplitude and phase were found by numerical optimization (using the gradient ascent pulse engineering (GRAPE) algorithm [1]) with the different durations of the RF field. These calculations allowed to estimate the optimal time for spins I=1 and I=3/2 and to compare it with the results obtained in our previous work [2]. For the spin I=1, we found that the value of optimal time obtained numerically is very close to the minimal time obtained analytically in [2] which equal to the total duration of the intervals of free evolution between rf pulses. For the spin I=3/2, the numerical and analytical optimal times also are close in case of the rotation between $|-½\rangle$ and $|+½\rangle$ states. But for the rotation between $|-3/2\rangle$ and $|-½\rangle$ (or $|+½\rangle$ and $|+3/2\rangle$) states the optimal time estimated numerically is less than analytical one. Hence the rf pulse sequences which perform this operation in a shorter time can be found. Moreover the numerical solution for the control field $u_\alpha(t)$ is more preferable from the point of view of the experimental realization because the rf field vary smoothly and have lower amplitude as compared with the pulse sequences in [2]. The presented results of numerical simulations are interesting in the view of an experimental implementation of quantum computation on quadrupole nuclei by NMR techniques.

This work was supported by the Russian Foundation for Basic Research (project. no. 09-07-00138) and Dynasty Foundation.

1. N. Khaneja, T. Reiss, C. Kehlet et al., “Optimal control of coupled spin dynamics: design of NMR pulse sequences by gradient ascent algorithms”, J. Magn. Reson., **172**, pp. 296-305, 2005
2. V. E. Zobov and V. P. Shauro, “Selective control of the states of multilevel quantum systems using nonselective rotation operators”, J. Exp. and Theor. Phys., **V. 108**, No. 1, pp. 5-17, 2009

Resonant dipole-dipole interaction of a few cold Rydberg atoms in a magneto-optical trap

D.B.Tretyakov[1], I.I.Beterov[1], V.M.Entin[1], I.I.Ryabtsev[1], P.L.Chapovsky[2]
1. Institute of Semiconductor Physics SB RAS, Novosibirsk,Russia, E-mail: dtret@isp.nsc.ru
2. Institute of Automation and Electrometry SB RAS, Novosibirsk, Russia

Long-range interactions of Rydberg atoms have been proposed for use in a quantum computer based on trapped neutral atoms [1,2]. We have studied the dipole-dipole interaction of a small definite number of cold rubidium Rydberg atoms in a magneto-optical trap (MOT) theoretically and experimentally.

The initial 37P Rydberg state was excited from 5P state by the two pulsed lasers in crossed-beam geometry. The laser beams were focused inside of the cold atom cloud and intersected at right angles, providing a small excitation volume of about 30 micrometers in size. Each laser pulse excited a few Rydberg atoms, which were detected by the selective field ionization technique using a channeltron that provides a single-atom resolution of up to 5 atoms.

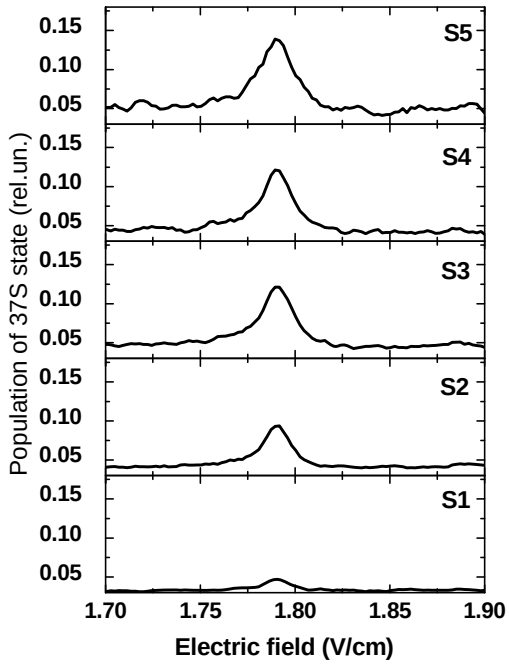

Fig. 1. The experimental spectra of the resonant dipole-dipole interaction observed in the Rb MOT for 1-5 detected Rydberg atoms.

We observed the Forster resonance transitions driven by the dipole-dipole interaction in the following scheme:

$$Rb(37P) + Rb(37P) \rightarrow Rb(37S) + Rb(38S).$$

Exact resonance for this energy-exchange process was achieved by Stark tuning of the Rydberg energy levels. The atomic signals were sorted over the number of detected atoms. The experimental spectra of the resonant dipole-dipole interaction for selectively detected 1 to 5 Rydberg atoms are shown in Fig. 1. The dependences of the peak heights and widths on the number of Rydberg atoms were analyzed and compared with theory using a many-particle Monte-Carlo model for definite number of Rydberg atoms randomly positioned in the excitation volume.

This work was supported by the Russian Academy of Science and Russian Foundation for Basic Research.

1. D.Jaksch *et al*, "Fast quantum gates for neutral atoms", Phys. Rev. Lett., 85, №10, pp.2208-2211, 2000.
2. M.D.Lukin *et al*, "Dipole blockade and quantum information processing in mesoscopic atomic ensembles", Phys. Rev. Lett., 87, 037901, 2001.

Problems of nano-sized and high aspect ratio features plasma etching

V. Lukichev[1], K. Rudenko[1], A. Orlikovsky[1] V. Yunkin[2]

1. Institute of Physics and Technology of Russian Academy of Sciences, Moscow, Russia. E-mail: lukichev@ftian.ru

2. Institute of Microelectronics Technology of Russian Academy of Sciences, Chernogolovka, Russia.

More than 20 years deep anisotropic plasma etching processes of silicon are under developing. Most details of them are well understood and processes are realized in modern semiconductor industry. Main problem appeared was so called aperture effect (also referred to as aspect ratio dependent etching, ARDE) or in general the decrease of the etching rate with the feature size shrinkage (or aspect ratio increase). It became essential at opening sizes below one micron. Several theories were suggested and different approaches were proposed to overcome it. The most challenging was etching of high aspect ratio (HAR) submicron structures like capacitors in DRAM and diffractive elements in optics. In the former case ARDE resulted in different depth and shape of features with different sizes. The problem was partly solved for given feature size (or very narrow range of sizes) by using RIE, ICP or MERIE systems and gas mixtures to passivate feature sidewalls while directed high energy ion flux bombardment assists bottom etching. Such approach has evident drawback: ion angle distribution has non-zero average divergence. So one can achieve only aspect ratios about reciprocal average angle. This means that usage of mixed chemistries which produce both active and passivating precursors in plasma has own limit.

Another approach realized in deep reactive ion etching (DRIE) utilizes chopped etching consisting of two separate steps, which are repeated: etching and passivation. This process was called Bosch one after the inventor and was based on high density inductively coupled (ICP) plasma sources. There is no need to have anisotropic etch step which is relatively short. Despite the Bosch process allows one to obtain high etch rate and to realize etching from through wafer to submicron size features with high aspect ratios, some serious drawbacks exist such as ARDE, notching at the insulating etch stop layer, microscopic nonuniformities, and feature sidewalls ripples. The former is not so crucial for several tens micron features used in standard MEMS but is very critical in optical structures.

Special issue is aspect ratio independent etching, e.g. in X-ray optics wedge layout where AR should range from several units to formally infinity.

We focus on demands of ITRS beyond 22 nm technology node for DRAM capacitors, nanotransistor structures, and nano-optical electromechanical systems (NOEMS) which involve plasma processing. We also discuss demands and problems of process monitoring including chamber wall conditions and small percentage of openings.

In addition to technological issues like materials and chemistries we consider physical limitations of HAR structures formation.

The investigation was supported by Russian Foundation for Basic Research, grant # 09-07-00359-a

Nucleation and growth of Ge nanoislands on pit-patterned Si substrates

J.V. Smagina[1*], P.L. Novikov[1], A.S. Deryabin[1], E.E. Rodyakina, D.A. Nasimov[1], B.I. Fomin[1], V.A. Zinovyev[1], A.V. Dvurechenskii[1,2]

1. *Institute of Semiconductor Physics SB RAS, 630090, Novosibirsk, Russia,*
2. *Novosibirsk State University, 630090, Novosibirsk, Russia.*

* *E-mail: smagina@isp.nsc.ru*

Dense and homogeneous arrays of Ge quantum dots (QDs) on Si are a promising object for applications in microelectronics. These applications require space arrangement of QDs arrays embedded in crystalline matrix. For that reason it's a challenge to develop an effective method of fabricating ensembles of Ge nanoislands on Si substrates. At present, there exist several approaches for controlling nucleation and heteroepitaxial growth of nanocrystals. These include preliminary deposition of submonolayer coatings formed by impurity elements (antimony, oxygen) [1], the formation of strained layers (the preliminary growth of solid solution layers) [2], generation of nucleation centers by the deviation from singular planes [3], pulsed irradiation by low-energy ions [4], etc. The great success in formation of space arranged QDs arrays was achieved by growth on pit-patterned substrates [5]. However, some aspects of the ordering process are not studied yet.

In this work we have studied the effect of temperature, amount of Ge deposited and crystalline surface orientation on the nucleation and growth of Ge nanoislands ensemble on shallow pit-patterned Si substrates. The pit patterning was performed by electron-beam lithography and subsequent plasma chemical etching. Circle-shaped pits with a diameter of 50 nm, a depth of 10 nm, and a periodicity of 100 nm were etched in the Si(111) and Si(100) substrates. The structures were grown by molecular-beam epitaxy at a deposition rate of approximately 0.1 ML/s in temperature range of 300–450 °C. The total amount of deposited germanium was varied from 3 to 7 atomic layers. The morphology of the surfaces were *ex situ* analyzed by atomic force microscopy.

Spatially ordered arrays of Ge nanoislands were obtained on Si(111) at low temperature (400 °C). Their size distribution (50±4 nm) is narrower than that for islands grown on unpatterned surface (42±14 nm). Initial stage of island growth was investigated. We have found that nucleation of islands occurs at the edge of the pits (2–3 islands per pit). Further deposition of Ge gives rise to coalescence of islands within each pit. Ge islands grown on Si(100) substrate were observed both in pits and between them. An island average size is ~10 nm, and islands density is $9 \cdot 10^{10}$ cm^{-2}. We believe that at higher temperatures (>450 °C) the fraction of Ge islands formed in pits should be increased.

The mechanism of island formation was studied by molecular dynamics (MD) and Monte Carlo (MC) calculations. Using MD calculations in the case of Si(100) the potential relief at the edge of a pit was built, and the paths of favorable Ge migration into the pits were determined. MC simulations were performed for Si(100) and Si(111) substrates. In the both cases MC simulations exhibit space arrangement effect at 400 °C.

This work was supported by RFBR (grants No.09-02-00882, 09-02-00377) and Russian Academy of Sciences.

1. C.S. Peng, et al. Appl. Phys. B, 62, pp. 2541, 2000.
2. N.V. Vostokov et al. Phys. Solid State, 47, pp. 26, 2005.
3. J. Zhu et al. Appl. Phys. Lett, 73, pp. 620, 1198.
4. J.V. Smagina, et al. JETP, 106, pp. 517-527, 2008.
5. G. Bauer, F. Schaffler, Phys. State. Sol. 203, pp. 3496, 2006.

Nanoscale Si/SiO_2 superlattices produced using plasmochemical technology

S.A. Arzhannikova[1,2], M.D. Efremov[1,2], A.Kh.Antonenko[1,2], V.A. Volodin[1,2], G.N. Kamaev[1,2], D.V. Marin[1,2], S.A. Kochubei[1], A.A.Voschenkov[1]

1. Institute of Semiconductor Physics, Russian Academy of Sciences, Novosibirsk, Russia, efremov@isp.nsc.ru, 2. Novosibirsk State University, Novosibirsk, Russia, nsm@nsm.nsu.ru

Silicon based superlattices attract scientists due to combination of well known good properties of Si/SiO_2 interface and possibility for realization of quantum properties at room temperatures due to large difference in forbidden zone values. Ways were elaborated for deposition of silicon dioxide films using hexamethyldisilozan and hexamethyldisiloxan, as well as amorphous silicon films from mixture of monosilane and argon. Analysis of capacitance characteristics reveals good electronic properties of the interface, so quite low fixed charge was detected (about $4\cdot10^9$см$^{-2}$) and interface density of states (from $5\cdot10^{11}cm^{-2}\cdot eV^{-1}$ in the middle of forbidden zone up to $5\cdot10^{12}cm^{-2}\cdot eV^{-1}$ near the edge of one). Achieved growth rates for deposition was allowed to deposit Si, SiO_2 films with thickness above 20nm. Mode for manufacturing of SiO_2 films with thickness above 2nm was found owing to oxidation of amorphous and crystalline silicon in plasma of pure oxygen. Multilayered structures were manufactured with interlaced layers of amorphous silicon and its oxide with correspondent thickness 5,15nm.

Thermal treatment leaded to modification of Raman spectra according to phase transformation (fig.1). After annealing the increasing of Raman signal was discovered both at $520cm^{-1}$ and at $480cm^{-1}$ possibly due to resonant effect. Increasing of the intensity near $520cm^{-1}$ interpreted as transformation of amorphous silicon into crystalline form. Electrical measurements reveal significant peculiarities connected with charge transport through prepared superlattices. At positive voltages and low frequency sharp increasing of capacitance was detected in correlation with conductivity behavior (fig.2). Possibly this effect is connected with alternative current originating from charge exchanging between substrate and silicon dioxide layer. The exchanging may be the sequence of recharging of small silicon clusters or crystallites formed in dielectric layer.

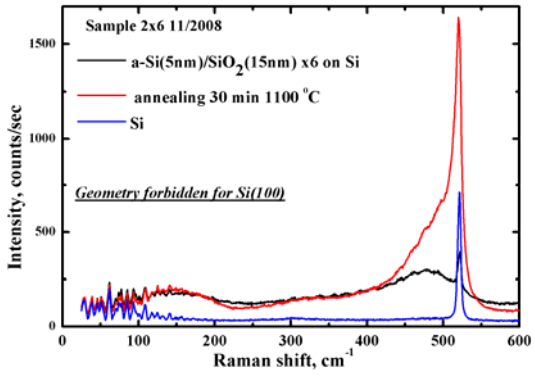

Fig. 1. Raman spectra for substrate (blue) and for SL (Si-5nm/SiO_2-15nm)x6 before (black) and after (red) annealing at 1100C, 30min.

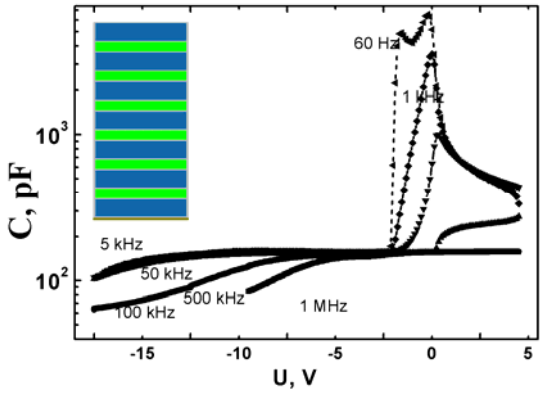

Fig. 2. Frequency dependent differential capacitance for MOS structure with multilayered dielectrics (Si-5nm/SiO_2-15nm)x6.

Impurity activation and nanocrystals formation using excimer lasers

M.D. Efremov[1,2], S.A. Arzhannikova[1,2], V.A. Volodin[1,2],
G.N. Kamaev[1,2], S.A. Kochubei[1], I.G.Neizvestny[1]
1. Institute of Semiconductor Physics, Russian Academy of Sciences, Novosibirsk, Russia, efremov@isp.nsc.ru, 2. Novosibirsk State University, Novosibirsk, Russia, nsm@nsm.nsu.ru

Amorphous silicon represents free-ordered material having significant meaning in modern applications. This paper represents itself the study simultaneous nucleation and impurity activation, contributions in conductivity which was seemed to distinguish difficultly.

Research of electronic properties was provided for amorphous films with silicon nanocrystals, formed at nanosecond laser irradiation. It was discovered, that for Si-nanocrystals with dimensions about 2nm changing of conductivity mechanism was detected with lowering of activation energy from 0.7eV down to 0.12-0.17eV. Calculations of temperature dependence for Fermi energy in amorphous Si-films was realized within representation of nanocrystals as multi-charged centers. Computation has demonstrated pinning Fermi energy close to values of energetic levels localized inside of nanocrystals, depending on background doping level.

For the similar laser treatments regimes transition of boron and phosphorus atoms in electrical active state was detected without melting of a-Si films. That allows to conserve initial spatial distributions of B,P atoms. Spread resistances as well as ampere-voltage (I-V), capacitance-voltage (C-V) characteristics for p-n junctions were studied revealing quite good electrical properties. Laser treatments at large energy density and thermal treatments leaded to full activation of boron and increase of p-n junction depth up to 400-500nm. Full concentration of boron was registered by means of SIMS method detecting spatial distribution variation (fig.1). Using Raman spectroscopy proved the activation due to observed increasing of the peak corresponding to Si-B vibrations when boron is found in tetrahedral configuration surrounded by Si atoms, i.e. in electrical active state. Plasma immersion and ion implantation were used for formation of initial samples, as well as doping during growth process, what gave variation of boron distribution depth from 20nm to 100nm.

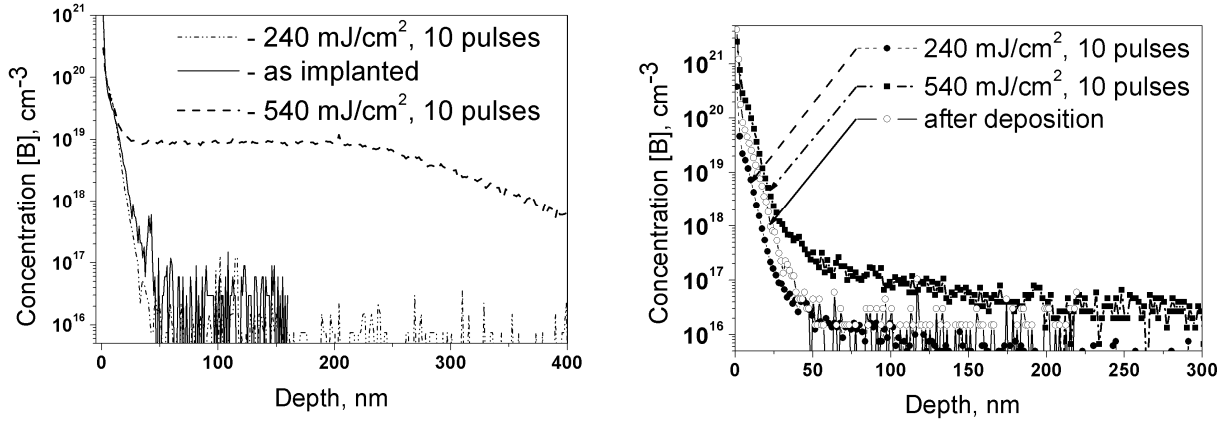

Fig. 1. SIMS profile for boron atoms both as prepared by means of plasma immersion implantation (left) and plasma chemical deposition (right) and after excimer laser treatments.

Femtosecond and nanosecond laser assistant formation of Si nanoclusters in silicon-rich nitride films

V.A. Volodin[1,2], T.T. Korchagina[1], G.N. Kamaev[1], A.H. Antonenko[1], J. Koch[3], B.N. Chichkov[3]

1. Institute of Semiconductor Physics, Russian Academy of Sciences, Lavrent'eva ave., 13, 630090, Novosibirsk, Russia, E-mail address: volodin@isp.nsc.ru *2.Novosibirsk State University, Pirogova street, 2, 630090, Novosibirsk, Russia. 3.Laser Zentrum Hannover, Hollerithallee 8, 30419 Hannover, Germany*

Semiconductor nanocrystals (NCs) embedded in dielectric films attract much interest due to their optical and electronical properties, which can be modified by varying its sizes. The dependence of energy of optical transition on the NC size is also called quantum-size effect. This effect for Si NCs in dielectric matrix becomes brightly apparent at room temperature, and because in some experiments a single NC reveals delta-function-like photoluminescence spectra [1], the NCs can be called as quantum dots. The NCs have shown significant promises for a wide range of nanoelectronic and optoelectronic applications. In metal-dielectric-semiconductor structures based on silicon-rich nitride (SRN) films an effective electroluminescence was achieved. Red, green and blue light emitting diodes were demonstrated [2]. SRN films are non-stoichiometric SiNx films (x<4/3). There are reproducible, not expensive, low temperature technologies for deposition of SRN films. The additional silicon atoms in some SRN films are randomly distributed in a SiN_x matrix. They do not form nanoclusters (random bonding - RB model). Some SRN films contain amorphous Si nanoclusters, which depends on growth condition. This situation is close to random mixture - RM model. The problems of formation of amorphous Si nanoclusters and its crystallization are topics in current research. The laser induced crystallization has several advantages comparing to long time high temperature furnace annealing [3]. This work is devoted to development of laser assisted formation of amorphous Si nanoclusters in SRN films and its crystallization.

The initial SRN films were deposited using low frequency plasma enhanced chemical vapor deposition technique on crystalline Si (100) and glass substrates. The stoichiometric parameter x in the SiN_x:H films was varied from 0.6 to 1.3 using various ratios of SiH_4 and NH_3 gases in reactor during deposition. Raman spectroscopy technique was used to identify the structure (amorphous or crystalline) of Si nanoclusters in the films.

The nanosecond pulse KrF and femtosecond pulse Ti-Sapphire laser (FemtoPower Compact Pro, Femtolasers Produktions GmbH) with a central wavelength of 800 nm and pulse duration of <30 fs were used for laser treatments of initial SRN films.

Raman data show that initial SRN films (with stoichiometric parameter x<1.2) contain amorphous Si nanoclusters. Laser treatments lead to crystallization of these clusters. The average sizes of Si NCs were estimated from Raman data. The sizes depend on stoichiometric parameter x and also on parameters of laser treatments. So, the average sizes of Si NCs can be controllable changed from 1-2 nm to 5-6 nm. It is very important that laser pulse treatments lead not only to crystallization of amorphous Si clusters existing in the initial films but also to formation of silicon nanoclusters in films with relatively low concentration of additional silicon atoms. It was supposed, that in the case of femtosecond laser treatments the non-linear effects play an important role in light absorption. Silicon nitride is dielectric with optical gap about 5 eV. Average energy of photons in Ti-sapphire laser is 1.5 eV. This is not enough for effective absorbance even in a-Si:H films with optical gap 1.5-1.9 eV. So, multi-photon processes should take place. Mechanism of phase transition can also be not purely thermal.

It should be noted that femtosecond laser treatments were applied for the first time for crystallization of amorphous silicon nanoclusters in SRN films. The laser fluences for crystallization were found for the films of various non-stoichiometries. The effect of laser assistant formation of amorphous Si nanoclusters in SRN films with relatively low concentration of additional silicon atoms was observed. The developed approach can be used for the creation of dielectric films with semiconductor nanoclusters on non-refractory substrates.

1. I.Sychugov, R.Juhasz, J.Valenta, and J.Linnros, Phys. Rev. Lett. **2005**, 94, 087405.
2. Nae-Man Park, Tae-Soo Kim, Seong-Ju Park. Appl. Phys. Lett. **2001**, 78, 2575.
3. V.A.Volodin, M.D.Efremov, V.A.Gritsenko, S.A.Kochubei. Appl. Phys. Lett. **1998**, 73, 1212.

Optical diagnostics of GaAs nanoheterostructures growth processes

I.P. Kazakov, E.V. Glazyrin, V.I. Tsekhosh
P.N. Lebedev Physical Institute of Russian Academy of Sciences, Moscow, Russia, E-mail address: ipkazakov@yandex.ru

During the recent years, optical reflectance observation methods are being widely developed as *in situ* diagnostics methods of semiconductor heterostructures growth processes. Being non-destructive, showing large probing depth, these methods are a significant supplement to commonly used reflectance high-energy electron diffraction (RHEED) in molecular beam epitaxy (MBE) technological processes. Moreover, for chemical vapour deposition growth processes optical methods are the only way of non-destructive *in situ* observation. In the present work the possibility of growth monitoring in visible and near-IR wavelenghts was studied *in situ* for heterostructures with ultrathin films (few monolayers thick).

Heterostructures for resonant tunneling diodes (RTD) with AlAs 2,3 nm/GaAs 4,0 nm/AlAs 2,0 nm active zone (Fig. 1) were grown by MBE on GaAs substrates (001). Various stages of heterostructures growth (oxide removal, buffer layer growth, active zone growth) were studied by Laytec EpiRAS IR TT optical spectrometer. Time dependences of reflectance and reflectance anisotropy were analyzed for normal incidence of the light beam with 500 nm and 950 nm light waves. Obtained dependences clearly indicated different processes occurring on heterostructures surface during growth: oxide desorption, surface reconstruction transition, changes of surface roughness.

Fig. 2 shows a time dependence of reflectance anisotropy signal at 495 nm wavelength during RTD active zone formation. GaAs/AlAs is clearly observed in the curves, despite the small thickness of the layers. Rapid changes of reflectance anisotropy signal on heterointerfaces are most likely caused by anisotropy induced by Ga atoms replaced by Al and vice versa, as the *in situ* RHEED patterns do not indicate reconstruction transition. It has been shown that the method of optical diagnostics, used throughout the whole process of RTD heterostructure growth, allows to gain the necessary information for fine-tuning and accurate control of MBE semiconductor growth technology.

The research was supported by RFFI grant № 08-02-00451-a

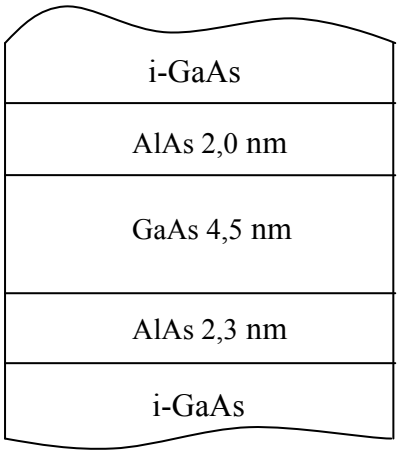

Fig. 1.Scheme of RTD active zone

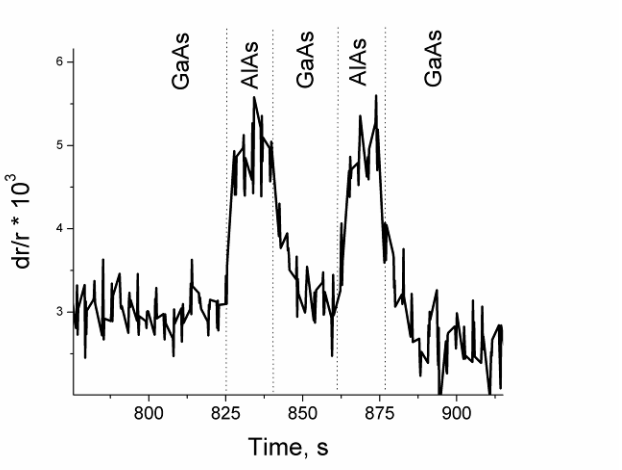

Fig. 2. Time dependence of reflectance anisotropy during RTD active zone formation

Low voltage micro lens ion beam column for nano-patterning with resolution of 1.5÷2 nm. Numerical simulation and prospects.

V. A. Zhukov[1], S. Kalbitzer[2], A. I. Titov[3]

1. Institute for Informatics and Automation, Russian Academy of Sciences, 199178 St. Petersburg, Russia, valery.zhukov2@gmail.com

2. Ion Beam Technology, D-69121 Heidelberg, Germany, skalbitzer@aol.com

3. St. Petersburg State Technical University, 195251 St. Petersburg, Russia, andrei.titov@rphf.spbstu.ru

In order to improve the spatial resolution in nano-patterning, one of the most important strategies is to lower the ion energy. Here, we present a possible strategy and methods to achieve the limit resolution in focused-ion-beam (FIB) microscopes for nano-patterning. Our strategy differs from the well-known FIB with LMIS and from so called the ML-2 ("Maskless" - 2) technology with using the ions of rare gases (CHARPAN Project) in the following aspects: (i) It employs an advanced oxygen ion source [1] on iridium super-tip with effective radius < of 1 nm and with current of 200 pA. (ii) The ion energy at the target is in interval of 500 ÷ 2000 eV so this technology is 'noninvasive'. (iii) Reactive Ion Etching (RIE) of organic targets (diamond, graphite, PMMA, etc.) by means of oxygen ions is used for nano-patterning at the nanometer scale instead of pure physical sputtering. (iiii) For reducing a chromatic aberration at decreasing of ion energy we here propose reducing the ion-optical column to a scale of tens of micrometers [2]. It is shown by computer simulation that the resolution (FWHM) thus obtained should be in interval of 1 ÷ 2 nm. This resolution not involving aberration correction [3] can be achieved only at the cost of reducing the current on a target to interval of 0.1 ÷ 0.5 pA that coincides with the low boundary of current interval in helium ion microscope [4]. The experimental nano-chip with size of 1x1 μm^2 and with depth of etching pits in 10 of atom mono layers can be processed during time in interval of 100 ÷ 20 seconds. At above mentioned values of current and energy only one ion can be transmitted through the device in one point of time. So problems with 'space charge' are absent.

This work was supported by the Russian Academy of Sciences within the framework of the research initiative "the base for elements of microelectronics, nano-electronics, quantum computers, materials for micro- and nano-electronics, micro-system engineering, solid-state electronics".

1. A. Knoblauch, Th. Miller, Ch. Klatt, S. Kalbitzer, "Electron and ion emission properties of iridium supertip field emitters", Nucl. Instr. and Meth. in Phys. Res**. B 139**, pp. 20–27, 1998.
2. V. A. Zhukov, "Achieving Sub-1.6-nm Resolutions of a Low-Voltage Microscopic Focused-Ion-Beam System Not Involving Aberration Correction Russian Microelectronics", **37 (**2), pp. 98–106, 2008.
3. V. A. Zhukov, A. I. Titov, "Using a Chromatic-Aberration Correction System to Achieve Sub-1.6-nm Resolutions of a Focused-Ion-Beam Microscope Designed for Characterization and Processing", Russian Microelectronics, **36 (5)**, pp. 279–287, 2007.
4. B. W. Ward, J. A. Notte, N. P. Economou, "Helium ion microscope: A new tool for nanoscale microscopy and metrology", J Vac. Sci. Technol. **B 24(6)**: pp.2871-74, 2006.

The influence of the suboxide layer structure on equivalent oxide thickness in nanoscale MIS-structure

Zaitsev N.A.[1], Krasnikov G.Ya.[1], Matyushkin I.V.[2]

1. JSC Mikron, Zelenograd, Russia, e-mail: zaitsev@mikron.ru
2. Moscow Institute of electronic technology, Zelenograd, Russia

EOT's (equivalent oxide thickness) value is defined usually under the formula (1):

$$\frac{EOT}{\varepsilon_{ox}} = \sum_i \frac{d_i}{\varepsilon_i} \tag{1}$$

Here are: i - number of dielectric layer, considering from silicon, d_i - a thickness of i-th layer, ε_i - its dielectric permittivity. We will try to improve definition (1) taking into account features of a structure of Si/SiO_2 interface, remaining within the classical physics. The urgency of consideration EOT in such aspect is connected by that at the overwhelming majority of technological ways of drawing alternative dielectrics the formation of a SiO_x suboxides thin transition layer on border with silicon is inevitable [1, 2]. Approximating the gate area S a square of channel length a and considering finiteness of the condenser size, we will receive for EOT the improved formula:

$$\widetilde{\varepsilon}_i = \varepsilon_i + \frac{2d_i}{\pi a}\ln\frac{a}{d_i}, \quad \Delta = \frac{\varepsilon_0 \overline{E} z}{\sigma} \qquad \frac{EOT}{\varepsilon_{ox}} = \sum_i \frac{d_i}{\varepsilon_i} - \Delta \qquad \frac{EOT}{\varepsilon_{ox}} = \left(1 + \frac{z\overline{E}}{U}\right)^{-1} \sum_i \frac{d_i}{\varepsilon_i} \tag{2}$$

Here are: ε_i - effective permittivity, z - a thickness suboxidelayer, σ – surface density of a charge in a silicon undersurface layer, E – induced by dipoles on this layer field. The account of both amendments leads to reduction EOT approximately on 12% (see also [2,3]).

References

1. S. Monaghan, J.C. Greer, S.D. Elliott. Phys Rev B 75, 245304 (2007)
2. F. Giustino, A. Bongiorno, A. Pasquarello. Applied Physics Letters, 86, 19 (2005).
3. N.A. Zaitsev, G.Ya. Krasnikov, I.V. Matyushkin. Poverhnost. 11, 117-123 (2002).

Semi-analytical model of a field-effect transistor with an ultra-thin channel

A. Khomyakov, V. Vyurkov
Institute of Physics and Technology, Russian Academy of Sciences, Moscow, Russia, vyurkov@ftian.ru

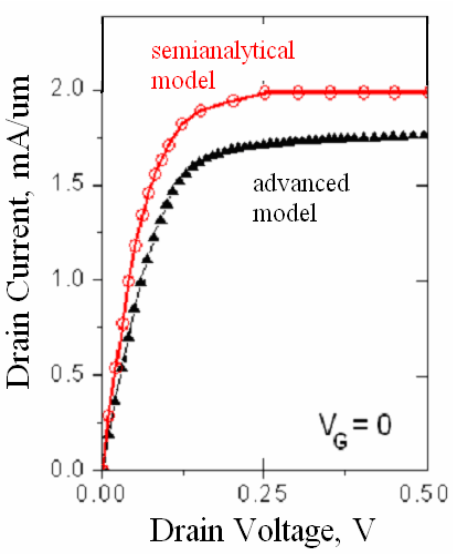

Compared to the simulation based on advanced models, that based on the analytical and semi-analytical models is much less time-consuming. It allows a swift evaluation of transistor characteristics with respect to different structure parameters. Such a kind of simulation may be successfully used at the preliminary stage of a transistor design and also for testing of advanced models.

Here we put forward a model which is applicable to description of a ballistic field-effect transistor with an ultra-thin channel. For instance, this transistor can be manufactured on a "silicon-on-insulator" wafer. The model accounts for single-gate and double-gate structures. It differently describes the regimes of a transistor above threshold and below threshold. The first implies an essential influence of charge inside the channel on a potential distribution; the second supposes a negligible charge inside the channel. Both approaches are mainly based upon an approximate solution of the Poisson equation.

The structure in simulation is as follows: a channel length 16nm, channel thickness 2nm, equivalent gate oxide thickness 1.5nm, and contact doping 10^{20}cm^{-3}. The semi-analytical model gives higher ON-state current (upper Fig.) than the advanced quantum model based upon Landauer-Buttiker approach [1, 2]. We attribute this to the influence of quantum reflection. The OFF-state regime is almost insensitive to the character of transport through the channel. Indeed, there is a perfect coincidence of sub-threshold swings in both models (below left Fig.). Remarkably, the single-gate transistor and the double-gate reveal the sub-threshold swings (below right Fig.) quite close to the theoretical limit 59 mV/dec at room temperature. It means that for a fairly thin channel there is no necessity to resort to a double-gate structure which is very inconvenient for fabrication.

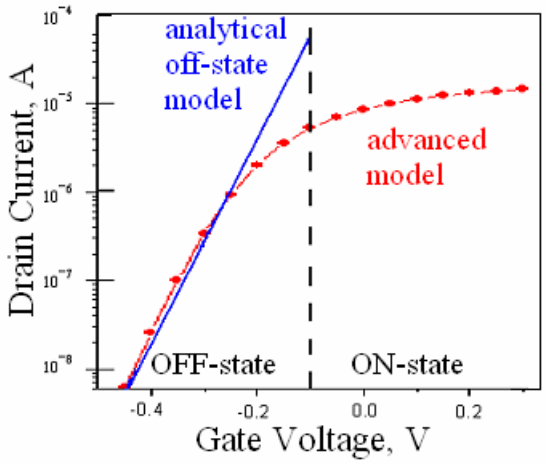

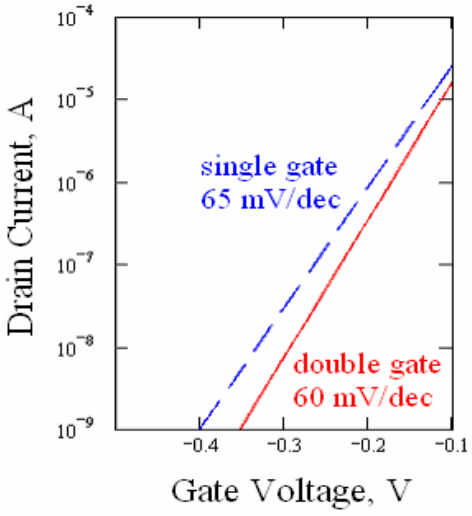

The research was supported via the grant # F793/8-05 of the Computer Company NIX (science@nix.ru) and the grant #08-07-00486-a of the Russian Basic Research Foundation.

1. V. Vyurkov , I. Semenikhin, V. Lukichev, A. Burenkov, and A. Orlikovsky, "All-quantum simulation of an ultra-small SOI MOSFET". Proc. SPIE, 7025, p. 70251K, 2008
2. A. Orlikovsky, V. Vyurkov, V. Lukichev, I. Semenikhin, A. Khomyakov, "All quantum simulation of ultrathin SOI MOSFET", in *Nanoscaled Semiconductor-on-Insulator Structures and Devices*. Springer, pp. 323-340, 2007

Impact of channel inhomogeneities on characteristics of a quantum field-effect transistor

V. Vyurkov, I. Semenikhin, V. Lukichev, A. Orlikovsky
Institute of Physics and Technology, Russian Academy of Sciences, Moscow, Russia, vyurkov@ftian.ru

The continuing progress in silicon VLSI technology motivates the transition to silicon-on-insulator (SOI) wafers. Just these structures definitely suppress short channel effects which substantially impair bulk MOSFET performance. The ultra-thin (1-5nm) fully depleted silicon will be a structure to take an ultimate advantage of SOI wafers and to provide an advancement of silicon technology to the extreme channel length. As a carrier wave length become comparable with the channel size the all-quantum simulation of such small devices becomes challenging.

The effective method for solution of a scattering problem for the stationary Schrödinger equation in a transistor channel of nanometer length with an arbitrary potential relief was developed [1, 2]. The method allows fulfilling a simulation of a field effect transistor based on Landauer-Buttiker approach. It has a distinct physical sense clearly based on the conception of a transistor channel as a quantum wire or quantum wave-guide. The necessary transmission coefficients are determined via a self-consistent solution of Schrödinger and Poisson equations. The results of simulation demonstrate the impact of realistic channel inhomogeneities on transistor characteristics.

The UTB SOI MOSFET in simulation is as follows: a gate length 10nm, spacers 5nm, channel thickness 2nm, channel width 5nm, equivalent gate oxide thickness 1.5nm, and source/drain contact doping $10^{20}cm^{-3}$.

A step-like corrugation of a channel wall diminishes ON-state current (left Fig.). A positively charged center augments ON-state current (right Fig.). Really it means the shifted threshold voltage. The charged center may originate in a random impurity inside the channel, or in interface defect, or in charged defect inside the gate dielectric. All kinds of inhomogeneities have much stronger impact on the current when they are located by the source contact compared with that located by the drain contact. The preliminary estimation of dispersion caused by realistic imperfectness of transistors in a circuit gives rise to 10-20%. In spite of former intuitive suspicions, it is not dramatic. However, some improvements of technology and materials for ultra-large integrated circuits may become challenging.

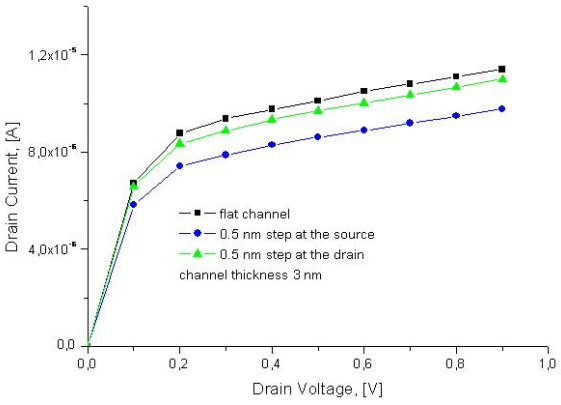

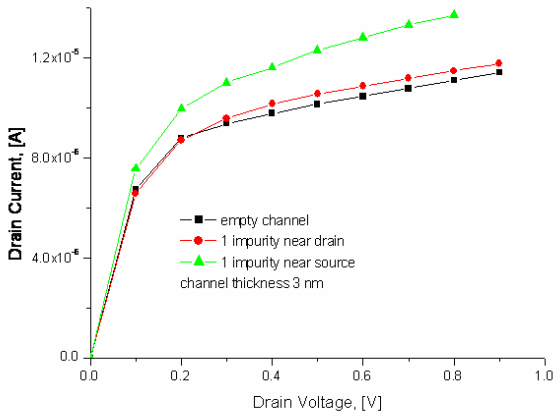

The research was supported via the grant # F793/8-05 of the Computer Company NIX (science@nix.ru) and the grant #08-07-00486-a of the Russian Foundation for Basic Research.

1. V. Vyurkov , I. Semenikhin, V. Lukichev, A. Burenkov, and A. Orlikovsky, "All-quantum simulation of an ultra-small SOI MOSFET". Proc. SPIE, 7025, p. 70251K, 2008

2. A. Orlikovsky, V. Vyurkov, V. Lukichev, I. Semenikhin, A. Khomyakov, "All quantum simulation of ultrathin SOI MOSFET", in *Nanoscaled Semiconductor-on-Insulator Structures and Devices*. Springer, pp. 323-340, 2007

Bulk and Nanoribbon Graphene Field-Effect Transistor Modeling

G. I. Zebrev[1], E.A. Zotkin[1], A.A. Tselykovskiy[1], E.V. Melnik[1], V. O. Turin[2]

[1]*Micro- and Nanoelectronics Department, National Research Nuclear University "MEPHI", Moscow, Russia, e-mail: gizebrev@mephi.ru*
[2]*Orel State Technical University, Orel, Russia, e-mail: voturin@ostu.ru*

Due to high mobility at room temperature, the gated two-dimensional (2D) graphene systems could become promising for high-speed transistor nanoelectronics [1]. Being a semimetal without energy gap and having finite conductivity at the point of electroneutrality, graphene hardly can be considered directly as a material for field-effect transistors (FETs) with the high ratio I_{ON}/I_{OFF}. It is possible to make energy gap (dependent only on graphene strip width) by using narrow (< 30 nm) nanoscale ribbons (GNR). The energy gap opens up in the GNRs due to quantization effects. In addition to the 2D confinement, the graphene electrons in narrow ribbons can be further quantized in transversal direction of wave vector. This transversal quantization is expected to result in a split of the original 2D energy dispersion of graphene into a number of one-dimensional (1D) modes. Electron transport and carrier statistics is significantly modified by this circumstance.

It is intended to discuss in this report the following topics:

- electrostatics of double-gated graphene field effect structure;
- key role of quantum capacitance in graphene [2];
- influence of edge scattering on conductance of narrow strips of graphene;
- diffusion-drift current and I-V characteristic of GNR and bulk graphene gated structures [3];
- near-interfacial defects and its influence on characteristics of graphene devices.

1. K. S. Novoselov, A. K. Geim, et al. "Electric field effect in atomically thin carbon films," *Science*, vol. 306, pp. 666-669, 2004.
2. G.I. Zebrev, "Graphene nanoelectronics: electrostatics and kinetics", Proceedings of the SPIE, Volume 7025, pp. 70250M-70250M-9 (2008).
3. G. I. Zebrev, "Electrostatics and diffusion-drift transport in graphene field effect transistors", MIEL 2008, Proceedings 26th International Conference on Microelectronics 2008, pp. 159-162.

Electron optical spin polarization in broken-gap heterostructures

A. Zakharova[1], K. A. Chao[2], I. Semenikhin[1]

1. Institute of Physics and Technology of the Russian Academy of Sciences, Moscow, Russia, E-mail address zakharova@ftian.ru 2. Department of Physics, Lund University, Lund, Sweden, and Department of Physics, Chemistry and Biology, Linköping University, Linköping, Sweden, E-mail address chao@ifm.liu.se

Spin-related phenomena can play an essential role in operation of different semiconductor quantum well devices based on zinc-blende materials such as field effect transistors, detectors and laser diodes, resonant tunneling structures. This is because the spin-orbit interaction and different symmetry breaking mechanisms create the specific electronic band structure in a quantum well of a device which characteristic feature is a spin split of energy levels belonging of the same subband. Spin split of levels in the quantum well results in the spin-dependent lateral transport along it, the spin-dependent resonant tunneling through the various quasi-bound states in the resonant tunneling structures, spin-dependent optical and infrared transitions between the states of different subbands caused by linearly or circularly polarized light. Due to the spin split of energy levels in the quantum wells combined with lateral current along the quantum well or perpendicular to interfaced tunneling transport, or the inter-subband excitation by the light circularly polarized in the plane different from the plane of the structure, the electron or hole spin polarization appears that is a foundation of new semiconductor devices based on spin manipulation. The interesting effects of electron optical spin polarization can exist in the broken-gap quantum wells to be studied here.

The electron optical spin polarization caused by circularly polarized light has been studied in bulk zinc-blende crystals [1] and semiconductor quantum wells made from zinc-blende materials grown along the [001] direction [2]. The reason of this effect is the different selection rules for optical excitation from the states with opposite spins. Simple selection rules in bulk materials read that the transitions with right-handed (left-handed) circularly polarized light can occur with the change of total angular momentum by 1(-1). The spin-orbit interaction and structural inversion asymmetry (SIA) modify these simple selection rules for the transitions between the states of different subbands in the quantum wells [2]. As a result, all spin-flip and spin-conserved transitions are allowed that influences the electron or hole spin polarization. The different mechanisms of bulk inversion asymmetry (BIA) and interface Hamiltonian (IH) can change considerably the optical matrix elements and the degree of electron optical spin polarization especially in InAs/GaSb broken-gap quantum wells where the InAs conduction and the GaSb valence bands overlap. As a result the electron, light-hole and heavy-hole states can hybridize that gives an additional characteristic features to the optical properties.

We present the detailed investigation of the influence of different inversion asymmetry mechanisms such as SIA, BIA and the interface low symmetry mechanisms (relativistic IH and non-relativistic IH) on the spin split of energy levels, optical matrix elements for the inter-subband transitions caused by circularly polarized light, and electron optical spin polarization in InAs/GaSb quantum wells. The calculations were performed using the eight-band Burt-Foreman envelope function theory. The self-consistent potential and the lattice-mismatched strain have been taken into account. We have found that BIA and IH modify the spin-split of levels and optical matrix elements considerably and give a giant increase of electron optical spin polarization.

1. M. I. Dyukonov and V. I. Perel, in *Optical orientation*, edited by F. Meier and Zakharchenya (Elsevier, Amsterdam, 1984), Chap. 2.

2. A. G. Mal'shukov and K. A. Chao, “Optoelectric spin injection in semiconductor heterostructures without a ferromagnet”, Phys. Rev. B, 65, 241308, 2002.

High-temperature magnetization and Mössbauer spectra of nanoparticles in a weak magnetic field

M. A. Chuev
Institute of Physics and Technology, Russian Academy of Sciences, Moscow, Russia, E-mail: chuev@ftian.ru

A number of techniques are applied to study the non-equilibrium magnetism of nanoparticles, among which the most informative seem to be the conventional magnetization measurements and Mössbauer spectroscopy. The corresponding shapes of the temperature- and field-dependent magnetization curves and Mössbauer spectra obviously supplies one with a large amount of information about physical characteristics inherent to the systems studied. The principal difference between these two complementary techniques is that they can probe magnetic properties of the same material in different frequency ranges: the magnetization measurements are carried out at lower frequencies (of about 1-1000 Hz) while Mössbauer spectroscopy can reveal the magnetic dynamics of nanoparticles at higher frequencies due to the Mössbauer time window (10^{-11}–10^{-6} s for ^{57}Fe nuclei).

The only way to extract the reach information from the experimental data is to define a model of the magnetic dynamics in order to describe the whole set of the experimental data for the sample studied. The general theory of stochastic relaxation of the uniform magnetization of ferromagnetic single-domain particles has been developed by Brown in the early 1960s [1]. However, its application in practical sense is restricted by only numerical simulations without any real analysis of not only the Mössbauer spectra of nanoparticles in a magnetic field, but even magnetization curves.

In order to describe the magnetic dynamics of an ensemble of nanoparticles in a magnetic field the alternative approach has been proposed, where the magnetization precession orbits are considered as stochastic states of each particle and the states (orbits) are characterized by the mean magnetization value for the corresponding trajectory [2,3]. In the framework of this approach the probabilities of transitions per unit time between the stochastic states can be defined by the statistical characteristic of the random field. This allows a general model of magnetic dynamics to be determined for calculating the magnetic characteristics in various measurement methods including the conventional ‘low-frequency’ magnetization measurements and Moessbauer spectroscopy. Qualitative analysis and numerical calculations within the ‘multilevel’ model supply one with theoretical evidences for the existence of the asymptotic high-temperature behavior of the magnetization of an ensemble of particles in a weak magnetic field, which is earlier predicted to be different from the classical Langevin limit for ideal superparamagnetic particles. Moreover, such a behavior has been already observed in the temperature dependence of the nickel nanoparticles magnetization [3,4].

Based on this approach, a simplified three-level stochastic model taking into account the magnetic anisotropy, precession and diffusion of uniform magnetization of single-domain particles is developed in order to describe the Mössbauer absorption spectra of an ensemble of magnetic nanoparticles in a weak magnetic field [5]. This model allows one to take into consideration physical mechanisms of formation of the magnetic hyperfine structure within the magnetic dynamics inherent to such materials. A number of qualitative effects observed in experimental Mössbauer spectra taken on small magnetic particles even in zero magnetic field can be self-consistently explained within the model in terms of the mean-field interparticle interaction. In particular, this model predicts the appearance of ^{57}Fe magnetic sextets with a small hyperfine splitting slightly dependent of the particle’s size and temperature in a weak magnetic field and at high temperature, which look like effective “doublets” of lines often observed in experimental spectra.

This work is financially supported by the Russian Foundation for Basic Research (projects No. 08-02-00388 and 09-02-12195).

1. W.F. Brown Jr., “Thermal fluctuations of a single-domain particle”, Phys. Rev., 130, pp. 1677-1686, 1963
2. M.A. Chuev, “Response from M.A. Chuev”, JETP Lett., 87, pp. 707-709, 2008
3. M.A. Chuev. “Non-Langevin high-temperature magnetization of nanoparticles in a weak magnetic field”, JETP, 108, pp. 249-259, 2009
4. J. Hesse, H. Bremers, O. Hupe, et al., “Different susceptibilities of nanosized single-domain particles derived from magnetisation measurements”, J. Magn. Magn. Mater., 212, pp.153-167, 2000
5. M.A. Chuev, “Mössbauer spectra of single-domain particles in a weak magnetic field”, J. Phys.: Condens. Matter., 20, pp. 505201 (1-10), 2008

Mössbauer study of nanomagnetics

V.I.Bachurin[1], I.N.Zakharova[1], M.A.Shipilin[2], A.M.Shipilin[3]

1. Yaroslavl State Technical University, Yaroslavl, Russia, e-mail: ship_yar@mail.ru.

2. P.G.Demidov Yroslavl State University, Yaroslavl, Russia, e-mail: ship_yar@mail.ru.

3. M.V. Lomonosov Moscow State University, Moscow, Russia, e-mail: amship@mail.ru

The interest to nanomagnetic substances is caused by their abundance in natural materials and by their application in different fields of technology. So, magnetic nanomaterials are perspective substances for microelectronics. Recently great attention is paid to the questions of magnetism integration in semi-conductor architecture of computers. Nanomagnetics may be used for the synthesis of ferromagnet-semiconductor hybrid with the properties of integrated and tunable system [1]. The use of magnetic anisotropy is of interest for the microelectromechanical systems obtained by filling microcapillaries with magnetics. In particular, ferrocolloids can be used as microcapillaries filling materials [2].

We studied nanodispersed magnetic oxides γ-Fe_2O_3 и Fe_3O_4 powders and magnetic fluids on their base. A typical magnetic fluid (so-called ferrofluid) is a colloid disposition of monodomain magnetic nanoparticles in fluid media stabilized by some surface-active substance (SAS).Our Mössbauer investigations of nanomagnetic oxides powders and magnetic fluids on their base have been carried out at temperatures from 100 to 300 K. Mössbauer spectra were obtained in geometry of absorption. According to the data of electron microscopy the average size of the particles varied from 7,5 to 18 nm in different investigated samples.

The properties of nanoparticles depend essentially on the state of their surface layer. The information about the state of "internal" and "surface" area of magnetic nanoparticles was one of the purposes of our study. This study includes the analysis of distribution functions of effective magnetic fields, which were restored by the data about Mössbauer spectra of ^{57}Fe in investigated samples. The distribution function of effective magnetic fields $p(H_n)$, restored on the basis of γ-Fe_2O_3 spectrum, is shown in the figure. This function has 2 maxima. One of them H_n = 485 kOe corresponds to effective magnetic field on the nuclei of iron ions belonging to the "internal" area of γ-Fe_2O_3 nanoparticles. The other maximum H_n = 435 kOe corresponds to similar field for nuclei of iron ions belonging to the "surface" area of the particles ("surface" atoms are devoid of half of exchange bonds compared to 'internal" atoms). The difference in effective fields of "surface" and "internal" atoms determined on the basis of $p(H_n)$ is in good agreement with the estimation of these fields in terms of molecular orbitals method [3]. The ratio of the areas under the plot maxima $p(H_n)$ was regarded as the ratio of volumes of "surface" and "internal" areas of the particle. The latter enabled us to estimate the particle size in the investigated γ-Fe_2O_3 powder . The result obtained agrees with the data on electron microscopy. The similar calculations were performed for magnetite powder and for investigated ferrofluids. It is important, that the essential decrease of maxima $p(H_n)$ fields is revealed for the Fe_3O_4 ferrofluids in comparison with disperse magnetite without surfactant. This decrease is equal to ~ 15 kOe for "internal" and ~ 60 kOe for "surfactant" ions. Apparently, it can be connected with redistribution of electron density on iron nuclei, that may arise because of chemosorption interaction between magnetic particle and surfactant.

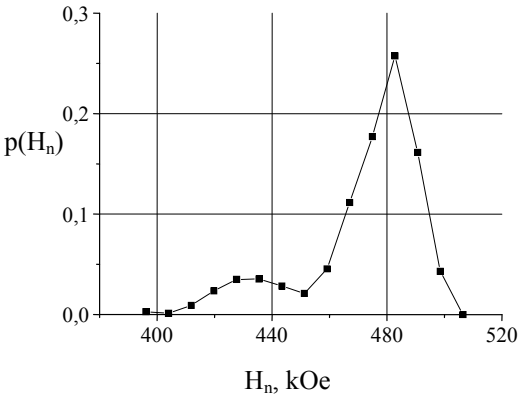

Fig. Dictribution fanction of effective magnetic field of γ-Fe_2O_3

The obtained data may be of interest in connection with investigation of the role of "surface" and "internal" atoms in magnetic properties of intended for the microelectronics nanomagnetics.

1. B.P.Zakharchenya, V.L.Korenev. Uspekhi Fizichskikh Nauk, 175 (6), pp. 630-635, 2005.
2. I.I.Amirov, O.V.Morozov, M.O.Izyumov, V.A.Kalnov, A.A.Orlikovsky, K.A.Valiev. Works FTI RAN. 2005. V. 18. P.173.
3. V.I.Nikolaev, V.S.Rusakov: *Mössbauer study of ferrites.* Moscow University Press, Moscow, 1985.

Ferromagnetic resonance and magnetoelastic demodulation in giant magnetostriction $TbCo_2$/FeCo nanostructured thin film

A. Klimov[1,2], Yu. Ignatov[2], S. Nikitov[2] N. Tiercelin[1], V. Preobrazhensky[1,3], P. Pernod[1]

[1] *LEMAC–IEMN CNRS UMR 8520, Ecole Centrale de Lille, 59652 Villeneuve d'Ascq cedex, France*

[2] *Kotel'nikov Institute of Radioengineering and Electronics (IRE RAS), 125009 Moscow, Russia*

[3] *Wave Research Center, A.M. Prokhorov General Physics Institute RAS, 119991 Moscow, Russia*

Magnetostrictive materials that can directly convert electromagnetic energy into elastic modes gained a lot of interest for making new types of microactuators [1]. Rare earth intermetalic compositions provide giant magnetostriction, large values of the electromechanical coupling factor, contact-less driving and easily can be scaled down to small lateral dimensions. The magnetoelastic sensitivity of micro-magneto-mechanical systems (MMMS) can increase about two order of value in the vicinity of spin reorientation transition (SRT) in giant magnetostriction thin films [2,3]. The area near SRT has a number of special dynamic and nonlinear features [3]. In particular high efficiency of sub-harmonic excitation of elastic vibrations was observed [4]. Magnetoelastic demodulation of electromagnetic waves can also become efficient near SRT [5]. This phenomenon is of interest for high frequency control of MMMS. For microwave demodulation one can expect the most preferable conditions when SRT is combined with ferromagnetic resonance (FMR) in a magnetostrictive film.

In the present report we study FMR properties of the 25x$TbCo_2$/FeCo bilayers of thickness 10 nm nanostructure deposited on Si cantilever and excitation of low frequency elastic vibrations of the cantilever due to magnetoelastic demodulation of microwave electromagnetic field at FMR frequency. The experiments have been carried out at high frequencies from below 1 GHz to above 4 GHz.

Calculations for imaginary part of magnetic susceptibility were made using Landau-Lifshitz equation. The results are compared with experimental FMR curves on Fig.1. In our case only one resonance peak was observed that is explained by strong attenuation of HF spin excitations in rare earth compounds. The results of calculations of magnetic field dependence of the resonant amplitude of elastic vibrations are presented on Fig.2 in comparison with the experimental data. According to the prediction and calculations the increase of amplitude of LF vibrations excited by HF electromagnetic field in FMR conditions near SRT is clearly seen.

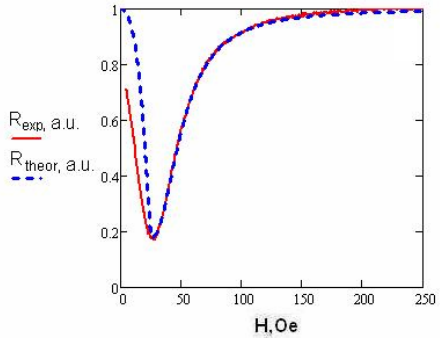

Fig.1. Magnetic field dependence of the HF reflection coefficient in R at FMR frequencies f = 1172 MHz, line-experiment, dashed line-theory.

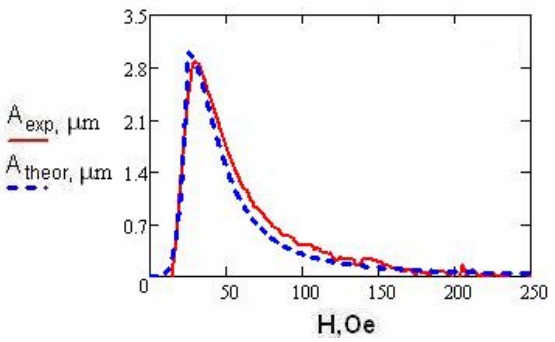

Fig.2. Amplitude of sample vibrations at FMR frequencies f = 1172 MHz, line-experiment, dashed line-theory.

The experimental studies of FMR and magnetoelastic demodulation in thin film $TbFe_2$/FeCo nanostructures deposited on Si cantilever shown that low-frequency vibrations of the cantilever can be amplified when FMR is excited by HF electromagnetic field near SRT. The phenomenon under consideration can find various applications in the field of MMMS controlled by HF electromagnetic field.

This work was supported by RFBR Grant No.05-02-19643-NCNIL_a and No. 08-02-00785-a.

[1] Quandt E. and Holleck H., Microsystem Technologies, **1**, pp. 178-84, 1995.
[2] Tiercelin N. et al., Journal of Magnetism and Magnetic Materials, **249**, pp. 519-23, 2002.
[3] Klimov A. et al., IEEE Trans. Mag, **42**, 10, 2006.
[4] Tiercelin N. et al., J. Ultrasonics, **38**, pp. 64-66, 2000.
[5] Buchel'nikov V., Dan'shin N., Tsymbal L. and Shavrov V., Phys. Usp., **39**, 547, 1996.

Odd-even effects in magnetic nanostructures

V.V. Kostyuchenko
*Institute of Physics and Te*chnology RAS, Yaroslavl Branch, *150007 Yaroslavl, Russia*
vkqubit@mail.ru

It is well known that there are differences between properties of magnetic multilayers with an odd and an even number of magnetic layers, when external magnetic field id applied along easy axis [1]. The magnetic properties of nanowires also depend on the parity of the chain length [2]. Thus the parity of objects number in nanostructure is a crucial parameter determining the properties of magnetic nanostructures.

In the present work the origin of this effect in the spin chain is analyzed in the framework of classical and quantum Heisenberg models. The common and distinct features of classical and quantum models are established. In the framework of classical Heisenberg model the solution to the problem of minimization of functional

$$H = J\sum_{i=1}^{N-1}\left(\mathbf{n}_i\mathbf{n}_{i+1}\right)+\sum_{i=1}^{N}\left[\frac{1}{2}k\left(n^x{}_i\right)^2-\left(\mathbf{hn}_i\right)\right], \qquad (1)$$

is needed. The exact analytical solution is obtained by using the technique of finite difference equations. The values of critical fields are calculated for the different orientation of external field with respect to the easy axis. It is shown that odd-even effect depends on the orientation of external field. The odd-even effect is more pronounced in field applied perpendicular to the easy axis.

The odd-even effect also exists in the framework of quantum Heisenberg model. In this case the magnetic properties of spin chain is described by the Hamiltonian

$$\hat{H} = J\sum_{i=1}^{N-1}\left(\hat{\mathbf{S}}_i\hat{\mathbf{S}}_{i+1}\right)+ g\mu_B H\sum_{i=1}^{N}\hat{S}_i^z . \qquad (2)$$

Made in the present work analytical and numerical calculations show essential differences between the odd-even effects within the framework of classical and quantum models. These calculations predict new effects and make clear the conditions of their experimental observation. The transition from quantum to classical model, when the spin value is increased, is also investigated.

1. R.W. Wang, D.L. Mills, E.E. Fullerton, Fullerton, J. E. Mattson, S. D. Bader, Phys. Rev. Lett., **72**, 920 (1994)
2. S. Lounis, P.H. Dederichs, and S. Blugel, Phys. Rev. Lett., **101**, 107204 (2008)

Magnetoresistance of multilayer ferromagnetic nanoparticles

S.N.Vdovichev, A.A.Fraerman, B.A.Gribkov, S.A.Gusev, A.Yu.Klimov, V.L.Mironov, V.V.Rogov
Institute for Physics of Microstructures, Russian Academy of Science, Nizhniy Novgorod, Russia,
vdovichev@ipm.sci-nnov.ru

The interest to multilayer system consists from ferromagnetic layers is due to possibility of fabrication of new type of data storage [1]. In general case, distribution of magnetization in laterally-confined magnetic multilayer is noncollinear and strongly depends on number of magnetic layers due to their magnetostatic interaction [2]. Magnetic anisotropy (K) of the system is determined by eccentricity of the particles. Interaction between magnetic layers due to magnetostatic interaction leads to their "antiferromagnetic" coupling with strength J. Behavior of the system in external magnetic field is determined by interplay of the two factors. If J>K, noncollinear phase is possible. In opposite case (J<K), only collinear states exist.

In the report the connection between magnetic states and transport properties of such systems is discussed. We observed the magnetoresistance of the particle CoFe(12 nm)/TaO_x(2 nm)/CoFe(8 nm) with different lateral sizes fabricated by electron lithography. The transport measurements were carried out in CPP geometry, see Fig. 1. Magnetic force microscopy was used for observation of magnetic states in the multilayer nanoparticles.

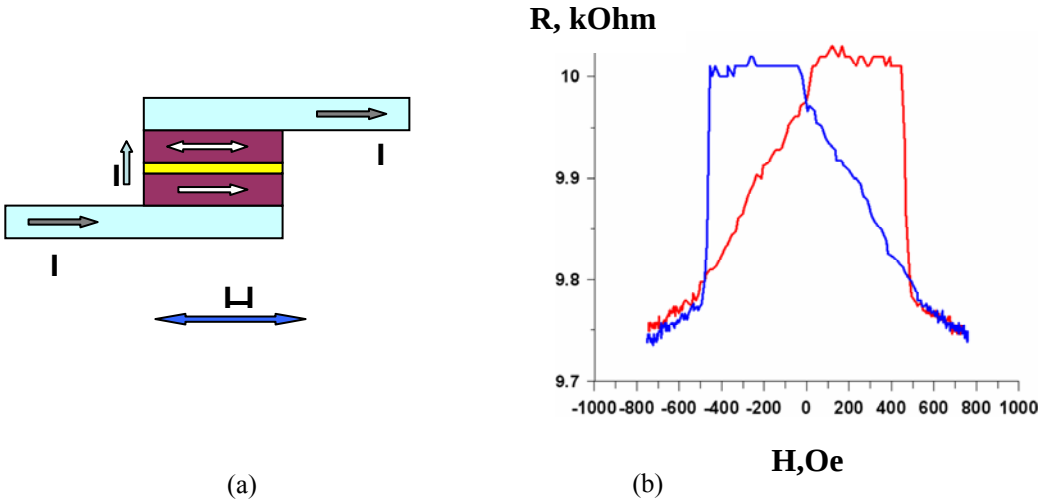

(a) (b)

Fig.1.(a) Architecture of multilayer magnetic element
(b) Dependence of the resistance on external magnetic field

Thus we demonstrated the first step for investigation of the transport properties for noncollinear magnetic systems with magnetostatic interaction between layers.

The work was supported by the RFBR and by BRHE #Y4-P-01-09.

1. Jian-Gang Zhu, Proceedings of IEEE, V.96, N.11, p.1786, 2008.
2. A. A. Fraerman et al, J. of Appl. Phys. 103, 073916, 2008.

SEM Probe Defocusing Method of Measurement of Linear Sizes of Nanorelief Elements

M.N. Filippov[1], Yu.A. Novikov[2], A.V. Rakov[3], P.A. Todua[3]

1. N.S. Kurnakov General and Inorganic Chemistry Institute of the Russian Academy of Sciences, Moscow, Russia, E-mail: MN@filippov.org.ru. 2. A.M. Prokhorov General Physics Institute of the Russian Academy of Sciences, Moscow, Russia, E-mail: nya@kapella.gpi.ru. 3. Center for Surface and Vacuum Research, Moscow, Russia, E-mail: fgupnicpv@mail.ru.

Scanning electron microscopes (SEM) play the leading role in linear size measurements of micro- and nanostructures elements. The examination of existing methods of measurements show that there are certain methods of measurement of elements sizes with trapezoid profile and big inclination angle of side walls (***d*** << ***s***, ***d*** – effective SEM probe diameter [1], ***s*** – projection of inclined side wall on the base plane of element). For small inclination angle structures (***d*** > ***s***) such methods are missing. However in micro- and nanoelectronics technology the structures with small inclination angles make the main part of microcircuit production

In [2] the SEM probe defocusing method of measurement of linear sizes of relief elements of nanostructures with small inclination angle of side walls was proposed. According to this method in the SEM working in SE mode one obtain the images of measured relief elements at different probe focusing (different probe diameter). Next the reference points on the SEM signal are selected, the distances between which characterize the element size and probe diameter and the dependence of its position on the probe diameter is determined. The extrapolation of these dependences to zero probe diameter gives a relief element size.

To extend the size range of the structure elements studied by SEM defocusing probe method the test-structures with big inclination angle of side walls (***d*** << ***s***) and test-structures satisfied the condition ***d*** < ***s***. were used. The positions of maxima and the borders of bottom bases of signals were used as reference points. It was discovered that in all cases the functional dependencies between the distance between reference points and probe diameter were linear. At the same time the sizes of all the reference lengths increase with the increase of ***d.*** It should be stressed that functional dependencies for the structures with small inclination angles of side walls (***d*** > ***s***) linking the distance between those reference points and probe diameter was also a linear one, but the reference length characterizing the distance between the signal maxima decreased with the increase of ***d*** [2]**.** This was the case when signal shapes for the structures with ***d*** > ***s*** and ***d*** < ***s*** were equal.

The possible mechanisms of signal formation in SEM in SE mode are discussed as well as the ways of measurement of structure elements' sizes of class ***d*** < ***s*** by the SEM electron probe defocusing method.

1. V.P. Gavrilenko, Yu.A. Novikov, A.V. Rakov, P.A. Todua, "Measurement of the parameters of the electron beam of a scanning electron microscope", Proc. of SPIE, 7042, pp.70420C-1 – 70420C-12, 2008
2. V. P. Gavrilenko, V. A. Kalnov, Yu. A. Novikov, A. A. Orlikovsky, A. V. Rakov, P. A. Todua, K. A. Valiev, E. N. Zhikharev, "Measurement of dimensions of resist mask elements below 100 nm with help of a scanning electron microscope", Proc. of SPIE, 7272, pp.727227-1 – 727227-9, 2009

SEM Relief Structure Images with Trapezoid Profile and Big Inclination Angle of Side Walls in Back Scattered Electrons

M.N. Filippov[1], Yu.A. Novikov[2], A.V. Rakov[3], P.A. Todua[3]

1. N.S. Kurnakov General and Inorganic Chemistry Institute of the Russian Academy of Sciences, Moscow, Russia, E-mail: MN@filippov.org.ru. 2. A.M. Prokhorov General Physics Institute of the Russian Academy of Sciences, Moscow, Russia, E-mail: nya@kapella.gpi.ru. 3. Center for Surface and Vacuum Research, Moscow, Russia, E-mail: fgupnicpv@mail.ru.

The influence of probe diameter on scanning electron microscope (SEM) signal formation in secondary electron (SE) and backscattered electron (BSE) modes was studied on SEM *S-4800 (Hitachi, Japan)* at the electron probe energy 20 keV. The measurement of probe diameter was carried out by defocusing of electron probe. Silicon structures with trapezoid profile of relief elements and big inclination angle of side walls (test object *MShPS-2.0K*) were studied. During the experiment the image registration of one and the same part of the structure in the SE (Fig.1) and BSE (Fig.2) modes was carried out.

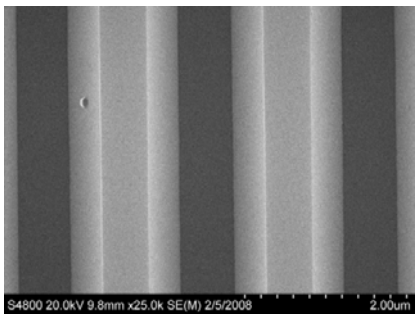

Fig.1

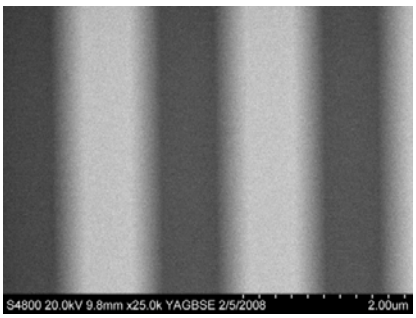

Fig.2

The probe diameter measurements were done by SE images. The probe diameter was varied in the range from 14 nm up to 75 nm. The SE signals (Fig.3) changed dramatically as probe diameter varied while the BSE signals (Fig.4) changed not more than the noise level (signals 1 are detected at probe diameter 14 nm and signals 2 – at probe diameter 75 nm).

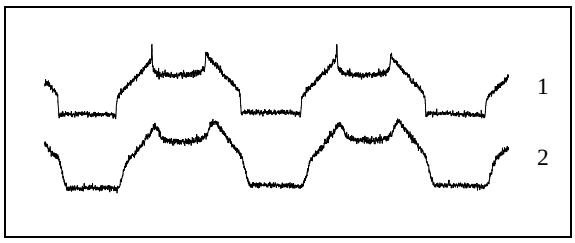

Fig.3

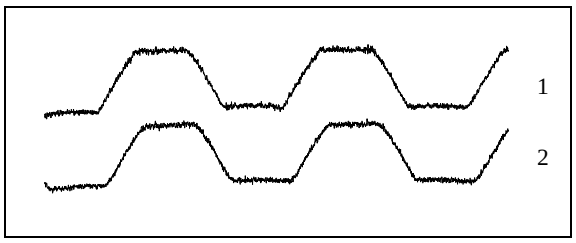

Fig.4

Thus, the shape and parameters of SEM signal in BSE mode are independent from the probe diameter. The possible mechanisms of SEM signal formation in BSE mode have been considered. A possibility to use the BSE mode of SEM for certification of linear sizes of test objects with trapezoid profile and big inclination angle of side walls has been discussed.

Combined electron-beam method of the diagnostic of microelectronic structures in scanning electron microscopy

F.A..Lukyanov[1] , N.A.Orlikovsky[2] , E.I.Rau[3] , R.A.Sennov[3]

1. *Moscow State University, Moscow, Russia*
2. *Institute of Physic and Technology RAS, Moscow, Russia*
3. *Institute of Microelectronics Technology and High-Purity Materials RAS, Chernogolovka, Moscow Region, Russia*

Non destructive "in depth" characterization of the multilayer structures plays an increasingly important role in modern microelectronics. Owing to their high 3-dimensional resolution, the electron beam microtomography of microelectronic devices can be used for this purpose via analysis of the energy distribution of the backscattered primaries electrons [1, 2]. The energy filtered backscattered electron (BSE) signals provide more depth information on the sample microstructures than the total BSE signals. Since BSEs which have lost a certain amount of energy are typically generated from a given depth in the sample, an energy-filtered image series represents two-dimensional slices of the sample at various depths below the surface. A compact electrostatic toroidal energy spectrometer specially adapted for SEM applications has been developed and will be described. The energy resolution of used toroidal spectrometer is about 1%, the lateral resolution remains at that for SEM under particular operating condition. The depth resolution by visual monitoring of each subsurface layer (microstructure) is in the 10-100 nm range. The distance below the surface at which microstructure can be resolved is typically 0.5 to 2 μm for silicon microelectronic devices. It is shown that from the BSE spectral curves the depth and thickness of buried film in multilayered structures or of different subsurface inhomogeneties can be estimated.

The second nondestructive contactless method of diagnostic, which can be carried out simultaneously with the BSE microtomography, is the local electron beam induced voltage (EBIV) method, which is a relatively analog of surface photo-voltage detection [3, 4]. This method can be successfully applied to examine surface and bulk electronic properties and to control the quality of semiconductor crystals. This technique allow to detect and characterize such features in semiconductor structures as dopant distribution, dislocations, stacking faults, precipitates, grain boundaries, microcracks, all local p-n junctions etc. It will be demonstrated that the EBIV method can be used for local contactless measurement of minority carrier diffusion length and lifetime.

Contacts to the sample are not required allowing inspection of initial wafers, partially fabricated devices and complete integrated circuits. Also, the microelectronic structures can be examined at several stage of processing. Our experiments show that bottom-side EBIV detection may be preferable to topside detection owing to minimization of topographic signal contribution, higher signal coupling efficiency and a less complex sample-detector mounting procedure.

A few examples of applications of combined electron-beam diagnostic methods will be presented. These experimental results demonstrate the potential of proposed methods.

The investigations were partly supported by Federal Agency for Science and Innovation (Rosnauka), grant N 01.648.12.3017.

[1] E.I.Rau, V.N.E.Robinson. "An Annular Toroidal Backscattered Electron Energy Analyzer for Use in scanning electron Microscopy". Scanning, **18**, pp.556-561, 1996

[2] H.Niedrig, E.I.Rau. "Information depth and spatial resolution in BSE microtomography in SEM". Nucl. Instr. Meth. in Phys. Res. (B), **142**, pp.523-534, 1998

[3] W.K.Wong, E.I.Rau, J.T.Thong. "Electron-acoustic and surface electron beam induced voltage signal formation in scanning electron microscopy analysis of semiconductors samples". Ultramicroscopy, **101**, pp.183-195, 2004

[4] S.Zhu, E.I.Rau, F.H.Yang. "A novel method of determining semiconductor parameters in EBIC and SEBIV modes of SEM", Semiconductor Sci. and Technol., **18**, pp.361-366, 2003

Problems of AFM-investigations of open sandwich MIM-structures

Gorlachev E.S., Mordvintsev V.M., Levin V.L.
Yaroslavl Branch of the Institute of Physics and Technology RAS, Yaroslavl, Russia
E-mail: Mordvintsev-Viktor@yandex.ru

One of the most important fields of the modern micro-, nanoelectronics is the development of a new generation non-volatile memory devices alternative to flash technology and designed for specialized applications (nuclear, space, military, etc.). A substantially novel concept of a nano-MIM (metal-insulator-metal) diode, which may serve as a base for the non-volatile electrically reprogrammable memory, was developed (see [1] and references therein). It is based on the process of electroforming – the self-organization of an insulating nanogap in the active conductive medium on an open insulator surface via electric current. It was shown that experimental samples of nano-MIM memory matrixes based on $W/SiO_2/Si$ open sandwich structures can be manufactured by standard methods of silicon technology and practically applied with high operating speed and outstanding radiation stability. However, there still is an important problem of the visualisation of conductive phase particles and insulating nanogap on the surface of the open SiO_2 edge. Such problem can be solved using atomic force microscopy (AFM). The aim of the present work was to determine AFM scanning parameters, which would allow to perform measurements of an open SiO_2 sidewall of the MIM-structure. For these experiments specially fabricated $W/SiO_2/Si$ open sandwich MIM-structures with removed upper electrode (W) were used. A sidewall of the 10-20 nm thick insulator layer (SiO_2) was open for the direct access AFM measurements. Surface topography research was carried out in contact mode using CSG11/TiN (NT-MDT) probes on Omicron UHV AFM/STM with limited scan range of 6×6 μm^2 and coarse movement in plane for x axis only, which considerably restricted our measurement capabilities. The elaboration of the research technique was firstly carried out using TGQ1 (NT-MDT) calibration grating array of SiO_2 square mesas with 21.5 nm height. Several factors limiting the AFM performance were established: the inherent piezoelectric scanner nonlinearity, hysteresis, creep, which all affect imaging and positioning. In particular, presence of creep in the vertical direction introduced artificial ridges and grooves near sidewalls, therefore its removal is crucial. Frequently met artifacts (distortions), such as broadening, edge overshoot and blurring, and also external noises and tip artifacts due to tip contamination and wear were revealed and excluded. Thus, if the tip is contaminated it may case severe blurring and instabilities, so the measurements should be performed in vacuum of 10^{-8}-10^{-10} Torr. It was determined that at scanning speed less then 50 nm/s, the distortion effects become negligibly small, while at large standard speeds of orders of thousands nm/s they result in the appearance of noticeable artifacts of a step profile. Recommended loop gain was 1%, because higher gains resulted in oscillations at the edge of the sidewalls, indicating momentary loss of contact between the probe and the sample. Choosing a feedback force set-point to a 0 nN reduced a contact friction while still kept stability of the contact. Also, scanning was conducted in such way that the cantilever mount tilt of 15° oriented the tip "into" the sidewall. As a result, the AFM parameters were experimentally obtained, which allow one to obtain "close-to-true" structure of SiO_2 sidewalls. Next, using obtained regimes, non-electroformed MIM-structures were explored. Good results for the sidewall profiles, corresponding to REM data, were obtained. Furthermore, the aim was to apply the conductive AFM (C-AFM) technique to these samples, when a conductive probe in contact mode is biased relatively to a sample and the resulting current obtained simultaneously with topography serves as a measure for the local conductivity. C-AFM measurements showed excellent distinguishing between dielectric and conductive layers of the MIM-structures; features of the resistance transition on the SiO_2 sidewall lower part were observed. C-AFM researches are prospective from the standpoint of the observation of an insulating nanogap. It is concluded that under developed regimes, considering the limitations of the current Omicron instrument, it is possible to provide sufficient sidewall information using a conventional AFM technique and to carry out local conductivity characterization of MIM-structure SiO_2 edge with nanometer resolution, which would allow us to research open SiO_2 edge of the electroformed MIM-diodes in the forthcoming experiments.

1. Mordvintsev V.M., Kudryavtsev S.E., Levin V.L., "High-stable nonvolatile electrically reprogrammable memory on self-formed conducting nanostructures", Nanotechnologies in Russia, **4**, No. 1-2, pp. 129-136, 2009

Correct measurements of capacity using atomic force microscope

A.A. Chouprik, A.S. Baturin
Moscow Institute of Physics and Technology, Dolgoprudny, Russia,
E-mail: chouprik@ckpmipt.ru

Microelectronic devices basically consist of an array of insulated-gate field-effect transistors, where the gate insulator is made of a very thin oxide film. Now the continued scaling of microelectronic devices to smaller and smaller size faces the problem of the replacement of the conventional SiO_2 gate insulator with a high dielectric constant (high-*k*) oxide. In next generation complementary metal-oxide-semiconductor (MOS) devices, the high-*k* candidate must have a SiO_2-free interface with the semiconductor. Somehow investigation of electrophysical properties of gate insulator in multilayer metal-oxide-semiconductor structures is actual problem at present. Key electrophysical parameters of MOS structures are got from the analysis of their current-voltage (*I*-*V*) and capacity-voltage (*C*-*V*) characteristics. For determination of electrophysical parameters of real MOS structures it is required *I*-*V* and *C*-*V* measurements with high spatial resolution. From this point of view atomic force microscope (AFM) is one of the promising tools.

There are some AFM methods of capacity measurements. Most methods are qualitative. Among them are noncontact scanning capacitance microscopy and contact scanning capacitance microscopy [1, 2]. Some producers announce quantitative methods of *C*-*V* curves measurements [3]. However these methods require special tools or special probes.

We propose AFM method of quantitative capacity measurements using any routine AFM that able to measure *I*-*V* curves applying saw-tooth bias voltage between probe and sample. From measured *I*-*V* curves bias current $I_b(V)$ are defined. Capacity of structures is defined as*:*

$$C(V) = \frac{I_b(V)}{\mathrm{d}V/\mathrm{d}t}, \qquad (1)$$

where d*V*/d*t* is a velocity of voltage variation. Proposed method allows measuring *I*-*V* and low-frequency *C*-*V* curves simultaneously. It is essential for calculation of actual *C*(*V*) at real MOS structures with leakage currents.

Proposing above mentioned method we have paid an essential attention to metrological aspects. Uncertainties of capacitance measurements by proposed method come from uncertainties in definition of bias current and velocity of voltage variation. Any short voltage peaks or high frequency noise (even with low amplitude), which are inessential for *I*-*V* curves at resistive samples, will be very pronounced in bias current and as a result in *C*-*V* curves. To minimize this imperfection we propose to use a high-frequency edge filter after built-in voltage source or use an external voltage supply. The derivative d*V*/d*t* (in eq. (1)) could be found numerically having *V*(*t*) dependence. However to minimize uncertainties we recommend to use an analog differentiation with further measurement of signal proportional to d*V*/d*t*. Uncertainties at bias current definition comes from self-noise of current preamplifier, quantization of ADC and temperature instabilities of current preamplifier gain coefficients. We propose to use an built-in preamplifier of AFM together with an accurate external voltage meter. So to improve accuracy of capacity measurement AFM is only used for probe positioning and for probe current preamplification. To ensure a stable contact of AFM probe with sample AFM probes were modified. Modification consists in Pt film deposition on the tip of probe using a technique of chemical vapor deposition induced by focused ion beam.

Method of quantitative capacity measurements was tested using commercial capacitors 11.5±0.5 pF, 26.0±0.5 pF, 40.3±0.5 pF and test structures Pt/SiO_2(280 nm)/Si(p-type, 10^{20}cm^{-3}), $NiSi/Al_2O_3$(2 nm)/HfO_2(4 nm)/Si(p-type, 10^{15}cm^{-3}) [4]. Actual capacities of capacitors and test structures were measured by calibrated LRC-meter Agilent E4980A. It was found that mismatch of results of capacity measurements by proposed method to actual values on test structures at most 0.6%.

Proposed method of quantitative capacity measurements allow to measure low-frequency *C*-*V* of micro- and nanostructures quantitatively with good accuracy.

1. V.V. Polyakov, I.V. Myagkov, G.A. Tregubov, An.V. Bykov, Proceedings of ICMNE-2005, O3-16
2. V.A. Bykov, An.V. Bykov, I.V. Myagkov, G.A. Tregubov, V.V. Polyakov, Patent RU 2289862
3. A. Born, R. Wiesendanger, J. Appl. Phys. A, 66, pp. S421-S426, 1998
4. Yu. Lebedinskii, A. Zenkevich, E. Guseva, J. Appl. Phys. 101, pp. 074504, 2007

Modeling of plasma reactive ion etching of ultra high aspect ratio Si trenches

I.I.Amirov[1], A.S.Shumilov[1], A.N.Kupriynov[1], V.F.Lukichev[2]

1. Physics-Technology Institute RAS Yaroslavl branch, Yaroslavl, Russia, amirov@yf-ftian.ru
Physics-Technology Institute Russian Academy of Sciences, Moscow, Russia, Vkalnov@ftian.ru

Improvement of Si etching capability for ultra high aspect ratio (UAR) (A/R >90) trench capacitor formation is one of important tasks of nanoelectronics [1]. Formation of these UAR structures can be performed in Bosch process in SF_6/fluorocarbon plasma. In this process the verticality of the trench walls is determined by the protective properties of fluorocarbon polymer film on the walls. The degree of passivity reduces with increasing of AR that is the cause of different type profile distortions [2]. To suppresses these phenomena during formation of UVA structures it is necessary to operate at the high density and energy ion fluxes, and narrow ion angle distribution. In this case the etching stage in SF_6 plasma is realized as reactive ion etching regime when the main source of etchant F-atoms are SF_5^+ ions. The goal of the work is a modeling of Bosh processes (SF_6/C_4F_8 plasma) in ion–reactive regime formation of UAR structures.
Modeling is performed with the help of EDPS simulator (Etch-deposition profile simulator) [3]. The method is based on the Monte Carlo simulation of fluxes of plasma particles, the string-cell model of profile representation and models of isotropic Si etching in the SF_6 plasma, ion-stimulated etching and deposition of polymer film.

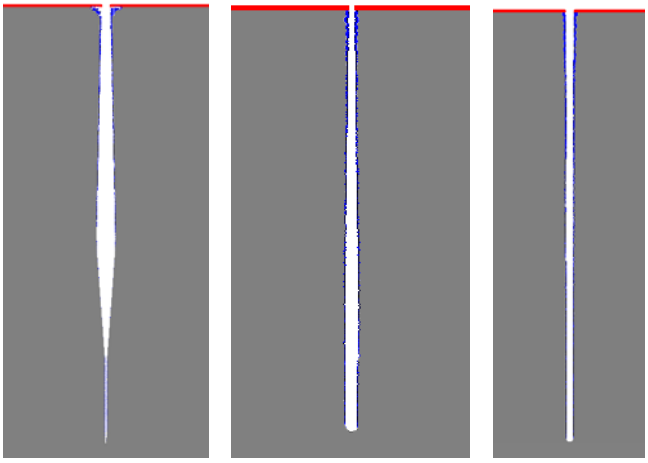

Fig.1. Profile formation of narrow trenches (width 25, 50 nm) at the different modeling parameter.
a) stop-effect,
a,b) bowing,
c) A/R=50

The ratio of ion to neutral fluxes, as well as ion energy and angle distributions, and others are parameters of model for understanding their influence on the trench profile evolution. Different effects of deep trenches formation – stop-effect, bowing (Fig.1) and UAR trenches (A=50) are received. According to experiments the etch rate of trench is slowly reduced in time. Modeling provides necessary information about the competing parameters in UAR trench formation and allows better control of the process performance.

1. *International Technology Roadmap for Semiconductors*, 2008.
2. M. A. Blauw, T. Zijlstra, E. van der Drift. Balancing the etching and passivation in time-multiplexed deep dry etching of silicon. J. Vac. Sci. Technol. B19, pp. 2930-2934, 2001
3. A.S. Shumolov, I.I. Amirov.“ Modeling of Deep Grooving of Silicon in the Process of Plasmochemical Cyclic Etching/Passivation. Russian Microelectronics, 2007, pp. 241–250, 2007

Plasma parameters and active particles kinetics in HBr dc glow discharges

A. Smirnov[1,2], A. Efremov[1], V. Svettsov[1], A. Islyaykin[2]
1. Ivanovo State University of Chemistry & Technology, Ivanovo, Russia, efremov@isuct.ru
2. Mikron JSC, Zelenograd, Moscow, Russia

Recently, the HBr-based plasmas are widely used in micro- and nanoelectronics technologies because of serious advantages in the "dry" etch processes of some materials. Particularly, the high anisotropy silicon etching was achieved due to a negligible spontaneous reaction between Br atoms and Si. In addition, the low etch rate of SiO_2 provides a high selectivity of Si etching with respect to oxide. Also, a highly uniform and clean etch process was reported for A^3B^5 semiconductors due to the chemical reactions of hydrogen atoms with the etched surface. However, though the practical use of HBr plasma has some evident perspectives, the development and optimization of the etch process is retarded by the insufficient knowledge of the plasma chemistry in this system.
In this work we carried out the study of plasma parameters and active species kinetics in HBr direct current (dc) glow discharges, using the 0-dimensional self-consistent model.
The set of equations included: 1) The steady-state Boltzmann kinetic equation without accounting for both electron-electron collisions and the second-order impacts; 2) The plasma conductivity equation; 3) The balance equations for neutral and charged particles in a steady-state approximation; 4) The quasi-neutrality conditions for densities of charged particles as well as for their fluxes to the reactor wall. The output parameters were electron energy distribution function (EEDF), mean electron energy ($\bar{\varepsilon}$) and drift rate, transport and kinetic coefficients of neutral and charged species, their volume-average densities and fluxes. As the self-consistency criterion, we used the balance equation for electrons in the approximation of "effective" diffusion coefficient. The set of cross-sections for HBr was composed on the base of Refs. [1-3].
The calculations showed that an increase in E/N results in the same behaviors of both the fraction of high-energy electrons in EEDF and the mean electron energy while in the low E/N region the EEDF is impoverished by the electrons with the energies of 2–3 eV. This effect is due to the electron energy losses through the rotational and vibrational excitations of HBr. The rate constants for high-threshold processes with $\varepsilon_{th} \geq \bar{\varepsilon}$ (ionization, electron excitation) correlate with the changes EEDF and mean electron energy, and the rate constants for low-threshold processes (rotational excitation, vibrational excitation, dissociative attachment) show a decrease with increasing E/N. This is because of decreasing fraction of "slow" electrons in the EEDF. In the range of E/N=4.5×10^{-16}–1.0×10^{-14} Vcm^2 the dissociation of HBr molecules realizes mainly through the excitation of $a^3\Pi$ state while the summary contribution of the $A^1\Pi$ и $t^3\Sigma$ states to the total dissociation rate varies in the range of 22–46%. This is due to the differences in corresponding cross-sections in a maximum of EEDF. Also, the contribution of dissociative attachment to the total dissociation rate is less than 10%.
It was found that the HBr molecules are the dominant neutral species in HBr plasma. The steady-state densities of HBr dissociation products are noticeably influenced by the atom-molecular processes, such as HBr+Br→Br_2+H (R1), HBr+H→H_2+Br (R2), Br_2+H→HBr+Br (R3) and H_2+Br→HBr+H (R4). The fast decay of H atoms in R2 and R3, which also represent the additional channels for the formation of Br atoms, results in a disproportion between Br and H densities, so that [Br]>>[H]. The densities of Br_2 and H_2 were found to be higher than the densities of atomic species. The reasons are the high formation rate of H_2 molecules in R2 as well as the high tree-body recombination rate of Br atoms.
An increase in gas pressure from 30-250 Pa results in decreasing electron density, but in increasing both absolute and relative negative ion densities. This results from increasing rate of dissociative attachment which becomes a dominant electron loss pathway for the pressures higher than 50 Pa. The reason is the high dissociative attachment cross-section, which provides the corresponding rate coefficient in the range of 4.55×10^{-10}-5.75×10^{-10} cm^3/s.

1. T.N. Rescigno, "Effective potential methods in variational treatments of electron-molecule collisions, II. Application to HBr", J. Chem. Phys., 104(1), pp.125-129, 1996
2. O. Šašić, S.Dujko, Z.Lj. Petrović, "Transport coefficients for electrons in mixtures of Ar and HBr", Jpn. J. Appl. Phys., 46(6A), pp. 3560-3565, 2007
3. M. Probst, H. Deutsch, K. Becker, T.D. Mark, "Calculations of absolute electron-impact ionization cross sections for molecules of technological relevance", Int. Journal of Mass Spectrometry, 206, pp.13–25, 2001

Mechanisms of film deposition from BCl_3-based plasma during dry etching

D. Shamiryan[1] , A.M. Efremov[2] , V. Serlenga[3] , M. R. Baklanov[1], W. Boullart[1]

1. IMEC, Leuven, Belgium, shamir@imec.be 2. Ivanovo State University of Chemistry and Technology, Ivanovo, Russia, 3. Instituto Universitario di Studi Superiori, Pavia, Italy

Continuous downscaling of semiconductor devices requires introduction of new materials in semiconductor manufacturing, which, in turn, requires new technological processes in order to integrate the new materials into the circuits. In particular, introduction of metal gates requires new plasma etch chemistries. One of those chemistries is based on BCl_3 plasma as it is known to etch metals, metal oxides and be selective over Si substrate. This plasma, however, has some peculiarities that sometimes are not well understood. One of those peculiarities of BCl_3 plasma is ability to deposit a film at certain conditions. The deposition of a film can significantly influence the etch results.

It was shown that depending on additives one can obtain a B-Cl film (from pure BCl_3 plasma), no film (BCl_3+5%O_2) or B-N film (BCl_3+N_2). We have already shown that those films have strong influence on the profile of TaN metal gates [1]. In this work we studied the mechanisms of film deposition from BCl_3 plasma.

In order to study film deposition from BCl_3-based plasma we exposed 200 mm Si wafers to pure BCl_3 plasma or BCl_3/O_2 mixture at different pressures with zero substrate bias. Plasma composition was monitored by optical emission spectroscopy (OES), deposited film thickness was measured by ellipsometry. The plasma was simulated by zero-dimensional model described elsewhere [2]. The model allows calculation of species density in the plasma and coverage fraction on the surface. We found that in pure BCl_3 plasma film thickness exponentially increases with decrease of pressure, while for BCl_3/O_2 mixture (O_2>20%) a reverse trend was observed: the film thickness linearly increased with pressure, as shown in Fig.1. No deposition observed for 3%<O2<20%. For pure BCl_3 plasma film thickness corresponds to the surface fraction of atomic B, as illustrated by Fig.2. Such behaviour is explained by the simulations where B is only consumed by Cl_2 through the reaction

$$B + Cl_2 \rightarrow BCl + Cl \qquad (1)$$

Since Cl_2 is not present in the plasma and can only be formed by recombination of Cl dissociated from BCl_x and its concentration drops with pressure, the concentration of B increases with pressure. When O_2 is added to the mixture, volatile BO_x compound are easily formed as observed by OES. With increase of O_2 concentration and pressure B_2O_3 film starts to deposit on the wafer.

In conclusion, pure BCl_3 deposits a B-Cl film with the B consumption as a limiting step. BCl_3/O_2 deposits B_2O_3 with, apparently, species density as a limiting factor.

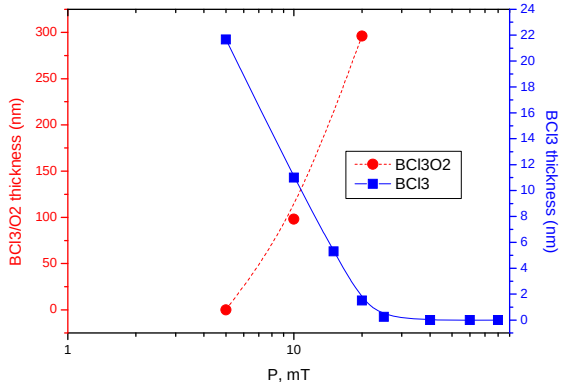

Fig. 1. Film thickness deposited from BCl_3 and BCl_3/O_2 plasma

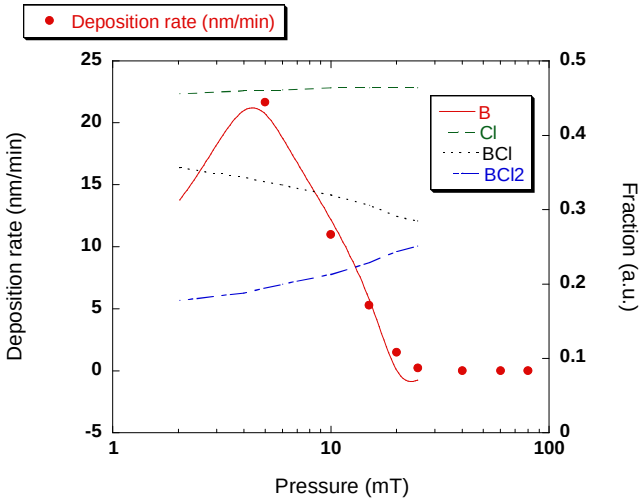

Fig. 2. Measured film thickness (circles) and calculated surface fractions of different species in pure BCl_3 plasma

1. D. Shamiryan *et al*. *55th AVS Symposium, 19-24 Oct 2008, Boston, USA*
2. M. Kim *et al*. J. Vac. Sci. Technol. A, 26, p.344, 2008

Excitation Mechanism of the B^+ Emission Line at 345.1 nm in Low-Temperature Plasma

V.P. Kudrya
Institute of Physics and Technology, Russian Academy of Sciences, Moscow, Russia, E-mail address kvp@ftian.ru

Boron-contained plasmas are widely used in contemporary microelectronic technology. For example, BF_3-based plasmas are used for boron implantation [1] and etching [2] of Si, BCl_3-based plasmas are used for etching of GaAs, Al [3], TaN [4], HfO_2, ZrO_2 [5], and so on, plasmas contained B_2H_6 and N_2 or NH_3 are used for BN thin film deposition [6].

The observed emission spectra of boron-contained molecular plasmas include strong lines at 249.7 nm (B, dublet, resonant transition) and at 345.1 nm (B^+, singlet). To use these lines for plasma diagnostics, understanding of excitation mechanisms is necessary. On the other side, the excitation mechanisms are also necessary for development of plasma kinetics numerical simulation. Nevertheless, the problem of excitation mechanisms for the mentioned emission lines is open to date.

In the report the results of the 345.1 nm line excitation mechanism investigation are presented. A comprehensive analysis of the radiative transition rates for the B^+ lower energy levels is carried out. The cross sections and rate constants of the electron impact excitation/de-excitation processes involved are also calculated. These fundamental data are used in a radiative-collisional model that results in the steady-state B^+ level population. An important feature of the model is taking into account the ladder excitation mechanism through the metastable level $2s2p\ ^3P^o$ by electron impact. This mechanism strongly changes the dependences of population (and line intensities) on the plasma electron temperature.

A dependence of the intensity relation for the 345.1 nm and 162.4 nm on the plasma electron temperature is also presented that can be used for plasma diagnostics.

1. K. Rudenko, S. Averkin, V. Lukichev, A. Orlikovsky, A. Pustovit, and A. Vyatkin, "Ultra shallow p^+-n junctions in Si produced by plasma immersion ion implantation", Proc. SPIE, 6260, 626003, pp.1-9, 2005.
2. D.C. Hays, K.B. Jung, Y.B. Hahn, E.S. Lambers, S.J. Pearton, J. Donahue, D. Johnson, and R.J. Shul, "Comparison of F_2-based gases for high-rate dry etching of Si", J. Electrochem. Soc., 146, pp.3812-3816, 1999.
3. R.J. Saia and B. Gorowitz, "High rate aluminum etching in a batch loaded reactive ion etcher", Solid State Techn., 26, pp.247-252, 1983.
4. M.H. Shin, M.S. Park, N.-E. Lee, J. Kim, C.Y. Kim, and J. Ahn, "Dry etching of TaN/HfO_2 gate-stack structure in $BCl_3/Ar/O_2$ inductively coupled plasmas", J. Vac. Sci. Technol. A, 24, pp.1373-1379, 2006.
5. L. Sha and J.P. Chang, "Plasma etching selectivity of ZrO_2 to Si in BCl_3/Cl_2 plasmas", J. Vac. Sci. Technol. A, 21, pp.1915-1922, 2003.
6. B.P. Lavrov, M. Osiac, A.V. Pipa, and J. Röpcke, "On the spectrometric detection of neutral species in a low-pressure plasma containing boron and hydrogen", Plasma Sources Sci. Technol., 12, pp.576-589, 2003.

De-processing technologies for modern VLSI based on grazing incident ion beams

A.F. Vyatkin
Institute of Microelectronics Technologies, Russian Academy of Sciences, Chernogolovka, Russia, Vyatkin@ipmt-hpm.ac.ru

With increased VLSI integration, cells are being miniaturized, and gate oxide films and capacitor insulating films are becoming thinner. Furthermore, multiple layers, trenches and other three-dimensional structures are making technological processes more complex. As a result, problems rooted in the processes occur more easily, resulting in various failures of integrated circuits (IC) and make it difficult to ensure their quality and reliability. Thus, failure analysis technologies are becoming more and more important in order to analyze process-related problems. Particularly, for failure analysis of ICs it is necessary to open and delayer a chip layer by layer in order to find a hidden defect or defects.

There are a lot of failure analysis techniques. Many of them are related to selective layer-by-layer plasma etching, reactive ion etching (RIE) or chemical etching of IC comprising different components and structures or some combination of these techniques. Depending on the desired information, de-layering of the integrated circuits is usually performed by either of two strategies, anisotropic removal of all dielectric layers, or sequential removal of all layers including conductors. In the first procedure, all dielectric layers are removed anisotropically down to the silicon surface, i.e. to the area of active devices. Metal conductors will be left sitting on top of pedestals of dielectric material. Anisotropic dielectric removal is useful, but in many situations defects or other features of interest may lie underneath conductors. In this case, it is necessary to remove metal and dielectric layers sequentially. Normally, inductively coupled plasma systems or straight RIE systems are used to perform sequential etching. In order to maintain planarity during sequential de-layering of an IC, it is desirable to stop each dielectric etch when a level is reached that is even with the next metal layer to be etched. Thus when the passivation is etched, it should be etched level with the base of the metal line. Since there is no etch stop between the dielectric layers, this process requires a timed etch.

Hence, novel techniques are required to get precise information about possible reasons of IC failures occurring at the different steps of IC processing. Grazing incidence ion irradiation of solids can be used for smoothing of surfaces and of growing films as well as for the formation of regular nanogrooves, ripple and dot patterns. Many of these processes are exploited successfully in nano- and microelectronics and in diagnostics for TEM sample preparation. In the present work, physical ion sputtering when ions incident upon solids at grazing angles is proposed as an instrument for integrated circuits failure analysis. Sample rotation must be added to the procedure as a option to provide uniform sequential etching of IC. It is well known that various IC components have different sputtering yields. It means that different portions of IC will have different etching rate and as a results the surface of etched IC will be far away of planarity. Meanwhile, sputtering rate depends on the incidence angle of ions used for solids etching. So, all steps which have aroused on the IC surface due to different etching rate of various IC components will meat incident ions at the angles characteristic for higher sputtering yields. As a result, planarization of an initially uneven IC surface should be expected during its bombardment by grazing incident ion beams. The dynamic equilibrium will exist at the assumed conditions and sequential planar layer-by-layer etching will be realized when etching front will move into the depth of IC.

To confirm described above scenario, experimental etching of standard microcircuits and specially prepared test samples by means of grazing incident ion beams has been performed. Ar+ ions with energy of 1 keV and ion current density of 0.5 mA have been used as etching ions. It was demonstrated that at incident angle of 85^0 off sample surface normal and sample rotation with 5 r/min IC comprising different components such as SiO_2, Al or Cu, TiN, W can be sequentially etched keeping planar surface and allowing to open each metallization layer separately from above and below laying layers. Test samples with rectangular Al protrusion on the top of oxidized silicon sample has been etched at the similar conditions. The evolution of the Al protrusion shape has been studied. About one hour of ion irradiation takes to achieve fully even surface of the sample. So, these experiments provide good proves of grazing incident ion beams applicability for sequential layer-by-layer IC etching.

Development of computer methods for multi nano-layer parameters measurements by X-Ray reflectometry

N.N. Gerasimenko[1], D.A. Kartashov[2], A.G. Turyansky[3]

1. *Moscow Institute of Electronic Technology, Moscow, Zelenograd, Russia, rmta@miee.ru.*
2. *JSC Mikron, Moscow, Zelenograd, Russia, dmitry_kartashov@mikron.ru.*
3. *LPI, Moscow, Russia, tour@sci.lebedev.ru.*

The results of implementation of multi-parameter optimized algorithms for data processing obtained with Relative X-Ray Reflectometry (RXRR) technique. This method is used for different multi nano-layer metal and dielectric films.

For data interpretation in X-ray reflectometry technique new algorithms are applied. This new algorithm includs genetic algorithm (GA) [1], extended GA and other GA modifications.

Recently, a novel algorithm that differs in interpretation approach (BA) has been developed [2]. In this paper efficiency of BA is being compared to different algorithms, including GA as well, using a set of test functions with number of variables from 2 to 10. Comparison shows that in 80 % of cases efficiency of BA surpasses efficiency of any other evolutionary algorithms, including GA. Distinctive feature of BA is the smaller quantity of the objective function addressing, which is necessary for finding of the solution with the defined accuracy in comparison with GA. It means actually shorter computation time.

Initially a set of interpretation algorithms was applied to X-ray reflectogram, obtained at simulated nanostructure models (Al on Si). As a result we have found that in some cases BA allows to reduce the error function up to 2 times compared to the classical GA at similar computation time.

Later the extended BA (eXtended Bees Algorithm, XBA) where relationship between values of the objective function and searching range was applied, was developed. This XB algorithm was applied for interpretation through others and showed the best results at decoding of simulated structures. Obtained fitting error was about 10^{-15} with number of layer from 1 to 5.

All considered algorithms (BA, GA [3] and XBA) were applied for interpretation of data obtained with measurement of platinum nano-films, grown upon silicon substrate. At a number of iterations starting from 500 steps (about one tenth of traditional number of steps for robust interpretation) the XBA showed the best result at any interpretation run.

Sufficient superiority of the XBA against other algorithms for interpretation task is revealed, in a starting from low number of iterations.

References:

1. Wormington, M., Panaccione, C., Matney, K. M., & Bowen, D. K. Characterization of structures from X-ray scattering data using genetic algorithms."Philos. Trans. R. Soc. Lond.", ***357***, pp.2827-2848. (1999)
2. The Bees Algorithm – A Novel Tool for Complex Optimisation Problems.
Pham DT, Ghanbarzadeh A, Koc E, Otri S, Rahim S and Zaidi M. The Bees Algorithm. Technical Note, Manufacturing Engineering Centre, Cardiff University, UK, (2005)
3. http://lancet.mit.edu/galib-2.4/

Experimental scheme for observation of anomalous Kossel effect in semiconductor structures

P. G. Medvedev, M. A. Chuev
Institute of Physics and Technology, Russian Academy of Sciences, Moscow, Russia, E-mail: mskmail@yandex.ru

The method of Kossel lines in its standard form was developed as early as in the mid-1930s. Three decades further on, it proved to be notably useful for determining the phase angle of scattering amplitudes, and therefore was widely adopted in x-ray structure determination. Recent years have seen a surge of interest in the emission of x rays from a crystal in relation to x-ray holography. In fact, this research topic covers both Kossel analysis and the well-known x-ray standing-wave method. Not requiring perfect translational symmetry, x-ray holography is applicable to imperfect crystals such as ones made up of macromolecules, impurities, or nanostructures, or crystals occurring in the internal atomic layers and the surrounding regions of heavy atoms in heterogeneous structures. Moreover, x-ray holography may serve to enhance the effectiveness of conventional crystallographic techniques. In 1991 Afanas'ev and Esayan [1] considered x-ray diffraction in extremely asymmetric schemes to predict the generation of an x-ray beam compressed up to several hundred times, propagating in the bulk of the crystal parallel to its surface. This prediction was verified by experiments employing the x-ray standing-wave method, photoelectrons being detected with a gas-flow proportional counter specifically designed for the experiments. Further, the large amount of compression suggested changes in the distribution of emission intensity within Kossel lines, and recent theoretical research indeed showed the distribution to appear as a sharp peak hundreds of times as intense as the background [2-4].

The simplest way of detecting anomalous Kossel lines is to use a crystal analyzer which must be made of the same material as the sample under investigation. In this case, in order to be able to disregard dispersion, use should be made of the same reflection for which the anomalous Kossel effect must be observed. In addition, the crystal analyzer should be oriented so that the reciprocal lattice vectors for the sample under investigation and the crystal analyzer lie in the plane of reflection. Rotating the crystal analyzer about a vertical axis, we can measure in this scheme the dependence of the reflected wave intensity on the angle of rotation of the crystal analyzer. The calculation of the diffraction-induced reflection (rocking) curve obtained in this experiment is reduced to the calculation of the convolution of the radiation intensity distribution function within the Kossel line with the reflection curve of the crystal analyzer in the angular interval determined by the system of gaps. In order to avoid the suppression of the observed effect to the background enhancement, we must cut a certain angular region of the order of ten angular minutes along the Kossel line in the vicinity of the radiation intensity peak with the help of a slit in front of the crystal analyzer and, in addition, choose the extremely asymmetric reflection in the analyzer to make the asymmetry coefficient large enough to ensure the formation of a narrow detection window in the crystal analyzer. In addition, the angle at which radiation emerges from the analyzer must be much larger than the specular reflection angle to ensure relatively simple detection of this radiation, preserving the maximum value of reflectivity. Also in calculations of proposed experimental scheme frequency dispersion of emerging radiation in Kossel line is considered.

This work is financially supported by the Russian Foundation for Basic Research (project No. 09-02-12164).

1. A.M. Afanasev and A.V. Esayan, "X-Ray Diffraction in Extremely Asymmetric Diffraction Schemes in the Vicinity of a "Degenerate" point", Phys. Stat. Sol. (a), 126, pp. 303-311, 1991
2. A.M. Afanasev, M.V. Kovalchuk and M.A. Chuev, "Kossel Lines in Extremely Asymmetric Diffraction Schemes", JETP Letters, 73, pp. 271-273, 2001
3. A.M. Afanasev, M.V. Koval'chuk, M.A. Chuev and P.G. Medvedev, "Kossel Lines as a New Type of X-Ray source", JETP, 95, pp. 472-479, 2002
4. P.G. Medvedev, A.M. Afanas'ev and M.A. Chuev, "Anomalous Kossel Effect in Semiconductor Structures", Russian Microelectronis, 35, pp. 359-371, 2006

Structural Investigation of Magnetic Digital Alloys

I.A. Subbotin[1], M.A. Chuev[2], V.V. Kvardakov[1], I.A. Likhachev[1], E.M. Pashaev[1]
[1]Russian Research Center "Kurchatov Institute", 123182 Moscow, Russia, E-mail: subbotin@kcsr.kiae.ru . [2]Institute of Physics and Technology, Russian Academy of Sciences, 117218 Moscow, Russia, E-mail: chuev@ftian.ru

Magnetic digital alloys, which are a periodic system of submonolayers of magnetic ions located between the nanometer layers of a semiconducting material in the form of the superlattice, demonstrate a number of unordinary electron and magnetic properties promising for designing devices for the writing and storage of information. In this work, we consider only the problem of the structural diagnostics of such materials on the basis of analyzing the high-resolution X-ray glancing-incidence mirror reflection [1].

The 15(Mn/GaSb) superlattice is grown on the GaAs(001) substrate by the laser ablation method with the suggested values of the superlattice period $d=L_1+L_2=3$ and 10 nm and ratio of the thicknesses of the Mn and GaSb layers $L_2/L_1= 0.2$ and is then coated with a GaSb layer with the thickness L_1. Measurements of X-ray investigations are carried out on a two-crystal x-ray spectrometer with collimated Cu $K_{\alpha 1}$ radiation from an x-ray tube with a power of 1.5 kW and a Si(111) monochromator. X-ray glancing-incidence reflection curve for the sample with d=10 nm displays a distinct two-humped first Bragg peak from the superlattice while that for the sample with d=3 nm is smooth without any signs of the Bragg peak. These facts are naturally related to an imperfect structural quality of the superlattices grown. A detailed treatment of the experimental X-ray data has allowed us to show that the electron density of the Mn-layers in digital-alloy superlattices corresponds to a mixture of Mn and GaSb into the layers, which has allowed us to estimate the diffusion depth of Mn atoms into adjacent GaSb thicker layers. The results of the analysis confirm all qualitative and quantitative estimates of the structural parameters of the really grown superlattice. Indeed, simple analysis of the recovered distribution profile shows that (i) the number of bilayers is equal to 14, eight of which form a certain "gradient buffer" on the substrate, (ii) the average thicknesses of the layer over the superlattice L_1 = 3.5(3) nm and L_2 = 3.8(3) nm, (iii) the electron density of the "manganese" layers corresponds to the mixing of Mn and GaSb in these layers, and (iv) the thickness of the distorted layer on the surface is L_N = 6.6(2) nm.

This work was financially supported by the Russian Foundation for Basic Research (grant No. 08-02-01462, 09-02-12164).

1. M. A. Chuev, I. A. Subbotin, E. M. Pashaev, V. V. Kvardakov and B. A. Aronzon. "Phase relations in analysis of glancing incidence X-ray rocking curves from superlattices". JETP Letters, 85, No. 1. pp. 17-22, 2007

Spectroscopic and scanning ellipsometry for investigation of surfaces, thin films and nanolayers

V. Tolmachev[1], T. Zvonareva[1], L. Portzel[1], V. Kudoyarova[1], T. Perova[2], V. Shvets[3] and S. Rykhlitskii[3]

1. *Ioffe Physical Technical Institute, Russian Academy of Sciences, St. Petersburg, 194021 Russia,*
2. *Department of Electronic and Electrical Engineering, University of Dublin, Trinity College, Dublin 2, Ireland,*
3. *Semiconductor Physics Institute SB RAS, Novosibirsk, Russia,*

E-mail address: tva@mail.ioffe.ru

The fabrication of new materials for deposition of thin films and nanolayers as well as the investigation of the surface of solids and processes at the "solid-liquid" interface requires an informative and non-destructive methods of characterisation. The optical methods and ellipsometry, in particular, are the most suitable techniques for these purposes. The ellipsometry is the method which analyse the polarisation variation of the light beam reflected from the investigated surface.

In this work the results of investigation of thin films of amorphous carbon – platinum (a-C:Pt) composites and a-$Si_xC:H_{(1-x)}$, using spectroscopic ellipsometer Spectroscan (Novosibirsk, Russia) are performed. The ellipsometric parameters Δ and ψ were measured in the range of wavelengths from 250 to 900 nm. For the data analysis the Bruggeman effective media approach for the determination of film composition and a Cauchy equation for determination of the dispersive parameters of a-C film have been used.

The modification of the surface of GaAs as a result of gas discharge effect was also investigated using spectroscopic ellipsometry. In case of the electrons influence the effective medium model includes a thin oxide film of Ga_2O_3 on the surface of the substrate, while in case of the ions influence, the effective medium model includes the amorphous a-GaAs, crystalline a-GaAs and voids.

Silicon membranes with thickness of a few hundreds nanometers can be obtained on Si-On-Insulator (SOI) structures by removing the excess layers using wet of reactive ion etching (Fig. 1 a). The area of thus obtained Si membrane windows can be varied from 5x5 μm^2 to 100x100 μm^2 (see Fig. 1 b). These structures can be utilised as sensing elements in bio-chemical micro-reactors. It is important to know the quality of these membranes as well as to determine very precisely the thickness of membrane in certain position of the fabricated Si window. For this analysis the single-wavelength scanning ellipsometer SCAN150 (Novosibirsk, Russia) have been used. The scanning of the original SOI structure as well as the window area has been carried out (Fig. 1 c). The thickness distribution across the area of Si membrane was analyzed, which provides information about high thickness uniformity (± 2 nm) within certain areas of membrane.

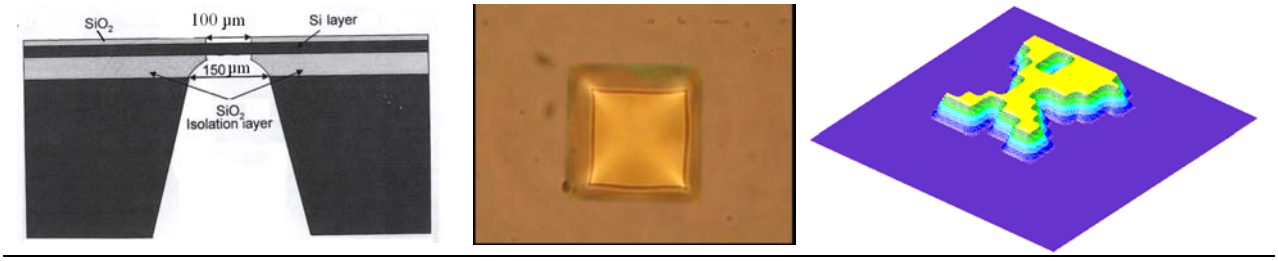

a b c

Fig.1 a) Schematic cross-section of Si membrane with thickness of 0.25 μm, fabricated on SOI structure, with area of 100x100 μm^2; b) top view of membrane obtained with optical microscope; c) thickness distribution(250-251 nm) within the membrane window area obtained by scanning ellipsometry.

The results of these investigation show that modern ellipsometry demonstrates a high sensitivity, self-descriptiveness, possibility of investigation of the modified solid surface as well as in-situ liquid/gas measurements with relatively high spatial resolution (3 mm for spectroscopic and 10 μm for single-wavelength ellipsometry). At the same time this technique is non-destructive and non-contact. However, this technique required mirror-like surface of the sample, high parallelism of the interfaces, as well as to use an accurate modelling of the investigated structure and their justification for application to a particular structure.

Temperature of one-side polished silicon wafer at different position relatively incoherent radiance source

V. I. Rudakov, V. V. Ovcharov, V. P. Prigara
Yaroslavl Branch of Institute of Physics and Technology RAS
E-mail: vladovcharov@rambler.ru

The influence of surface roughness on the temperature of a silicon wafer during incoherent radiance heating was studied. The time-temperature diagrams of heating and cooling processing for p-type lightly doped Si wafers (12 Om·cm) with double-side polished and one-side polished surfaces with different position of a rough surface facing the heater were measured. A comparison of the stationary temperatures of the wafers under the same heating conditions in a hot-wall method film-growth reactor for temperature ranging from 100 to 250°C was made. It was found that under the same experimental conditions the maximum stationary temperatures are observed for the one–side polished wafers with a rough surface facing the heater and the minimum ones for the two-side polished. The stationary temperatures for the one-side polished wafers with a polished surface facing the heater have intermediate values. The differences of the stationary temperatures corresponding to the equal heating conditions are decreased with lower radiation power. The maximum values of this difference ~10°C are observed at maximum wafer temperature ~ 250°C, and minimum ones ~5°C at the minimum stationary temperatures ~150°C. The optical model of rough surface was proposed. In accordance with the model the roughness surface is put in correspondence to the damaged layer with a neglecting thickness possessing its own optical characteristics: reflectance R_d and linear extinction coefficient k_d. The relation between the optical characteristics of the damaged layer valid for the opaque wafers, suggesting that all the radiation "underreflecting" from the rough surface is absorbed in the damaged layer is proposed. In the framework of this model the optical parameter describing the degree of surface roughness is introduced. The dependences of absorbance of silicon wafers on the value of this optical parameter and the position of rough surface with respect to the radiation heater are studied theoretically. Our model explains the experimental data obtained.

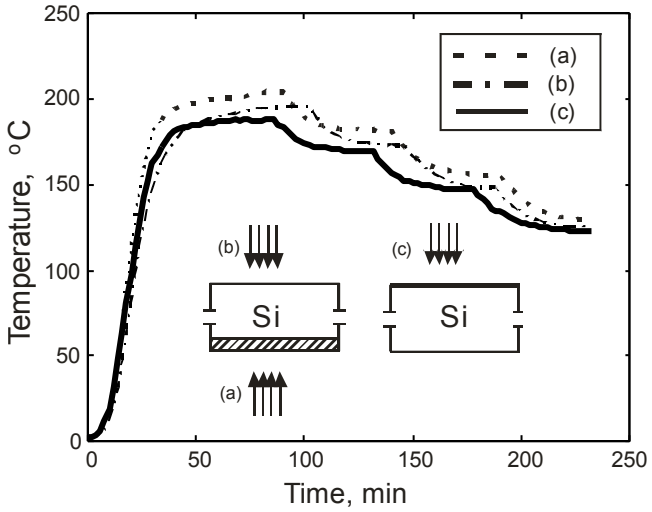

Fig.1. Time–temperature diagrams of heating and cooling lightly doped silicon wafer (100) orientation during incoherent irradiation. a) the one-side polished wafer facing by grinded side to heating source; b) the one-side polished wafer facing by polished side to heating source; c) the two-side polished wafer.

Quantum computer without uncontrollable Coulomb interaction among space-based qubits

S. Filippov, V. Vyurkov
Institute of Physics and Technology, Russian Academy of Sciences, Moscow, Russia, vyurkov@ftian.ru

The main disadvantage of quantum computers based on space states in quantum dots is an uncontrollable interaction between even distant qubits due to long-range Coulomb forces. The rough estimation of phase decoherence time for realistic two double quantum dot (DQD) qubits of a size 10nm placed at a relatively long distance 100nm from each other gives rise to $10^{-10}s$ which is far from practical requirements. It should be underlined that unlike to all other sources of decoherence this one cannot be suppressed by lowering the temperature.

Recently an implementation of qubits [1, 2] where no charge transfer occurs during computation was put forward. Encoding and processing of quantum information is merely performed on symmetric and antisymmetric states in DQDs. However, the original proposal implies an identity of quantum dots and perfect symmetry of the structure. Here we withdraw this severe obstacle on way of experimental realization and show that the proposed construction, in fact, could do without foregoing restrictions. Nevertheless, an aspiration to perfect symmetry and identical quantum dots should remain with the aim to diminish decoherence caused by voltage fluctuations on gates. Fortunately, those fluctuations become small at low temperature.

A qubit is implemented in two DQDs (Fig.1). A DQD consists of a pair of quantum dots with a single electron. The electrode E operates on the strength of exchange interaction between electrons in DQDs. The electrode T varies tunneling coupling between quantum dots constituting a DQD. The dots may have different size and shape. The only demand is that the ground state energy of all dots in a circuit must be equal. It could be meet by placing additional gates nearby quantum dots (not shown in Fig. 1). A quantum computer is composed as a chain of qubits separated by gates operating on the strength of exchange interaction between adjacent DQDs (Fig. 2).

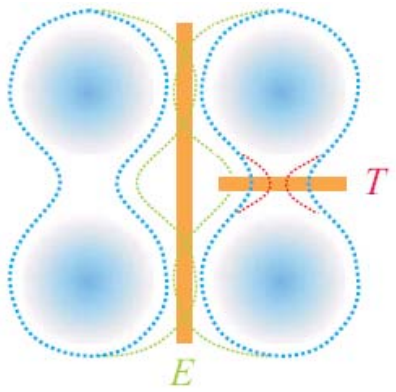

Fig. 1. Single qubit.

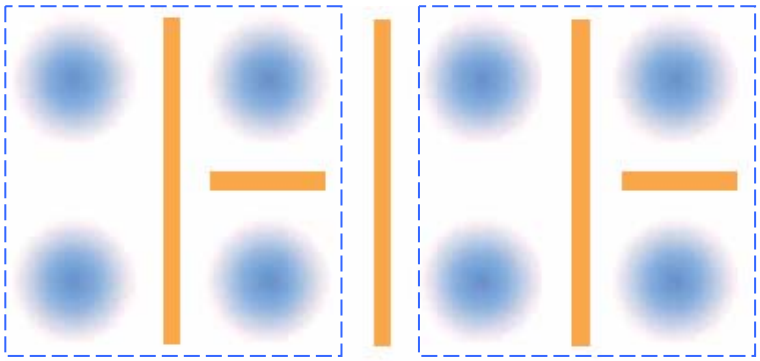

Fig. 2. Two neighbor qubits.

Lately, the possibility of CNOT operation between any pair of qubits in a computer was proved [2]. This opens prospects to universal quantum computing.

The research was supported via the grant # F793/8-05 of the Computer Company NIX (science@nix.ru) and the grant #08-07-00486-a of the Russian Basic Research Foundation.

1. V.V.V'yurkov and L.Y.Gorelik, "Charge based quantum computer without charge transfer", arXiv: quant-ph/0009099, 2000
2. S. Filippov, V. Vyurkov, and L. Gorelik, "Quantum computing based on space states without charge transfer", arXiv: quant-ph/0903.1056v2, 2009

Quantum information transfer protocol via optimized single-electron transport in semiconductor nanostructure

Alexander V. Tsukanov

Institute of Physics and Technology, RAS, Moscow, Russia, email: tsukanov@ftian.ru

In this work, we investigate a problem of interqubit connections at large distances. As the example, we consider two qubits presented by electronic spins in singly-charged semiconductor quantum dots (see figure). The distance between the qubits is supposed to be sufficiently large to neglect direct exchange interaction of the qubit spins. The effective (indirect) qubit coupling is achieved making use of the third (probe) electron. At the beginning of the algorithm its spin is initialized. In fact, the probe electron serves as a flying qubit that at the first step interacts with one qubit electron so that their spins become entangled *(1)* and, being transported to another qubit electron via an auxiliary structure *(2)*, it transfers information about first qubit to the second one *(3)*. So the electron's spin degree of freedom contains qubit state whereas electron's charge degree of freedom plays role of an information bus. To shuttle probe electron between edge structure dots, the resonant electromagnetic pulse is applied to the structure. We discuss how to optimize the information transfer process via appropriate engineering of the nanostructure potential $U(x)$ as well as the driving pulse amplitude $E0$ and frequency ω.

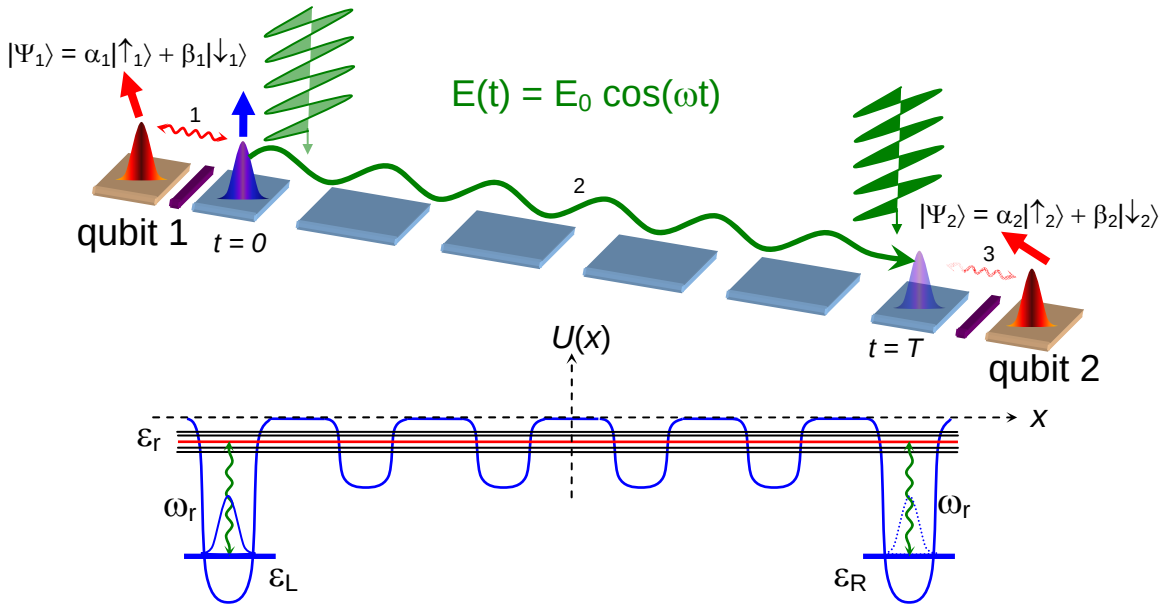

Outlook for the application of Ge/Si quantum dots in quantum calculations

A. Zinovieva[1], A. Nenashev[1], A. Dvurechenskii[1], A. I. Nikiforov[1], A. Lyubin[1], L. Kulik[2]

1. *Institute of Semiconductor Physics, Russian Academy of Sciences, Novosibirsk, Russia, aigul@isp.nsc.ru*
2. *Institute of Chemical Kinetics and Combustion, Novosibirsk, Russian Academy of Sciences Russia, chemphy@kinetics.nsc.ru*

For successful quantum calculations using spin states the fulfillment of three main conditions is required: an existence of entangled states, a possibility of one-qubit and two-qubit operations and a long spin relaxation time. Strong confinement of electrons in quantum dots (QDs) leads to a significant increase of spin lifetimes due to the absence of spin-flip mechanisms governed by the momentum relaxation. An extremely long spin lifetime is expected in zero-dimensional structures based on Si due to the weak spin-orbit (SO) coupling in this material. A promising way to the creation of zero-dimensional structures is the strain epitaxy. Semiconductor QDs fabricated by this technique can be controllably positioned and electronically coupled. The Ge/Si heterosystem is one of the most suitable systems for strong electron confinement in all three dimensions in Si. The electron is localized in a potential well emerging due to the strain in Si nearby a Ge QD. The strain is maximum near the apex of the QD and decays in Si, thus forming a triangular potential well for the electrons. A very long spin relaxation time can be expected for electrons localized in this potential well. However, the main structural property of the electron potential wells in the system containing Ge/Si quantum dots is the absence of mirror symmetry across the growth plane (100). Therefore the SO interaction in this system can provide an intense spin relaxation and shorter spin lifetimes. The present work is devoted to the experimental and theoretical study of main characteristics important for quantum calculations in the Ge/Si nanostructures with quantum dots.

Theoretical calculations and experimental study show that the binding energy of electron can be significantly increased by creation of Ge/Si QD multilayer structure or embedding of Ge QD layer into two-dimensional strained $Si_{1-x}Ge_x/Si/ Si_{1-x}Ge_x$ channel. EPR measurements in continuous wave *(cw)* and pulsed (spin echo) mode were performed. We observed a new EPR signal with anisotropic line width. An analysis of the obtained g-tensor values confirms electron localization in the strain-induced potential wells in the vicinity of the Ge dots. For explanation of EPR line width behavior we proposed a model of anisotropic spin relaxation due to the interaction of electron spin with the effective magnetic field, lying in the plane of the QD array (analog of Bychkov-Rashba field). This magnetic field arises during tunneling of electron between QDs. Each tunnelling event causes the spin precession in the effective magnetic field and this provokes the spin flip after several times of random tunnelling events. This model implies a special relation between values of T_2 (a coherence time) and T_1 (a spin population relaxation time), $T_2=2T_1$, if the external magnetic field is perpendicular to the QD array plane. The measurements of spin echo confirm this model of spin relaxation. We obtain the required relation between T_1 and T_2 for electrons localized in four-fold stacked multilayer structure with Ge QDs. The measured coherence time reaches the value ~20 μs, while the relaxation time T_1 consists of ~ 10 μs. Since the spin orientation loses preferentially during tunnelling between QDs, the increasing spin lifetimes can be expected in a well-separated QD array, where tunneling transitions between QDs are suppressed.

The results of these experiments can be used as a basis for direct single-qubit operations with electrons strongly confined in all three dimensions in Si. For two-qubit operations one needs the sufficient tunnelling coupling of QDs. We propose to use two layers of QDs: first layer with well separated QDs for storage of information between logic operations and second layer with tunnel-coupled QDs for performing logic operations. The QDs in the second layer are positioned exactly over QDs in the first layer, and the distance between them allows transferring the electron in z-direction between QD layers by applying voltage to the gates located over the QDs. We establish that the tunneling between QD layers in z-direction does not lead to the loss of spin information (due to relaxation of component S_z). We have investigated theoretically the tunneling coupling between QDs in the plane of QD layer. Our approach [1] allows to study the dependence of tunneling coupling on size, form, composition of QDs and on the distance between them. The results of this study will be useful for designing of elementary cell for quantum computation.

This work was supported by RFBR (Grants 08-02-00121, 09-02-90480) and SB RAS (integration project “Developments of physical principles of building of logic elements based on QD nanostructures”).

1. A. F. Zinovieva, A. V. Nenashev, A. V. Dvurechenskii. “Hole spin relaxation during the tunneling between coupled quantum dots” Phys. Rev. B, **71**, p.033310, 2005.

The quantum dynamics of two coupled large spins

V.E. Zobov
L.V.Kirensky Institute of Physics, SB Russian Academy of Sciences,Krasnoyarsk, Russia, rsa@iph.krasn.ru

In recent years, quantum computation not only on quantum systems with two levels (qubits) but on d-level systems (qudits) is investigated. Qudit quantum information processing employs fewer coupled quantum systems: a considerable advantage for the experimental realization of quantum computing. A particle with large spin S, for example a quadrupole nucleus or a single-molecule magnet, can be treated as a qudit with d=2S+1. Interactions of the spin with a static magnetic field and with an electric field gradient result in formation non-equidistant energy levels, allowing to selective control of the states. The question can be point: is there limitation in S? Some expect the quantum-to-classical transition, when the value of S increase, (see [1-3], for example), some don't [4-6].

In this work we study dynamics in a two-spin system governed by an Ising-like Hamiltonian

$$H_{SS} = -(J/S)S_1^Z S_2^Z ,$$

where S_i^α is α-components (α=X,Y,Z) of spin i and ħ=1 is assumed. We calculate the time evolution of X-projections of the spins and the squared I-concurrence [7], which is used as a measure of entanglement. We suppose the two-spin state be a pure product state at initial time and we consider two variants: the spin-coherent states – eigenstates of S_i^X with maximal X-projection [5, 6, 8] and the uniform superposition states [9]:

$$|\Psi_{coh}\rangle = |S\rangle_X = \frac{1}{2^S}\sum_{m=-S}^{m=S}\left(\begin{array}{c}2S\\S+m\end{array}\right)^{1/2}|m\rangle_Z , \qquad |\Psi_{sup}\rangle = \frac{1}{d^{1/2}}\sum_{m=-S}^{m=S}|m\rangle_Z ,$$

where $|m\rangle_Z$ is the eigenstate of S_i^Z. In the first variant the X-projection evolution at S>>1, t<<T ($T = 4\pi S/J$ is the period [1]) is described by a Gaussian function

$$F(t) = <S^X(t)>/<S^X(0)> , \qquad F_{coh}(t) = (\cos Jt/2S)^{2S} \cong \exp\left(-(Jt)^2/4S\right),$$

and in the limit S→∞ we have motion of two classical magnetic moments. Whereas the concurrence and hence entanglement grow in time upon the maximal value C^2=1 as S→∞. For its time evolution at S>>1, t<<T we have obtained the asymptotic formula

$$C^2 = \frac{d}{d-1}\left(1 - Tr_1\rho_1^2\right), \qquad C_{coh}^2 \cong \left(1+\frac{1}{2S}\right)\left(1 - \frac{1}{\sqrt{1+J^2t^2}}\left(1 - erf\sqrt{\frac{J^2t^2+1}{8S}}\right) - \frac{1}{\sqrt{2\pi S}}\right).$$

For the uniform superposition states at any S the quantum properties are observed to a greater degree then for the spin-coherent states. Thus, the large spins can demonstrate both quantum and classical properties depending on a preparation state and observe conditions. It is impotent for us that the quantum mechanics do not put limits on values of S for the quantum computing on qudits represented by large spins.

This work was supported by the Russian Foundation for Basic Research (project. no. 09-07-00138).

1. B.C. Sanders, Phys. Rev. A **40**, 2417 (1989).
2. J.L. Garcia-Palacios, S Dattagupta, Phys. Rev. Lett. **95**, 190401 (2005).
3. A. Polkovnikov, "Representation of quantum dynamics of interacting systems through classical trajectories", cond-mat/0905.3384.
4. A Cabello, Phys. Rev. A **65**, 062105 (2002).
5. S. Ghose, P.M. Alsing, B.C. Sanders, I.H. Deutsch, Phys. Rev. A **72**, 014102 (2005).
6. G. Burlak, I. Sainz, A.B. Klimov, "Entanglement enhancement for two spins assisted by two phase kicks", quant-ph/0906.2986.
7. P. Rungta, V. Buzek, C.V. Caves et al., Phys. Rev. A **64**, 042315 (2001).
8. Y.Yang, W.Liu, Z. Sun, X. Wang, Phys. Rev. A **79**, 054104 (2009).
9. X. Lu, X. Wang, Y.Yang, J. Chen, Quantum Inf. Comput., **8**, 671 (2008); quant-ph/0803.1032.

Can entanglement fluctuate?

M. A. Yurishchev
Institute of Problems of Chemical Physics, Russian Academy of Sciences, Chernogolovka, Moscow Region, 142432 Russia; E-mail: yur@itp.ac.ru

It is discussed a problem of entanglement-entropy fluctuations .The consideration is done with examples of a two-qubit system [1] and quantum Ising chain.

It is shown that the fluctuations in the two-qubit system are absent in the fully entangled and, vice versa, in separable states. On the other hand, there is a region where the entanglement fluctuations are greater than the entanglement itself (the region of strong fluctuations) [1].

In the case of a quantum Ising chain, the fluctuations of entanglement equal zero in the limits of fully ordered and fully disordered states. It is found also that the absolute fluctuations of entanglement entropy diverge at the critical point. However the relative fluctuations of entanglement stay finite in the vicinity of the second-order phase transition.

This work is supported by the Russian Foundation for Basic Research (project no. 07-07-00048) and by the Presidium of the Russian Academy of Sciences (programme no. 18).

1. E. B. Fel’dman and M. A. Yurishchev, “Fluctuations of quantum entanglement”, Pis’ma v ZhETF 90, issue 1, 2009

Quantum cryptography system using phase-time coding and resistant to PNS attack

D.A. Kronberg[1] , S.N.Molotkov[1,2,3]

1. *Faculty of Computational Mathematics and Cybernetics, Moscow State University, Moscow, 119992 Russia*
2. *Institute of Solid State Physics, Russian Academy of Sciences, Chernogolovka, Moscow region, 142432 Russia*
3. *Academy of Cryptography of the Russian Federation, Moscow, 121552 Russia*

E-mail: dmitry.kronberg@gmail.com, sergei.molotkov@gmail.com

A new set of quantum key distribution protocols is proposed. For this set the detection of eavesdropping has two parameters: output bit error rate and the counting rate in the control time slot. For the single-photon source with orthogonal states and no counts in the control time slot, the protocol guarantees secure key distribution if the bit error rate in the sifted key does not exceed 50%, which is theoretical limit. In the case of weak coherent pulses on the source side, when the PNS attack is available, this protocol also provides the largest distance, up to which secure key distribution can be implemented.

Entanglement measure for multipartite pure states and its numerical calculation

A. Yu. Chernyavskiy[1]

1. *Institute of Physics & Technology of RAS (FTIAN), Moscow, Russia, andrey.chernyavskiy@gmail.com*

The quantification of quantum entanglement is a very important and still open question in quantum informatics and physics. We describe an entanglement measure for pure multiparticle states (the minimum of Shannon's entropy of orthogonal measurements). This measure is additive and monotone under LOCC. In addition, this measure is extended to fermionic states. For two-qubit states it coincides with the entropy of the Schmidt decomposition (reduced von Neumann entropy) and for two-fermion states it coincides with entropy of the Slater decomposition.
A method for numerical calculation of this measure by genetic algorithms is also presented. Moreover, the calculation of multiqubit entanglement measure is implemented for CUDA (high performance parallel computations on graphics processing units).

This work is partially supported by RFBR grant 09-01-00347-a.

1. A. Yu. Chernyavskiy, "The computable measure of quantum entanglement of multiqubit states", Mikroelektronika, 2009, Vol. 38, No.3, pp. 217–223
2. A.Y. Chernyavskiy, "Multiparticle analogue of Schmidt coefficients", Quantum Computers and Computing, 2008, 8 (1), pp. 141-148.

Quantum Computing with Collective Ensembles of Multilevel Systems

E. Brion, K. Mølmer, and M. Saffman
Laboratoire Aime Cotton (CNRS), Orsay, France

We propose a new physical approach for encoding and processing of quantum information in ensembles of multilevel quantum systems, where the different bits are not carried by individual particles but associated with the collective population of different internal levels. One- and two-bit gates are implemented by collective internal state transitions taking place in the presence of an excitation blockade mechanism, which restricts the population of each internal state to the values zero and unity.

Quantum computers with 10$\leftrightarrow$20 bits can be built via this scheme in single trapped clouds of ground state atoms subject to the Rydberg excitation blockade mechanism, and the linear dependence between register size and the number of internal quantum states in atoms offers realistic means to reach larger registers.

Spin-1/2 systems with simple two- and three-dimensional geometrical configurations: state transfer and entanglement between different nodes

S.I.Doronin, E.B.Fel'dman and A.I.Zenchuk
Institute of Problems of Chemical Physics, Russian Academy of Sciences, Chernogolovka, Moscow reg.,Russia, zenchuk@itp.ac.ru

The problem of either perfect or high probability transfer of the arbitrary quantum state in spin systems is important due to the development of the quantum computing and quantum communication systems. Most of papers investigating this problem consider the end-to-end perfect state transfer (PST) in spin chains using two basic approaches based on: (a) spin chains with properly distributed coupling constants [1,2] and nearest neighbor approximation and (b) spin chains with remote end nodes [3] involving interactions among all nodes. The problem of end-to-end entanglement [4] and its relationship with end-to-end state transfer [5] has also been considered but many aspects of this problem have not been clarified yet.

In [6] we generalize the problem of the quantum state transfer and consider the high probability state transfers (HPSTs) between arbitrary nodes (not only between end nodes) of the spin-1/2 system with XXZ Hamiltonian involving interactions between all nodes. This generalization is important in revealing the quantum objects which may be candidates for (a) the quantum register where the state transfer between all cells is required or (b) the commutator which distributes the information among different quantum clusters. It seemed out that the simple two- and three-dimensional configurations are preferable for this purpose instead of one-dimensional spin chains. Namely these configurations reveal relatively short time intervals required for the quantum state transfers with probabilities exceeding 90%. We study the rectangle and parallelepiped spin systems of four and eight nodes respectively with proper ratios of their edjes (namely proper ratios of edjes provide all possible HPSTs) and find the parameters of the HPSTs (i.e. probability amplitudes and appropriate time intervals required for the state transfers) between any two nodes of these systems.

We also consider the relationship between the probabilities of the state transfers between different nodes of arbitrary spin system and entanglements between appropriate subsystems of this system using both Wootters [5] and positive partial transpose (PPT) criteria. In particular we introduce explicit formulae relating double negativity $N_{A,B}$ as the measure of entanglement between some subsystems A and B of the whole quantum system and excited state transfer probabilities between different nodes of the spin system. These formulae have been successfully applied to the above mentioned rectangle and parallelepiped spin-1/2 systems revealing a relationship between the state transfer probabilities and node-to-node, edge-to-edge and side-to-side entanglements therein. More precisely, the HPST between the *n*th and *m*th nodes requires strong entanglement between these nodes if only both these nodes belong to the same shortest edge of the rectangle or the parallelepiped. Otherwise these nodes are not entangled with each other while entanglements between edges and sides define the state transfer process.

1. M.Christandl, N.Datta, A.Ekert and A.J.Landahl, "Perfect State Transfer in Quantum Spin Networks", Phys.Rev.Lett. 92, 187902 (2004)
2. P.Karbach and J.Stolze, "Spin chains as perfect quantum state mirrors", Phys.Rev.A, 72, 030301(R) (2005)
3. G.Gualdi, V.Kostak, I.Marzoli and P.Tombesi, "Perfect state transfer in long-range interacting spin chains", Phys.Rev. A, 78, 022325 (2008)
4. L.Campos Venuti, S.M.Giampaolo, F.Illuminati and P.Zanardi, "Long-distance entanglement and quantum teleportation in XX spin chains", Phys.Rev.A 76, 052328 (2007)
5. G.Gualdi, I.Marzoli and P.Tombesi, "Entanglement generation and perfect state transfer in ferromagnetic qubit chains", New J.Phys., 11 063038 (2009)
6. S.I.Doronin, E.B.Fel'dman and A.I.Zenchuk, "Relationship between probabilities of the state transfers and entanglements in spin systems with simple geometrical configurations", Phys. Rev. A 79, 042310 (2009)

Flux-qubit and the law of angular momentum conservation

A.V. Nikulov
Institute of Microelectronics Technology, Russian Academy of Sciences,
142432 Chernogolovka, Moscow District, Russia. E-mail: nikulov@ipmt-hpm.ac.ru

The essence of the fundamental difference of quantum bit from classical bit is the possibility of coherence superposition of two states. The superposition of states is the cardinal positive principle of quantum mechanics according to L.D. Landau [1] and many other theorists. But there is important to keep in mind that, as the Einstein - Podolsky - Rosen paradox has demonstrated [2], the superposition principle can not be interpreted as a method of description of a local reality. The founders of quantum mechanics realized clearly that superposition, as well as the quantum formalism on the whole, can describe only phenomena, but no a reality. This fundamental difference quantum mechanics from all other physical theories was the subject of hot debate between they [3-5]. It is clear from [4] and other publications that three cardinal reasons: indeterminism, a duality and a problem with the conservation laws observed in some quantum phenomena forced Bohr to accept the positivism point of view, rejected by Einstein [3]. Bohr hoped that his complementarity, uncertainty principle by Heisenberg and the superposition principle can describe in a best way these paradoxical features. The absence of a causality of phenomena described by the superposition principle Schrodinger demonstrated clearly with help of his cat paradox [6]. The problem with the law of conservation may be illustrated with help of the Stern–Gerlach experiment [7] described very well with superposition of spin-1/2 states [1] and its collapse at measurement [8]. Measuring in consecutive order z-projection $|\Psi>_z = |\uparrow>$, x - projection $|\Psi>_z = (|\uparrow> + |\downarrow>)/\sqrt{2}$ and z-projection $|\Psi>_z = |\downarrow>$ of spin-1/2 we can obtain with the probability 1/2 the angular momentum at the first $\hbar/2$ and the third $(-\hbar/2)$ measurements differing in the Planck's constant $\hbar/2 - (-\hbar/2) = \hbar$. This causeless change of the angular momentum does not overstep the limits of the uncertainty relation and therefore is permissible according to the universally recognized quantum formalism. But any causeless change of the angular momentum on a value $\Delta M_p >> \hbar$ is considered as impossible. Therefore the assumptions on macroscopic quantum tunnelling [9] and on superposition of two macroscopically distinct quantum states [10] of superconducting loop with $M_p \approx 10^5\ \hbar$ and $M_p \approx -10^5\ \hbar$, considered as flux qubit by many authors [11], contradict not only to the fundamental law of angular momentum conservation but also to the quantum formalism. A motive of this mass and funny mistake and its significance for the quantum computation problem will be considered in this work.

1. L. D. Landau and E. M. Lifshitz, *Quantum Mechanics: Non-Relativistic Theory*, Volume 3, Third Edition, Elsevier Science, Oxford, 1977.
2. A. Einstein, B. Podolsky, and N. Rosen ”Can Quantum - Mechanical Description of Physical Reality Be Considered Complete?” Phys. Rev. 47, pp. 777-780, 1935.
3. A. Einstein, “Remarks concerning the essays brought together in this co-operative volume”, *Albert Einstein philosopher – scientist*. Ed. by Schillp P.A. Evanston, Illinois, pp. 665-688, 1949.
4. N. Bohr, “Discussion with Einstein on Epistemological Problems in Atomic Physics”, *Albert Einstein philosopher – scientist*. Ed. by P.A. Schillp. Evanston, Illinois, pp. 201-241, 1949.
5. G. Greenstein and A.G. Zajonc, *The Quantum Challenge. Modern Research on the Foundation of Quantum Mechanics.* Second Edition. Jones and Bartlett Publishers, Sudbury, Massachusetts, 2006.
6. E. Schrodinger, "Discussion of probability relations between separated systems," Proc. Cambridge Phil. Soc, 31, pp. 555-563, 1935.
7. W. Gerlach and O. Stern, "Das magnetische Moment des Silberatoms", Zeitschrift für Physik 9, pp. 353–355, 1922.
8. J. von Neumann, *Mathematishe Grundlagen der Quantem-mechanik.* Springer, Berlin, 1932; *Mathematical Foundations of Quantum Mechanics*. Princeton, NJ: Princeton University Press, 1955.
9. F. Balestro, J. Claudon, J. P. Pekola, and O. Buisson, Evidence of Two-Dimensional Macroscopic Quantum Tunneling of a Current-Biased dc SQUID. Phys. Rev. Lett. 91, 158301, 2003.
10. J. Clarke and F.K. Wilhelm, “Superconducting quantum bits”. Nature 453, pp.1031–1042, 2008.
11. Makhlin, Y., Schön, G. & Shnirman, “A. Quantum-state engineering with Josephson junction devices”. Rev. Mod. Phys. 73, pp. 357–400, 2001.

Implementation of the quantum order-finding algorithm by adiabatic evolution of two qudits

A. S. Ermilov, V. E. Zobov
L. V. Kirensky Institute of Physics, Russian Academy of Sciences, Siberian Branch, 660036, Krasnoyarsk, Russia
nord@ngs.ru, rsa@iph.krasn.ru

The quantum order-finding algorithm is well known and even has demonstrational realization on the system of five qubits [1]. Moreover, we developed a numerical model of the adiabatic realization of this algorithm [2]. On the other hand, the extension of the order-finding algorithm is already suggested for system of some d-level basic elements (qudits) [3]. Such multilevel systems are interested for investigation because can have different advantages to ordinary qubits. For example, it appears in the fault tolerance, in the rate of increase of Hilbert space dimension with increasing number of qudits.

In this work we combine our attainments to make computer simulation of the adiabatic realization of the quantum algorithm on the system of two interactive qudits. In this case, the order-finding algorithm can be implemented by a sequence of some unitary operators [3]:

$$|\Psi\rangle = U|0\rangle, \qquad U = QFT_1^{\dagger} \times SUM_{12} \times QFT_1 = QFT_1^{\dagger} \times QFT_2^{\dagger} \times P_{12}(\alpha) \times QFT_2 \times QFT_1. \tag{1}$$

To obtain adiabatic equivalent of this circuit, it is needed to introduce new operators [2, 4]:

$$K = -i \cdot \log(U), \qquad U(s) = \exp(isK), \qquad s = t/T, \qquad U(0) = 1, \; U(1) = U. \tag{2}$$

Then adiabatic realization of quantum algorithm will be determined by following evolution operator

$$|\Psi(T)\rangle = U_T|0\rangle, \qquad U_T = \hat{P}\exp\left(-i \cdot T\int_0^1 H(s) \cdot ds\right), \qquad H(s) = U(s)H(0)U^{\dagger}(s). \tag{3}$$

Time dependent Hamiltonian H(s) varies continuously from the initial Hamiltonian H(0), whose ground state $|0\rangle$ is easy to construct, to the final Hamiltonian H(1), whose ground state $|\Psi\rangle$ encodes the solution of the problem under study. If the Hamiltonian varies sufficiently slowly, then the quantum adiabatic theorem guarantees that the quantum computer is in the ground state with a high probability.

To realize U_T experimentally, it is needed to come from continuous transformation to discrete one ($s = {}^{n}/_{N}$, $\Delta t = {}^{T}/_{N} = \text{const}$, $N = {}^{T}/_{\Delta t}$ is dimensionless evolution time). As result, for some finite Δt, the evolution operator can be written as:

$$U_T \approx \prod_{n=0}^{N} \exp\left(-i\frac{T}{N}H\left(\frac{n}{N}\right)\right) = \prod_{n=0}^{N} U\left(\frac{n}{N}\right) \cdot \exp\left(-i\frac{T}{N}H(0)\right) \cdot U^{\dagger}\left(\frac{n}{N}\right) = U \cdot \left(\exp\left(-i\frac{T}{N}H(0)\right) \cdot U^{\dagger}\left(\frac{1}{N}\right)\right)^{N}. \tag{4}$$

Introducing parameter $s = {}^{1}/_{N}$ into circuit (1) allows us to represent it in form (4):

$$U(s) = U(1/N) = QFT_1^{\dagger} \times QFT_2^{\dagger} \times P_{12}(\alpha/N) \times QFT_2 \times QFT_1. \tag{5}$$

To illustrate derived algorithm two qudits were taken with $d_1 = 8$ and $d_2 = 4$. These qudits can be represented by two quadrupole nuclei with spins $I_1 = {}^{7}/_{2}$ and $I_2 = {}^{3}/_{2}$ are placed into static magnetic field and electric field gradient and controlled by radio frequency (RF) pulses. Then initial Hamiltonian will be written as [3]:

$$H(0) = -\omega_1 I_{1Z} - \omega_2 I_{2Z} + q_1\left(I_{1Z}^2 - 21/4\right) + q_2\left(I_{2Z}^2 - 5/4\right) - JI_{1Z}I_{2Z}. \tag{6}$$

The quantum Fourier transform operators (QFT) can be obtained as subsequences such of RF pulses. It is described in detail in the papers [3] and [5]. The operator of the controlled phase shift P_{12} is complex and consists from free system evolution during the specified time interval and additional subsequence of some RF pulses [3]. As result, quantum order-finding algorithm can be realized adiabatically by combining RF pulses and time intervals of free evolution.

Described algorithm was simulated for different evolution times within the bounds of selected model. The degree of agreement between computed value and ideal one was estimated and to error value was calculated.

This work was supported by the Russian Foundation for Basic Research (project no. 09-07-00138).

1. L. M. K. Vandersypen, M. Steffen, G. Breyta, et al., *Phys. Rev. Lett.*, **85**, p. 5452, 2000
2. V. E. Zobov, A. S. Ermilov, *Theor. Math. Phys.*, **150** (**3**), p. 393, 2007
3. V. E. Zobov, V. P. Shauro, A. S. Ermilov, *JETP Letters*, **87** (**6**), p. 334, 2008
4. M. S. Siu, *Phys. Rev. A*, **71**, p. 062314, 2005
5. A. S. Ermilov, V. E. Zobov, *Opt. Spectrosc.*, **103** (**6**), p. 969, 2007

NMR Saturation and Entanglement in Solids

M. Kutcherov
Siberian Federal University, Krasnoyarsk 660041, Russia, MKucherov@sfu-kras.ru

We consider the magnetic resonance in the rotating reference frame of a system of dipolar coupled spins. This assumption is justified because the transformed spin Hamiltonian is effectively time independent and the spin-lattice interaction is small. The theory is extended into the region where $\beta\overline{E} \geq 1$ (β is the inverse dipole temperature, $\overline{E}$ is the interaction energy at the average distance between the spins).
Then we consider the adiabatic demagnetization in the rotating reference frame (ADRF) for the nuclear spins s =½ in an external magnetic field. The demagnetization starts with the offset of the external magnetic field (in frequency units) from the Larmor frequency being several times greater than $\overline{E}$. For the first time the approximate equations of the two temperature theory of saturation are formulated for the whole temperature region and the heat capacities for real systems are calculated [1]. In Figure we choose $\overline{E}^{-1}$ as unit timescale. We see entanglement as measured by the concurrence in the steady state.

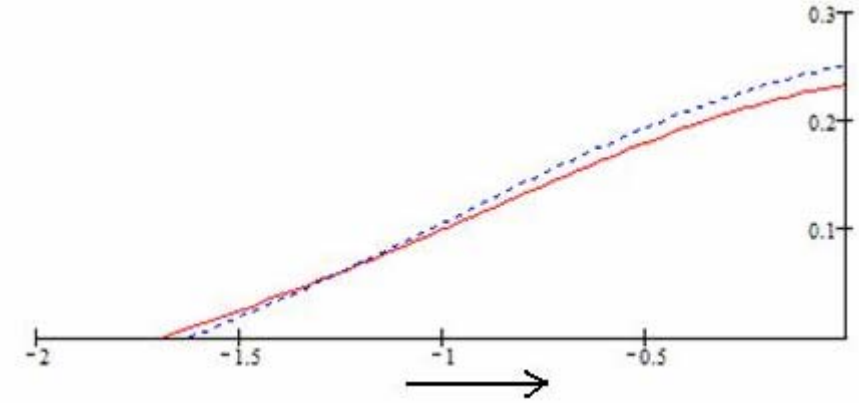

Figure. Time development of entanglement for ADRF. Comparison of exact (continuous line) and approximate (dotted line) concurrence values for neighboring spins for a closed chain of spins ½ with nearest- and next-nearest-neighbor interactions in the absence of relaxation.

The solutions of the approximate kinetic equations are analyzed. For different subsystem sizes, we have found from numerical simulations the temperatures at which subsystems of a one-dimensional spin chain and a plane spin cluster become entangled. These temperatures are of the order of microkelvins. There is a weak dependence of the temperature on the space dimension of the system [2].
Finally we want to compare steady-state entanglement with and without reset [3]. The entanglement may still retain in solid-state systems at high temperature. A simple mechanism, where nuclear spins are randomly reset to some standard initial state, can result in an entangled steady state. We find that the temperature range where one can find entangled steady states is much higher with the reset mechanism.

1. M.M. Kucherov, “Effective control of quantum spin registers”, Doklady TUSURa, 1(19), part 2, pp.27-29, 2009
2. S.I. Doronin, E.B. Fel’dman, M.M. Kucherov and A.N. Pyrkov, “Entanglement of systems of dipolar coupled nuclear spins at the adiabatic demagnetization”, J. Phys.: Cond. Matter, 21, 025601 (5pp), 2009
3. L. Hartmann, W. Dür, and H.J. Briegel, “Entanglement and its dynamics in open, dissipative systems”, New J. Phys. 9, 230 (30pp), 2007

Quantum Scattering on Dypole Potential in Adiabatic Approximation

K.S. Arakelov.

M.V.Lomonosov Moscow State University, Russia

Determination of electronic properties of molecular objects on the basis of nanodevices transport characteristics

V.A. Malinin, V.V.Shorokhov, E.S. Soldatov.
Faculty of Physics, Moscow State University, 119899 Moscow, Russia

The most intriguing challenge of the last decade is to determine electronic properties (single-particle spectrum, charge spectrum, effective electric capacitance) of single molecular objects (molecules, molecular clusters, nanogranules, etc.) by using nanoelectronic devices. The opportunity of such determination had previously been identified by investigations of transport characteristics of single-molecular transistors with discrete energy spectrum of the central island. In such devices, the electron transfer through individual single-particle molecular energy levels leads to vertical steps of tunneling current on the transport characteristics. In the future, by identifying patterns of these vertical steps on the transport characteristics it will be possible to determine the electronic and charge spectra of molecular objects located on the substrate in nanoelectronic devices and hence their electric capacity and effective size.

The main goal of this work is to develop a methodology to determine discrete energy spectra of molecular objects by use of transport characteristic data of single-molecular transistors.

In this work, it was shown that discrete energy spectra of molecular object can be determined on the basis of transport characteristics of molecular single-electron transistor at room temperature for molecular objects with a characteristic size of 2-3 nm. Measurement of stability diagram of molecular single-electron transistor is necessary to determine the charge and discrete energy spectra of a molecular object. The minimum range of control voltage of stability diagram should allow measuring at least 3 charge states of the molecular transistor. The range of tunneling voltage of stability diagram is determined by the number of tunnel current steps. Their number should be at least 2, which gives at least 2 energy levels involved into tunnel transport of electrons.

In our work we have investigated influence of single-particle levels of specially selected electron energy spectra on transport characteristics of molecular single-electron transistor. Regions appearance condition with equal tunnel current on the stability diagram was obtained. A new way to establish a clear correspondence of quantum numbers sets of molecular object and regions of constant tunnel current on the stability diagram has developed. An order of changing quantum numbers sets for transfer from one region to another on the stability diagram has been ascertained. For electron transport through a small number of energy levels (less than 5), an analytical expression for the height of tunnel current steps based on the analysis of quantum states participating in tunneling transport has been derived. Also it has found that the tunneling current through the island of single-electron transistor is determined by a combination of tunneling rate through each single-particle energy level with rational coefficients. It has been shown that in the case of non-equidistant spectra of molecular object stability diagram consists of rhombic polygons with different sizes.

This work has been supported by RFBR (Pr. No. 09-07-00272-a) and ISTC (Pr. No. № 3457).

Highly doped SOI based single-electron transistor: noise characteristics and charge sensitivity

D.E. Presnov[1], *V.S. Vlasenko*[2], S.V. Amitonov[2], V.A. Krupenin[2]
[1]Nuclear Physics Institute, Moscow State University, 119899 Moscow, Russia
[2]Laboratory of Cryoelectronics, Moscow State University, 119899 Moscow, Russia,
kivals@mail.ru

We have developed and studied SOI based SET transistor structures that demonstrate classical behavior: changes between Coulomb blockade and fully conductive states and periodical modulation of transport current controlled by the gate electrode voltage. This type of SET transistor can be used as ultra-sensitive electrometer. Advantages of the chosen fabrication method compared with other types of SET devices [1-2] are: simpler fabrication technology, mechanical solidity, higher stability to overvoltage, higher operating temperatures at the lithography resolutions, the opportunity to manufacture suspended devices.

The experimental structures were fabricated from highly doped (10^{20} cm^{-3}) silicon-on insulator film. We used SOI material with 55 nm thick silicon layer and 150 nm insulating SiO_2 layer placed on a silicon substrate which was prepared with the bonding method. The fabrication method for the SET structures contains the following stages: ion implantation of SOI film with P^+ ions; e-beam lithography for the structure patterning; forming of a metal mask by the evaporation of Al through the suspended 2-layers resist mask prepared with an electron- and photolithography; forming of nanostructures by the reactive-ion etching of SOI film through the formed metal mask; reactive-ion etching process of Si for further downsizing of the fabricated structure and final adjustment of the transistor parameters.

For the effective comparison several SOI based SET transistors were fabricated with a characteristics extremely close to those of the $Al/AlO_x/Al$ based transistors, e.g. without further etching of the structures. Size of the central island was about 100 nm.

IV-curves of the investigated samples were measured with different gate voltages applied and in the wide temperature range: from 30 mK to 1 K. The offset voltage of the Coulomb blockade was about 1 mV. The *IV*-curves shape and their behavior versus gate voltage were close to those of traditional Al/AlO_x SET transistors. SOI based SET transistor demonstrated blockade and completely conductive states at $V < V_{off}$ depending on the applied gate voltage.

The modulation curves of the transistor demonstrate current oscillations depending on the bias voltage. The modulation amplitude increases with the increasing of the bias voltage. Its maximum corresponds to the bias voltage very close to the offset. This behavior correlates well with the behavior of the traditional SET transistor modulation curve. The maximum charge sensitivity SET transistor demonstrates with a bias voltage of 1 mV in the highest slope point of the modulation curve. This value was estimated to be 15 nA/*e*, which is 3-4 times greater than typical charge sensitivity of traditional SET transistors.

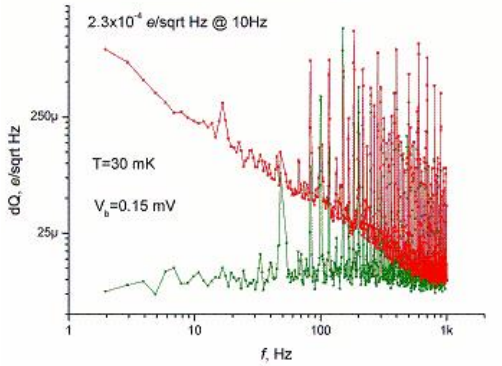

Fig. 1. *Noise characteristic of a typical SET transistor based on SOI.*

The charge noise of the highly doped SOI based SET transistor at 10 Hz was measured as $2{,}7 \times 10^{-4} e/Hz^{1/2}$ at bias voltage of 1 mV and $2{,}3 \times 10^{-4} e/Hz^{1/2}$ at 0.15 mV and temperature 30 mK (Fig. 1). The increasing of the current through SOI SET transistor causes the increasing of its charge noise exactly as in the traditional SET transistor case. The spectrum of this noise is close to the *1/f* function in the voltage range 0,1 – 100 Hz. This is a common situation for the Al/AlO_x SET transistors where the sources of charge noise are located in the dielectric substrate. Probably the suspended structures could solve the problem of excess charge noise for SOI based SET devices [1].

Authors wish to express gratitude to prof. M.Yu. Kupriyanov for useful discussions during this work.

1. V.A. Krupenin, D.E. Presnov, M.V. Savvateev, H.Scherer, A.B. Zorin, J. Niemeyer, “Noise in Al single-electron transistor of stacked design”, *J. App. Phys.* **84** 6 (1998), 3212-3215
2. Yukinori Ono, Kenji Yamakazi, Masao Nagase, Seiji Horiguchi, Kenji Shiraishi, Yasuo Takahashi, “Single-electron and quantum SOI devices”, *MEE* **59** (2001), 435-442

Nanocarbon films with electronic conductivity

N.F. Savchenko, M.B. Guseva, V.V. Khvostov, Yu. A. Korobov, A.F. Alexandrov
Physics Department, M.V. Lomonosov Moscow State University, Leninskie gory, Moscow State University, Physics Dept., Moscow, 119899 Russia, E-mail: n.f.savchenko@gmail.com

Electronic conductivity was discovered in diamond films that were produced by the method of chemical vapor deposition (CVD) with ion assisted irradiation (Ar^+) on p-Si surface with sublayer of superdispersed diamond. The obtained p-Si/diamond heterojunction demonstrated photo electromotive force 0.40 V in visible spectrum. Investigation of the structure of these films identified regions with diffraction pattern that is different from the diamond diffraction pattern by presence of forbidden reflections, and, specifically, by presence of the face-centered cubic (FCC) phase of carbon.

For the first time, FCC-carbon was discovered in carbon films, synthesized by ion-assisted condensation of carbon after annealing it at temperature E=350C [1]. Afterwards, similar structures were found in carbon samples obtained by use of various methods: transformation of graphite by high-temperature high-pressure treatment [2], chemical treatment in hydrogen plasma with argon and oxygen [3], plasmochemical synthesis, etching of diamond films in atmosphere of atomic hydrogen [4]. FCC-carbon phase in these reports was identified by means of structural electron-microscope and X-ray investigations. Since the crystal lattice constant of the FCC-carbon is very close to that of diamond, most researchers considered FCC-carbon to be a diamond with abnormal diffraction pattern. That is why in literature this carbon phase is often called "n-diamond" or "x-diamond". But the fact that presence of FCC-carbon phase changes electrophysical properties of diamond is the most convincing evidence that FCC-carbon is an allotropic phase of carbon.

The films of FCC carbon have been thoroughly examined by methods of high-resolution electron microscopy and methods of electron spectroscopy (HREM, ESCA, Auger spectroscopy, EELS, PES, FTIR spectroscopy). These studies showed that both atomic and electronic structure of FCC-carbon significantly differ from those of diamond [5, 6]. High-resolution electron microscopy shows evidence that the atomic structure of the FCC-carbon corresponds to the crystal structure with the distance between atoms equal to 2.5Å (compared to 1.54Å in diamond). Energy features in electron structure indicate absence of s- and p-orbitals hybridization in carbon atoms in this phase. For comparison, diamond has valence electrons in sp^3-hybridization state. Width of forbidden zone in FCC carbon was found to be 3.5 eV (comparing to 5.5 eV in diamond). According to the data, obtained by electron spectroscopy, the upper of valence band in FCC carbon is by 1.5 eV higher than the one of diamond. Plasmon energy of FCC is equal to 23 eV (33 eV in diamond). From this fact, FCC density was calculated to be equal 1.61 gram/cm^3, which is by 2.18 times less than that of diamond.

Theoretical analysis of FCC-carbon electronic structure was conducted taking into account Hubbard model and this analysis explained dielectric properties on the basis of coulomb correlations. With use of the density of electronic states in FCC-carbon, photoelectric properties of diamond with admixture of FCC-carbon were explained as injection of electrons from the FCC-carbon valence band to the conductivity band of diamond.

By performing analysis of energy diagrams of diamond and FCC-carbon as Mott-Hubbard's semiconductor, n-type conductivity of diamond doped with FCC-carbon was explained.

1. L.S. Palatnik, M.B. Guseva, V.G. Babaev, N.F. Savchenko and I.I. Falko, "On γ-carbon", Sov. Phys. JETP, **87**, 3(9), pp.914-917, 1984
2. H Hirai, K. Kondo, "Modified phases of diamond formed under shock compression and rapid quenching", Science, **253**, pp.772-774, 1991
3. S. Jarkov, Y. Titarenko, G. Churilov, "Electron microscopy studies of fcc carbon particles", Carbon, **36**, pp.595-597, 1998
4. I. Konyashin, A. Zern, J. Mayer, F. Aldinger, V. Babaev, V. Khvostov, M. Guseva, "A new carbon modification: "n-diamond" or face-centred cubic carbon?", Diamond Relat. Mater, **10**, pp.99–102, 2001
5. M. Fatow, I. Konyashin, V. Babaev, M. Guseva, V. Khvostov, N. Savtchenko, "Carbon modification with fcc crystal structure", Vacuum, **68**, pp.75–78, 2003
6. M.B. Guseva, V.G. Babaev, I.Yu. Konyashin, N.F. Savchenko, V.V. Khvostov et al., "New phase of carbon with fcc lattice", Poverhnost, Rentgenovskie, sinkhrotronnie i neitronnie issledovaniya, **3**, pp.28-35, 2004

Secondary-emission properties of the carbon films

V.V. Khvostov, M.B. Guseva, N.F. Savchenko, Yu. A. Korobov, N.D. Novikov
Physics Department, M.V. Lomonosov Moscow State University, Leninskie gory, Moscow State University, Physics Dept., Moscow, 119899 Russia, E-mail: vkhv@yandex.ru

Prospects in the field of development of small-scale systems, first of all, are associated with carbon materials. This is due to the unique features of the carbon that allow formation both ideal two-dimensional (graphene) and one-dimensional (chain carbon) structures and hybrid objects (fullerene, nanotubes, etc). The electrophysical properties of various carbon forms cover range from the wide-band dielectrics to the metals, what makes it possible to implement the idea of C-tronics - development of the new kind of electronics on the basis of carbon.

In view of this, it is extremely important and timely to carry on studies of the electrophysical properties of the films of nano-structured carbon for the purpose of development on their basis of instruments and devices, that work on fundamentally different (quantum) physical effects.

In this work, we present results of studies of the secondary electron emission of the films of linear-chain carbon (LCC) [1] (for transparency) and carbon films with the face-centered cubic (FCC) phase [2] (for reflection).

The mechanism of secondary electron emission can be subdivided into three stages: generation of hot electrons, transport of electrons to the emitting surface, output of secondary electrons into the vacuum by overcoming the potential near-surface barrier.

Linear-chain carbon, which has one-dimensional structure, possesses high efficiency of the electron generation and has high electron mobility, which ensures effective transport of electrons along the chains. On the basis of these two parameters LCC has advantage over all currently existing materials.

Diamond has low energy of affinity (low potential barrier for the output of electrons into the vacuum), which must ensure high secondary emission. However, the conducted studies of the emissive properties of diamond-like films have not shown the expected high secondary-emission coefficient, which is explained by the low conductivity of diamond. Due to this fact, measurement of the secondary emission of carbon films with the FCC phase is of interest, since they have high electronic conductivity.

Experimental studies of the secondary-electron emissive characteristics of carbonic films were conducted on the scanning electron microscope LEO-1455VP. Measurements were made in the energy range of primary electrons from 200 eV to 4 keV. Films with a thickness from 50 to 500 nm were investigated.

The conducted investigations of films of linear-chain carbon showed anomalously high secondary emission for transparency. The secondary emission of FCC films grows with an increase in the extraction field by the Schottky's mechanism; and that is an indication of the over-barrier emission of secondary electrons. The energy spectrum of secondary electrons indicates that emission of excited electrons takes place from the resonance electron levels of this structure.

Studies of FCC films showed that dependence of the secondary-emission coefficient on the energy of primary electrons has a maximum, whose energy is determined by the thickness of the film. Maximum secondary electron emission coefficient is found to be 3-5. A comparatively low value of the secondary-emission coefficient of the films is probably associated with the high work function.

1. Babaev V.G., Guseva M.B., N.D.Novikov, Khvostov V.V., and Flood P., “Carbon material with a Highly Ordered Linear-Chain Structure”, in *Polyynes Synthesis, Properties, and Applications* edited by Franco Cataldo, Taylor & Francis, Boca Raton London, New York,2006

2. M.B. Guseva, V.G. Babaev, I.Yu. Konyashin, N.F. Savchenko, V.V. Khvostov et al., “New phase of carbon with fcc lattice”, Poverhnost, Rentgenovskie, sinkhrotronnie i neitronnie issledovaniya, **3**, pp.28-35, 2004

Investigation of auto-emission diodes with CNT emitters under small inter-electrode distance conditions

S. Orlov[1], O. Gushchin[1], S. Yanovich[1], V. Shyshko[1], O. Perveeva[1], N. Savinsky[2]
1. Mikron JSC, Zelenograd, Russia, E-mail: orlov@mikron.ru.
2. Yaroslavl branch of Russian Academy of Science, Yaroslavl, Russia.

Unique carbon nano-tubes (CNT) features are considered to be advanced basis for nanoelectronic devices [1, 2, 3]. Auto-emission devices are the most promising approach. Therefore operation of auto-emission prototypes with micron scale distance between electrodes is of major interest. This paper presents a study of emission properties diode type structures with different inter-electrode distance. For the purposes of the study special integrated anode cell was designed and allowed to conduct electric measurement under different ambient conditions.

Emission structures for investigation were fabricated with cathalitic vertical CNT arrays growth in HTCVD process in ethanol/hydrogen gas mixture upon cobalt cathalitic seed layer. While investigating CNT auto-emission diodes characteristics it was found that CNT emitters demonstrate emission density up to 150 mA/cm^2 along with quite low emission threshold voltage about 2.0 V/μm. All samples demonstrated stable emission during observed period when measured under air conditions.

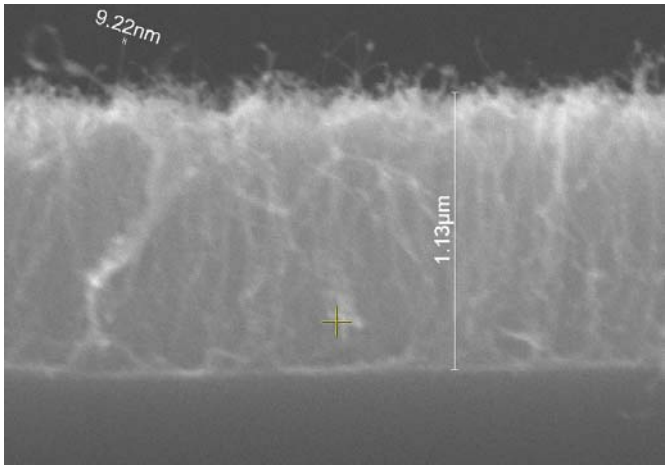

Fig.1. CNT emission layer cross-section

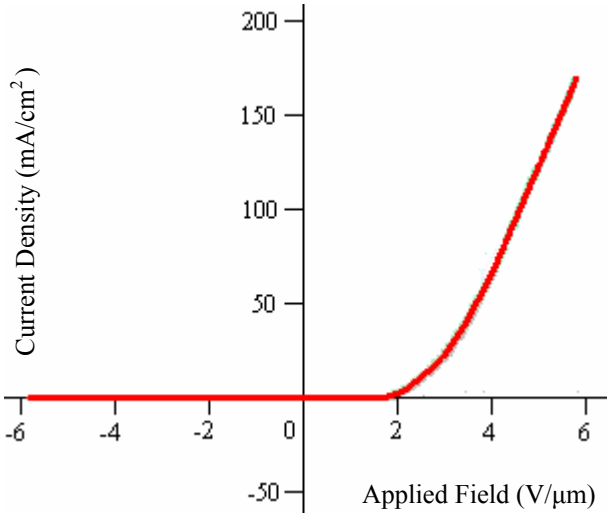

Fig.2. 2.5 μm distant CNT diode structure emission characteristic

1. G. Chai, L. Chow // *Carbon* 45, 2007. P. 281.
2. I.Shinji , Y.Masato , I.Nobuyuki , Y.Hiroshi // *Japanese Journal of Applied Physics.* 2008. Vol. 47. No. 1. pp. 700–702
3. David S. Y. Shaw J // *Applied Physics Letters* V.80, N 1. 2002. pp118-120

Design of 3D nano-carbon emitter based autoemission devices

N. Savinski[1], M.Gitlin[1], A. Shornikov [1]

[1]*Yaroslavl branch of Institute of Physics & Technology (IPT),Russian Academy of Sciences E-mail Savinski1@yandex.ru*

Vacuum auto-electron micro-devices AEMD have certain advantages over semiconductor devices. The major are temperature operation range (from – 130° till + 300°C) and resistance to radiation impact. These features are due to the nature of auto-electron emission. The next advantages are related to its super performance as ballistic electron transfer from cathode to anode is a matter of sub-picosecond range. The general trend of vacuum electronics development at recent years is research of ways to shrink low voltage AEMD by design and process means. Following this trend the design based on nanotechnology in general and self-organizing nanostructure process in particular is considered more and more attractive. CNT FEC array is the only functional nanoscale element of device. CNT FEC arrays have excellent features. Along with exciting gain due to self-organizing process CNT within FEC arrays are formed at distances compared with its diameter. Furthermore CNT arrays grow vertically only in case when distance between CNT is so small that Van der Waals interaction takes place. As we already mentioned above emitters at the central area of FEC array are screened, emission current may be unstable as intensively operating edge CNT may burnout. But is each sole CNT-emitter, grid, anode isolate with vacuum surrounding screening problem may be suppressed. This shall cause sufficient emission current density increase because of increase of effective emitter quantity per square unit. Another target is formation of nanoscale vacuum inter-electrode distance which is a matter for device performance limits and power consumption. Such distance shall be not more than CNT diameter. AEND performance is determined by cathode-anode electron transition along with respective electrodes capacitance. As there is certain electric field non-uniformity at cathode-grid high field level space and grid-anode space with better field uniformity but lower field level, cathode-anode electron transition time $\tau_{k\text{-}a}$ should be determined as a sum of respective times

$$\tau_{k\text{-}a} = \tau_{k\text{-}g} + \tau_{g\text{-}a} ,$$

where $\tau_{k\text{-}g}$ is transition time for cathode-grid space and $\tau_{g\text{-}a}$ is transition time for grid-anode space Let's expect 1V voltage is applied to grid and 4V voltage is applied to anode. Along with estimation of $(d_{k-g} - h_k)$ and $(d_{g-a} - h_a)$ about 5nm each we get accordingly

$$\tau_{k-g} = 16.85 * 10^{-15} s \quad \tau_{g-a} = 5.62 * 10^{-15} \quad \tau_{k-a} = 22.47 * 10^{-15} s.$$

Cutoff frequency may be evaluated as

$$f_m = \frac{1}{2\pi\tau} \approx 7.1 * 10^{12}\ \text{Hz}$$

Residual gas pressure one has in vacuum micro-devices is about 1-3 * 10^{-6} Pa. The main reason to have such high vacuum level in auto-emission micro-devices is to provide stable cathode emission current

Table 1. One-molecule residual gas pressure vs cathode-anode distance when channel diameter is 10nm.

d , nm	5	10	30	50
P , Pa	1910	955	318	190

With these results we get good news that extremely high vacuum is not mandatory factor for efficient performance of nano-triode. Definitely a lot of technological restrictions and difficulties are eliminated.

1 Savinski.N.G., ShornikovA.A., Gitlin M.L.,Orlov S.M., Gutschin.O.P., Petryhin G.N, Growth of carbon nano structures by an alcoholic catalytic chemical vapor deposition for field emission.// Abstract of Nanotechnology forum Rusnanotech 2008, Moskow/

ZnO nanorods for device application

O.V. Kononenko [1], A.N. Red'kin [1], A.N. Baranov[2], A.N. Panin[1, 4], M.V. Shestakov[3], V.T. Volkov[1], A.I. Il'in[1], E.E. Vdovin[1]

1. Institute of Microelectronics Technology and High Purity Materials, Russian Academy of Sciences, Chernogolovka, Russia, E-mail adderss: oleg@iptm.ru. 2. Moscow State University, Chemistry Department, Moscow, Russia, 3. Moscow State University, Department of Materials Science, Moscow, Russia, 4. Quantum-functional Semiconductor Research Center, Department of Physics, Dongguk University, Seoul, Korea

Zinc oxide is one of the most important functional semiconductor oxides with a direct wide band gap (3.37 eV) and with a large excitation binding energy (60 meV).
One-dimensional semiconductor nanostructures have in recent years attracted much attention due to their potential use as building blocks for future electronics and photonics, as well as for life-science applications. A large variety of ZnO quasi one-dimensional structures have been demonstrated [1]. The large surface area of the nanorods and bio-safe characteristics of ZnO makes them attractive for gas and chemical sensing and biomedical applications, and the ability to control their nucleation sites makes them candidates for microlasers or memory arrays. The initial reports show a pronounced sensitivity of the nanowire conductivity to UV illumination and the presence of oxygen in the measurement ambient. Recently, a wide variety of nanodevices including UV photodetectors [2], sensors [3], field effect transistors (FET) [4] and light emitting device arrays have been fabricated utilizing ZnO nanorods. The fact that ZnO can be grown at low temperatures on cheap substrates such as glass also makes it attractive for transparent electronics.
ZnO nanorods was grown on silicon substrates. Nanorods showed high structural performance and good optical characteristics. Planar and vertical structures from zinc oxide nanorods were fabricated and I-V characteristics were measured. Vertical structures on the basis of ZnO nanorods and NiO films demonstrated diode I-V characteristics and sensitivity to UV irradiation (Fig.1).
ZnO nanorods doped by Cr were synthesized by heating the mixture of solution processed Zn precursor with $NaCl\text{-}Li_2CO_3$ salt. The nanorods have sngle crystalline structure and blue-green luminescence. Resistivity of the nanorod is about 1 Ω·cm in the dark. The strong UV response of the nanorods is observed. Si back gate Field Effect Transistor fabricated from ZnO:Cr nanorod is n-channel and demonstrates enhancement-mode behavior (Fig.2).

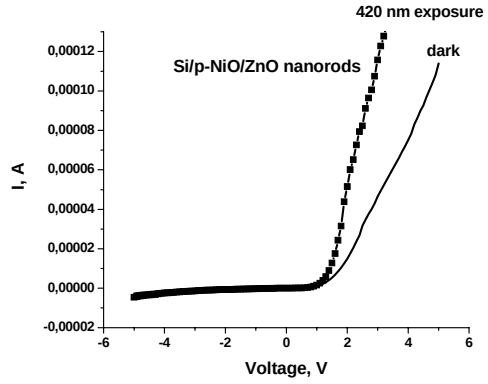

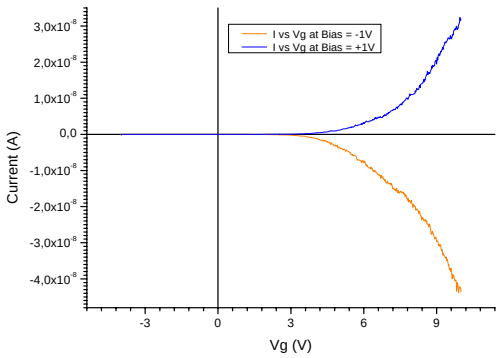

This work has been supported in part by the Russian Foundation for Basic Research, grant No.07-08-00514-a.

1. Z.L. Wang, "Nanostructures of zinc oxide", Mater. Today**,** 7**,** pp.26-33, 2004
2. O. Harnack, C. Pacholski, H. Weller, A. Yasuda, J. M. Wessels, "Rectifying Behavior of Electrically Aligned ZnO Nanorods", Nano Lett., 3, pp.1099-1101, 2003
3. S. J. Pearton, B. S. Kang, L. C. Tien, D. P. Norton, Y. W. Heo, F. Ren, "ZnO-based nanowires", NANO: Brief Reports and Reviews, 2, pp.201–211, 2007
4. W I. Park, J S. Kim, G-C. Yi, M. H. Bae, H-J. Lee, "Fabrication and electrical characteristics of high-performance ZnO nanorod field-effect transistors", Appl. Phys. Lett., 85, pp.5052-5054, 2004

Observation of spin injection in ballistic nanostructures Mo(001)/Py

G.M. Mikhailov, V.Yu. Vinnichenko, A.V. Chernykh, I.V. Malikov, Piatkin S.V.
Institute of microelectronic technology and high purity materials RAS, Chernogolovka, Russia,
E-mail address mikhailo@ipmt-hpm.ac.ru

Electron spin polarization caused by the current flowing across ferromagnetic and normal (F/N) metal interface is the most powerful approach for origination of spin imbalance in normal metals and attracts much attention in spintronics developing. It was demonstrated [1,2] that the effect of spin injection is observed for hybrid F/N nanostructures fabricated by planar technology. In these investigations, the polycrystalline copper, aluminum and silver films were used as normal metals during nanostructure fabrication. In present work, we investigate the hybrid F/N nanostructures, composed from Py and Mo (or W), where normal metal part is formed by singlecrystalline normal metal film with large residual electron mobility. Under low temperatures, the electrons in normal metal part possess large electron mean free path exceeding the distance between two polycrystalline ferromagnetic electrodes that used as spin injector and detector. This allows investigating ballistic spin injection.

Hybrid Mo(001)/Py nanostructure fabrication was performed during two-step technology using R-plane sapphire as a substrate. At first, two polycrystalline Py-electrodes with two reservoirs at their ends were fabricated by “lift off” procedure using electron lithography. In the second step, Mo(001) film of 80 nm thickness was epitaxially grown by pulse laser deposition technique under ultra high vacuum, which forms singlecrystalline and polycrystalline regions on sapphire and Py-electrodes, respectively. The subtractive technology with use of nanomask fabrication and ion milling was applied to fabricate single crystalline Mo(001) junction connected two Py-electrodes. The width of the junction was 900 nm and its length 500 nm.

Electric measurements were performed at liquid helium and room temperatures by four-probe technique using lock-in system. Both magnetoresistance measurement with in-plane magnetic field of ferromagnetic electrodes, normal metal junction and also the transfer resistance that characterized spin injection were carried out. We found that Py-electrodes were remagnetized at magnetic field 120 and 160 Oe. Reswitching fields depend on the ferromagnetic electrode width, the wider Py-electrode has smaller reswitching field. Magnetic field dependence of the transfer resistance exhibits typical behavior specific for spin injection. It is observed in the magnetic field range limited by reswitching fields of Py-electrodes. Magnitude of spin injection signal depends on the sample temperature. By this experiment, we demonstrate for the first time ballistic spin injection in hybrid Mo(001)/Py nanostructures.

Acknowledgement

The work was supported by the RFBR grant 07-07-00119-a.

1. F. J. Jedema, M. S. Nijboer, A. T. Filip, and van Wees “Spin injection and spin accumulation in all-metal mesoscopic spin valves”, Physical Review B **67**, 085319 (2003)
2. T. Kimura and J. Otani “Large Spin Accumulation in a Permalloy-Silver Lateral Spin Valve” Phys. Rev. Letters, PRL **99**, 196604 (2007).

Formation of Voids in Silicon-Based Structures Annealed in Non-Isothermal Reactor

Yu. I. Denisenko
Institute of Physics and Technology, Yaroslavl Branch, RAS,
Universitetskaya, 21, Yaroslavl, 150007, Russia, E-mail: den-yur55@mail.ru

Open volume defects (voids, nanopores, nanocavities), which obtained in silicon crystal substrates without the use of electrochemical processes, are now of considerable interest from both technological and scientific points of view. The traditional fabrication route of the defects formation involves production of gas (helium, hydrogen) bubbles by implantation with doses $(0.8 \div 15) \cdot 10^{16}$ ions/cm^{-2} and subsequent removal of the gas by annealing at temperatures above 400 ^{0}C. Depending on process regimes, a buried layer with nanopores that are dispersed throughout the thickness of the layer [1] or arranged in one plane parallel to crystal surface [2] can be formed. Another approach to voids formation can be based on the Kirkendall effect in the planar layered structure of $Ni/Ni_2Si/Si$ has been represented in [3]. All the layers with voids can perform the next important functions in device structures - effective sinks for mobile interstitial atoms or metal ions, deep level defects for life-time monitoring in power devices, compensators of stresses on the border of heterostructures, centers of luminescence due to Si -dopant complexes, etc.

The aim of the present work is further development the engineering of layers with voids in silicon substrates. Suggested the overall porosity in the substrates can be increased by the way of bulk diffusion of excess vacancies generated during annealing in non-isothermal reactor (NIR). The substrates are developed with the using high-dose implantation of phosphorus and oxygen. During annealing in the NIR (1100 ^{0}C, 5 minutes, at presence of the axial $\nabla T = \pm 70$ K/cm), the emerged buried oxide phase separates an influence of the region with irradiative vacancy-type defects (at the surface) from the region with excess interstitials (in the depth). The conditions for division of point defects fluxes are created, in which the direct recombination between vacancies and interstitials became difficult. At the same time, indirect recombination through inserted recombination centers may be possible. This increases the chemical potential of vacancies, thus, increasing probability the appearance of viable nucleus of pore. At condition of “low” thermal budgets of annealing procedures, the phase remains as a barrier to any flow of vacancies to recombine on the surface, while serves as a source of phosphorus diffusion into the substrate. It has been investigated the influence of the ∇T in two directions on the pores formation. After subsequent isothermal annealing (1150 ^{0}C, $1 \div 4$ hours), on the “cold” side of the substrate, within the boundaries of phosphorus diffusion zone, the arising nucleuses got their development to both single- and double-octahedral voids. At that time, on the "hot" side of the substrate, impact of dislocations formation causes the microcracks. Corresponding SEM images of the cleaved structures are presented.

1. V. Rainery, M. Saggio, E. Rimini, “Voids in silicon by He implantation: From basic to applications”, J. Mater. Res. **15**, pp. 1449-1476, 2000
2. N. Hueging, M. Luysberg, H. Trinkause, et al., “Quantative pressure and strain field analysis of helium precipitates in silicon”, J. Mater. Sci., **41**, pp. 4454-4465, 2006
3. K.N. Tu, U. Gösele, “Hollow nanostructures based on the Kirkendall effect: Design and stability considerations”, Appl. Phys. Lett., **86**, 093111, 2005

Si wires deposition by magnetron sputtering method

S.Evlashin[1], N. Suetin[1], V.Krivchenko[1].

1. D.V. Skobeltsyn Institute of Nuclear Physics Lomonosov Moscow State University
E-mail address: stevlashin@gmail.com .

Silicon is used in the main part of solar cells (SC) as materials for photoelectronic conversion of solar energy. To get high efficiency SC it is necessary to use high purity Si where diffusion length of minority carrier is comparable with wafer thickness. Therefore the lifetime of the minority carrier has to be at least 20 mcs. It's possible for high pure Si which is rather expensive. The main aims of solar energy engineers are the increasing of the power conversion efficiency of SC and the reducing of their price.

To reduce the price of SC it has been proposed to use cheaper materials with a high level of impurities or a high density of defects, but these materials have very low lifetime of the minority carrier. One of the solutions of the problem can be the transition from conventional planar geometry SC to radial geometry with the radial direction of p-n junction oriented with the rod axis parallel to the incident light direction. High-aspect-ratio (length/diameter) Si wires allow use of material of sufficient thickness to obtain good optical absorption while simultaneously providing short collection lengths for excited carriers in a direction normal to the light absorption.

Si wires of micron and submicron size can be produced on inexpensive substrates by chemical vapor deposition (CVD), plasma enhanced chemical vapor deposition (PECVD), molecular beam epitaxy (MBE), plasma chemical epitaxy and liquid etching methods.

We suggest a new method of Si wires synthesis involving magnetron sputtering of solid target. This method is simple, safe and cheaper in compare with the listed above. Moreover, applying doped silicon as a target allows making structures with the predetermined type of conductivity.

In this work we show that magnetron sputtering method permits growing Si wires in the micron range. Si(100) substrates with gold deposited films is used as a substrate. Au film thickness was ranged within 2 and 20 nm. We have studied the influence of silicon atom flows and substrate temperature on the growth of different Si structures. It was found that Si wires have different morphology, which depends on the Si flux. We have also researched the substrate temperature regime and determined the most optimal temperature of growth.

Nanocrystalline silicon on sapphire

D. Pavlov, P. Shilyaev, E. Korotkov, N. Krivulin
University of Nizhniy Novgorod, Nizhniy Novgorod, Russia, e-mail address: korotkov_ev@phys.unn.ru

The methods of producing of high density massifs of nanoislands are based on effects of self-assembly during the epitaxy process (for example, epitaxial growth of Ge on Si). During the molecular beam epitaxy (MBE) of Ge on Si in the initial stages of growth thin Ge layer is formed on the Si substrate. Due to mismatch of lattice parameters of Ge and Si (4.2 %) this layer is characterized by the existence of compression strains. The relief of strains is realized owing to the formation of the three-dimensional Ge islands on the layer surface (Stranski-Krastanow mechanism) [1]. The shape and the size of islands (hut or dome) depend on growth time and substrate temperature.

The object of our investigation is the molecular beam epitaxy (MBE) silicon on sapphire (SOS) heterostructure. The discrepancy of lattice parameter of (100) silicon and ($1\bar{1}02$) sapphire is 4-12 %. It was established, that in the early stages of chemical vapor deposition (CVD) of SOS layers nucleation centers are formed, which evolve into hemispherical islands covering just a fraction of the sapphire surface (Volmer-Weber mechanism) [2]. As more material is deposited a greater fraction of sapphire surface is covered by islands. The minimal thickness of continuous (imperforated) SOS layer is 60-80 nm substrate surface structure. There is not any evidence about the self-assembly in the initial stages of growth of silicon on sapphire layers, which were obtained using the MBE method.

Ultra thin SOS layers were grown by the MBE. The sapphire substrates were previously annealed during the 30 min under the 1300°C. The pressure in the chamber at the time of epitaxy did not exceed 7×10^{-7} Torr. The temperature of substrate was 450-800°C. The deposition rate was 2.5-5 Å/s, growth time varied from 30 sec up to 10 min. The surface morphology of SOS layers were studied by means of atomic force microscopy (AFM). The films structures were investigated by means of reflection of high energy electron diffraction (RHEED).

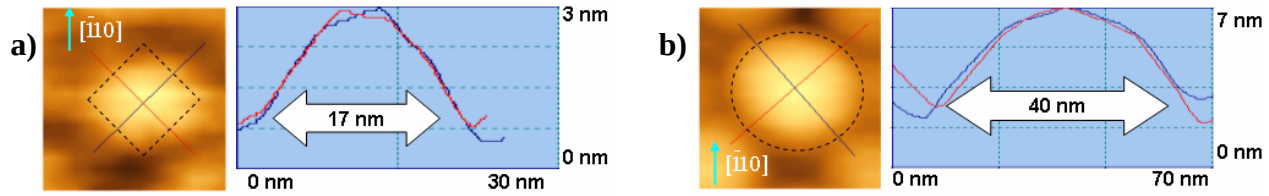

Fig. 1. Silicon islands on sapphire with: a) pyramidal shape; b) domelike shape.

The massif of Si islands is formed in the initial stages after 30 sec of molecular beam epitaxy of silicon on sapphire on substrate surface. If the substrate temperature during the growth process did not exceed the 650°C there was pyramidal shape of islands (Fig. 1-a). The lateral size of such clusters was about 20 nm, the height – 3 nm, the surface density - 2×10^{11} cm^{-2}. The shape of Si islands growing under the 650°C and higher was domelike (Fig. 1-b). The average size of dome clusters were 40 nm, and their surface density was about 10^{10} cm^{-2}. After the 1 min of silicon deposition all islands have dome shape. With substrate temperature increasing, the islands sizes were decreased, and the density of clusters was raised. The RHEED patterns of SOS layers, which were grown during the 30 sec, contain the reflexes, which confirm the single-crystal structure of the islands. But the intensity of reflexes at the RHEED patterns is reduced with the substrate temperature decreasing. The additional rings at the patterns of low-temperature grown (500°C) SOS confirm the fraction of polycrystalline structure of the film. After the 1 min of silicon deposition the SOS layer is imperforated. The minimal thickness of such film is 30 nm. The existence of the extra spots at the RHEED patterns of such layers certify the appearance of twinning defects, which are formed due to the coalescence of islands with different orientation.

This work was financially supported by CRDF Post-Doctoral Fellowship Supplemental Award (Y4-P-01-07) and Ministry of Education and Science of the Russian Federation (Project RNP 2.1.1/3626).

1. K. Bruner, “Si/Ge nanostructures”, Rep. Prog. Phys., 65, pp. 27-75, 2002
2. M.S.Abrahams, C.J. Buiocchi, R. T. Smith et al., “Early growth of silicon on sapphire. I. Transmission electron microscopy”, J. Appl. Phys., 47, pp. 5139-5150, 1976

Formation of the atomically smooth surface of gold film and the binding of gold nanoparticles on it by the self-assembly method

A.N. Kuturov[1], E.S. Soldatov[2], L.A. Polyakova[3], S.P. Gubin[3]
[1]*P.N. Lebedev Physical Institute of the Russian Academy of Science, Moscow, Russia, kuturov@cryolab.ru*
[2]*M.V. Lomonosov Moscow State University, Moscow, Russia, esold@phys.msu.ru*
[3]*Institute of General Inorganic Chemistry of the Russian Academy of Science, Moscow, Russia*

The creation of molecular transistor is one of the promising ways in electronics mainstream. To create molecular transistor it's necessary to put the molecular nano-object to the system of electrodes. We have developed the technique of the surface's roughness decrease of gold films to atomic level. This technique consists of the accurate annealing of fresh-evaporated gold films by the free flame of gas-jet or hot plate. To make a smooth film we must use an atomically smooth base and anneal the gold film just after evaporation. The samples of mica with dimensions of 8 mm * 8 mm, thickness 0.2 mm were evaporated and annealed in free flame of gas-jet (T~700ºC) or on hot plate at temperature 250ºC to obtain the atomically smooth surface of gold film. The atomically smooth (roughness ~ 0.2 nm) regions have a sizes 50-100 nm. The time from the end of evaporation process to the beginning of annealing process should be not more than 10 hours and not more than 2 days to the implementation of self-assembly process and the analysis of results. We suppose that this limit time is caused by relax processes in film after evaporation and annealing.

There was developed the method of gold nano-objects with dimensions 5-25 nm binding on the gold film evaporated and annealed on atomically smooth mica base. This method consists of the process in which at first evaporated and annealed gold film was treated by dithiol solution (1,2-ethanedithiol or 1,4-butanedithiol) with concentration of 0.05 g/mg and after that the samples were treated by the solution of gold nanoparticles ($2*10^{-3}$ – $2.5*10^{-5}$ mol/l). We show that dithiol groups should be used instead of single-thiol groups in the self-assembly process of gold nanoparticles on gold film surface. We have sorted out the optimal concentrations of gold nanoparticles in various solvents, temperature and process duration which exclude the nanoparticles' conglomeration and guarantee the uniform distribution of nanoparticles on film surface. The data which confirm the absence of nanoparticles' conglutination can be obtained during the examination of samples with Scanning Tunneling Microscope (at voltage 0.17 V and current 0.54 nA) and Scanning Electron Microscope (at accelerating potential 20 kV). These examinations demonstrate that the uniform distribution of nanoparticles on gold surface with the density of about 1 particle per 5000 nm^2 and the dimensions of deposited nanoparticles are 5-25 nm.

Thus the technique of gold film surface flattening was developed. There was demonstrated the necessity of the use of atomically smooth base. There were obtained the optimal process' characteristics and determined the main important characteristics including the time stability of obtained structures. There was developed the technique of the binding of 5-25 nm gold nanoparticles on surface by self-assembly process. There was obtained the uniform distribution of chemically binded nanoparticles on surface with the density of about 1 nanoparticle per 5000 nm^2.

The work was supported by RFBR (project 09-07-00272-a and 08-03-00681-a), ISTC (project 3457), and Fundamental Investigations' Programs of Presidium RAS (20П10 and ОХ2.3).

1. Nogues, C. and M. Wanunu // Surface Science. 2004. **573**, N. 3. P. 383-389

LGD-technology of FM/SC hybrid nanostructrures

A.S.Sigov[1], A.V. Abramov[2], L.A.Bityutskaya [3], E.V. Bogatikov[3], M.V.Grechkina[3], Yu.I. Dikarev[3], A.P.Lazarev[2], E.A.Pankratova[2], V.M.Rubinshtein[3], A.V.Tuchin[3]

1. MIREA, Moscow, Russia, E-mail: rector@mirea.ru 2. «Rosbiokvant» Ltd, Voronezh, Russia 3. Voronezh State University, Voronezh, Russia, E-mail: me144@phys.vsu.ru

Combined application of the charge and magnetic properties of electrons in spintronics is a challenge for researchers working in the field of micro- and nanoelectronics. Development and design of spintronic devices requires an integrated approach based on nanotechnology principles: a search for magnetic materials compatible with silicon technologies, quantum-confined simulation of magnetic nanostructures, development of technologies using non-equilibrium processes of formation for the self-organized nanostructures, elaboration of metrology for magnetic nanostructures and so on.

A serious outbreak to the industrial spintronics was the discovery of magnetic properties in the wire-crystals of ferromagnetic metals silicides [1]. Magnetic properties of the free-standing and deposited nanoclusters of ferromagnetic materials considerably differ from those ones for the bulk materials. Atoms on the cluster surface are characterized by the reduced coordination number and a narrow width of the density of states band at the Fermi level. This results in the increase of the spin and orbital moments of the atoms in a cluster. The effect the number of the atoms and their configuration on the spin anisotropy was investigated under simulation of magnetic nanoclusters of ferromagnetic metals and their silicides by the density functional theory method in Gaussian software suite within the quasimolecular approximation. Considerable influence of d-electrons on the redistribution of electron density was found to take place thus providing a new prospect for the use of ensembles of the clusters made of ferromagnetic metal silicides applied as the memory cells.

Using the original technique developed by the authors – local plasma-chemical maskless etching in localized gas discharge (LGD) a technology of obtaining for nanoheterostructures of FM/SC (Ferromagnetic/Semiconductor) type is discussed. It allows to realize in the common technological cycle three functions: cleaning, dimension etching and local deposition of ferromagnetic materials under formation of hybrid nanostructures on semiconductor or dielectric substrates including multi-layered ones. Under etching with a localized gas discharge it is applied for the formation of the patterns with a preset topology without the use of masks on the surface of different materials. Preliminary “negative” or “positive” image of the etch pattern is pre-settled on the plane electrode arranged above the processed material. For the optimal combination of the gas pressure P and the length of discharge gap L discharge localization takes place in a complete correspondence with the electrode configuration. If the noble gases are used for plasma formation then this way of treatment makes possible to perform a discrete controllable deposition.

This technology allows to form a system of as disordered as regular nanostructures on the chip with the controllable nanocluster sizes and controllable interface quality. The sizes and density distribution of nanostructures can be controlled by varying the size and topology of the plasma electrode. This can solve the problem of single-domain structure and increasing of Curie point for magnetic semiconductors. The problem of the interface quality on the one hand is determined by matching of cleaning, dimension etching and local deposition of nanostructures and on the other hand – by the choice of materials providing a coherent intergrowth of a substrate and ferromagnetic layer. Using such an approach FM layer in a hybrid structure of FM/SC can be considered as self-organized 2D magnetic sublattice embedded into crystalline matrix of semiconductor. These conditions are realized in non-equilibrium state of the plasma discharge. Thus, to solve the problems of industrial spintronics LGD method has the indisputable advantages and attractiveness over the routine plasmachemical technologies and some other technologies (CVD, MBE).Using LGD technologies layers of magnetic nanoclusters of cobalt and nickel silicides on silicon were obtained with the controllable size of 20-60 nm.

The work was performed within the frames of epy federal purpose program «Investigations and elaborations on the priority directions of the development of the science and technological complex for 2007-2012 years», contract № 02.513.11.3393.

1. K. Seo, K.S.Varadwaj, P.Mohanty et al., “Magnetic properties of single-crystalline CoSi nanowires”, Nano Lett., 7, pp.1240-1245, 2007.

Preparation of electrodes for molecular transistor by focused ion beam.

I.V. Sapkov[1], V.V. Kolesov[2], E.S. Soldatov[1]
1. Department of Physics, Moscow State University, Russia, esold@phys.msu.ru. 2. Kotel'nikov Institute of Radioengineering & Electronics of Russian Academy of Sciences, Moscow, Russia, kvv@cplire.ru.

Miniaturization of element base is of particular interest for contemporary microelectronics. It is expected that in future we will be able to construct such small elements as only tens and units of nanometers and therefore to create new devices. These devices, for example, can be based on molecular single-electron transistor (i.e. a molecule placed between two electrodes, while a gate-electrode electrostatically controls molecular potential). It operates on the basis of single-electron tunneling.

The problem of creation of such device can be split into two parts [1]. The first one is to create leading electrodes with a small (3-5 nm) gap between them, which allows investigation to be made with nanometer sized objects. The second problem is placing and binding of a single molecule between such electrodes.

We have demonstrated [2] the method where the gap was formed after additional deposition of metal into relatively wide gap (about 100 nm) between suspended electrodes. This method allows iterative fitting of a gap's width, because a gap can be reconstructed through electromigration in the case of bridging of electrodes. To our knowledge it's the only method with such possibility. It is obvious that starting width of a gap should be as small as possible. We used focused ion beam (FIB) microscope ("NanoLab9000", gallium ion source, spot size <10 nm) to get such small gaps.

Samples with metal (short-circuited) wires were prepared on silicon base covered with 400 nm surface layer of SiO_2 using a conventional lithography technique. Metal wires consist of two layers: 2 nm (Ti) / 18 nm (Au). Each metal wire ends both sides with contact pad (1x1,5mm). Electrical characteristics (I-V's) was measured with device based on picoammeter Keithley-6487, PC and specially constructed measuring probe which permits to prescribe current between 0 – 10 mA range and voltage between 0 – 50 V. I-V's of the sample are measured before and after using of FIB microscope to investigate the change in conductivity of a sample. Atomic force microscopy was used to control height profile of milled structure and re-deposition effects.

Focused ion beam microscope operated at currents of about 1 pA, smallest possible width of a beam and different depths into the substrate. For optimal milling parameters a gap's width about 30 nm was obtained. These gaps can be used as great starting gaps in the method described earlier. All I-V's demonstrate increase in resistance from 400 Ohm before milling to dozens of MOhm after milling. The latter values can't be explained as conductivity either silicone dioxide, not continuous metal film in the gap. It is possible that such resistance is due to partial implantation of gallium ions into the substrate in the area of a gap. We observe small amount of metal redeposited onto electrodes in case of metal milling as bulges on the ends of electrodes, but it is not significant for our method. Also we found that we can escape the most danger step in formation of "undercut" in the area of gap with anisotropic RDE which was found destructive for metal electrodes. To provide this vertical etching of silicone dioxide FIB was also used. No visible redeposition of silicone dioxide is also satisfactory result for a method. Additionally, we used FIB to form narrow nanowires and only then cut them with a gap. It allows us to obtain gaps with small cross-section area that is attractive for a single-molecule trapping during transistor implementation.

Thus, we have tested possibilities of focused ion beam microscope and showed that it's using allow to decrease width of stating gaps to values of about 30 nm. It is facilitate farther processing and quality of a gap. It also allows modernization of the processing sequence. The change in substrate's conductivity was observed, but it is not essential because of following processing of the sample. In situ production of different topological simple nanostructures was demonstrated. Such devices can be particularly interesting for constructing of element base of nanoelectronics.

This work was supported by RFBR (project 09-07-00272-a) and ISTC (№ 3457).

[1] E.A. Osorio, T. Bjornholm, J.M. Lehn, M. Ruben, H.S.J. van der Zant, "Single-molecule transport in three-terminal devices", J. Phys.: Condens. Matter, **20**, pp. 374121-374135, 2008

[2] I.V. Sapkov, E.S. Soldatov, V.G. Elensky, "Method of creation of monomolecular transistor with overhanging electrodes ", *Proc. SPIE. Nanosctructures and Nanodevices*, 7025, 70250P, 2008.

Formation of molecular transistor electrodes by electromigration

A.S. Stepanov[1], E.S. Soldatov[2], O.V. Snigirev[1,2]

1. IMP, RRC "Kurchatov Institute", Russia, stepanov@cryolab.ru
2. M.V. Lomonosov Moscow State University, Russia, esold@phys.msu.ru

The trend towards miniaturization of components of sub - 10 nm range of electronic devices and increase the density of integration of the elements requires to find new approaches to their creation. One promising direction is to create a molecular transistor. Thin-film gold electrode system with gap between them in a few (< 5 nm) nanometers is a basis of such a transistor.

Method based on the effect of electromigration often used to create such gap [1]. In this work we have carried out experiments to study the thin film electrode with sub-10 nm nanogaps obtained by this method. To be able to control the process of electromigration at nano-scale we must to have a fast feedback scheme. It is estimated that the characteristic time of the restructuring of the gold films in the formation of the gap lies in the range of 10 - 50 ms. A shift of about 10^5 atoms of gold occurs during this time [2]. On the basis of computer, A / D board Advantech PCI-1713, and D / A converter Advantech PCI-1720 we constructed setup, being able to respond to the changing profile of torn film with the time ~ 20 us. This allowed us to very precisely control the process of film rupture, formation the gap and the time to stop him just at the proper moment. It's very important to obtain extremely small gaps.

Chips with dimensions 10x10 mm of standard silicon wafers with deposited e-beam resist and evaporated gold served samples for the electromigration in our work [3]. At the center of the chip a system of gold electrodes (thickness 50 nm) with a thin (15 nm) and a narrow region (width 200 nm, length 3 mm) has been built. Gold evaporated on the Ti buffer layer with thickness of 2 nm. Ti typically used to provide adhesion of the Au film on SiO_2 substrate. Electromigration in the regime with continuous increase of voltage in the range of 0 – 10 V with the rate 10 mV/s was conducted on these samples. The resistance change of the bridge 4 times was stopping criteria in our experiments. Current density in the sample reaches 10^6 A/sm^2 during the process of restructuring the film.

The resulting gaps with sizes 5 - 10 nm were studied in the scanning electron microscope (SEM), followed by measurement of their I-V curves. It was found that conductivity of the gap was higher than the estimates for the geometry of gaps. This indicates that lying under the gold titanium layer shunting nanogap and prevents the formation of molecular transistors. To resolve this problem, we have abandoned the evaporation of Au on SiO_2, requiring to use a buffer layer, and investigated the possibility of deposition the necessary strips of gold on the dielectric layer of Al_2O_3, without a buffer layer. Layers of Al_2O_3 were obtained by oxidation of a thin film of Al in an atmosphere of oxygen for 20 minutes. Experiments have shown that the obtained nanostructures have sufficient adhesion and gold are well retained on the surface without any additional buffer layers.

Implementation of the electromigration process in such samples showed that gaps with size of about 5 nm can be obtained.

As a result, in the present work setup with a small (~ 20 us) response times was designed and constructed, allowing to produce gaps of width 5 - 10 nm in the Au films. It was shown the need for evaporating Au without buffer layer, made thin (15 nm) and narrow (200 nm) Au film on the surface of Al_2O_3 without adhesion layer. Electromigration held on such films and received nanoelectrodes with wide gaps ~ 5 nm suitable for the manufacture of single-molecular transistors based on them.

This work was supported by RFBR (project 09-07-00272-a) and ISTC (project number 3457).

1. Park, H., A. K. L. Lim, et al. "Fabrication of metallic electrodes with nanometer separation by electromigration." Applied Physics Letters 75, pp. 301-303, 1999.
2. Heersche, H. B., G. Lientschnig, et al. "In situ imaging of electromigration-induced nanogap formation by transmission electron microscopy." Applied Physics Letters 91: 072107-3, 2007.
3. Soldatov E.S., Khanin V.V., Kolesov V.V., Presnov D.E., et al. "Room temperature molecular single-electron transistor." Usp.Fiz.Nauk. vol. 168, pp. 217-219, 1998.

PECVD carbon nanostructure formation using DC glow discharge

D.G. Gromov, S.A. Gavrilov, I.S. Chulkov

Moscow Institute of Electronic Technology (Technical University), Moscow, Russia, E-mail:gromov@optolink.ru, 124498 Moscow, Zelenograd, Russia

In the last years the new carbon nanomaterials such as carbon nanotubes, fullerene, diamond-like films are strenuously studied because of their potential possibility for applications. They show the especial structural, mechanical and electrical properties.

The most commonly used method of carbon nanostructure synthesis is chemical vapor deposition (CVD). CVD is simple and economically sound method for carbon nanostructure synthesis. This method provides the controlled growth with desired forms, but it allows to use carbon-contained substances in different aggregative states (liquid, solid and vapour). The plasma using during CVD (PECVD) enables more intensive dissociation of carbon-contained substance and carbon nanostructure synthesis temperature reduction.

We have produced the plant of plasma enhanced chemical vapour deposition of carbon nanostructures on the base of the triode ion-plasmas system for thin film deposition. In the produced plant the DC glow discharge plasma is used. It has the follow features:

- It is possible the deposition of catalytic agent (Fe, Ni, Fe-Ni alloy having any composition) by triode ion-plasmas sputtering of corresponding target in the united vacuum cycle with CVD process;
- catalytic agent sputtering can be carried out directly during CVD process;
- catalytic agent sputtering can be introduced in reaction region consisting of gas-vapour mixture during CVD process;
- It is possible the realization of ion bombardment of substrate and growing structure by ions from plasma. For this the direct negative voltage bias can be applied on the substrate;
- The high frequency voltage bias can be applied on the substrate also.

In the realized experiment series nickel has been used as catalytic agent. It was deposited on the heated substrate surface by nickel target sputtering directly prior to CVD process. Hexane and argon were used as carbon source and gas-carrier respectively.

The first series of the realized experiments showed that the produced plant allows to produce the different carbon structures in dependence on formation conditions (Fig.1).

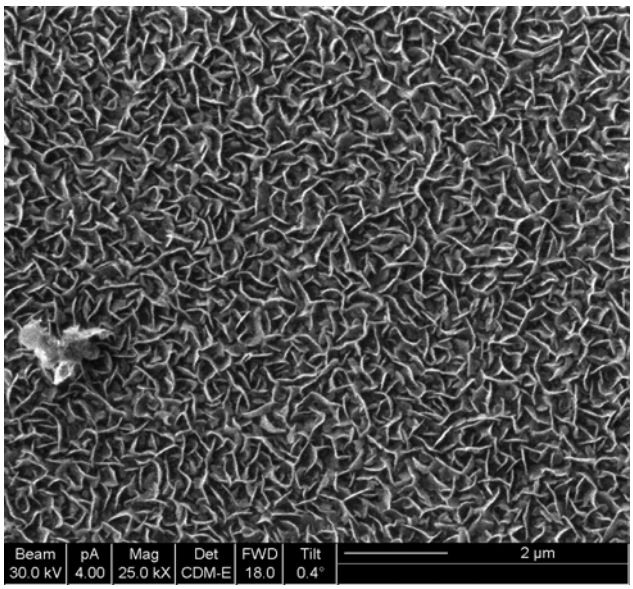

a)

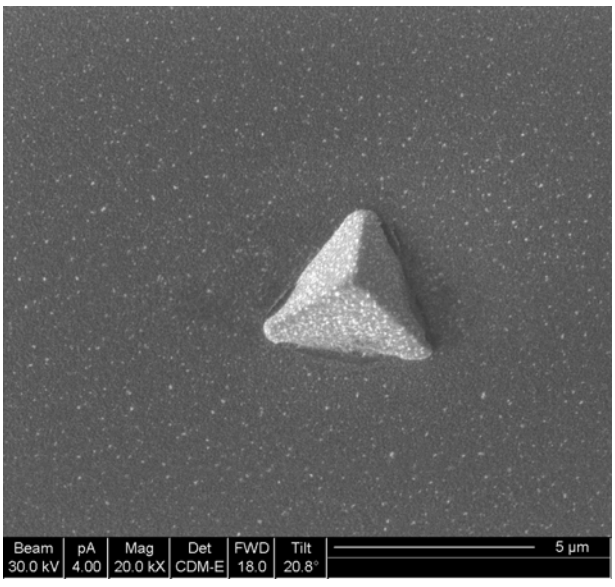

b)

Fig.1. The morphology of the formed carbon layers: a) scales; b) pyramids.

The electrophysical properties of the produced carbon structures have been studied. The structure formation mechanism is discussed.

Physical limitations of reliability in microwave microelectronic devices operating in periodical pulse mode

A.G. Vasiliev, V.F. Sinkevich
FSUE "Science and Production Enterprise "Pulsar" Moscow, Russia, pulsar@dol.ru

The analysis of microelectronic devices that failed while operating in periodical pulse mode (a basic operating mode of microwave modules for radar station) showed:

- time to failure varies within wide range;
- the failure is catastrophic and is followed by local destruction of multilayer metallization.

It was found out, that the main mechanism of those failures is connected with material fatigue in metallization layers. This mechanism is caused by fundamental temperature variation on the crystal boundary in periodical pulse mode. The amplitude of temperature variation can reach 120÷150 ºC, and the amount of variations - 10^{10} cycles. That leads to periodically changing mechanical stress on the boundary of heterogenetic materials (Si-Ti-Pt-Au-SiO_2) because of different temperature coefficient of their linear expansion. As a result the degradation process leads to breakdown voltage decrease and catastrophic failure.

Here were discussed the ways of reliability growth in microelectronic devices while operating in impulse periodical modes.

Principal problems of quality improvement for high-speed planar transmission lines issued from studies of high-*Q* microstrip resonators

A. P. Chernyaev[2], V. A. Dravin[1], A. Yu. Golovanov[1,2], A. L. Karuzskii[1], A. E. Krapivka[1], A. N. Lykov[1], V. N. Murzin[1], A. V. Perestoronin[1], A. M. Tskhovrebov[1], and N. A. Volchkov[1]

1. P. N. Lebedev Physical Institute of Russian Academy of Sciences, Moscow, Russia, E-mail address karuz@sci.lebedev.ru 2. Moscow Institute of Physics and Technology (State University), Dolgoprudny, Moscow District, Russia, E-mail address chernyaev49@mail.ru

Synchronous machine recognition of the content of a talking man's speech is the most important challenge to recent electronics [1]. Requirements to hardware for this task were formulated early in previous editions of the book in the eighties as a critical minimal computation rate, which should be an order of value higher than the achieved up to now several-GHz-range frequencies. Noteworthy the recent several-GHz level has been estimated in that time as the one else critical value of computation rate required to fulfill another global challenge of machine image processing, which seems to be practically implementing now. Required for human voice recognition frequencies order of ten-GHz correspond to centimeter range of wavelengths, which become to be comparable with geometrical dimensions of a computational device. That can increase a significance of coherent wave effects, including the resonance effects, in transmission lines of a computational device as it has been pointed out early concerning development of the Josephson-junction-based computer. In recent computers most of the circuits, which transmit electrical signals, comprise exclusively integrated planar microstrip-like lines. So the principal problems of quality improvement for the broadband high-speed planar transmission lines may grow important. Quality of a high-speed transmission line is determined by its dispersive and dissipative characteristics, which are directly related to the quality-factor (Q) of resonators constructed of a finite segment of this transmission line, and may be characterized by results issued from measurements of Q of the resonators. In the case of planar integrated transmission lines the Q-factor of microstrip-like resonators should be studied. Such investigation is of a great interest also for applications of microstrips as positive loop-back passive elements in monolithic high-speed resonance-tunneling semiconductor heterostructure-based THz wave oscillators [2], as high-Q microwave resonators in thin film superconductor circuits with high critical temperature and in measuring schemas for studying physical effects and properties, including the use of recently found effect of significant retardation in microstrip microwave systems, which opens a novel experimental approach to investigations of spatial dispersion effects [3].

The problem of improvement of Q-factor of microstrip resonators, which belong to the type of semi-open resonators (open waveguide resonators), was not studied in any detailed systematic formulation previously. This is a consequence of the semi-open nature of resonator, which results in inherently continuous spectrum of resonances and to the respective possibility of an existence of radiative losses even for an ideal resonator made of not dissipating materials. In this report the results of rather systematic study of superconductor high-Q microstrip resonators in the frequency range of order 10 GHz are presented. Relative contributions of the spectral (geometrical and non-dissipative properties of materials), on one hand, and of the dissipative (losses in materials) characteristics, on another hand, into the limitation of the maximal achievable quality-factors are investigated. It is shown that the achieved by now highest Q-factors of microstrip resonators in cm wavelength range $Q \geq 10^5$ are limited dominantly by the spectral properties of microstrip resonators.

This work is supported by PFI OFN RAN IV.12. "MPR", by RFFI (08-02-00513), by the Ministry of Education and Science of Russia from VCP RNPVS 2.1.1, №5904, from AVCP RNPVS 2.1.1/500.

1. Iu. K. Pozhela. *Physics of High-Speed Transistors.* Plenum Publishing Corporation, New York, 2007

2. A. L. Karuzskii, V. A. Dravin, A. S. Ignatyev, A. E. Krapivka, Yu. A. Mityagin, V. N. Murzin, A. V. Perestoronin, A. M. Tskhovrebov, "Microstrip stabilized semiconductor quantum-well generator for millimeter and submillimeter wavelength range", in *International Conference on Millimeter and Submillimeter Waves and Applications III, August 5-8, 1996, Denver, Colorado, USA*. M. N. Afsar, editor, Proc. SPIE Vol.2842, p.319-327, SPIE, Bellingham, WA, 1996

3. A. P. Chernyaev, M. Chiba, A. L. Karuzskii, A. N. Lykov, V. N. Murzin, A. V. Perestoronin and Yu. V. Vishnyakov. "Retardation effect in microstrips and microwave detection of spatial dispersion in superconductors", Journal of Physics and Chemistry of Solids, **69**, pp. 3313-3316, 2008

Effect of Conductivity Triggering: Studying and Optimization of MOS-like Structures

A.E. Berdnikov, A.A. Popov, A.A. Mironenko, V.D. Chernomordick, A.V.Perminov
Yaroslavl Branch of Institute of Physics & Technology of Russian Academy of Sciences, 150007, Russia
e-mail: imiraslab4@yandex.ru

Earlier we found out effect of conductivity triggering [1]. It consists in switching of MOS-like structure in high conductive state at supplying of one polarity and threshold size voltage, and in low conductive state at supplying of others polarity and threshold size voltage. The conductive state can be kept long time. Dielectric in MOS-like structure was prepared by a method of low-frequency PECVD. The creation of non-volatile memory devices with cross-bar topology is possible on the basis of conductivity triggering effect. The similar effect was earlier observed in similar structures on chalcogenide glasses with one silver electrode [2] and on structures with polymer dielectric, containing of metal clusters [3,4].

For study of the mechanism of conductivity triggering effect the investigations of conductivity were carried out at various temperatures. It was revealed that the conductivity grows at decrease of temperature. Such dependence can be explained by reduction of spread resistance due to increase of free path of carriers in the semiconductor. It shows that the conductivity through dielectric is carried out on the small size channels.

The parameters of conductivity triggering effect were investigated in depending on the area of MOS-like structures. It was established that the dependencies on the area have a statistical property. At reduction of the area the average values of a threshold voltage of switching are increased. It can be explained that the precursors of conducting channels are formed as a result of self-organising during dielectric growth. However conductivity is realised only through one channel, which has the least value of a threshold switching voltage.

High values of a current and voltage of conductivity switching for MOS-like structures with the small area provide the energy dissipation increasing. In result the probability of destruction of structures with occur of dielectric breakdown increases. The changed designs of MOS-like structures were developed. In particular, the increase of resistance of the semiconductor raises stability of switching.

Method of control of LF PECVD was developed, allowing independently assigning of rate of plasma chemical reactions in gas region and on growth surface. The principle of this method consists in individual adjustment of parameters of the gas discharge. The optimisation of technological process of dielectric like film production with various technological parameters was carried out.

On the basis of the experimental data analysis the model of effect is developed. It is supposed, the channels of conductivity under influence of an initial unlocking voltage in dielectric film appear. The flow of carriers through these channels is defined by the charge placed on built - in during LF PECVD process nanosize clusters. It was defined that 1-2 channels of conductivity work simultaneously in structure. The measurements of temperature dependence have shown that the diameter of the channel is much less than length of free path of carriers. The parameters of switching effect of conductivity depend on properties of the channel and located around it clusters of a material with smaller band-gap.

The test structure of the memory device with cross-bar topology was developed and produced.

1. A.E. Berdnikov, A.A. Popov, A.A. Mironenko, V.D. Chernomordick. Abstracts of International Conference «Micro- and nanoelectronics – 2007», Oct.1th-5th, 2007, Moscow-Zvenigorod, Russia, O2-3
2. B.T. Kolomietz, G.A. Andreev etc., Pribori i sistemi upravleniya (rus), 4, 27 (1980)
3. W. Wu, G.-Y. Jung, D.L. Olynick, J. Straznicky, Z. Li, X. Li, D.A.A. Ohlberg, Y. Chen, S.-Y.Wang, J.A. Liddle, W.M. Tong, R. Stanley Williams, Appl. Phys. A 80, 1173–1178 (2005)
4. J. Campbell Scott, Luisa D. Bozano, Adv. Mater. 19, 1452 (2007)

Design and application features of nonvolatile memory based on ferroelectric thin films

A. Marycheva[1], N. Zaitsev[2]

1. *Moscow Institute of Electronic Engineering (TU), Zelenograd, Russia, E-mail address arabella@mikron.ru.*
2. *Micron Corp., Zelenograd,, Russia, E-mail address: zaitcev@mikron.ru*

There is a great demand for different types of nonvolatile memory nowadays on the market. One of them is Ferroelectric Random Access Memory (FRAM). It uses the phenomena of ferroelectricity, the ability of some materials to keep electric polarization that can be reversed by the application of an external electric field. The FRAM memory cell consist of the thin ferroelectric film placed between two electrodes. The crystal of ferroelectric consists of the cells with an unsteady atoms in the middle [1-3]. By applying of the electric field, this atom can be moved back and forth between two stable positions. The atom remains in either of the positions even without outer field, so ferroelectrics are able to remember two states, representing logical "1" and "0". Among others the described memory is shockproof and resistant to various types of radiation, that makes it potentially useful in space applications.

The FRAM memory modules produced by Ramtron company have cell structure based on the two transistors and two ferroelectric capacitors [1,4]. Such a structure provides high reliability, but is geometrically large. The size of the cell, as well as the cost of the memory, can be reduced by using only one transistor and one capacitor. There are many other solutions except these two basic above and many research centers are working on it.

FRAM is faster and consume less power then it's competitors - EEPROM and Flash memories. For example FRAM's read/write cycle is only 150 ns long, versus 10 ms of EEPROM/Flash's one [1]. The current is 20mA and 90 mA accordingly. The maximum of write/rewrite cycles is several times higher for FRAM as compared with EEPROM or floating gate memory. The last one is able perform up to 1e06 write cycles, and this is too few for data collecting applications. FRAM can be rewrote more than 1e10 times (fig.1).

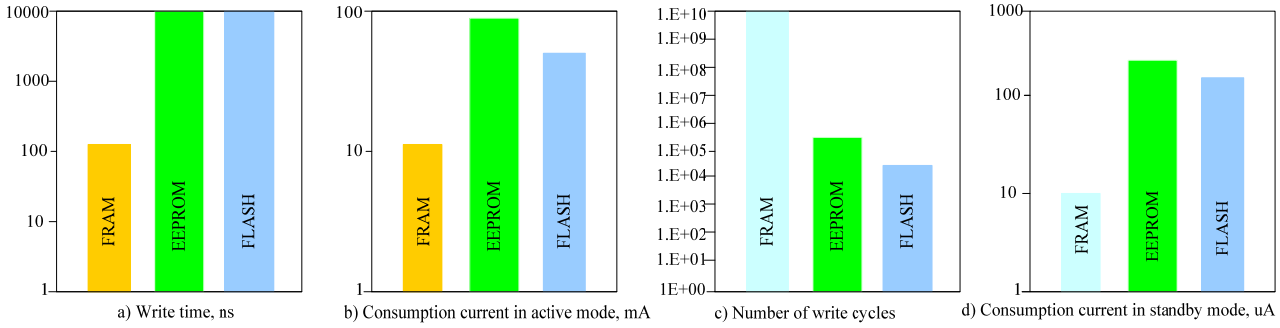

Fig.1. Comparison characteristics of different technologies of memory.

There is a probability of oxide layer destruction in the floating gate memories, due to stressful conditions of the writing/erasing cycle. FRAM does not have it, and that dramatically improves it's durability. The writing cycle of the floating gate memory takes long time and needs relatively high voltage. Whose two factors lead to high power consumption. Quite the reverse, FRAM almost does not consume power.

Since reading and writing are the same physical process in case of FRAM, there are almost the same currents in either of them [2]. The relatively low voltage in addition leads to lower power supply requirements and reduces the electromagnetic interference emitted by the circuit.

Thanks to shot reprogramming cycle, low currents in active mode and standby mode, FRAM is an ideal solution for RFID applications, where radiofrequency acts as the data channel and the power source in the same time [2]. Ferroelectric based memory cell is considered as prospective solution for nonvolatile random access memory applications.

1. Dobrusenko S. Ferroelectric RAM by Ramtron International // Electronics: Science, Technology, Business. №4, 2003
2. Temchenko V. It's time to use FRAM // Electronic components. №1, 2000
3. Layans M., Glas A. Ferroelectrics and similar materials. Mir, Moscow, 1981
4. http://www.ramtron.com/

Research of SONOS non -volatile memory elements

Orlov O.[1], N.Shelepin[1]

1. *Mikron JSC, Moscow, Russia, E-mail addres:o_orlov@mikron.ru , shelepin@mikron.ru*

NVM ICs comprise additional high voltage blocks to provide information re-writing in the memory array. Attempts to reduce NVM cell reprogramming voltage and make process compatible to CMOS is considered an actual task [1,2].

Currently Mikron JSC has fabricated p- and n-type sample MONOS transistors with re-writing voltage about 8-9V. This paper deals with p- and n-type SONOS NVM cells investigation in respect of different choice of major ONO stack parameters [2,3]. Based on physical analysis and simulation computation certain meanings of key layer thicknesses were taken for performance evaluation: tunneling oxide thickness from 2.0 to 2.5 nm, blocking oxide thickness 5.0 nm and nitride thickness within the range 5.0 - 8.0 nm. All major cell operation states were analyzed: writing , erasing of information and storage.

Regarding n-type SONOS NVM cell writing was conducted under the following conditions: Vd = Vs = Vsub = 0 V, Vg = 9 V, where d – drain, s – source, g – gate and sub stands for "substrate". Erasing conditions were taken as Vd = Vs = Vsub = 0 V, Vg = –9 V.
In case of p-type cell all the meaning were inverted.

For SONOS NVM test structures (W/L =50/50) the following dependences were obtained:
- threshold voltage (Vt) dependence upon programming voltage value (U) with 10 ms pulse;
- threshold voltage dependence upon programming pulse duration with programming voltage –9V and +9B;
- threshold voltage dependence upon number of programming pulses +9V and –9B with pulse duration 10 ms and pulse repetition cycle 30 ms.

Cells (W/L =16/1.6) were investigated as well and threshold voltage dependence upon the storage time was obtained for programming voltage +9V and –9B.

It was found that repeatable threshold voltage shift among all the samples is repeatable for corresponding programming conditions. Acceptable writing characteristics with memory window about 2 V after reprogramming were obtained only for samples with nitride thickness of 8.0 nm. For such a structure optimal operation conditions were considered as following: writing and erasing voltage 8-9 V; writing cycle duration 0.5 – 1.0 ms, erasing cycle duration 2 – 10 ms. This operation mode provides more than 10^5 cycles available. SONOS NVM cell are very sensitive to the quality and repeatability of such processes steps as tunneling oxide, blocking oxide, nitride, poly-silicon gate deposition along with consequent doping, and respectively it is very sensitive to the quality and condition of layers boundaries and interfaces within ONO structure. These flow steps are responsible for basic SONOS NVM cell parameters and in general are compatible with CMOS process. Comparison of n-type cells with tunneling oxide of 2.0 nm and 2.5 nm showed the difference of threshold voltage shift caused by three decades storage period change: for 2.0 nm tunneling oxide cell Vt shifted about 1.0 V while for 2.5 nm tunneling oxide cell Vt shift was about 30% less – 0.7 V. Evaluation of storage time based on approximation for long periods demonstrate storage times about hundred years with room temperature condition and taking 0.5 V memory window as a criterion.

1. S.M. Sze. Physics of Semiconductor Devices. John Willey and Sons, New York, 1981
2. J. Bu, M. H. White, /Design considerations in scaled. SONOS nonvolatile memory device //, Solid-State Electronics., vol. 45, pp. 113-120 (2001)
3. V. A. Gritsenko, H. Wong, J. B. Xu et al., J. Appl. Phys. 86, 3234 (1999)

Research and optimisation of anodic joint process of SOI microelectromechanical strain transducer with glass reference element

L. Sokolov[1], N.Parfenov[1], S. Timoshenkov[2], V. Kalugin[2]
1. Moscow Aviation Institute, Moscow, Russia, e-mail pnm334@mai.ru.
2. Moscow Institute of Electronic Technology (Technical University), Moscow, Russia

There is a number of papers dedicated to research of anodic joint of silicon and 'Pyrex'-type glass in electrostatic field, among which the most valueable are [1…2].
Science and research problem of making of high-temperature high-stable SOI integrated absolute pressure transducers and sensors based on them, working in rough conditions of aronautical and space on-board electronic systems, cannot be solved in full without developing and implementation of SOI transducers anodic joint with glass.
The special feature of anodic joint for SOI structures is the presence of a dielectric layer (e.g. made of glass) after solid integral strain frame forming in instrument layer of SOI structure (see fig.1). Thus in high-voltage power source circuit an additional resistance from glass is inserted in series.
In this report there are brought the results of research and optimisation of anodic joint process for samples of SOI strain transducer with 'Pyrex'-type glass reference element specially finished for fusion. There also are microphotographs of morfology of samples' surface being etched up to silicon.
The photographs acquired via Veeco atomic-force microscope show the dimensions of glass nanoparticles (the glass-like system of BaO- Al_2O_3 – SiO_2, average size being less than 100 nm), which were used for silicon plates fusion process and silicon membrane etching after having the glass removed. The microrelief of samples' surface with nano-impurities of oxides is studied.
According the results of research and optimization of fusion mode parameters the specimens of strain modules based on undetachable joint of with glass.

1. W.H.Ko. J.T. Suminto. G.J. Yeh. *Micromachining and Micropackaging of Transducers*, edited by C.D. Fung, P.W. Cheung, W.H. Ko and D.C. Fleming. Elsevier Science Publishers B.V., Amsterdam, 1985
2. Eniko T. Enikov, James G. Boyd A. *Finite – Element Formulation for Anodic Bonding // Smart Materials Structures*, vol.32, pp.737-750, 2000

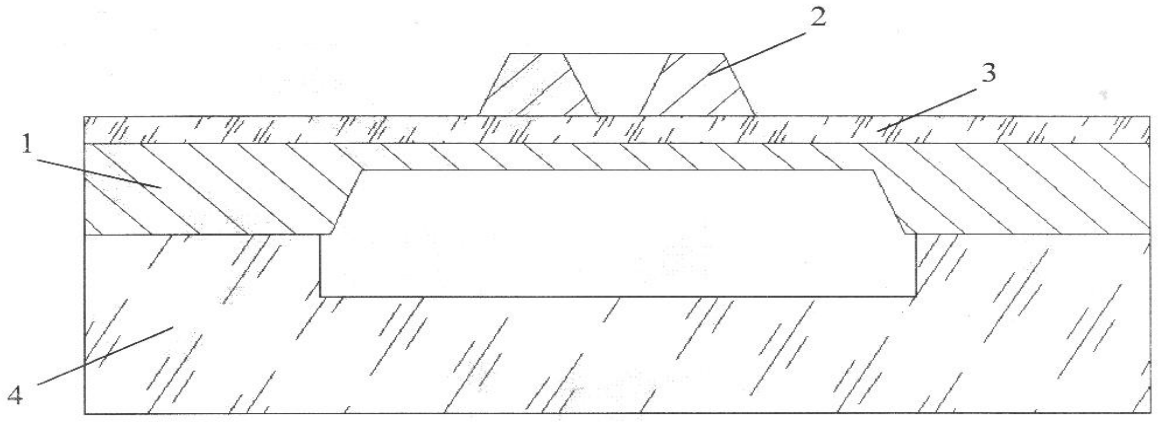

Fig.1 Cross-section of strain module of absolute pressure: 1 – Microelectromechanical SOI transducer with solid strain frame (tensoframe), 2, 3 – dielectric layer of SOI structure, 4 – reference element.

Experimental research of the Magnetotransistor in a double well

A. Kozlov[1], Yu. Parmenov[1], R. Tikhonov[2]
1. *Moscow State Institute of Electronic Engineering – Technical University, anton@dsd.miee.ru;*
2. *2. SMC "Technical University", R.Tikhonov@tcen.ru*

Now the most actual direction in the microelectronics are designing and creation of physical sizes sensors. They are very applied in various branches of a science and technics. The most claimed are a magnetic field sensors which allow to measure such physical parameters as screen angle, an incline, a careen, a trim difference, an azimuth, a speed, an acceleration, a distance up to object and many other things.

On a basis before [1,2] lead researches by a device-technological modelling it is shown, that to the most effective integrated magnetosensitivity element as a magnetic field sensors can serve a lateral dual-collector bipolar magnetotransistor executed in double diffusion well (DCBMTDW). The given device has low factor of nonlinearity of a target differential signal in a wide range of an induction of a magnetic field, high magnetic sensitivity, average values of power consumption and the sizes.

The experimental researches executed on base SMC "Technological Center" MIET of DCBMTDW samples were carried out. For creation of a magnetic field the electromagnet with values of a magnetic induction size from 3 up to 180 mT was used. Transistors samples were located in a backlash of an electromagnet so that lines of a magnetic field introduction were parallel to the long party of the emitter. The magnetotransistor in a magnetic field it was included in an electric circuit under the circuit with the common emitter by means of the common voltage supply and a resistive divider. Measurements of dependence of relative and absolute DCBMTDW sensitivity with different distances the base - emitter from a total current of a *p*-well (base) and a *n*-well were carried out.

Measurements were carried out with the help of digital voltmeters B7-40 at a voltage supply V_{DC} = 9 V and loading resistance in collectors 546 kOhm for 16 and 32-1 samples and 9 kOhm for a 2a16 sample. The choice of a working point was provided with the task of current I_{BW} through block of resistance R4831 in the incorporated contacts to a *p*-well (base) and to a *n*-well. The emitter was united with contact to *p*-substrate and connected to the common potential. In circuits of collectors equal high-resistance loading R_{C1}=R_{C2} were used. Collector resistance values changed. On the common contact of a *p*-well (base) and a *n*-well voltage supply V_{DC} concerning potential of the emitter moved. The magnetic field with induction *B* was directed in the coil by change of a current of the solenoid creating a magnetic field in samples, placed inside the solenoid.

At measurement of sensitivity dependence an induction the current changed proportionally for creation of a magnetic induction in a range 10 - 100 mT with step 10 mT. At increase in distance L_{BE} with 2 up to 32 um sensitivity raises with 1,7 up to 49 V/T at the chosen value of a current of base - well I_{BW} = 4,3 mT.

Definition of differential an absolute voltage sensitivity was spent by digital voltmeter B7-40 on change of a potential difference between collectors V_{C1} (*B*)-V_{C2} (*B*) in view of initial offset V_{C1} (0)-V_{C2} (0):

$$S_{AV} = \frac{(V_{C1}(B) - V_{C2}(B)) - (V_{C1}(0) - V_{C2}(0))}{B} \quad (1)$$

Practical realization of developed design of DCBMTDW is carried out. On the basis SMC "Technological Center" MIET test crystals with DCBMTDW are made and investigated. Measurements on the basis of the received values of currents of transistors in magnetic field *B*=100 mT have shown VACH and calculation relative current sensitivity (RCS) that the developed transistors possess increased RCS $SRI \approx 1{,}082\ T^{-1}$ that on the average in 2,5-3 times is higher, than size RCS of DCBMT in single diffusion well. Comparison of experiment results and calculations confirms validity of the developed technique of modelling and adequacy of numerical modelling.

1. Anton V. Kozlov, Robert D. Tikhonov / Device-technological Modelling of Bipolar Transistor with Base in the Well // 9th International Workshops and Tutorials on Electron Devices and Materials (EDM-2008), Table of Contents, 1-5 july, Erlagol, 2008, pp. 69-73.

2. R.D. Tikhonov, A.V. Kozlov, Yu.A. Chernova, S.A. Polomoshnov / Increase sensitivity of the Sensor based on bipolar magnetotransistor by minimization initial output offset // International Siberian Conference on Control and Communications (SIBCON-2009), Proceedings, Russia, Tomsk, March 27-28, 2009, pp. 216-221.

The amplifier-concentrator of electrons as the base element of the emission electronics.

E.Il`ichev, A.Kuleshov, E.Poltoratskii, G.Rychkov
State Research Institute of Physical Problems,
Zelenograd, Moscow, Russia, e-mail: polt@niifp.ru

Development of digitized television, satellite communication and radiolocation results in to construct powerful microwave devices with frequency up to 200 GHz. To design these devices it is need cold cathode with current density more then 10 A/cm^2. We propose amplifier-concentrator of electrons (ACE) as cold cathode. ACS is a through hole (1) having form of the truncated pyramid (see fig.1).

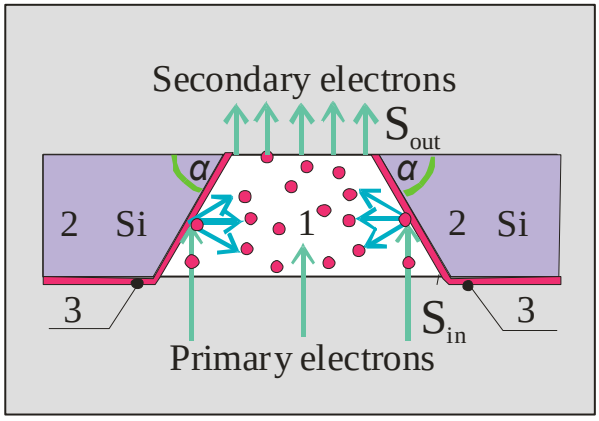

Fig. 1

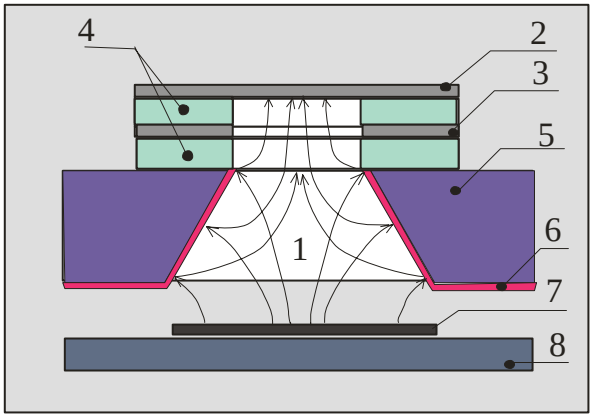

Fig.2

The hole is made in silicon plate (2) and the hole walls are coated with boron doped diamond polycrystalline film (3). If primary electrons with energy E are incident on the film then secondary electron are born and part of them are emitted to vacuum [1].

The optimal value of E for which the number of secondary electrons become maximal can be estimated as [1]

$$E_{opt}\ [keV] = \left[25 L \rho \Gamma (1/m + 1) / Sin\alpha\right]^{0.625} \qquad (1)$$

where ρ=3.51 g/cm^3 for diamond, Γ- gamma function, $m \approx 1.9$, L- diffusion length (for polycrystalline diamond film 0.016 $\mu m < L <$ 0.16 μm [1]), α = 54.7^0. From Eq.(1) one obtains maximal number secondary electrons $N_{max} \approx 1.2 \cdot 10^3 h L^{0.6}$[$\mu m$] where $h \approx 0.2$-0.5 [1]. Considering electron concentration at the output ACE and the electron multiplication factor we can obtain current density yield K up to $N_{max} S_{in}/S_{out}$ where S_{in} (S_{out}) input (output) hole square. In experiment we have $K \approx 30$.

ACE can be used as base electron source for creating microelectronic vacuum integrating circuits. As example Fig. 2 shows the triode design: 1-silicon plate, 2-ACE, 3-diamond film, 4-anode, 5-gate, 6-insulator, 7-primary electrons source, 8-substrate.

1. V.Dvorkin, N.Dzbanovsky, N.Suetin, E.Poltoratsky, G.Rychkov, E Il`ichev.” Secondary electron emission from CVD diamond films”, Diamond Relat, Mater. 12, pp. 2208-2218, 2003.

Piezoelectric current generator through filamentary nanocrystals of zinc oxide

M. Nazarkin, S. Gavrilov.
Moscow Institute of Electronic Technologies (Technical University), E-mail: mikleo@mail.ru

The development of renewable energy sources make scientist to look for new materials to create more efficient and environmentally friendly methods of electricity production. One of this material is zinc oxide which band gap width is 3.37 eV. Because of its unique set of properties, based on it is possible to create the set of instruments and devices [1].

Thus [2] was created power generator, based on the piezoelectric effect filament array of zinc oxide nanocrystals. When bent nanofilament ZnO at its ends appear a potential difference. The big drawback is described in [2] design is an upper electrode, which is an array of the edge, which touch only to part of nanocrystals ZnO. Because of this the efficiency of such construction is not high enough.

As part of this work was designed a construction of generator, in which the upper electrode was used self-nanostructured material - porous anodic aluminum oxide coated thin gold foil. The generator is an assembly consisting of the lower and upper electrodes, with the array of zinc oxide nanocrystals among them.

Formation of microelectromechanical generator was as follows:

At the pre-laundered first oxidized silicon substrate by magnetron sputtering through a mask applied Si_3N_4 layer thickness 600 nm, which employee spacer. Then through a mask applied Ni layer, which thickness is 300 nm, as the lower electrode. Then on top of it through a mask applied seed layer of ZnO: Al thickness of 20 nm with a resistivity 12MoHm*cm. On the structure obtained by chemical deposition was formed an array of nanocrystals ZnO For deposition using an aqueous solution: 0.4 M NaOH and ·0.01 M $(Zn(NO_3)_2)\cdot 6H_2O$. After the deposition of ZnO nanocrystals the structure was washed in ionless water.

On the pre-laundered second oxidized silicon substrate by magnetron sputtering was applied a layer of aluminum 300 nm thick. Further from aluminum layer with electrochemical means formed layer of porous anodic aluminum oxide in 0.1 M solution of H_3PO_4. Then on its surface is deposited Au layer thickness 400 nm, a second electrode.

The next stage involves the assembly of the generator. The second wafer substrate layer of gold dropped down to an array of ZnO nanocrystals on the first substrate. The last stage was installed on the perimeter of the structure of an elastic hermetic glue, which, on the one hand, must allow movement of the second wafer on the first and, on the other hand, inhibit the absorption of moisture array of nanocrystals.

The control of each stage was carried out using scanning electron microscopy (SEM). The length of nanocrystals is about 1 micron, with a diameter of about 20 nm. Average pore diameter of anodic Al_2O_3 coated with gold was around 100 nm.

Study on vibration measurement system collected samples revealed the presence of dependence of its response to the frequency and amplitude of oscillations. The frequency response of the device of mechanical vibrations at a constant acceleration of 1g. Over 400 Hz steady tone. This showed an increase in resonance signal at frequencies 520, 1000 and 4000 Hz. The maximum response of 80 mV, to expedite 1g was obtained at a frequency of oscillation 4kHz. Attention is drawn to the fact that a change in the tone generator in the time it repeats the sinusoid mechanical vibrations. A comparative analysis of the device and the generator is described in [2]. The big difference of investigated samples from the generator described in [2] was the presence of positive and negative parts of sinusoids, which cannot be said of the generator in [2], where there was only a positive component. In our case, ZnO nanocrystal inserted into the pores of anodic Al_2O_3. Because of this zinc oxide nanocrystal always refer to the upper electrode. In its neutral (zero) state they are already bent. Therefore, in the event of mechanical vibrations, and further their bent generates a positive charge, and if extension negative.

Thus the presence of positive and negative components of the signal with the linear dependence of the signal from the acceleration, allows using this device not only as a generator of power, but also as an accelerometer.

1. ZnO – nanostructures, defects, and devices Lukas Schmidt-Mende* and Judith L. MacManus-Driscoll, Department of Materials Science, University of Cambridge, Pembroke Street, CB2 3QZ, Cambridge, UK ,may 2007 vol_10, № 5.

2. Direct-Current Nanogenerator Driven by Ultrasonic Waves, Xudong Wang, et al. Science 316, 102 (2007);

New type of high efficiency power supply of digital units

Y. Chaplygin[1], V.Losev[1]

1. *Moscow State Institute of Electronic Engineering, Moscow, Russia, E-mail address: dsd@miee.ru*

One of the possible techniques to reduces the power consumption in digital CMOS circuits is to slow down the charge transport [1]. This slowdown can be achieved by introducing an inductor in the charging path. Additionally, the inductor can act as an energy storage element, conserving the energy that is normally dissipated during discharging. LC-resonant circuit together with the parasitic capacitances from the circuit is formed.

The resonance type drivers have a greatest power efficiency. The analysis of resonance drivers with the LC-resonator and the fixed loading, working in a condition of autogeneration is carried out.

Regularities of power consumption in drivers with impulse power pumping are parsed. The optimum range duration of pumping pulses and best values of switching devices resistance is established.

Principal difficulty of resonance type drivers realization will consist in synchronization of two and more generators for deriving pulses with number of phases, major two, and also provide the necessary pumping impulse frequency which should be equal to a resonance frequency of LC-network.

This problem has been solved by use the automatic control system of pumping power regulatory based on the ring oscillator. The flow chart of operation of the adiabatic driver designed based on the ring oscillator and the functional block diagram providing a possibility of build-up of the driver with the arbitrary number of clock phases is offered. On the basis of theoretical signature analysis of a self-regulation system requirements to performances of its blocks, amplitudes of output pulses providing high stabilization are formulated.

Functional models of basic units of a self-regulation system are offered. On the basis of these models behavioral simulation of the 4-phase adiabatic driver is carried out. Outcomes of simulation have confirmed a possibility of deriving of high stabilization of output pulses amplitude at formulated requirements realization.

The electric circuits of basic units of the automatic control system - comparators, the integrating amplifier and the saw-tooth generator area designed.

It is shown, that at use of a hinged among choke on each clock trunk the efficiency of the driver can attain 90 % on 600 MHz frequency and 80 % on 1 GHz frequency at output pulses amplitude ~ 3V. For the 4-phase drivers which are not using interconnection components, the efficiency of the driver can attain 50 % on 700 MHz frequency and is boosted up to 75 % at decrease of frequency. At increase of output pulses phases number the efficiency will increase.

Estimated accounts show, that for a chip containing more $4 \cdot 10^3$ gates, the relative area of adiabatic power supplies on a chip can make less than 10 %.

Problems of operation comprised in search of optimum modes of management by switching devices of the driver, research power consumption regularities in drivers and control units, and also development of a procedure of their optimum designing and research of dynamic characteristics.

Investigations were carried out by analytical methods, and also by computer simulation methods.

The obtained results can be used in adiabatic device of information processing with midget power consumption, synchronous digital VLSI (drivers of clock pulses), memory device (drivers of pulses of sampling), the charge-coupled storage device (drivers of clock pulses) and other device containing high-electrical capacity rails.

1. Losev V.V, Staroselsky V.I. The elementary adiabatic logic gates for digital information processing system. Int. Conf. “Micro- and nanoelectronics – 2005” ICMNE-2005. Moscow-Zvenigorod, Russia. Oct. 3-7,. Abstracts, O1-22. 2005.

The theoretical analysis of electronic thermal properties of the interfaces between multiband superconductors and a normal metal

I.A. Devyatov[1], M.Yu. Romashka[1], A.V. Semenov[2], P.A. Krutitskii[3], M.Yu. Kupriyanov[1]

1. Lomonosov Moscow State University Skobeltsyn Institute of Nuclear Physics, 119991 Moscow, Russia, igor-devyatov@yandex.ru. 2. Moscow State Pedagogical University, 119992 Moscow, Russia, a_sem2@mail.ru. 3. Keldysh Institute for Applied Mathematics, 125047 Moscow, Russia, biem@mail.ru.

Investigations of the electronic thermal properties of the interfaces between a normal metal and high-temperature superconductors are important for correct design of modern low-temperature electronic refrigerators and bolometers [1,2]. Multiband superconductivity, recently discovered in ferropnictides [3] and in magnesium diboride [4], is the suitable choice due to isotropic order parameter in it, in contrast with strongly anisotropic d-wave superconductivity in high-Tc cuprates, which is destructive for electronic refrigeration and bolometric applications [2]. Moreover, recent calculations of Andreev spectra and subgup bound states in ferropnictides [5], taking into account coherent multiband interference effects in $s_{\pm}$ sign-reversal order parameter model [6], predict possible suppression of Andreev reflection for clean boundaries between ferropnictides and a normal metal. This Andreev reflection suppression can improve electronic refrigerator quality, in a similar way as additional ferromagnetic layer, suggested in [7].

Up to now there was no calculation of electronic thermal properties of the interfaces between a normal metal and novel multiband superconductors. In this paper we calculate the thermal flux and electron thermal conductivity of the boundary between normal metal and novel multiband superconductors. In this calculations both s_{++} and $s_{\pm}$ sign-reversal order parameter models [6] for multiband superconductor is used, taking into account coherent multiband interference effect [5]. We suggest, that the interface is smooth in an atomic scale and clean, so BTK model [8] for transmission and reflection probabilities of the interface is used. The possible microrefregerating and bolometric application of this structures is discussed.

The work is supported by RFBR grants 09-02-01351-a, 09-02-12351-офи_м.

1. F. Giazotto, T. Heikkila, A. Luukanen, A.M. Savin and J.P. Pekola, “Opportunities for mesoscopics in thermometry and refrigeration: Physics and applications”, Rev. Mod. Phys., **78**, pp. 217-275, 2006
2. I.A. Devyatov, M.Yu. Kupriyanov, L.S. Kuzmin, A.A. Golubov, and M. Willander, “Electronic Thermal Properties of the Interface between a Normal Metal and a High-Temperature Superconductor Material”, JETP, **90**, pp. 1050-1057, 2000
3. Y. Kamihara *et.al*., J. Am. Chem. Soc., **130**, p. 3296, 2008
4. J. Nagamatsu, N. Nakagawa, T. Muranaka, Y. Zenitani, J. Akimitsu, “Superconductivity at 39 K in magnesium diboride”, Nature, **410**, pp. 63-64, 2001
5. A.A. Golubov, A. Brinkman, O.V. Dolgov, I.I Mazin, Y. Tanaka, “Andreev spectra and subgup bound states in multiband superconductors”, arXiv:0812.5057v1.
6. I.I. Mazin, D.J. Singh, M.D. Johannes, and M.H. Du, “Unconventional Superconductivity with a Sign Reversal in the Order Parameter of $LaFeAsO_{1-x}F_x$”, Phys. Rev. Lett, **101**, pp. 057003-1- 057003-4, 2008
7. F. Giazotto, F. Taddei, R. Fazio and F. Beltram, “Ultraefficient cooling in ferromagnet-superconductor microrefrigerators”, Appl. Phys. Lett., **80**, pp. 3784-3786, 2002
8. G.E. Blonder, M. Tinkham, and T.M. Klapwijk, “Transition from metallic to tunneling regimes in superconducting microconstrictions: Excess current, charge imbalance, and supercurrent conversion”, Phys. Rev. B, **25**, pp. 4515-4532, 1982

Microscopic theory of thermal phase slips in diffuse superconducting wires

A.V. Semenov[1], I.A. Devyatov[2], P.A. Krutitskii[3], M.Yu. Kupriyanov[2]
1. Moscow State Pedagogical University, 119992 Moscow, Russia, a_sem2@mail.ru. 2. Lomonosov Moscow State University Skobeltsyn Institute of Nuclear Physics, 119991 Moscow, Russia, igor-devyatov@yandex.ru. 3. Keldysh Institute for Applied Mathematics, 125047 Moscow, Russia, biem@mail.ru.

The investigations of the phase slips phenomenon are important for deriving the answer on a fundamental question, important for the superconducting electronics: up to what value it is possible to reduce the width of a superconducting strip, that it keeps the ability to carry a current without dissipation. Per the last few years new theoretical results [1-3] was obtained, which essentially improved our understanding of this problem, in comparison with the first theories [4,5].These new theoretical results include calculations of quantum phase slip rate [1], essential for extremely low operating temperatures, the correction of McCumber-Halperin result [4] for the preexponential factor in phase slip frequency, obtained via reconsideration of phase-slip center problem with the aid of the imaginary time effective action technique [2], as well as the calculation of free-energy barrier versus supercurrent dependence in clean superconducting wires at arbitrary temperature, using Eilenberger equations [3]. But up to now there was no calculation of free-energy barrier value versus supercurrent dependence in the whole temperature range for the case of diffuse superconductor, which is the most important for the comparison with the experimental results.
In this work we consider the phase slip process for the case of diffuse superconductor in a framework of Usadel equation in Matsubara technique. We calculate numerically coordinate-dependent Green functions corresponded to saddle point in the configuration space and obtain the dependence of the free-energy barrier on the supercurrent.
The work is supported by RFBR grants 09-02-01351-a, 09-02-12351-офи_м.

1. D. S. Golubev and A. D. Zaikin, “Quantum tunneling of the order parameter in superconducting nanowires”, Phys. Rev. B **64**, pp. 014504-1 - 014504-8, 2001
2. D. S. Golubev and A. D. Zaikin, “Thermally activated phase slips in superconducting nanowires”, Phys. Rev. B **78**, pp. 144502-1 - 144502-8, 2008
3. A. Zharov, A. Lopatin, A. E. Koshelev, and V. M. Vinokur, “Microscopic Theory of Thermal Phase Slips in Clean Narrow Superconducting Wires” , Phys. Rev. Lett. **98**, pp. 197005-1- 197005-4, 2007
4. J.S. Langer and V. Amegaokar, “Intrinsic Resistive Transition in Narrow Superconducting Channels”, Phys. Rev. **164**, pp. 498-510, 1967
5. D.E. McCumber, B.I. Halperin, “Time Scale of Intrinsic Resistive Fluctuations in Thin Superconducting Wires”, Phys. Rev. B **1**, pp. 1054-1070, 1970

Characteristics of Nb/α-Si/Nb Josephson junction arrays at frequencies of 68 - 75 GHz.

A.L. Gudkov[1], A.A. Gogin[1], A.I. Kozlov[1], A.N. Samys[1], I.Ya. Krasnopolin[2]
1. CJSC "Compelst", FSUE "SRIPP n. F.V. Lykin", Moscow, Zelenograd, Russia, E-mail: gudkov@niifp.ru
2. FSUE "VNIIMS", Moscow, Russia, E-mail: krasnopolin@vniims.ru

In superconducting integrated circuits (SCIC) of the fundamental frequency-voltage converters basically two types of junctions are used: junctions with hysteretic current-voltage characteristic (tunnel type Nb/AlO_x/Nb, so-called SIS junctions [1,2]), and junctions with direct conductivity (so-called SNS junctions) with nonhysteretic current-voltage characteristic [3,4]. Josephson junctions of SNS type with single-valued (nonhysteretic) current-voltage characteristic are required for the development of Programmable Josephson Voltage Standard (PJVS) with stable output voltage and possibility of fast switching of quantum voltages under computer control.

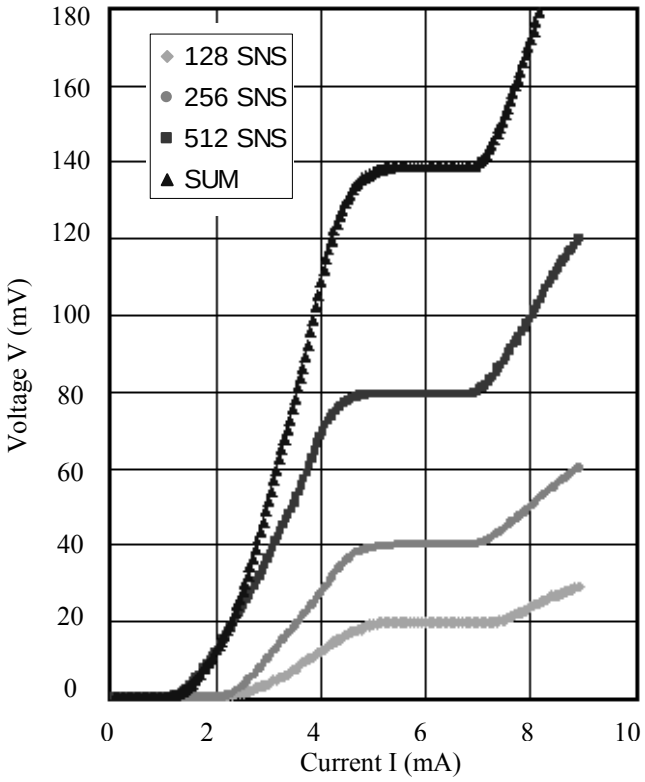

Fig 1. Current-voltage characteristics of 128, 256, 512 sections and their sum (the top curve) of the array of 1024 Nb/α-Si/Nb Josephson junctions under 75 GHz microwave radiation.

This work presents the experimental results of the researches of Josephson junction arrays with SNS junctions as base elements of the frequency-voltage converter for PJVS. Characteristics of arrays up to 1024 junctions, made on the basis of planar Nb/α-Si/Nb Josephson junctions have been investigated. The area of planar junctions is 9×9 μm^2. The junction arrays have been patterned in the form of two microstrips of 15 μm width. These strips form an open slot line with the spacing of 4 μm. The array of series-connected SNS junctions is divided into binary sections with number of 1, 2, 4, 8.... 512, 1024 junctions. The contact pads for independent bias sources are made for each binary segment of this array.

The dc-characteristics of the experimental SCIC samples were measured. The values of the critical current of single junctions are in the range I_c = 4,0 - 8,0 mA. The values of characteristic voltage are $V_c = I_cR_n$ = 100 - 150 μV. Metrological characteristics of experimental SCIC samples were investigated on the JVS apparatus of VNIIMS. The high quality steps (the maximum amplitude up to 2 - 4 mA) were observed at driving frequencies of 68 - 75 GHz. At frequency of 75 GHz current steps were observed in the range of voltage 150 μV - 150 mV on the measured binary arrays (1 - 1024 junctions) (fig. 1). The voltage, generated by series-connected junctions, is the sum of voltages of all biased junctions in the array. Thus, by switching of bias currents in binary groups of k - digit array, it is possible to reproduce as stable constant levels of voltage, as a staircase synthesis of alternating voltage in the range from - 150 mV to + 150 mV with the minimum step 150 μV.

1. R. Poepel. The Josephson Effect and Voltage Standards. Metrologia. V.29. P.153-174. 1992.
2. A. Gudkov, A. Gogin, A. Kozlov, A. Samys, I. Krasnopolin. DC voltage standard. Superconducting IC on the basis of Josephson junctions. Electronics: a science, technology, business. №6. P. 90-93. 2007
3. H.Yamamori, M. Ishizaki, M. Itoh, A. Shoji. NbN/TiN_x/NbN/TiN_x/Nb double-barrier junction for programmable voltage standards. Applied Physics Letters. V.80, №8, P.1415-1417. 2002.
4. A.L. Gudkov "Josephson junctions and areas of their applications". Electronic industry. №3. P. 77-87. 2004.

Transport properties of josephson junctions with ferromagnetic layers

T.Yu. Karminskaya[1], A.A. Golubov[2], M.Yu. Kupriyanov[1], A.S. Sidorenko[3]

1. Nuclear Physics Institute, Moscow State University, 119992 Moscow, Russia.

2. Faculty of Science and Technology and MESA+ Institute of Nanotechnology, University of Twente, P.O. Box 217, 7500 AE Enschede, The Netherlands.

3. Institute of Electronic Engineering and Industrial Technologies Chisinau, Moldova.

The novel S-FN-S and S-FNF-S types of Josephson junctions (S - superconductor, F - ferromagnet, N - normal metal) suggested in [1-3] provide the opportunity for solution of several challenging problems, which still exists in SFS spin valve devices. They are the problem of enhancement of the decay length of critical current, I_C, and the problem of realization of control upon the junction parameters by changing the mutual orientation of magnetization vectors of ferromagnetic films. The results obtained in [1-3] are essentially based on the assumption that the thickness, d_F, d_N, of all the films in FNF multilayer are small compared to their decay lengths (ξ_F, ξ_N). In real structures the requirement $d_N << \xi_N$ can be easily fulfilled, while the inequality $d_F << \xi_F$ is difficult to achieve due to the smallness of ξ_F and finite roughness of NF interfaces. Therefore the solution of two dimensional problem is needed.

In this work we will concentrate on properties of a S-FN-S junction and perform the calculation of its critical current beyond the limits of small F and N film thicknesses for two dimensional geometry. We have considered that NF interface has finite transparency and that N and F metals have different transport parameters. The critical current of S-FN-S Josephson junctions is calculated in the framework of linearized Usadel equations. The dependence of I_C on the distance, L, between superconductors and thicknesses of ferromagnetic and normal layers is analyzed. We discuss practically interesting parameters of the structure. These results are important for possible applications of S-FN-S and S-FNF-S Josephson junctions as spin valve Josephson devices.

Also the conductance of ferromagnetic conductor is studied in the presence of induced long-triplet correlations from SF bilayer for the case of noncollinear vectors of magnetization of F layers.

The work is supported by RFBR grants 08-02-90105-Mol_a, 09-02-12176-ofi_m.

1. T. Yu. Karminskaya and M. Yu. Kupriyanov, Pis'ma Zh. Eksp. Teor. Fiz. 85, 343 (2007) [JETP Lett. 85, 286 (2007)].

2. T. Yu. Karminskaya and M. Yu. Kupriyanov, Pis'ma Zh. Eksp. Teor. Fiz. 85, 343 (2007) [JETP Lett. 86, 61 (2007)].

3. T. Yu. Karminskaya, M. Yu. Kupriyanov, and A. A. Golubov, Pis'ma Zh.Eksp. Teor. Fiz. 87 657 (2008) [JETP Lett., 87, 570 (2008)].

Bi-SQUID with linear transfer function

V. Kornev[1] , I. Soloviev[1] , N. Klenov[1], O. Mukhanov[2]
1. *Moscow State University, Moscow 119991, Russia, kornev@phys.msu.ru.*
2. *HYPRES, 175 Clearbrook Road, Elmsford, NY 10523, USA*

.In case of conventional low-frequency SQUID systems, improved linearity and dynamic range are obtained using an external feedback loop with limited bandwidth. That is unfeasible in case one designs a SQUID-based system with very broad bandwidth. In this paper, we present the modified dc SQUID directly capable of providing highly linear voltage response. As for dynamic range, one can use a serial array of the SQUIDs to elevate it up to the value compared with the response linearity.

We modified conventional dc SQUID (see Fig. 1*a*) by the addition of a nonlinear inductive element shunting the linear inductance of the loop coupling RF magnetic flux into the SQUID. The nonlinear inductive element is a Josephson junction (see Fig. 1*b*) that remains in its superconductive state during operation. This nonlinear element modifies the nonlinear transfer function of the SQUID to produce higher linearity transfer function, thus increasing the utility of the device as a linear amplifier. The additional

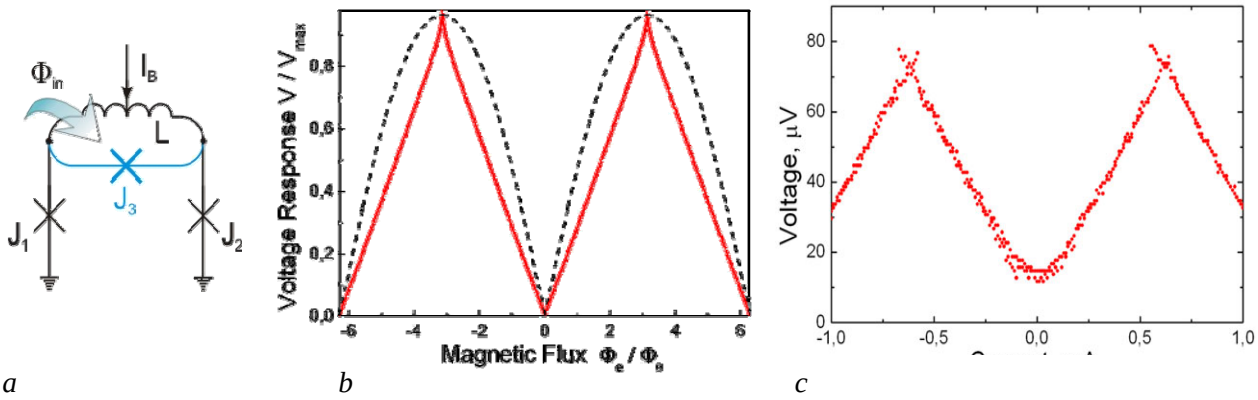

a *b* *c*

Fig. 1. *Bi-SQUID schematic (a); the calculated voltage response of conventional dc SQUID (dash line) and bi-SQUID (solid line) with normalized inductance l = 1 at bias current $I_b = 2I_c$ and $I_{c3} = 1.1\ I_c$ (b); experimental results for bi-SQUID with equal critical currents of all junctions and inductive parameter l = 1.4 (c).*

junction and main inductance form a single-junction SQUID. In such a way, the modified dc SQUID can be called as bi-SQUID. Such a bi-SQUID provides extremely high linearity for proper selection of critical current of shunt junction. This is somewhat surprising, since a Josephson junction is a nonlinear inductance. However, it seems that the junction nonlinearity can act to counter the nonlinearity of the device, to achieve an improved linearity of up to 120 dB for significant loop inductance.

We designed, fabricated and tested single bi-SQUID, serial arrays of bi-SQUIDs and a prototype of an active electrically small antenna based on bi-SQUID-array. The circuits were fabricated using a 4.5 kA/cm^2 Nb HYPRES process. The shunt junction critical current is not of the optimal value at the implemented inductance parameter. As a result, the observed voltage response is not perfectly linear, although it shows a clear triangular shape. The observed hysteretic peculiarities at tops of the voltage response reflect the fact that normalized inductance of one-junction SQUID exceeds 1. The obtained experimental data are in good correspondence with results of numerical simulation. The prototype of an active electrically small antenna based on serial array of 12 bi-SQUIDs was fabricated as well. Each bi-SQUID was equipped with a large superconducting loop to sense magnetic component *B* of an incident electromagnetic wave. To perform an initial test of such an antenna, a large-size strip coil was introduced in the fabricated chip to excite low-frequency magnetic field. The antenna voltage response is quite the same as the one observed for array of bi-SQUIDs with a control current strip line for magnetic flux application.

This work was supported in part by the ONR via CRDF Grant RUP1-1493-MO-05, and Russian Grants for Scientific Schools 5408.2008.2 and 133.2008.2.

Authors thank Mikhail Kupriyanov of MSU for fruitful discussions, Alex Kirichenko and Henrik Engseth of HYPRES for advice in design and testing.

Modeling of optical integrated circuit of a multiplexer/splitter on a basis of a photonic crystal structure

M.Belkin, K.Kostenko
Moscow State Technical University of Radio-Engineering, Electronics and Automation belkin@mirea.ru

Photonic crystal structured optical integrated circuits (OIC) are promising philosophy for the future generation of fiber-optic telecom systems equipment design. The major structural unit of the OICs two-dimensional photonic crystal (2DPhC) is allowed a newer opportunity to control the lightwave fluxes due to the availability of the band gaps in electromagnetic states density for a specified frequency range of the nearest IR range. Introduction of the distortions in the photonic crystal structure allows to create various devices, for example, waveguides, resonators, filters, splitters, etc. [1].

For example, removing a row of atoms in the crystal lattice, it can be done photonic crystal waveguide. After the ultra-short pulse advancing through the photonic crystal its spectrum has the band gaps that transparency is near zero. Incident plane wave emitting from usual optical waveguide of predefined width creates the spot of greater width on the interface of the photonic crystal waveguide. Changing the atom radius and the period of the photonic crystal lattice it can be affecting on the degrees of the electromagnetic field penetration in band gaps.

Basic element of the photonic crystal structured OIC is waveguide devices with a transmission matrix 1x2 (Y-junction), that can be used as a part of the multiport optical splitters/demultiplexers. One of the basic problem during a modeling of such devices is uniform radiating power distribution.

The method and results of the modeling of the Y-junction splitter using CrystalWave (Photon Design, Inc.) tool [2] are presented. As a result of simulation experience of waveguide splitters of the microwave range [3], it's necessary to introduce an additional linkage element in a place of flux splitting for the uniform distribution of the radiation and reducing of the insertion loss. The solution of this problem is ensured in the researching photonic crystal structure by adding a linkage element in a suburb of the splitting plane [4]. Changing its large and small ellipsis radius, it was selected form of the element (Fig.1). In the result, transmittance characteristics of the Y-junction splitter in the telecom range of 1,5…1,6 μm is presented depending on its sizes and displacement. Also transmittance characteristics of the mentioned above splitter depending on atom size and photonic crystal lattice are highlighted.

In the reverse direction this splitter acts as a part of the multiport multiplexer for an optical transmitting module of the fiber-optic wavelength-division multiplexed system. Research results for the optical parameters of the OIC in the multiplexing mode are specified.

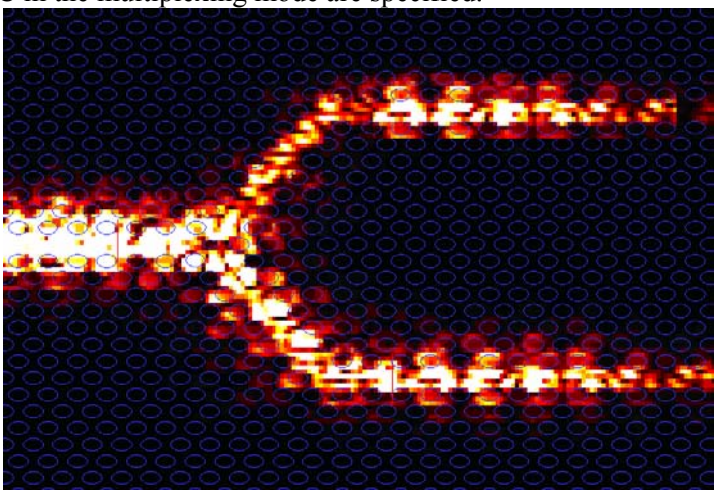

Fig.1

1. M.Bayindir , E.Ozbay, "Band-dropping via coupled photonic crystal waveguides", *Optics Express*, **10**, No.22, P.1279-1284, 2002
2. www.photond.com
3. J.L. Altman. *Microwave circuits*. D. Van Nostrand Company Inc., New York, 1964
4. S. G. Johnson and J. D. Joannopoulos. *Photonic Crystals: The Road from Theory to Practice*, Kluwer, 2002

Computer-aided design of the high-efficient laser module for microwave-band fiber optic systems

M. Belkin, A. Loparev
Moscow State Technical University of Radio-Engineering, Electronics and Automation. Moscow, Russia, e-mail: belkin@mirea.ru

As known, nowadays multichannel analog fiber-optical systems occupy in information-advanced countries the extensive niche in multiservice hybrid fiber-coax (HFC) networks. Other important direction of developing analog fiber-optical systems concerns with microwave-band radar systems where they can be effectively used in various paths of the multi-element phased array antennas. One more perspective area is the radio-over-fiber (RoF) systems that have been actively investigated recently.

For realization of the above-state systems laser modules in which effective electro-optical conversion on the modulation frequencies in microwave band is carried out are required. The general speed of the most widespread laser module with so-called direct modulation at the expense of an injection current control is equally defined not only by the technological features of a laser chip, but its construction, and also by a design of electrical input of the laser module in which the given chip is established.

The reasons for it within microwave modulation range are the parasitic electrical effects arising due to influence of a design of electric inputs of a laser chip and assembly elements demanded for its connection to the output of a modulating signal [1].

The basic disadvantages of a traditional design of a laser chip and its electrical node are the essential restriction of modulation bandwidth because of influence of the input node's parasitic elements: inductance of the connecting wires and insulator capacitance. Confirming to it on Fig. 1 the results of small-signal modulation performance modeling of a laser chip with the own modulation bandwidth of 11 GHz (squares) are presented. On the figure modulation performance of a laser module based on the same laser chip due to its connection to a microstrip line by means of two gold wires and pyroceramic insulator is shown also (triangles). As appears from the figure, use of such approach to the input leads construction results in approximately twofold reduction of a modulation bandwidth.

One of the realistic decisions of the highlighted problem consists in using laser chip with a unilateral arrangement of the leads and the electrical inputs construction on the basis of coplanar waveguide. In the module the laser crystal is mounted on the coplanar waveguide's termination by the flip chip technique. The technical result lies in expansion of modulation bandwidth of a semiconductor laser module with microwave modulation band at the expense of an exception of the above parasitic electrical effects influence. For increasing the overall electro-optical conversion efficiency of the laser module it is necessary to carry out the matching of impedances of a signal source (usually, active 50 Ohm) and a laser chip (usually, complex) in all modulation band of the fiber-optical system.

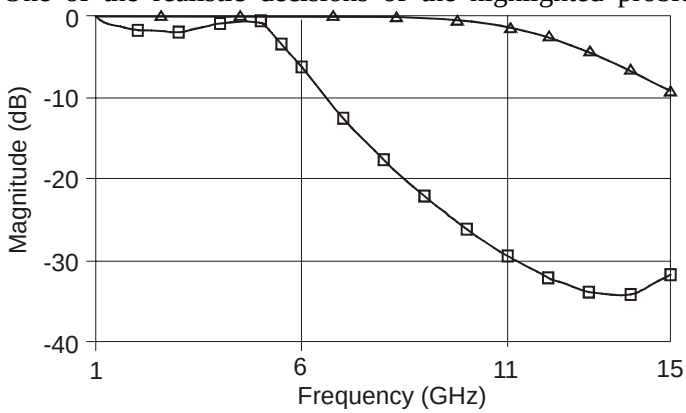

Figure 1. Modeling the laser's frequency-modulation characteristic

In the paper following the above described decisions the results of computer-aided design of the laser module's hybrid IC for an analog fiber-optical system with an operating range from 9.75 to 10.25 GHz, are highlighted. Our estimation has shown that the use of the offered technique allows to expand the highest frequency of the direct current modulation by 30-40% and to increase the efficiency of the electro-optical conversion by 10-12 dB.

References:

1. *Semiconductor Injection Lasers / In book: Semiconductors and semimetals. Vol. 22. Lightwave Communications Technology. / Ed. by* W.T.Tsang. - New York: Academic press. 1985. – 250 pp.

Numerical methods for calculation of optical properties of layered structures

S.A. Dyakov[1,4], V.A. Tolmachev[1,2], E.V. Astrova[2], S.G. Tikhodeev[3], V.Y.Timoshenko[4], T.S. Perova[1]

1. Trinity College Dublin, Dublin 2, Ireland. 2. Ioffe Physical Technical Institute, RAS, St. Petersburg, 194021, Russia 3. General Physics Institute, RAS, Vavilova 38, Moscow 119991, Russia. 4. Faculty of Physics, Moscow University, Leninskie Gory 1, 119991 Moscow, Russia. perovat@tcd.ie

The evaluation of propagation of the electromagnetic waves through the layered media is the task which is important for many areas of physics and engineering. A periodical Si-Air structures, served as one-dimensional photonic crystals (1D PC), were investigated in this work.

Grooved silicon structures were fabricated by photo-electro chemical etching of <100> Si. Samples consist of five silicon walls of 3.3 μm width. Period of the structure was 7 μm. Optical properties of the grooved structures were measured at normal incidence of light of different polarizations with a Digilab FTS-60A Fourier spectrometer in conjunction with UMA-500 IR microscope in the spectral range of 450–6000 cm^{-1}.

The well known 2x2 transfer matrix method, proposed by Abeles [1], can be used for simulation of light propagation through the layered media and for calculation of the reflection and the transmission coefficients at a given angle of incidence. However, in our experimental set up the cone-like shape of the light beam was used. The reflection and transmission coefficients of grooved silicon depend strongly on the angle of incidence. Thus, some disagreement between experimental and theoretical results is expected (Fig.1, left). In order to take into account the cone-like shape of incident light we propose integrating the reflection and transmission coefficients over the range of incident angles from 5° to 30°. We named this approach as a modified 2x2 transfer matrix method. As follows from Fig. 1 (right) the modified 2x2 matrix method demonstrates much better agreement with experimental spectrum for one of the investigated structure.

We note that in spite of it universality, the 2x2 transfer matrix method is not applicable to the thick layers and to the anisotropic media. In order to deal with these applications some other approaches can be used. The S-matrix method was pioneered by Ko and Inkson [2] for simulation of structures with thick layers. The 4x4 transfer matrix method is the generalization of 2x2 matrix method. The later can be used in the case of anisotropic components of the layered structure [3].

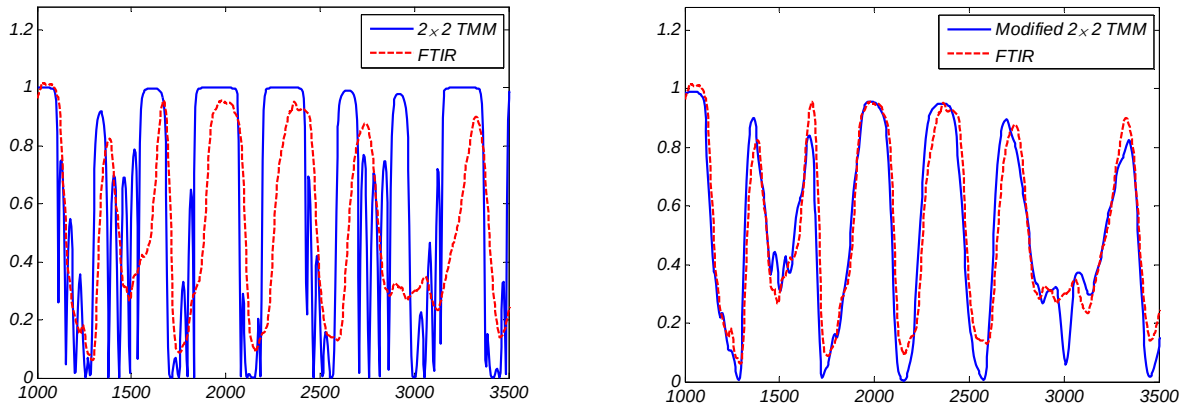

Fig.1 Reflectance spectra simulated by 2x2 transfer matrix method (left) and modified transfer matrix method (fight) as well as measured by FTIR.

1. R.M.A. Azzam, N.M. Bashara. *Ellipsometry and Polarized Light*. North-Holland Personal Libriary, 1987, pp.332-338.
2. D.Y.K. Ko and J.C. Inkson. "Matrix Method For Tunneling in Heterostructures: Resonant Tunneling in Multilayer System", Phys. Rev. B., 38, pp. 9945-9951, 1988
3. A. Yariv and P. Yeh. *Optical Waves in Crystals*, Wiley, New York, 1984

Vertical double range photocell with polysilicon photodiode, volume resonator and a photoelement with isotype potential p+ barrier in the substrate for UV application

I.V. Vanyushin[1], V.A. Gergel[2], N.M. Gorshkova[2], A.G. Klimkovich[1]

1. LCC "SensorIC", Moscow, Russia.

2. Kotel`nikov Institute of Radio Engineering and Electronics, Russian Academy of Sciences, Moscow, Russia, E-mail address: natali_gorshkova@bkl.ru

Integral silicon optical sensors, which have became a characteristic feature of the contemporary CMOS technology, are the point of interest in various fields of specific applications, such as cameras for machinery vision, technical, fire-alarm and security systems. The simplicity of integration of photo (image) sensor and signal processing circuits in a single chip provides a lower cost of the ultimate device, lower power consumption, and leads to a creation of single-chip cameras, which detect optical radiation in the whole spectral range, provided by silicon material possibilities.

For machinery vision systems (which are used, for example, in micro- and nano-technology fabs), and for fire-alarm notification systems it is necessary to detect a radiation (or take an image) in ultraviolet (UV) range. In the case of fire-alarm systems it is very important to reject parasitic spectral components of input radiation, for example, in the visible range, and usually such rejection is being achieved with the use of external optical band-stop filters. Such filters have limited throughput performance and, thus, give lower sensor gain. That's why in developing of an integral UV sensor it is more perspective to form the spectral sensibility needed directly on the sensor's chip. The most interesting photo sensors of this type are those, which use the well known spectral dispersion of light absorption by depth in silicon for a specific spectral range selection. This allows to convert almost all incident radiation to electric signal. One of the most effective structures here is a photocell, where potential barriers for minority carriers are used [1], because its selectiveness, contrary to vertical p-n junctions stack, much higher due to a rejection of unnecessary diffusion photo-current components generated by longer wavelengths. Spectral selectivity adjustment can be performed here by a simple boron implantation into a desired depth. For visible and infrared (IR) silicon applications (wavelengths are from 380 nm to ~1200 nm) the fabrication technology of such sensors is rather simple — achievable depths values in a standard CMOS tech process for appropriate potential barriers are just about photon absorption depths (~0.35 ...~2.5 um) for this spectrum range. As for UV application, ultra-shallow barriers about 0.3 um should be used, and significant modifications of CMOS tech process are needed. Another way is the well known polysilicon lateral photodiode placed on an insulator, when the active area thickness is about ~0.1...0.3 um.

Thin-film polysilicon photodiodes, placed above a silicon wafer and separated from the wafer by an insulator, are known as «cavity resonant photodiodes». By means of the polysilicon and insulator film thicknesses variation the spectral sensitivity of the photodiode can be varied and sometimes optimized for higher quantum efficiency and better gain slope on some wavelengths. One of the main problems for such "two-films" structure is a parasitic sensitivity with additional interference maxima in the long wavelength range (more than 420 nm), caused by photon absorption properties of silicon (polysilicon) and interference properties of the thin film structure, and additional optical filters should be used here.

Rejection of unneeded photo-electrical signal for wavelengths >380 nm in the cavity resonant photodiode can be significantly improved by implementation of a photocell with a potential barrier in a silicon wafer under the polysilicon photodiode. The whole structure can be considered as a vertical (with respect to the wafer) differential two-band photocell, whose structure includes two photoelements — one for UV range and another for visible; the sensitivity in UV range is provided by the thickness of the polysilicon photodiode, gain slope and cut effectiveness adjusted by optical thicknesses of polysilicon and insulator (SiO_2), and rejection of a signal generated by visible and IR radiations is performed by weighted subtracting of a photocurrent from the photocell with a potential barrier. As an example, band-sensitive UV photocell was simulated. It provides sensitivity in UV range <400 nm, rejection of signals detected in visible and IR ranges (>400 nm), and can be realized in a standard CMOS tech flow.

1. Gergel' V.A., Vanyushin I.V., Tishin Yu.I., Zimoglyad V.A., "Adjusting the Spectral Response of Silicon Photodiodes by Additional Dopant Implantation", Russian Microelectronics, vol. 34 (3), pp. 155–159, 2005

Formation of One-Dimensional Photonic Crystals by Means of Photo-Electrochemical Etching of Silicon

Yu.A. Zharova[1], G.V. Fedulova[1], E.V. Astrova[1], V.A. Ermakov[2] and T.S. Perova[2]
1.Ioffe Physical Technical Institute, Russian Academy of Sciences, St.Petersburg, Russia,
E-mai address: piliouguina@mail.ioffe.ru, GalyaFedulova@mail.ioffe.ru, east@mail.ioffe.ru
2. Department of Electronic and Electrical Engineering, University of Dublin, Trinity College, Ireland,
E-mail address: ermakov@tcd.ie, perovat@tcd.ie

Elements for integrated optics are based on structures designed for in-plane light propagation. One of the promising techniques to fabricate one-dimensional photonic crystals (1D PC) for photonic integrated circuits is photo-electrochemical etching (PECE) of (100)-oriented n-Si. The technique was first developed for manufacturing of regular two-dimensional (2D) arrays of macropores [1]. Recently it has been extended further for fabrication of deep wall arrays initiated by linear seeds on the surface [2]. Under the certain conditions macropores, aligned along the seeds [3], can merge and form a 1D periodic structure (Fig.1). Dependence of the trench formation on current density and period of seeds was investigated for Si substrates of different resistivity. Based on these investigations the design rules for formation of a 1D wall array were formulated [4]. The characteristic feature of 1D arrays fabricated by PECE is the corrugated structure of the silicon side-walls, which retain traces of the macro-pores (Fig.2). It has been shown that the wall roughness has a substantial impact on the optical properties of PCs [5, 6]. There are two major reasons for the wall corrugation: 1) incomplete macropore merging and 2) twinning effect [4]. The wall irregularities were investigated by the atomic force microscopy (AFM). Figure 3 shows the dependence of the height of the wall relief on the reduced current density j/j_{PS}, where j_{PS} is the critical current density corresponding to the transition from pore formation mode to electropolishing. The experimental results on additional smoothing of the side-walls using chemical etching of the 1D PC structures in alkaline solutions and under high temperature oxidation are presented.

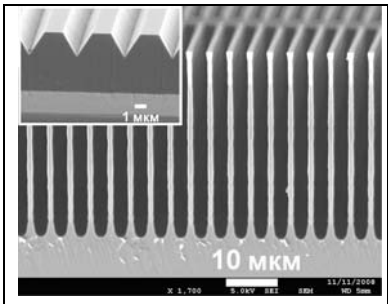

Fig.1 Cross-section SEM image of a 1D PC fabricated by PECE. Inset shows linear V–shaped seeds on the surface

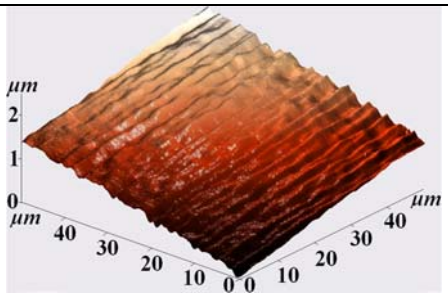

Fig. 2 AFM image of a Si wall relief

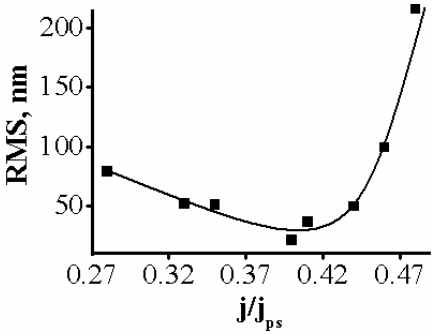

Fig.3 Root mean square (RMS) of the wall irregularities as a function of reduced current density j/j_{PS} found for the structure with period 9 μm on Si of 15 Ohm.cm resistivity

1. V. Lehmann and H. Foll. “Formation mechanism and properties of electrochemically etched trenches in n-type silicon”, J. Electrochem. Soc., **137**, pp.653-659, 1990
2. G. Barillaro at al., “Dimensional Constraints on High Aspect Ratio Silicon Microstructures Fabricated by HF Photoelectrochemical Etching”, J. Electrochem. Soc., **149**, pp.180-185, 2002
3. E.V. Astrova at al., “Photo-electrochemical etching of macro-pores in silicon with grooves as etch seeds”, Phys. Stat. Sol.(a), **206**, pp.1235-1239, 2009
4. E.V. Astrova and G.V. Fedulova. “Formation of deep periodic trenches in photo-electrochemical etching of n-type silicon”, J. Micromech. Microeng., **19**, 2009, http://stacks.iop.org/JMM/19/000000
5. E.V. Astrova, at al., “One-dimensional photonic crystals fabricated by photo-electrochemical etching of silicon”, Bulletin of the Russian Academy of Sciences. Physics, to be published
6. E.V. Astrova, at al., “Silicon periodic structures and their liquid crystal composites”, Solid State Phenomena, **156-158**, pp.547-554, 2010, http://www.scientific.net

Titanium dioxide with carbon nanotubes nanocomposite for new generation solar cells

A. Dronov , S. Gavrilov
Moscow Institute of Electronic Technologies (Technical University), E-mail:noiz@mail.ru

Storage, manufacture and energy transformation are one of mainstreams of development of a science and technics in which considerable economic benefit of nanotechnology introduction is expected. It becomes real if conditions of mass production and wide availability of the developed technologies are provided. Creation on a basis nanocristaline titania of photo-electric converters is an introduction vivid example of nanotechnology workings out in manufacture of solar cells. Such solar batteries made on flexible substrates, at the expense of the low cost price of manufacture and unique mass and overall characteristics can become a basis for creation portable charging devices.

The present work is devoted development of the concept of solar cells with an extremely thin absorption layer (SCETAL) which are a link between second and a third generation of photo-electric converters.

SCETAL is including pellucid emulsion substrate with a conducting coating, nanostructured electron acceptor in the capacity of which acts TiO_2, extremely thin absorbing layer and acceptor of holes. Sampling of substances for such structure is carried out on the underplate energy band diagram of the multilayered heterostructure containing the built in electric field which provides separation photooscillated electrons and holes.

It is known, that efficiency of real solar cells (SC) depends on recombination on boundary lines of transitions, and also consecutive and bypassing resistance of an element.

During early researches it has been find out that, the basic contribution to consecutive resistance brings in TiO_2 layer.

On decrease in consecutive resistance in an electron acceptor layer addition of leading corpuscles in gained layers titanium oxide can serve one of solutions. It was offered to use in the capacity of a substance for decrease in consecutive resistance leading carbon nanotubes. Having the drawn down structure which allows them to form the connected structures on all thickness of a layer, even at the small concentration, the given substance is capable to lower considerably consecutive resistance of titanium oxide layer, practically not influencing on structure optical transmission.

Physicotechnological bases of forming and research nanocomposite TiO_2 / carbon nanotubes (CNT) acting in a role of electron acceptor with SCETAL have been in-process offered, and also the basic functional characteristics of gained arrangements are investigated.

Sedimentation TiO_2 led a method of controllable plunging of vertically positioned in solutions isopropoxide of titan in isopropanol with addition in a solution carbon nanotubes in various concentration. Vibrationless pluging was carried by the automated complex for "layer by layer" forming films by a plunging method.

During researches voltage-current characteristics of solar cells was made on the basis of produced nanocomposite, and also optical transmission spectra of nanocomposites with various concentration carbon nanotubes have been gained.

From the gained data we see, that at low concentrations of CNT in TiO_2 layer the efficiency of the solar cell increases. However at the further increase of carbon nanotubes concentration decreasing efficiency that speaks about electrical breakdown in an electron acceptor layer since the carbon conducting material joints the gained heterogeneous junction on surfaces of layer TiO_2 and bottom contact electrode of SC is observed. In our opinion it occurs owing to decomposition of the spirit which is in carbon nanotubes when annealing the nanocomposite. As at dissolvent decomposition in CNT it is destroying titanium oxide who environs it.

Thus, researches have shown, that at increase in quantity carbon nanotubes in a solution, consecutive resistance of semi-conductor layer TiO_2 decreased, that has allowed to increase efficiency of the given solar cells. Also it has been find out, that high concentration of nanotubes leads to a structure electrical breakdown. On the basis of research of spectra of optical transmission it has been revealed, that addition of carbon nanotubes does not influence optical penetrability of a layer of nanocomposites.

1. S. A. Gavrilov, A. A. Dronov, et. al. , “Ways to Increase the Efficiency of Solar Cells with Extremely Thin Absorption Layers”, J. Nanotechnologies in Russia, vol.4, no. 3, pp.237-243, 2009

Application of linear-chain carbon nano-films in optoelectronic devices

M.B. Guseva*, P.B. Konstantinov**, Y.A. Kontsevoy**, N.N. Novikov*, A.S. Skrileov**, V.V. Khvostov*, V.V. Chernokozhin**

** - Physical faculty of Lomonosov Moscow State University Moscow, Russia, ** - FSUE "Science and Production Enterprise "Pulsar" Moscow, Russia, pulsar@dol.ru*

Linear-chain carbon films (LCC films) are new materials of nanoelectronics and they posses a set of unique properties: anisotropy of conductivity, high value of free path length of electrons in the films, a possibility to multiply the amount of electrons, coming from the film during the absorption of high energy electrons.

LCC films are made in plasma discharge in the pulse mode. The whole process is organized in such a way that almost all energy of the pulse discharge is being transformed in kinetic energy of ions; it means that the operating mode of Laval nozzle that is widely used in jet-motors is being actualized. On the basis of C_2^+ ions energy one can calculate the speed of ion's transmission. It's about 7-10 km/sec. With such parameters of pulse discharge carbon molecular beam turns into linear-chains already within the supersonic stream of carbon ions. So the pulse mode discharge corresponds to the conditions when the carbon linear-chains –C≡C-C≡C–C≡C- are being formed in the supersonic stream of carbon molecules, that are stable even at 4000˚C, while all the molecules with graphite and diamond bonds are being totally destroyed as their bonding energy is much lower. Carbon ions charge neutralization on the condensate is being processed with the help of "cold" plasma electrons and that lets remove the charge of substrate surface and not use additional accelerant potential for the carbon ions on the surface. During one impulse a 4-5 Å film is being evaporated.

Raman spectroscopy of the films indicated the peak in the region of 2100 cm^{-1}, which definitely characterizes linear sp^1-bonds. Scanning tunneling microscopy indicated tunneling transparence of LCC films. It means that an LCC film consists of nonoverlapping high conductive chains.

There were held researches connected with the conductivity of LCC films along and across the chains. Conductivity for the current across the chains was investigated using contact microstructure on the dielectric substrate. Lateral film resistance with thickness of 10 nm and more is about 10^{10} Ohm/square. When decreasing the thickness up to 1 nm the resistance increases up to 10^{14} Ohm/square. With that transverse film resistivity is some ranks lower than lateral resistivity. That gives an opportunity to use films as resistive layers in vacuum optoelectronic devices based on internal photoelectric effect (transmitting TV tubes) and photoelectric emission (electron-optical image intensifier).

Usually the resistive layers that are meant to decrease the accumulation electrode surface charging by the electrons of a scanning spot, are made of antimony triselenide films and cadmium compounds. It's really hard to manipulate the resistivity level of these layers. Moreover this kind of layers can partially vaporize during the technological warming. Application of LCC films enables to eliminate totally the surface charging without missing the resolution ability.

The CCD matrix with interline transfer for electron-optical image intensifier with the mesh size10x10 um^2 was used as an experimental model of suggested construction [1]. The film evaporated on the matrix surface had the lateral resistivity of $3 \cdot 10^8$ Ohm·cm and the transverse resistivity of $2 \cdot 10^3$ Ohm·cm. That helped us to exclude totally the parasitic coupling among matrix elements and to realize "leaking off" of the electron charge into the meshes.

1. Positive solution d/d 17.02.2009 on application for an invention #2007134969 d/d 20.09.2007

Critical temperature of SF and SFS multilayres with arbitrary electron mean free path in F and S films.

M.Yu. Kupriyanov[1], A.I. Buzdin[1], A.A. Golubov[2]

[1] *Nuclear Physics Institute, Moscow State University, 119992 Moscow, Russia.*

[2] *Centre de Physique Moleculaire Optique et Hertzienne, Universite Bordeaux 1-UMR 5798, CNRS, F-33405 Talence Cedex, France.*

[3] *Faculty of Science and Technology and MESA+ Institute of Nanotechnology, University of Twente, P.O. Box 217, 7500 AE Enschede, The Netherlands.*

In the last few years there is a considerable interest to the structures composed from superconducting (S) and ferromagnetic (F) interlayers [1-3]. Among the most important results achieved in this field there were the experimental evidence of so-called reentrance behavior of superconductivity in SF bilayers [4,5], as well as the observations of non-monotonic dependence of critical temperature of SF and FSF structures upon a thickness of ferromagnetic layers (see, e.g. [6]). The problem of theoretical calculations of critical temperature of SF and FSF structures has been also intensively analyzed (see e.g. [7-14]). Most of calculations had been done in a dirty limit and only in a few publications the clean limit had been also studied [9-12].

Up to now there was no calculation of T_C for SF bilayer and SFS trilayer under arbitrary mean free path in both S and F films. In this work we will attack this problem by developing a method, which has permitted to transfer the problem of T_C evaluation from solution of integro-differential Eilenberger equations in both S and F films to sufficiently more simple integral equation for a parameter $B(\theta)$. This parameter is a function of the angle θ between SF interface normal and the direction of Fermy velocity v_f in F metal and relates via boundary conditions the Eilenberger functions in F and S materials at SF interface.

Two types of SF interfaces have been considered. They are the interfaces having small transparencies or them, which are transparent and smooth in an atomic scale and connected the metals having essentially different Fermy velocities, $v_s >> v_f$.

The work is supported by RFBR grants 08-02-90105-Mol_a, 08-02-90012-Bel_a.

1. A. A. Golubov, M. Yu. Kupriyanov, and E. Il'ichev, Rev. Mod. Phys. 76, 411 (2004).
2. A. I. Buzdin, Rev. Mod. Phys. 77, 935 (2005).
3. F. S. Bergeret, A. F. Volkov, K. B. Efetov, Rev. Mod. Phys. 77, 1321 (2005).
4. V. Zdravkov, A. Sidorenko, G. Obermeier, S. Gsell, M. Schreck, C. Muller, S. Horn, R. Tidecks, and L. R. Tagirov, Phys. Rev. Lett. 97, 057004 (2006).
5. A. S. Sidorenko, V. I. Zdravkov, J. Kehrle et all, Pis'ma Zh. Eksp. Teor. Fiz. 90, N2 (2009).
6. I. A. Garifullin, D. A. Tikhonov, N. N. Garif'yanov et all, Physical Review B 70 054505 (2004).
7. B. P. Vodopyanov, L. R. Tagirov, Pis'ma Zh. Eksp. Teor. Fiz. 78 555 (2003).
8. Ya. V. Fominov, N. M. Chtchelkatchev, and A. A. Golubov, Physical Review B 66 014507 (2002)
9. M. Zareyan, W. Belzig, and Yu. V. Nazarov, Physical Review B 65 184505 (2002).
10. F. S. Bergeret, A. F. Volkov, and K. B. Efetov, Phys. Rev.B 64, 134506 (2001).
11. F. S. Bergeret, A. F. Volkov, and K. B. Efetov, Physical Review B 65 134505 (2002).
12. Zareyan1 : M. Zareyan, W. Belzig, and Yu. V. Nazarov, Physical Review Letters 86 308 (2001).
13. Ya. V. Fominov, N. M. Chtchelkatchev, A. A. Golubov, JETP Lett. 74 96 (2001).
14. M. Faure, A. I. Buzdin, A. A. Golubov, and M. Yu. Kupriyanov, Physical Review B 73 064505 (2006).

Experimental study of differential SQIF-structures

V. Kornev[1] , I. Soloviev[1] , N. Klenov[1], O. Mukhanov[2]

1. *Moscow State University, Moscow 119991, Russia, kornev@phys.msu.ru.*
2. *HYPRES, 175 Clearbrook Road, Elmsford, NY 10523, USA*

In conventional low-frequency SQUID systems, improved linearity and dynamic range are obtained using an external feedback loop with limited bandwidth. That is impractical in case one designs SQUID-based systems with very broad bandwidth. There are good reasons to associate the problem solution with Josephson-junction array structures. It is expected that the multi-element systems should provide the increase in dynamic range with number of elements N as well as highly linear voltage response due to special design technique [1]. We analyzed both the key parameters and the design issues for the multi-element Josephson structures capable of providing both the high dynamic range and the highly linear voltage response. As a consequence of the analysis, we proposed Josephson-junction structures capable of providing a SQIF-like highly linear voltage response (see Fig.1). The structures are based on the use of a differential scheme (see Fig.2) of two magnetically frustrated parallel SQIFs with special distribution of the cell areas $a(x)$ along the array. We found the particular distribution $a(a)$ which allows providing response linearity up to 100 dB (see Fig. 1). One should note that finite (non-zero) value of coupling inductances l between Josephson junctions in parallel array (and SQIF) is of fundamental importance for all principal characteristics of the array, since it imposes limitations on coupling radius - an effective number N_{eff} of the junctions which take part in the voltage response formation. The limited coupling radius value also stops increase in dynamic range when number of junctions becomes exceeding coupling radius. To study the frequency-dependent coupling radius, we performed numerical simulation of the parallel Josephson-junction array in the presence of thermal fluctuations. The obtained results were used at elaboration of the reported SQIF-based circuits.

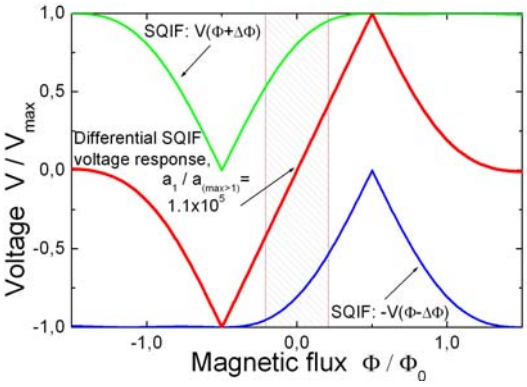

Fig. 1. *Voltage response of differential scheme of two SQIFs with the found area distribution.*

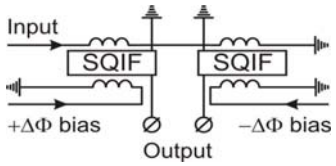

Fig. 2. *Differential scheme.*

We designed and fabricated two-dimensional structure which is differential circuit of two magnetically frustrated serial arrays of 10 parallel SQIFs each containing 10 Josephson junctions. Low-ohmic resistors shunting coupling inductances were used to increase the mentioned above effective number N_{eff}.up to about 10. Fig. 3 shows the experimentally observed voltage response which fully fits with the one obtained by numerical simulation for the corresponding parameters.

Fabrication of the serial arrays using standard niobium technology with two superconducting ground planes is accompanied by the substantially high stray capacitances. In order to decrease the stray capacitance impact, one can use individual double ground planes for each SQIF forming either separate double ground planes or overlapped double ground plane sections. The experimentally observed IV curve of the array with the separate double ground planes shows full agreement with the one calculated in the absence of stray capacitances.

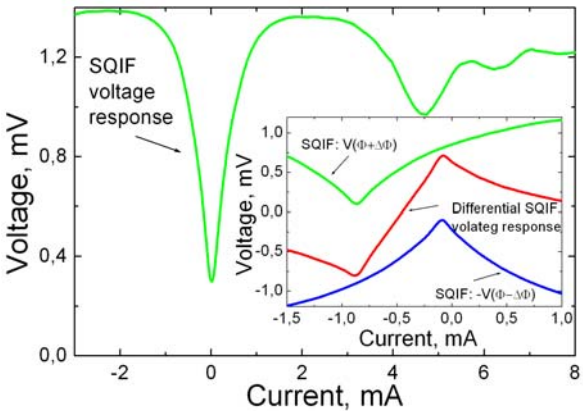

Fig. 3. *The experimentally observed SQIF voltage response. Inset shows voltage response of the differential scheme of two frustrated SQIFs.*

REFERENCES

[1] V. K. Kornev, I. I. Soloviev, N. V. Klenov and O. A. Mukhanov, *IEEE/CSC&ESAS European Superconductivity News Forum (ESNF)*, No 6, # 2EPM03.

Quantum interferometers on multichain of josephson junctions

A. Karuzskiy[1], G. Kuleshova[2], A. Tshovrebov[1], L. Zherikhina[1],
1. Lebedev Physical Institute, Russian Academy of Science, Moscow 119991, Russia; e-mail: tshovrebov@rambler.ru,
2. Moscow Engineering Physics Institute (State University) , Moscow 115409, Russia

Multicontact (n=100÷10000) chains consecutively-connected of josephson junctions initially has been developed for creating of Volta standards. We suggest to use such chains in superconducting quantum interferometers (SQUIDs) substituting by them each individual josephson junctions into SQUID. The paradoxicality given suggestion consists in the fact that formally such substitution shall be to sensitivity reduction SQUIDa on magnetic flux. Really the phase difference on each sides of one josephson junction now will be to granulate on a part, applied to each of n junctions: $I = I_J \sin\Delta\varphi = I_J \sin\frac{2\pi\Phi}{\Phi_0} \Rightarrow I = I_J \sin\frac{\Delta\varphi}{n}\varphi = I_J \sin\frac{2\pi\Phi}{n\Phi_0}$. On the one hand it means the reduction in n the time of interferometer phase sensitivity $\Delta\varphi \Rightarrow \frac{1}{n}\Delta\varphi$, but on the other hand this is equal to growth in n the time of flux quantum $\Phi_0 \Rightarrow n\Phi_0$, where $\Phi_0 = \frac{\pi\hbar}{e} = 2{,}07\times10^{-15}\,Wb$. In two arms SQUID of direct current (DC-SQUID) n the multiple increase of quantum period will reduce in n the time the derivative $\frac{\partial I_{\max\Sigma}}{\partial\Phi}$ of interference dependence $I_{\max\Sigma} = 2I_J\cos\left(\frac{\pi\Phi}{n\Phi_0}\right)$. However, the derivative $\frac{\partial V}{\partial\Phi}$ of periodic voltage dependability $V=V(\Phi)$ registered by the DC-SQUID electronics in this case is not will decrease, because respectively in n the time will increase the total tunneling resistance of all consecutively-connected the josephson junctions. On similar reasons after replacement of single josephson junction by chains of junction resulting sensitivity of the RF-SQUID, working at periodic current, nor will fall. For interferometers of both types n multiple growth of quantum period will allow to meet condition $LI_J < n\Phi_0$ in case of large significances of inductance of superconducting circuit SQUID. In DC-SQUID (fig.1) this condition guarantees the uniqueness its operating characteristic. Significant in n the multiple growth L in DC-SQUID provides $\sqrt{n}$ the multiple growth of transmission factor of variation of magnetic flux, injected in SQUID by means of superconducting transformer (in case of n=1000 transmission factor is to grow by thirty times). For RF-SQUID (fig.2) the condition $LI_J < n\Phi_0/2\pi$ will allow to pass on the unhysteretic mode in case of technically more accessible inductance significances of SQUID operating coil, providing at the same time the high coefficient of stream transfer in coil. So in anhysteretic condition in RF-SQUID dissipation direct channel of energy is absent, this device will have nonzero noise temperature only in measure of the association with «external dissipative electronics». At the same time the resolution of this RF-SQUID on magnetic flux is estimated at the level of $\delta\Phi = 10^{-9}\,\Phi_0/\sqrt{Hz}$ [1,2].

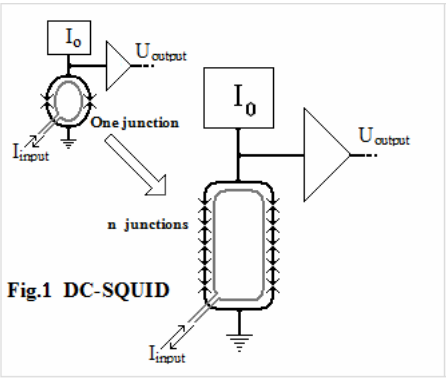

Fig.1 DC-SQUID

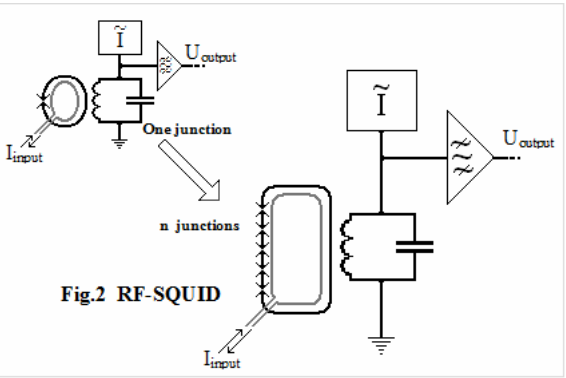

Fig.2 RF-SQUID

1. K. K. Likharev, B. T. Ulrikh. Systems with Josephson contacts. Moscow Univ. Press (1978).
2. A. I. Golovashkin, G. V. Kuleshova, A. M. Tskhovrebov, L. N. Zherikhina Proceedings FPS'08 (the 3d Int. Conf. «Fundamental Problem of HTSC»), pp. 292-293, Moscow/Zvenigorod (2008)

Propagation of magnetostatic surface waves in ferromagnetic films with variable thickness.

Ignatov Yu.A., Scheglov V.I., Klimov A.A., Nikitov S.A.
Kotel'nikov Institute of Radio Engineering and Electronics (IRE RAS), Moscow, yury.ignatov@gmail.com.

Magnetostatic surface waves (MSSW) propagating in symmetric ferromagnetic films with variable thickness are investigated. The external magnetic field was assumed to be tangential to the film surface, while the MSSW were propagating at a random angle to the symmetry plane. The dispersion characteristics of the magnetostatic surface waves were calculated using WKB approximation and the internal error of this method was estimated.

As a result of WKB approximation we have an imaginary component of the wave number. This term is defined by a geometric factor. The wave amplitude is increasing as the film becomes thinner. An arbitrary functional dependence of the thickness on the coordinate was considered as well as the linear dependence.

In addition, we have investigated the one-dimensional magnonic structure based on the film with variable thickness and found some motivating practical applications of them. The method of calculation was based on a model similar to the Kronig-Penney model. Some results of the theory are presented in Fig. 1 and Fig. 2.

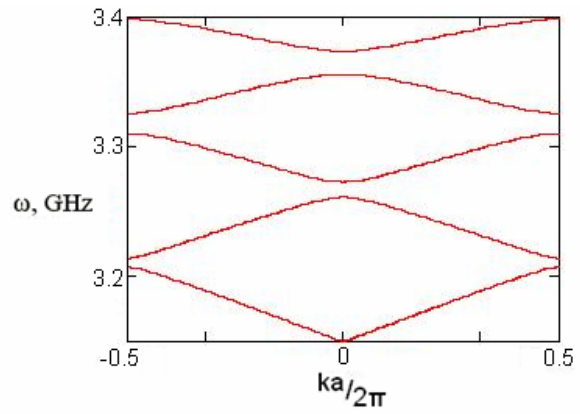

Fig. 1. Band-gap structure of MSSW in ferromagnetic film with the spatial periodic structure (period a = 10 μm).

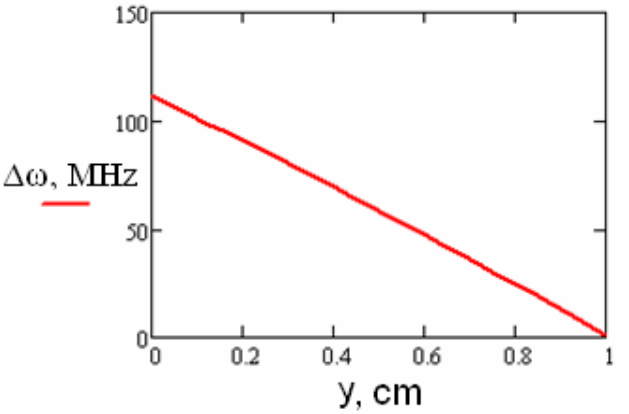

Fig. 2. Band-gap frequency dependence on the coordinate is decreasing as the thickness decreases (for the angular coefficient $\xi = 0.99$ cm^{-1}).

We have worked out an idea to build a comb filter and a narrow-band filter based on thin films with spatially variable thickness and the spatial periodic structure. As a result of thin film band-gap structures, the transmission properties of such filters were found to be dependent on the film length and the angle coefficient. Technical characteristics of few structures were estimated. The estimation was based on a model similar to the Beer-Lambert model in optics. There is a possibility to select a transmission bandwidth of 10 MHz for the structure with linearly decreasing thickness from 10 μm to 2 μm for the waves propagating in the structure of the length 1 cm.

This work was supported by RFBR Grant No. 08-02-00785-a.

[1] Yu. V. Gulyaev, S. A. Nikitov, L. V. Zhivotovskii et al., "Ferromagnetic films with magnon bandgap periodic structures: Magnon crystals", JETP Lett., **77**, 670, pp. 567-570, 2003.
[2] F. Villa and J. A. Gaspar-Armenta, "Photonic crystal to photonic crystal surface modes: narrow-bandpass filters", Opt. Express, **12**, pp. 2338-2355, 2004.
[3] J. D. Joannopoulos, S. G. Johnson, J. N. Winn, R. De Meade. *Photonic Crystals. Molding the flow of light. Second edition.* Princeton University Press, Princeton, 2008.

Modification of magnetic domain structures in Co film using the atomic force microscopy nano-oxidation

A. Bukharaev[1,2], D. Biziaev[1], P. Borodin[1], I. Merkutov[2]
1. Zavoisky Physical Technical Institute of Russian Academy of Sciences, Kazan, Russia, dbiziaev@inbox.ru
2. Kazan State University, Kazan, Russia, a_bukharaev@kfti.knc.ru

Lithography techniques based on local anodic oxidation of the ferromagnetic film by the tip of the atomic force microscope (AFM) allowed one to fabricate the planar-type Ni magnetoresistive structures [1].
In this report we present our first results AFM nano-oxidation of Co film 30 nm thick. The patterned microstructures were obtained by vacuum evaporation of Co through the mask with 25x25 μm^2 holes on the high oriented pyrolytic graphite substrate. Spreading resistance and magnetic force microscopy (MFM) imaging before and after AFM lithography were performed scanning probe microscope Solver P47 (NT-MDT). Fig.1a demonstrates the AFM image of a single microparticle after the local oxidation along the two crossed lines at 10 V bias between the AFM tip and sample. The corresponding spreading resistance image (fig.1b) confirms that the local oxidation along two crossed lines was performed. The width of Co oxide nanowires (white crossed lines in fig.1a and the black ones in fig.1b) was about 1μm in this case. Fig.1c and d demonstrate the MFM images of the same planar microparticle before and after the local oxidation. It is obvious that after the local oxidation along two crossed lines the initial microparticle was divided into four magnetic non-interacting fragments. The MFM images corresponding to these fragments are typical for the planar Co particles with such size and shape [2]. In our experiments the minimal Co oxide nanowire width 200 nm was reached.
Thus our results demonstrate that it is possible to create particles with the desired magnetization structure using the AFM nano-oxidation.

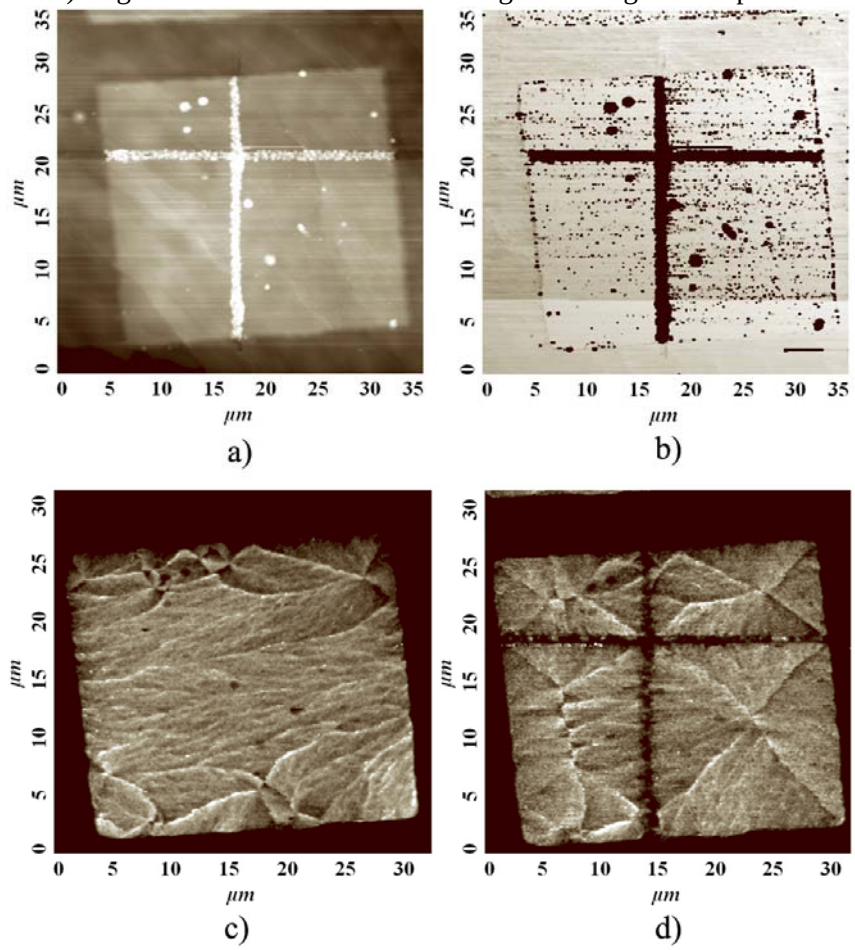

Fig.1. AFM (a), spreading resistance (b) and MFM (c,d) images before (c) and after (a,b,d) local oxidation.

This work was supported by the Russian Foundation of Basic Research (Grant 09-02-00568) and by the Programs of RAS.

[1] Y. Tomoda et al., "Planar-type ferromagnetic tunnel junctions fabricated by SPM local oxidation" JMMM, 310, pp. e641–e643, 2007
[2] S. Blomeier et al., "Micromagnetism and magnetization reversal of embedded ferromagnetic elements" Phys.Rev.B, 74, pp. 184405-1 – 184405-12, 2006

Investigations of magnetic states in multilayer submicron ferromagnetic particles

A.A.Fraerman, B.A.Gribkov, S.A.Gusev, A.Yu.Klimov, V.L.Mironov, V.V.Rogov, S.N.Vdovichev,
Institute for physics of microstructures RAS, Nizhny Novgorod, Russia, E-mail: bg@ipm.sci-nnov.ru

In this work we present our results in experimental investigations of the magnetic states within multilayer ferromagnetic submicron particles. This type of submicron structures attracts considerable attention because of its possible application as a magnetic storage and spintronic devices [2, 3]. Ordered arrays of submicron multilayer ferromagnetic particles were fabricated by means of electron lithography and ion etching process [1]. The distribution of remanent magnetization and investigations of remagnetization reversal process were performed using multimode scanning probe microscopes "Solver-HV" and “Solver PRO” (NT-MDT, Moscow, Russia).

Two configurations of magnetic states were observed in two-layer ferromagnetic elliptical particles (two uniformly magnetized layers of ferromagnetic material (Co), separated by nonmagnetic Si interlayer; dimensions of particles 400 × 250 nm): ferromagnetic - magnetization directions in Co layers oriented in the same direction along long axis of the particle; and antiferromagnetic - magnetization directions in Co layers oriented in the opposite directions. MFM tip induced remagnetization effects in these two-layer particles were investigated. Transitions between ferromagnetic and antiferromagnetic configuration and effects of reorientation in antiferromagnetic configuration of were observed.

For investigations of transport properties the special two-layer ferromagnetic submicron structures (CoFe ferromagnetic layers with tunnel TaO interlayer and surrounding metallic wires for current measurements) were fabricated. It was found, that resistance (current-flow was perpendicular to multilayer structure) of fabricated two-layer structures depends on external magnetic field. The value of TMR effect was about 3% at room temperature.

Distribution of magnetic states within tri-layer discs with diameter 300 nm was investigated. These tri-layer structures consisted of three ferromagnetic uniformly magnetised Co layers separated by nonmagnetic spacers. The spiral non-collinear magnetization distribution in tri-layer ferromagnetic discs was observed.

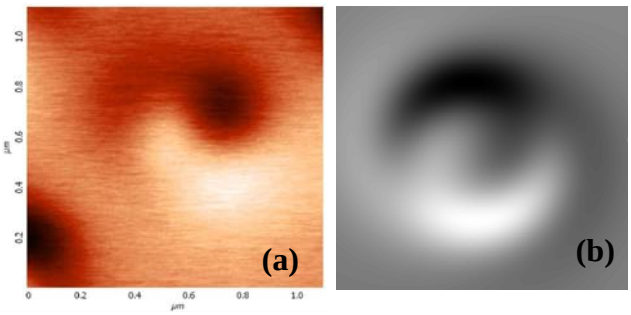

Experimental (a) and theoretically calculated (b) MFM images of spiral non-collinear distribution in tri-layer ferromagnetic submicron disc.

The realization of non-collinear states is not only of interest for basic investigations of nanomagnets, but they could also be used in spintronic devices [2, 3]. This work was partly supported by the RFBR.

1. A.A.Fraerman, S.A.Gusev, L.A.Mazo et al. Phys. Rev. B 65, p. 064424, 2002
2. S.S.Parkin, K.P.Roche, et. al. J. Appl. Phys. 85, p. 5828, 1999
3. I. Zutic, J. Fabian, et. al. Rev. of Mod. Phys. 76, pp. 323-410, 2004

Fe/MgO/Fe heterostructures on r-sapphire for single-crystal magnetic tunnel junctions

A. Chernykh, V. Vinnichenko, L. Fomin, and G. Mikhailov
Institute of Microelectronics Technology & High Purity Materials, Russian Academy of Sciences, 142432 Chernogolovka, Moscow Region, Russia, mikhailo@ipmt-hpm.ac.ru

The single-crystal Fe/MgO/Fe magnetic tunnel junctions (MTJ) are of great scientific and commercial interest due to both their giant magnetoresistance ratio (up to 180% at room temperature) and capabilities to study a coherent spin-dependent tunneling [1]. Basic requirement for fabrication of such junctions is growing initial heteroepitaxial Fe/MgO/Fe films with perfect crystalline structure layers and atomically flat interfaces. The great importance is in the choice of suitable for film growth substrates. At present, this multilayered films are growing on singlecrystalline MgO(001), Fe whiskers and GaAs(001) with MgO(001) underlayer [2] substrates. The aim of this work is growing the heteroepitaxial Fe/MgO/Fe films on r-plane sapphire substrates with MgO(001) underlayer, as well to optimize the growth conditions (mainly substrate temperature) for MgO and Fe films regarding the highest possible quality of tri-layered heterostructure Fe-MgO-Fe(001) within the experimental approach developed in this work.

Experiment. The Fe(001) and MgO(001) layers were grown by pulse laser deposition on r-plane of sapphire. Fe(001) layers were deposited on MgO(001) surface in vacuum of 10^{-7}-10^{-8} torr, MgO layers were synthesized on Fe(001) surface by the laser evaporating the metal Mg target in the presence of molecular oxygen at pressure of 2 mtorr. The growth process was performed at different substrate temperature in the range of 200-500^{o}C. The surface morphology and crystal orientation of the deposited layers were monitored by atomic-force microscopy and X-ray diffraction. The crystal structure quality and the interface smoothness of Fe layers were integrally characterized by the residual electron mean free path (MFP), which was found from electrical measurements through the residual resistances ratio (RRR = R(300K)/R(4.2K)). Residual MFP is very sensitive to the structure defects and the surface roughness of metal films [3] and allows regarding the film quality for their growth optimization. It depends quasi-linearly on the film thickness and in the perfect singlecrystalline thin Fe film exceeds its thickness.

Results. As for MgO(001) layers, 2D-growth was observed at 300 – 500°C. This allowed to grow thin 5-10 nm thick layers with surface roughness of 0,2 – 0,3 nm, that noticeably less than a tunnel thickness of MgO layer. As for Fe(001) layers, the surface roughness of 0,3 – 0,5 nm was found at growth temperatures 300-380°C. MFP exceeds Fe(001) layer thickness by a factor of 1.4 to 1.7.

The Fe(001)(60nm)/MgO(001)(5nm)/Fe(001)(10nm)/MgO(001)(10nm) layers were epitaxially deposed in series on r-plane sapphire in optimal growth conditions. X-ray diffraction and RRR measurements have confirmed a single-crystal growth and high quality of the grown heterostructural films.

Acknowledgement

The work was supported by the grant of Russian Academy of Sciences Division of Information technology and Nanotechnology.

1. S. Yuasa, T. Nagahama, A. Fukushima, Y. Suzuki1 and K. Ando, “Giant room-temperature magnetoresistance in single-crystal Fe/MgO/Fe magnetic tunnel junctions”, Nature materials, **3**, pp.868-871, 2004

2. C. M. Boubeta, J.L. Menendez, J.L. Costa-Kramer, J.M. Garcia, J.V. Anguita, B. Bescos, A. Cebollada, F. Briones, A.V. Chernykh, I.V. Malikov and G.M. Mikhailov, “Epitaxial metallic nanostructures on GaAs”, Surf. Science, 482-485, pp.910-915, 2001

3. G.M. Mikhailov, I.V. Malikov, A.V. Chernykh, “Novel Class of Low-Dimensional Metallic Structures, Characterized by Surface Dominated Electron Transport”, Phys., Low-Dim. Struct., **3/4**, pp.1-24, 1999

Epitaxial Fe_3O_4 films for spin valve applications

Malikov I.V., Mikhailov G.M.
Institute of Microelectronic Technology and High Purity Materials, Russian Academy of Sciences, Chernogolovka, Russia, *malikov@ipmt-hpm.ac.ru*

Half-metallic materials, such as CrO_2, $La_{0.7}Sr_{0.3}MnO_3$ (LSMO), and Fe_3O_4 are highly attractive for spintronics applications because of their high spin polarization. Among these materials, magnetite (Fe_3O_4) is superior to others because of its high Curie temperature (T_c) of 858 K, which is crucial for thermal stability in device applications. In addition, magnetite has proven to be a ferromagnetic material with a high spin polarization (ca. 100%) at the Fermi level, which results in a metallic minority spin channel and a semiconductor majority spin channel. Besides the utilization of spin electronics, magnetite can also be used in tunneling magnetoresistance (TMR), spin-transfer torque switching (STS) and giant magnetoresistive (GMR) devices.

Magnetite (Fe_3O_4) has the so-called cubic inverse spinel structure in which the Fe cations occupy interstices of a face-centered-cubic (fcc) close packed frame of oxygen ions (a=8.396Å). The eight tetrahedral (*A*) sites are solely occupied by Fe31, while the 16 octahedral (*B*) sites are equally shared by Fe31 and Fe21 ions. Rapid hopping of electrons between Fe21 and Fe31 ions in the *B* sites results in good room-temperature conductivity. Upon cooling, bulk Fe_3O_4 undergoes a metal–insulator transition (Verwey transition [1]) at a temperature T_V~120 K, where the electron hopping is frozen and the conductivity decreases by about two orders of magnitude.

Different deposition methods such as excimer laser ablation of Fe_3O_4 target prepared by a standard solid-state reaction method, and reactive MBE in oxygen at pressures 10^{-1}-10^{-6} Torr, temperatures 250-450^{o}C (including oxygen plasma assisted deposition) and growth rates about one monolayer per mimute were used for Fe_3O_4 films growth. Except polycrystalline magnetit films epitaxial Fe_3O_4 ones have been grown on various substrates including MgO (100), MgO (110), Al_2O_3 (0001), $MgAl_2O_4$, and $SrTiO_3$. A number of differences have been observed in the transport and magnetic properties of thin films as compared to bulk magnetite. In particular, the Verwey transition is broadened and shifted to lower temperatures in the case of the former (their T_V varied in the range of 65–155.5 K). This has been ascribed as the interaction between the film and the substrate, resulting in stress and rigid structural coupling of the film. Unfortunately, most of these films have exhibited anomalous or undesired magnetic properties. The anomalous behavior includes unsaturated magnetization at applied fields as large as 70 kOe as well as out-of-plane magnetic moments. These properties have been associated with structural defects.

Fe_3O_4 films are known to grow epitaxially on the Al_2O_3 (0001) substrate despite the lattice mismatch being of ~8%. Because of the large mismatch the films exhibit a columnar island formation during growth. MgO single crystal substrates provide an excellent template for the growth of epitaxial Fe_3O_4 films, owing to the small lattice mismatch between the film and the substrate (0.34%). The misfit (close to a factor of 2) between the cation sublattices tends to introduce film defects, such as antiphase boundaries (APBs). These defects form as a consequence of the difference in translational and rotational symmetries between the thin film and the substrate. The presence of APBs introduces local modifications of the structure and alters the magnetic interaction at the boundary, inducing an additional antiferromagnetic exchange. The effect of APBs can be observed both in transport and magnetic properties, with increases in resistivity and magnetoresistance and making the films hard to saturate even with strong fields of up to several tesla. Recently, it has been shown that the presence of APBs in Fe_3O_4 films can be manipulated to form anisotropic array, if vicinal substrates are used as the template.

Magnetit is epitaxially compatibal with iron. Our results on mutual epitaxial growth of Fe, Ni, Mo, W, and MgO on single crystal sapphire substrates are promising to use different epitaxial films combinations for spintronic applications. It is important that all these materials [2] including magnetit Fe_3O_4 may be coherently grown on GaAs(001) and Si(001) substrates, with regards of their practical applications.

1. Friedrich Walz, “The Verwey transition—a topical review“,J. Phys.: Condens. Matter **14** (2002) R285–R340.
2. C. M. Boubeta, J.L. Menendez, J.L. Costa-Kramer, J.M. Garcia, J.V. Anguita, B. Bescos, A. Cebollada, F. Briones, A.V. Chernykh, I.V. Malikov and G.M. Mikhailov, “Epitaxial metallic nanostructures on GaAs”, Surface Science 482-485 (2001) 910-915.

Investigation of domain wall pinning and nanostructures remagnetization of epitaxial Fe structures with use of magnetic force contrast and magnetoresistance measurements

G.M. Mikhailov, V.Yu. Vinnichenko, L.A. Fomin, K.M. Kalach, I.V. Malikov,
Institute of microelectronic technology and high purity materials RAS, Chernogolovka, Russia,
E-mail address fomin@ipmt-hpm.ac.ru

Electronic devices with magnetoresistive effects demand small reswitching fields (coercive forces, H_c) regarding their successful application. Coercive force of ferromagnets depends on many factors, in particular domain wall pinning by bulk and surface defects. Usually, domain wall pinning is investigated by dynamic methods with use of UHF techniques [1]. Nevertheless, these techniques do not allow to visualize a domain wall in an external magnetic field in a quasistatic regime, which is often of interest for functional devices. In this work, an effect of surface roughness on domain wall pinning in the regime of quasistatic remagnetization is investigated for epitaxial Fe structures.

For this investigation, we applied a magnetic force microscope (MFM) [2] developed on the base of P47 Solver NTMDT with options of external controllable magnetic field and electron transport measurements. The magnetic field source involves a water-cooled coil including a controllable current source. The magnetic field is supplied to the sample with the help of a magnetic core. The sample was placed in the gap of the cores. For precise monitoring of the magnetic field near the sample, a Hall sensor was used. Magnetic field is controlled by external signal generated by MFM. Electronic transport measurements of the sample were performed using a special holder with electric contacts allowing four-probe measurements. It was placed in the gap of the cores together with the sample. An electric signal from the sample was measured by lock-in system. The output electric signal from lock-in system was supplied into an input of MFM ADC and imaged by the controlling program of the device. In order to reduce an undesirable effect of atmospheric water on the sample and for electric screening of the device against electromagnetic noise an external metallic cover with an air drying system was made. To improve reliability of MFM contrast measurements, different magnetic coatings (Co, Fe, Ni, Fe-Ni, CoSm) for MFM probes were tested to optimize their sensitivity, resolution and magnetic properties in an external magnetic field..

During epitaxial Fe structures study, we found that domain wall pinning is small in the structures bulk, while majority pinning centers are due to surface roughness. This results in correlation between experimental data on a coercive force H_c, a roughness amplitude S_q and a roughness correlation length L_c. For the films grown at different conditions, we found a linear dependence H_c versus S_q^2 at small S_q, which comes to a saturation at large S_q. The linear dependence at small S_q was theoretically predicted [3] for ultrathin ferromagnetic films, also, the pinning mechanism investigated in cited work was differ from those found in our study. Saturation can be explained by the fact that at large S_q the film is already not perfect in the bulk and the pinning is also originated on bulk structural defects. The applied techniques on magnetic force contrast and magnetoresistance measurements complementary corroborate each other.

Acknowledgement

The work was supported by the grant of Russian Academy of Sciences Presidium on Nanotechnology.

1. V.V. Volkov, V.A. Bokov, “Domain wall dynamics in ferromagnets”, Phys. Sol. St., **50**, pp.199-228, 2008.
2. P. Grutter, H.J. Mamin, and D. Rugar, *Scanning Probe Microscopy II*, New York, Springer Verlag, 1991.
3. P. Bruno, G. Bayreuther, P. Beauvillain, C. Chappert, G. Lugert, D. Renard, J.P. Renard and J. Seiden, “Hysteresis properties of ultra thin ferromagnetic films”, J. App. Phys. **68** pp. 5759-5766, 1990.

Dependence of two-layer structures Cu/Co magnetoresistance on thickness of copper

V. Naumov
Yaroslavl Branch, Physicotechnological Institute, Russian Academy of Sciences, Yaroslavl, Russia, vvnau@rambler.ru

Two-layer structures Cu/Co have been made by magnetron method on Si substrates with thermal oxide thickness of 200 nm. During deposition the constant magnetic field (120 Oe) has been applied along a substrate surface for formation of the certain easy axis direction. Thickness of cobalt films for different series was 1,3 and 1,7 nm. In each series thickness of copper varied from zero up to several nanometers. The control of films thickness was carried out by profilometric measurement thicker cobalt and copper films (~ 40 nm) obtained in similar conditions. Investigated area was a rectangular 5x7 mm located between copper contacts deposited through a mask. Measurement of anisotropic magnetoresistance has been executed by a bridge method. Management of a constant external magnetic field was carried out by a source of a direct current manually. In all samples the electric current flew along an easy axis. The external magnetic field from -300 Oe up to 300 Oe was put along a surface of samples. Curves of longitudinal (a field along a current) and transversal (a field across a current) magnetoresistive effects were measured. The coercive force was defined from curves of longitudinal magnetoresistance. Relative change of transversal magnetoresistance of samples $\delta_S = \Delta R_S / R_S$ (MR ratio) was an object of research. If to assume, that layers of cobalt and copper represent parallel connection and copper does not possess magnetoresistive effect then MR ratio is expressed as

$$\delta_S = \frac{\Delta R_S}{R_S} = \frac{R_{MAX}}{R_{MIN}} - 1 = \frac{R_{Co} R_{Cu}}{(R_{Co} + R_{Cu})} \cdot \frac{(R_{Co} - \Delta R_{Co} + R_{Cu})}{(R_{Co} - \Delta R_{Co}) R_{Cu}} - 1 = \frac{R_{Cu} \Delta R_{Co}}{(R_{Co} + R_{Cu}) \cdot (R_{Co} - \Delta R_{Co})} . \quad (1)$$

From expression (1) we receive expression for $\delta_{Co} = \Delta R_{Co} / R_{Co}$ which should not depend on copper layer thickness

$$\delta_{Co} = \frac{\delta_S}{R_{Cu}/(R_{Co} + R_{Cu}) + \delta_S} , \quad R_{Cu} = \frac{R_{Co} R_S}{R_{Co} - R_S} . \quad (2)$$

In figure 1 dependences of δ_S, δ_{Co} and coercive forces of structures Cu/Co on thickness of a copper layer for two values of cobalt thickness are shown.

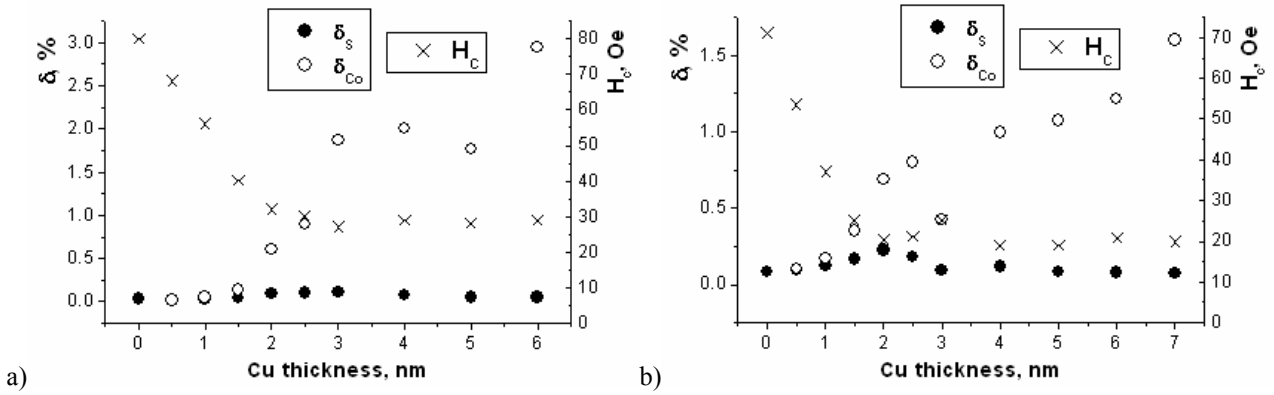

Fig. 1. Dependence of δ_S, δ_{Co} and coercive forces of Cu/Co structures on thickness of a copper layer.
a) Cobalt thickness 1.3 nm, b) cobalt thickness 1.7 nm.

It is visible, that δ_{Co} increases at increase in thickness of a copper layer though should remain constant. Besides coercive force Cu/Co structure with increase of thickness of copper decreases. The reasons of such behavior of Cu/Co structures will be discussed.

Study of size effect on switching characteristics of spinvalve GMR sensor

O.S. Trushin[1] , E.Yu. Buchin[1] , V.F. Bochkarev[1], N. Barabanova[2]
[1]*Yaroslavl Branch of the Institute of Physics and Technology of Russian Academy of Sciences, Yaroslavl, Russia, oleg_trushin@lenta.ru.*
[2].*Department of Physics, Yaroslavl State University, Yaroslavl, Russia*

Magnetic field sensors based on Giant Magnetic Resistivity(GMR) effect find wide range of applications in modern technology[1]. High sensitivity at low fields and low cost make these sensors very competitive at a market. The most popular design of these sensors based on spin-valve structures. Typical spin-valve structure consists of three thin film layers of magnetic and non-magnetic materials[2]. Very important problem in designing GMR sensors is the effect of size and shape of sensor element on its functional parameters.

In this work we present the results of experimental and theoretical study of size effect on switching characteristics of spin-valve structures. This is important problem for optimization of functional characteristics of magnetic field sensors on GMR effect. Standard spin-valve multilayer structures Py(5nm)/Cu(3nm)/Co(5nm)/Py(5nm)/SiO2/Si were grown by RF magnetron sputtering deposition. Sensor elements of rectangular shape with variable sizes were fabricated using ion sputtering lithography process. Sensor switching characteristics were acquired using home made computer controlled experimental set-up for measuring magnetoresistivity[3]. As the result the dependence of GMR response on device sizes was investigated. We find that decreasing of sensor element width with fixed length(increasing length/width aspect ratio) leads to increasing coercitivity of both magnetic layers (free and fixed). We also performed micromagnetic modeling using OOMMF code[4] of these sensor elements to verify experimental findings. The results showed similar trend for increasing coercitivity with reducing sensor width. This is due to increase of magnetostatic contribution to the total energy because of shape anisotropy[5].

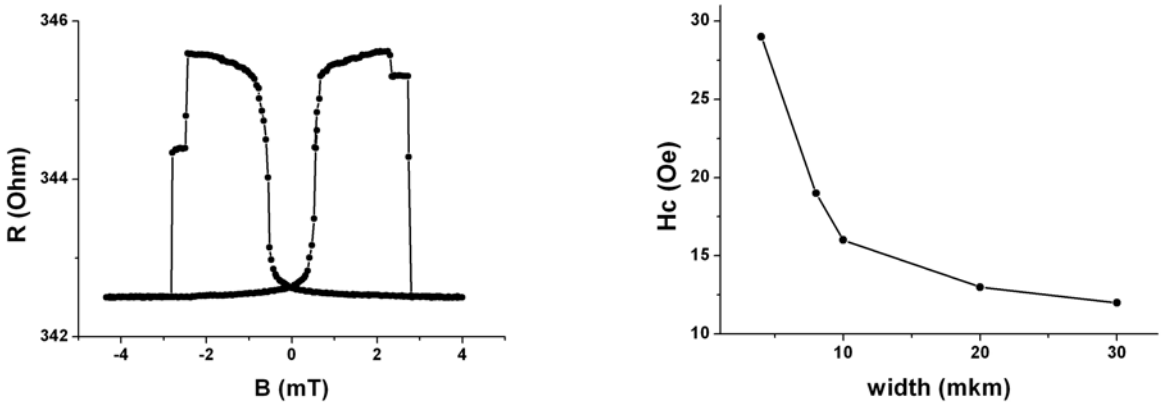

a) **b)**

Fig.1 a) GMR response curve for Py/Cu/Co spin-valve sensor with the following dimensions: width 4 mkm, and length 100 mkm and b) Dependence of fixed layer (Co) coercitivity (Hc) on sensor width.

1. S. Tumanski *Thin magnetoresistive sensor*s, IOP publishing Ltd., Bristol, 2001.
2. R. Coehorn “Giant magnetoresistance and magnetic interactions in exchange-biased spin-valves”, in *Handbook of magnetic materials*, volume **15**, Elsevier Science, Amsterdam, 2003.
3. O.S. Trushin, D.A. Kokanov, V.F. Bochkarev, V.V. Naumov, E.Y. Buchin, “An automated stand for express-diagnostics of magnetoresitive structures”, Russian Microelectronics, **38**, pp.257-259, 2009.
4. M.J. Donahue and D.G. Porter, “OOMMF User's Guide, Version 1.0”, Interagency Report NISTIR 6376, National Institute of Standards and Technology, Gaitthersburg, MD, 1999.
5. O. Trushin, N. Barabanova, and V.P. Alekseev, “Study of magnetic characteristics of permalloy nanostructures by micromagnetic modeling”, Russian Microelectronics, **38**, pp. 198, 2009.

GMR sensor design optimization using micromagnetic simulations

O.S. Trushin[1], N. Barabanova[2], V.P. Alexeev[2]
[1]*Yaroslavl Branch of the Institute of Physics and Technology of Russian Academy of Sciences, Yaroslavl, Russia, oleg_trushin@lenta.ru.*
[2]*Department of Physics, Yaroslavl State University, Yaroslavl, Russia*

Magnetic field sensors based on Giant Magnetic Resistivity(GMR) effect find wide range of applications in modern technology[1]. High sensitivity at low fields and low cost make these sensors very competitive at a market. The most popular design of these sensors based on spin-valve structures. Such structure consists of three thin film layers of magnetic and non-magnetic materials[2]. Very important problem in designing GMR sensors is the effect of size and shape of sensor element on its functional parameters.
In this work we are using micromagnetic simulations to study size effect of sensor element on its magnetic reversal. The model system consists of 3 layers: free layer – Py (3 nm), spacer – Cu(3 nm), fixed layer – Co(3nm). Sensor element has rectangular shape with fixed length (long side) equal to 5 mkm and variable width (short side) in the range 0.1-1 mkm.
We used OOMMF code[3] for these simulations. It became very popular tool in micromagnetic studies. We tested this program before for single layer Py nanostructure [4].
Typical magnetization reversal curve obtained for three layer spin-valve sensor element is shown in Fig.1. Our simulations showed that reducing sensor width leads to increasing coercitivity of both magnetic layers (free and fixed). It is due to increasing contribution of magnetostatic term in total energy because of growth of shape anisotropy.

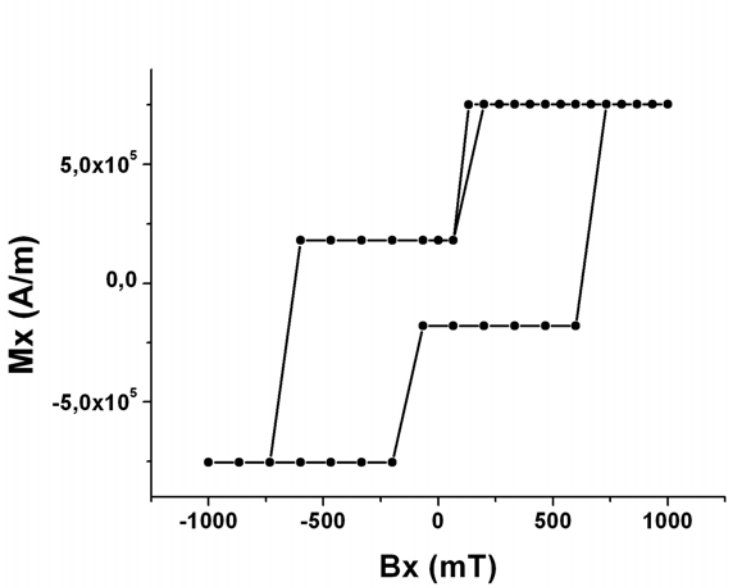

Fig.1 Magnetization reversal curve calculated with OOMMF package for Py/Cu/Co spinvalve sensor with lateral dimensions: width 1 mkm, length 5 mkm.

1. S. Tumanski *Thin magnetoresistive sensors*, IOP publishing Ltd., Bristol, 2001.
2. R. Coehorn “Giant magnetoresistance and magnetic interactions in exchange-biased spin-valves”, in *Handbook of magnetic materials*, volume **15**, Elsevier Science, Amsterdam, 2003.
3. M.J. Donahue and D.G. Porter, “OOMMF User's Guide, Version 1.0”, Interagency Report NISTIR 6376, National Institute of Standards and Technology, Gaitthersburg, MD, 1999.
4. O. Trushin, N. Barabanova, and V.P. Alekseev, “Study of magnetic characteristics of permalloy nanostructures by micromagnetic modeling”, Russian Microelectronics, **38**, pp. 198, 2009.

Optical and thermal effects in polymers with superparamagnetic impurities

R.M. Aynbinder

Institute of Chemical Technology, Prague, Czekh Republic, romain@inbox.ru

The use of nanomaterials opens up great prospects due to unique properties appearance of the nano-sized materials. Currently, diagnostic systems and effective methods of therapy based on nanoparticles are designed.

The aim of this work is the creation, experimental and theoretical study of miniature porous structures of polymer-based with magnetic iron oxide nanoparticles that are able to change their local properties (heating due to magnetic impurities, porosity, pore diameter) under the influence of external impacts (magnetic field, pH, temperature, chemical composition of the solution). Nanoparticles of iron oxide used for the creation of local heating centers in the dielectric polymer matrix, which offers opportunities for biomedical application of magnetic nanoparticles: biosensors, controlled local hyperthermia of tumors, targeted drug delivery, etc.

Theoretic research of nanoparticles in the polymer matrix under the influence of electromagnetic radiation (based on the Mie theory) was undertaken. The influence of the form of nanoparticles - a spherical or non-spherical (e.g., ellipsoidal) for the optical extinction spectra of nanoparticles was dicussed. We consider the physical processes responsible for the peculiarities of the experimental optical spectra of polymers with nanoparticles.

Also we have studied the remagnetization effects of single-domain (so-called superparamagnetic) particles by the external magnetic field (in the framework of the Stoner-Wohlfarth theory). For the iron oxide nanoparticles with a size less than the critical (which is about 10 nm) with the easy axis symmetry the value of critical field at which the switch of the spin system of the metastable state to stable was calculated. And, finally, we computed the value of thermal energy released nanoparticles due to absorbtion of energy of magnetic field (with the amplitude of the field exceeds the critical value) due to Larmor precession of the spin from metastable state into a stable during the time of the order of the spin - lattice relaxation. This energy value agrees well with experimental data.

Ferromagnetic resonance study of thin $Si_{65}Mn_{35}$ layer

S. Kapelnitsky[1,2]

1. *Russian Research Centre "Kurchatov Institute", Moscow, Russia, E-mail:kapelnitski@gmail.com.*
2. *Institute of Physics and Technology, Russian Academy of Sciences, Moscow , Russia*

Recently heavily doped thin $Si_{1-x}Mn_x$ layers are proposed as possible candidates for the realization of the spin injection in spintronic devices due to hysteresis-like character of the anomalous Hall effect at temperatures up to 230 K indicating the presence of the spin polarization of holes at high temperatures [1]. Magnetic and transport properties strongly depend on synthesis conditions and the thickness of layers. It is found that these features manifest that these materials are in non-equilibrium state and contain several different phases. Magnetic structure and origin of high T_c ferromagnetism in these layers is not yet clear.

Samples having 35 % of Mn were prepared by means of the laser epitaxy on single crystal GaAs substrate at T_g=350 °C. The thickness of layer was around 55 nm. Magnetic resonance spectra (absorption derivative) have been measured at 9.42 GHz in magnetic fields up to 1 T using Bruker ESP 300 EPR spectrometer in the temperature range from 115K to 295 K.

Complex multi-peak spectra are observed at room temperature due to the diverse resonance conditions for clusters constituting the layer. These spectra collapse, and strong resonance signal of the FMR uniform mode (besides weaker additional signals) is observed at T<200 K. The appearance of the nearly Lorentzian FMR signal points out the existence of strong exchange interaction between clusters. The resonance field depends on angle between the layer plane and the orientation of the external magnetic field, this dependence follows Kittel's equations for FMR of thin ferromagnetic disk. The angular dependence of resonance field shows neglible field of magnetic anisotropy besides the demagnetizing field of layer.

Values of magnetization and g-factor are derived from the temperature dependence of the resonance fields H_{rp} and H_{rn} , applied in-plane and normal to plane of the layers, correspondingly. It is obtained that g=2.03 in the temperature range 115 K - 200 K indicating quenched orbital moment of Mn and the layer magnetization is around 56 G at T=115 K. Corresponding average moment per Mn is μ_{Mn}=0.32 μ_B that is one order of magnitude lower then magnetic moment of Mn^{2+} ion. The Curie temperature estimated from FMR data achieves 230 K.

Observed high magnitudes of the Curie temperatures and low μ_{Mn} values are discussed within the framework of a model described in [2]. This model suggested that tetrahedral interstitial Mn (Mn_T) atoms together with intervening substitutional Mn (Mn_{Si}) ion assemble complexes of the Mn_T -Mn_{Si}-Mn_T type with the ferromagnetic interaction between Mn ions. Further experimental and theoretical study is required to explain strong ferromagnetic inter-clusters interaction mediated by Mn-Si matrix.

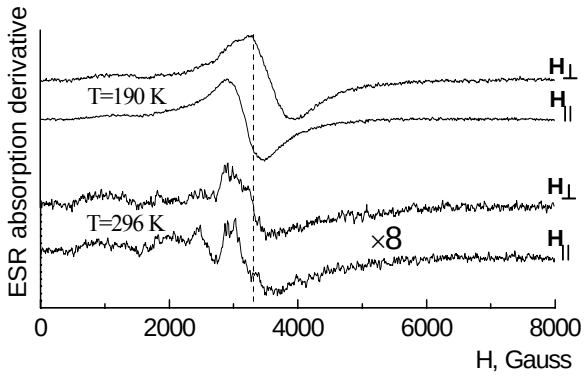

Fig. 1. ESR spectra (absorption derivative) at $\omega/(2\pi)$=9.42 GHz. Vertical dashed line represent the value $H_o=\hbar\omega/(g\mu_B)$, with g=2.03

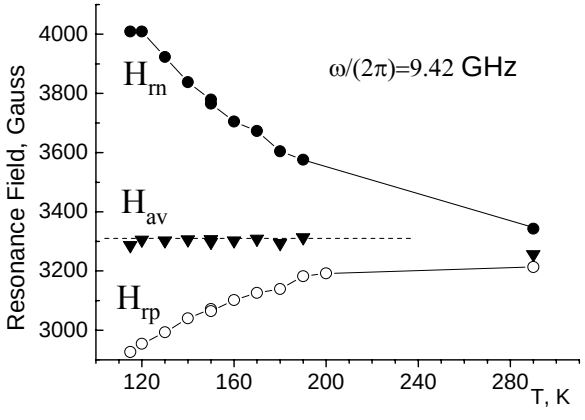

Fig. 2. Resonance fields H_{rp} (-○-), H_{rn} (-●-) (in plane and normal to the layer plane resp.) and the values of $H_{av}=(1/3)*(2H_{rp},+H_{rn})\approx\hbar\omega/(g\mu_B)$ (-▼-) vs T. Dashed line represent the value H_0=3308 G.

1. S.N. Nikolaev, B.A. Aronzon, V.V. Rylkov *et al.,* "Anomalous Hall effect in Si films heavily doped with Mn", JETP Lett., **89**, pp.707-712, 2009

2. Quinghua Liu, Wensheng Yan, He Wei *et al.,* "Energetic stability, electronic structure, and magnetism in Mn-doped silicon dilute magnetic semiconductors", Phys. Rev. B, **77**, pp.245211-245217, 2008

Calculation of the characteristics of electron transport through molecular clusters

Y.S. Gerasimov[1] , V.V. Shorokhov[2] , E.S. Soldatov[2] , O.V. Snigirev[1,2]
1. IMP, RRC " Kurchatov Institute", Moscow, Russia, secretariat@imp.kiae.ru. 2. Faculty of Physics, Moscow State University, Moscow, Russia, dean@phys.msu.su

There is no doubt that the creation of nanoscale molecular electronic devices with a weak coupling is the most intriguing problem of the next decade. The key to the construction of such devices is to be found in studying the electron tunnel transport through single molecular objects and in the development of the classification of the electronic properties of these objects, depending on their spatial structure and chemical structure. A solution of this classification problem will facilitate to move for the design and creation of more complex nanoscale molecular electronic devices eventually.

In the current work single-electron molecular energy spectra of small molecules of carborane $C_2B_{10}H_{12}$, fullerene C_{60} and platinum molecular cluster $Pt_5(CO)_6(PPh_3)_4$ were calculated for the first time for their different ground and excited charge states by means of quantum mechanical methods (Hartree-Fock and Møller-Plesset). Basing on the data, effective capacitance parameters and the transport spectrum of single-electron states of each of the molecules were estimated. These parameters determine the features of tunneling transport of electrons process through the molecule and allow to simplify the method of calculating the transport characteristics of single-molecular transistors and molecular single-electron devices in future almost without any loss of completeness and accuracy of description.

Using Monte Carlo simulation method transport characteristics of monomolecular single-electron transistor are calculated in approximation of low energy relaxation of electrons in a molecule ($t_{rel} > 10^{-10}$s) for the molecules of carborane, fullerene and molecular cluster of platinum as a central conducting island. The subsequent analysis of volt-current characteristics of such a transistor for the molecules of that small size gave an opportunity to come to a conclusion that the tunnel current's value is determined mostly by a small number of charge and energy states of a molecule.

A comparison of the calculation results with available experimental data [1] is done**.** In particular this comparison of the calculated and previously received experimental volt-current characteristics of monomolecular single-electron transistor based on fullerene molecule C_{60} revealed the difference of the Coulomb blockade size of the tunnel current for more than 10 times. The size of the Coulomb blockade in the experiment was 60 mV while the data of simulation defined one to be over 0.76 V. This difference in the Coulomb blockade value of nano-transistor based on fullerene molecule evidently indicates that in case of real experimental situation the molecule is surrounded by a *coat* of various molecular groups (e.g. phinyl ones, etc.) connecting it to the environment. Therefore, such a nanoscale object differs significantly from the specified one in the simulation model. Moreover, the influence of electromagnetic environment on the process of tunnel transport hasn't been taken into account in the assumed calculation model.

For the molecular transistor based on carborane the simulated volt-current characteristics are compared with previously experimentally measured characteristics for the molecular transistor based on carborane cluster molecule $1,7\text{-}(H_3)_2\text{-}1,2\text{-}C_2B_{10}H_9Tl(OCOCF_3)_2$. The width of the Coulomb blockade region at room temperature as a result of the calculation turned out to be less than 90mV. In experimental work [2] it was less than 50 mV. This discrepancy indicates that the tunneling current in the transistor flows not only through the carborane group but through the thallium center as well.

This work has been supported by RFBR (Pr. No. 09-07-00272-a) and ISTC (Pr. No. № 3457).

1. H. Park, J. Park, A. K. L. Lim, E. H. Anderson, A. P. Alivisatos, P. L. McEuen, "Nanomechanical oscillations in a single-c60 transistor", Nature, **407**, p.57, 2000
2. E.S. Soldatov, V.V. Khanin, A.S. Trifonov, S.P. Gubin, V.V. Kolesov, D.E. Presnov, "Room temperature molecular single-electron transistor", JETP Lett., **64**, pp.510-514, 1996

Investigation of segregation effect in InGaAs/GaAs quantum wells by means a computer simulation

A.N.Baryshev, S.V.Khazanova

- *Nizhni Novgorod University im.N.I.Lobachevskogo, NIzhni Novgorod, Russia*
- *khazanova@phys.unn.ru*

Quantum wells (QW) based on III/V heterostructures have gained much interest during recent years due to their applications in optoelectronic devices. Because the optical properties of nanostructure devices are governed by the size and composition distribution, detailed understanding of the growth kinetics has both technological and fundamental importance. As is known growth of InxGa1-xAs ternary alloy is influenced by processes such as segregation and diffusion. The processes have been observed during such as molecular beam epitaxy and metal-organic vapor epitaxy [1].

In this report, we present the theoretical study of the growth kinetics and optical properties of InxGa1-xAs/GaAs heterostructures (0,x,0.2), taking into account segregation effect. Using a Monte Carlo technique, a numerical modeling of the epitaxial growth was performed for a heterostructure containing an InxGa1-xAs quantum well (QW) surrounded by two GaAs barriers, grown in the [001] direction or close to it, in the case of a vicinal substrate. The model includes the effect of isomorphic deformation of the underlying atomic layers onto the energy parameters of adatoms in the growing monolayer.

Within the effective mass approximation, the dependence of the $e_1 - hh_1$ transition energy on the degree of In/Ga segregation and, consequently, on the growth conditions and substrate miscut angle was calculated. The calculations of the quantized energy levels in InGaAs/GaAs QWs were performed with realistic composition profiles (i.e. those obtained by the Monte Carlo modeling), taking into account the corresponding distribution of the elastic deformation. Our calculations show that the segregation effect leads to a considerable blue shift of the transition energy. According to the modeling results, the shift and broadening of the QW photoluminescence peak increase for higher growth temperatures and substrate miscut angles. Our results are in good agreement with the literature data [2].

1. Ю.Н. Дроздов, Н.В.Байдусь, Б.Н.Звонков, ФТП, 37, 203, 2003
2. S. Martini, A. A. Quivy, A. Tabata, et al, J. Appl. Phys., 90, p.2280, 2001.

Simulation of impurity diffusion at the formation of ultrashallow active areas in silicon-based FET

F. Komarov[1], O. Velichko[2], A. Mironov[1], G. Zayats[3], A. Komarov[1], V. Tsurko[3]

1. Institute of Applied Physics Problems, 7 Kurchatov Street, 220108 Minsk, Belarus, KomarovF@bsu.by 2. Belarusian State University of Informatics and Radioelectronics, 6 P. Brovka Street, 220013 Minsk, Belarus 3. Institute of Mathematics, Academy of Sciences of Belarus, 11 Surganov Street, 220072 Minsk, Belarus

One of ways of shallow p-n-junction formation in silicon-based ultra large integrated circuits (IC) technology is the expansion of opportunities of traditional technologies, namely ion implantation with the subsequent thermal processing. The fabrication of new generation IC is associated with the application of low-energy (below 10 keV) ion implantation and rapid (less than 60 seconds) thermal annealing. Such conditions correspond to the technological stages of the formation of p-n-junctions at the depth of 30 nm or less. It is significant that in this case the effect of “uphill” diffusion of the impurity in surface region of a crystal is observed during thermal annealing [1, 2].

Necessity to obtain calculated profiles of the impurity distribution adequate to real ones assumes use of high-level kinetic diffusion models as well as application of high-quality computing algorithms. Even recent versions of known simulation software do not give an opportunity to model precisely enough distribution of impurity after low-energy implantation and the subsequent rapid thermal annealing. In the present work, we demonstrate an approach considering determining features of such processes.

A model of the diffusion of dopant atoms implanted in silicon is presented. The model is based on the creation and migration of dopant-vacancy and dopant-self interstitial complexes. It accounts process nonlinearity and influence of non-stationary distribution of defects as well as electric fields and elastic stress on the migration of atoms. The finite-difference method is applied to numerical approximation of the obtained system of nonlinear equations. Estimate of accuracy is obtained. Numerical simulation results are in a reasonable agreement with experimental data. The proposed method enables to predict observable experimentally “kink and tail” profile shapes, the “uphill” diffusion and local maxima formation at a crystal surface.

1. D. Girginoudi, N. Georguolas, A. Thanailakis, E.A. Polycroniadis, “Studies of ultra shallow n+-p junctions formed by low-energy As implantation”, Materials Science and Engineering B, 114–115, pp. 381-385, 2004

2. F.F. Komarov, O.I. Velichko, V.A. Dobrushkin, A.M. Mironov, “Mechanisms of arsenic clustering in silicon”, Phys. Rev. B, 74, pp. 035205-1–035205-10, 2006

Modeling of the interfacial separation work in relation to impurity concentrations in adjoining materials

I. Alekseev, T. Makhviladze, A. Minushev, M. Sarychev
Institute of Physics and Technology, Russian Academy of Sciences, Moscow, Russia, minakh@mail.ru

Adhesion properties of interfaces built up from the solid thin-film materials are essential for modern methods of multilayer structures fabrication widely used in micro- and nanoelectronics. The interfacial surface tension and separation work are the most important parameters responsible for adhesion strength of an interface. The parameters have to depend strongly on lattice defects containing in the conjugate material layers due to penetration of these defects into the interface. Therefore a model that is capable of describing dependences of this kind would be very useful, for practical purposes, in order to predict the adhesion strength and reliability of multilayer structures.

Recently [1] we developed the general approach and the thermodynamic theory of interfacial adhesion between materials, which may contain various point defects. The foundations of the approach and the theory are the Gibbs equation for description of the interface thermodynamics and kinetic equations for defect production/annihilation. The theory has been applied to the cases that lattice defects are vacancies, vacancy clusters, and impurity atoms. For all types of defects, now we are capable of modeling the interfacial surface tension and separation work and of analyzing their dependences on the defect concentrations.

Based on the general theory [1], in the present work we develop the numerical model for the separation work analysis in the specific case that defects are interstitial or substitutional impurities. The comprehensive numerical analysis of the equations for the separation work has been performed for each type of defects. In particular it has been found numerically that the separation work as a function of the impurity concentrations can vanish and become negative. One of these calculated curves for the temperature T = 500 K is presented in the figure (*WI* is the dimensionless separation work, C is the impurity concentration in one of the materials, and the impurity concentration in the other one is considered to be zero).

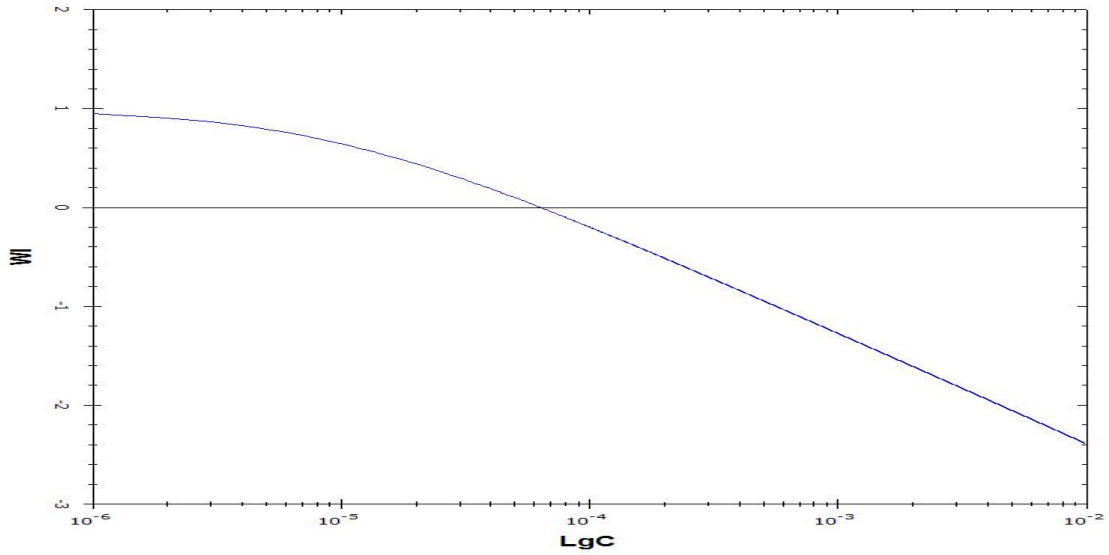

The separation work behavior of this type, that was founded here, means that the multilayer structure is thermodynamically unstable for the concentrations larger than ~$6 \cdot 10^{-4}$ (see Fig.), and at certain defect concentrations the interface may fall into the state, for that the spontaneous separation is more preferable. This effect can be used in practice in order to improve microelectronic structures reliability. The numerical modeling results over a wide range of material parameters and temperatures for each type of defects are presented and the results were used as a base for study of adhesion strength of various interfaces.

1. R.V. Goldstein, T.M. Makhviladze, M.E. Sarychev, “Influence of impurities on the interfacial separation work for conjugate materials”, Poverkhnost’ (Journal of Surface Investigation), №12, 2009 (to be published) (in Russian)

Energetics and atomic mechanisms of strain relaxation in heteroepitaxial systems

O. Trushin[1] , J Jalkanen[2] , E. Granato[3] , S-C. Ying[4], T. Ala-Nissila[2]
[1] *Institute of Physics and Technology of Russian Academy of Sciences, Yaroslavl Branch, Yaroslavl, Russia, oleg_trushin@lenta.ru.*
[2]*Department of Engineering Physics, Helsinki University of Technology, FIN-02015 TKK, Espoo, Finland,*
[3]*Laboratrorio Associado de Sensores e Materiais, Instituto National de Pesquisas Espaciais, 12227-010 Sao Jose dos Campos, SP, Brazil,*
[4]*Department of Physics, Brown University, Providence, RI 02912, USA*

We present a review of recent theoretical studies of different atomistic mechanisms of strain relaxation in heteroepitaxial systems[1]. We explore these systems in two and three dimensions using different semi-empirical interatomic potentials from simple Lennard-Jones type to more realistic many-body embedded atom method potentials[2]. In all cases we use a universal molecular static method for generating minimum energy paths for transitions from the coherent epitaxial (defect free) state to the state containing an isolated defect (localized or extended). This procedure consists of two stages. At the first stage we perform defect activation using Repulsive Bias Potential method[3]. This is followed by a systematic search for the minimum energy paths using nudged elastic band method[4]. We focus attention on two types of isolated defects which are shown in Fig.1. As the result we were able to understand many general features of the atomic mechanisms and estimate energetics of strain relaxation in metal/metal systems.

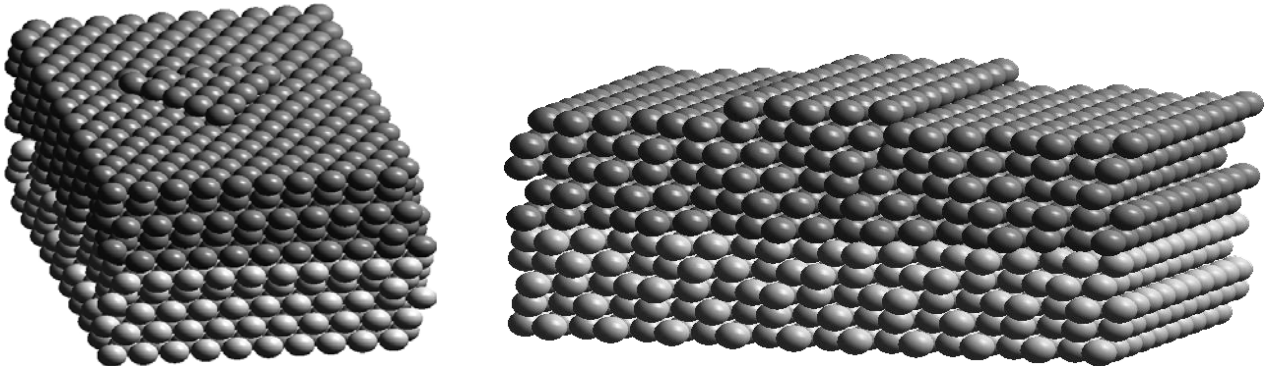

a) b)

Fig.1 Two types of isolated defects generated through RBP method: a) - local defect (stacking fault tetrahedron), b) - extended defect (misfit edge dislocation). Dark color balls represent atoms of the film and light color substrate.

1. O. Trushin, J. Jalkanen, E. Granato, S. C. Ying and T. Ala-Nissila, “Atomistic studies of strain relaxation in heteroepitaxial systems”, J. Phys.: Condens. Matter, **21**, pp.084211, 2009.
2. S. M. Foiles, M. I. Baskes and M. S. Daw, “Embedded atom method functions for fcc metals Cu,Ag,Au,Ni,Pd,Pt and their alloys”, Phys. Rev. B, **33**, pp.7983, 1986.
3. O. Trushin, P. Salo, T. Ala-Nissila and S.-C. Ying, “Searching for transition paths in multidimensional space with a fixed repulsive bias potential”, Phys. Rev. B, **69**, pp. 033405, 2004.
4. H. Jonsson, G. Mills and K. W. Jacobsen “Nudged elastic band method for finding minimum energy paths of transitions”, *Classical and Quantum Dynamics in Condensed Phase Simulations*, ed. By B.J. Berne et al, World Scientific, Singapore, 1998.

Off-lattice self-learning kinetic Monte-Carlo: application to 2D cluster diffusion on metal surfaces

O. Trushin[1] , A. Makin[2] , T. S. Rahman[3]
[1] *Institute of Physics and Technology of Russian Academy of Sciences, Yaroslavl Branch, Yaroslavl, Russia, oleg_trushin@lenta.ru.*
[2.] *Department of Physics, Yaroslavl State University, Yaroslavl, Russia*
[3] *Department of Physics, University of Central Florida, Orlando, FL, USA*

Atomic transport on crystal surfaces plays an important role in thin film growth. Understanding of atomic mechanisms of surface diffusion is needed for development of predictive growth models. In this paper we report developments of the kinetic Monte Carlo (KMC) method with improved accuracy and increased versatility for the description of cluster diffusivity on metal surfaces[1]. The on-lattice constraint built into our recently proposed self-learning KMC (SLKMC)[2] is released, leaving atoms free to occupy 'off-lattice' positions to accommodate several processes responsible for small-cluster diffusion, periphery atom motion and heteroepitaxial growth. This technique combines the ideas embedded in the SLKMC method, with a new pattern-recognition scheme, fitted to an off-lattice model in which relative atomic positions are used to characterize and store configurations. Application of a combination of the 'drag' and the repulsive bias potential (RBP)[3] methods for saddle point searches allows the treatment of concerted cluster, and multiple- and single-atom, motions on an equal footing. We present applications of this off-lattice SLKMC to the diffusion of 2D islands of Cu (containing 2–30 atoms) on Cu(111) (Fig.1) and Ag(111), using the interatomic potential from the embedded-atom method[4]. For the hetero-system Cu/Ag(111), this technique has uncovered mechanisms involving concerted motions such as shear, breathing and commensurate–incommensurate occupancies.

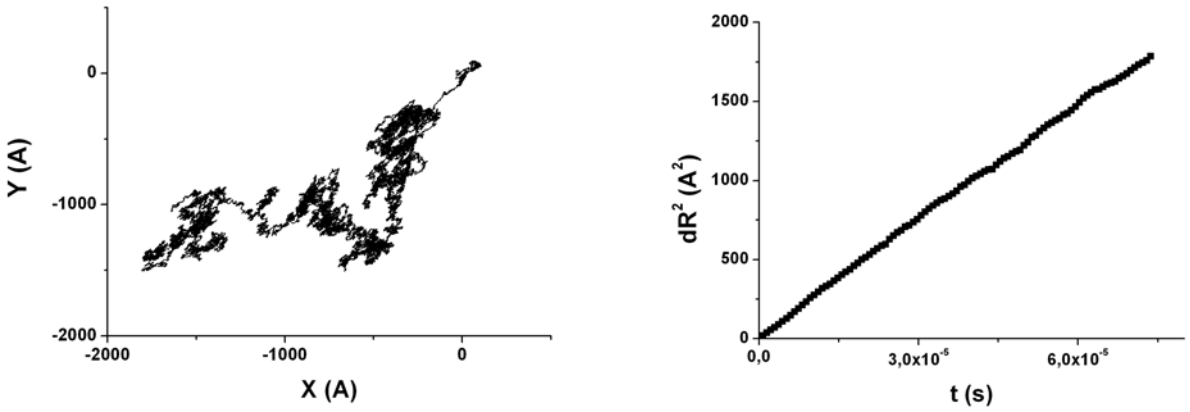

Fig.1 Trajectory of center of mass motion (a) and Mean Square Displacement versus time (b) for 7-atom Cu cluster on Cu(111).

1. A. Kara, O. Trushin, H. Yildirim and T. S. Rahman, "Off-lattice self-learning kinetic Monte Carlo: application to 2D cluster diffusion on the fcc(111) surface", J. Phys.: Condens. Matter , **21**, pp. 084213, 2009.
2. O. Trushin, A. Karim, A. Kara and T. S. Rahman, "Self-learning kinetic Monte-Carlo method: Application to Cu(111)", Phys. Rev. B, **72**, pp. 115401, 2005.
3. O. Trushin, P. Salo, T. Ala-Nissila and S.-C. Ying, "Searching for transition paths in multidimensional space with a fixed repulsive bias potential", Phys. Rev. B, **69**, pp. 033405, 2004.
4. S. M. Foiles, M. I. Baskes and M. S. Daw, "Embedded atom method functions for fcc metals Cu,Ag,Au,Ni,Pd,Pt and their alloys", Phys. Rev. B, **33**, pp.7983, 1986.

Nanoobject sizes of defects in porous systems and defective materials according ADAP method. Part I

[1]Timoshenkov S.P., [1,2] Svetlov-Prokop'ev E.P., [1]Grafutin V.I.
[1]*Moscow Institute of Electronic Technology (Technical University), TU- MIET, Zelenograd, proezd 4806, bulding 5, Moscow, Russia, , E-mail:spt@miee.ru*
[2]*«State Science Centre of the Russian Federation- A.I.Alikhanov Institute for theoretical and experimental physics», str. B.Cheremushkinskaya, 25, Moscow, Russia, E-mail:epprokopiev@mail.ru*

It is known [1], that positrons effectively probe free nanoobject volumes (basically vacancies, divacancies and pores) with the sizes ≤ 1-100 nanometer both in metals and alloys, and in semiconductors and porous systems. We receive on the basis of model of movement of a particle in a plane limited by round cylindrical absolutely impenetrable wall [2-4], more correct formulas for definition of radiuses R_c cylindrical (symbol c) and the specified formulas of radiuses spherical (symbol sp) of nanopores in the width a component of angular distribution of annihilation photons (ADAP) $\theta_{1/2}$ and energies E_{1c} and E_{sp} of the basic parapositronium state, annihilated in pores in porous silicon and aluminium dioxyde

$$R_c[\overset{0}{A}] = \frac{21{,}1}{\theta_{1/2}[mrad]}, R_c[\overset{0}{A}] = \left(\frac{30{,}58}{E_{1c}(eV)}\right)^{1/2}, \quad (1)$$

$$R_{sp}[\overset{0}{A}] = \frac{16{,}6}{(\theta_{1/2})[mrad]}, R_{sp}[\overset{0}{A}] = \left(\frac{18{,}85}{E_{1sp}(eV)}\right)^{1/2}, \quad (2)$$

where R and $\theta_{1/2}$ are expressed in Å and $mrad$ accordingly.

Experiments have shown [1], that the basic part of positrons is in porous silicon from positron states no positronium type in volume of pores annihilated. We shall consider, that such type positron states are the positrons localized in volume of pores in the same way, as well as positronium atoms. In this case formulas (1) and (2) will be transformed in

$$R_c[\overset{0}{A}] = \left(\frac{61{,}1}{E_{1sp}(eV)}\right)^{1/2}, R_c[\overset{0}{A}] = \frac{29{,}7}{\theta_{1/2}[mrad]}, \quad (3)$$

$$R_{sp}[\overset{0}{A}] = \left(\frac{37{,}7}{E_{1sp}(eV)}\right)^{1/2}, R_{sp}[\overset{0}{A}] = \frac{23{,}4}{\theta_{1/2}[mrad]}, \quad (4)$$

For experimental value in porous silicon $\theta_{1/2} = 0{,}8$ мрад [1], have received average value of radius of cylindrical times $R \approx 26{,}4$ Å ≈ 3 nanometer. Their concentration in a porous layer has appeared equal ~ $5{,}6 \cdot 10^{13}$ cm^{-3}.

1. E.P. Prokop'ev, V.I. Grafutin, S.P. Timoshenkov, Yu.V. Funtikov, Opportunities of research of porous systems and nanomaterials by a method of positron annihilation spectroscopy, Russian Journal of Nondestructive Testing (Rus), №10, p.700, 2008.
2. I.E. Irodov, Collection of problems on the nuclear physics (Rus.). Moscow: Gosatomizdat, 1960.
3. Z. Flugge, Problems in the quantum mechanics, V. 1, Moscow. Publishing house LKI, 2008.
4. John Börd. The engineering mathematics, Moscow. Izd. Dom «Dodeka-XXI», 2008.

Nanoobject sizes of defects in porous systems and defective materials according ADAP method. Part II

[1]Timoshenkov S.P., [1,2] Svetlov-Prokop'ev E.P., [1]Grafutin V.I.
[1]*Moscow Institute of Electronic Technology (Technical University), TU- MIET, Zelenograd, proezd 4806, bulding 5, Moscow, Russia, , E-mail:spt@miee.ru*
[2]*«State Science Centre of the Russian Federation- A.I.Alikhanov Institute for theoretical and experimental physics», str. B.Cheremushkinskaya, 25, Moscow, Russia, E-mail:epprokopiev@mail.ru*

Thus, on energy in a annihilation place on external valent electrons E it is possible to find also radiuses of pores, using only ADAP data. For this purpose we shall result the expression connecting energy of annihilated electron-positron pair with $\theta_{1/2}$ ($FWHM$ (full width half-maximum)) (see ref. [1] in Part I)

$$E = 6{,}9 \cdot 10^{-2} (\theta_{1/2})_g^2 \qquad (5)$$

Here *E*-energy in eV, and $(\theta_{1/2})_g$ - ($FWHM$ (full width half-maximum)) full width of ADAP curve in мрад. So for samples of silicon the measured size $(\theta_{1/2})_g$ has made 11,1 мрад and to it there corresponds average energy of electron-positron pairs, equal $E = 8{,}5$ eV and caused by average energy of electrons an external environment of atom of silicon on a wall of a pore which can be accepted equal energy of electron on an external environment of the isolated atom of silicon. Thus it is considered, that up to annihilation a positron and positronium are in pore thermalized and the measured energy is defined, basically, energy of electron. Tabulared value of energy for $Si(3p^2\ ^3P_0)$ an electronic external environment of silicon $E(Si) = 8{,}1517$ эВ [1]. As we see, the consent of these sizes energies E and $E(Si)$ quite satisfactory. Thus, positrons are basically on external valent electrons of silicon atoms of "wall" of a pore annihilated. It is possible to believe, that the difference of sizes $E - E(Si) = 0{,}35$ эВ is caused by the contribution of energy of bond of the positron which is being a pore in energy of annihilated electron-positron pairs. In this case for definition of the size of cylindrical pores it is rational to use expression (3)

$$R_c = \left(61{,}1/[E - E(Si)]\right)^{1/2}, \qquad (6)$$

Thus, at value $E = E - E(Si) = 0{,}35$ eV for the size of pores is equal 13,2 Å.

Further with value $R_{tr} \approx 13{,}2$ Å have defined average value of section of capture of a positron defects $\sigma_{tr} \approx 5{,}5 \cdot 10^{-14}$ of cm^2. For estimations of average values of concentration of pores have accepted $k_{tr} \approx 7{,}9 \cdot 10^8$ s^{-1}, $\sigma_{tr} \approx 5{,}5 \cdot 10^{-14}$ cm^2 and $v \approx 10^7$ cm/s. Have received value of concentration of pores $N_{tr} = k_{tr} / v \cdot \sigma_{tr} \approx 1{,}4 \cdot 10^{15}$ cm^{-3}.

Knowing the general porosity (45 %) [1] and average volume of a pore, we can estimate concentration of pores from simple geometrical reasons and, having compared it with calculated N_{tr} to check up reliability of accepted assumptions. Certain by us under the formula (2) average size of times $R_{tr} \approx 3$ of nanometer there corresponds their average volume $V_{tr} = \pi R_{tr}^2 \cdot h \approx 2{,}8 \cdot 10^{-16}$ of cm^{-3}, here h - thickness of a layer of porous silicon. For a case of " dense packing » such pores their concentration proceeding from size of the general porosity 0,45 could be equal $N_{tr}^G \sim 0{,}45/V_{tr} = 1{,}6 \cdot 10^{15}$ cm^{-3}. Divergences of size N_{tr}^G with us the certain concentration $N_{tr} = 1{,}4 \cdot 10^{15}$ of cm^{-3} it is not so great. Thus, the samples of porous silicon studied by ADAP method is represent microporous cylindrical nanoobjects with the sizes of the order 3 nanometers and concentration 10^{15} of cm^{-3}.

1. Physical sizes: Directory, Moscow. Energoatomizdat, 1991.

Calculation of electrophysical parameters of thin undoped GaAs-in-Al_2O_3 quantum nanowires and single-wall armchair carbon nanotubes

D.V. Pozdnyakov[1], A.V. Borzdov[1], V.M. Borzdov[1], V.A. Labunov[2]
1. Belarusian State University, Minsk, Belarus, pozdnyakov@bsu.by
2. Belarusian State University of Informatics and Radioelectronics, Minsk, Belarus, labunov@its.bsuir.edu.by

Presently such device structures as the quantum nanoconductors with one-dimensional electron gas are very attractive physical objects. It is mainly caused by their advantages over the device structures with three- and two-dimensional electron gas from practical point of view, particularly in the field of nanoelectronics. Thin undoped GaAs-in-Al_2O_3 quantum nanowires as well as single-wall armchair carbon nanotubes occupy a great niche among the quantum-dimensional structures with one-dimensional electron gas. At that the physico-mathematical basis, by means of which one can develop software allowing electrophysical parameters of the nanowires and the nanotubes characterized by some physical and topological parameters to be calculated, has already been created by now [1–7]. So the purpose of this study is software development as well as calculation of some electrophysical parameters of the thin undoped GaAs-in-Al_2O_3 quantum nanowires and the single-wall armchair carbon nanotubes.

In accordance with the purpose the influence of the cross-section size, the temperature, the Fermi level and the value of electric field strength on a number of electrophysical parameters of the structures mentioned above has been investigated by using a numerical solution of the one-dimensional Boltzmann transport equation taking into account all the dominant scatterers of electrons in the considered structures.

1. D.V. Pozdnyakov, V.O. Galenchik, A.V. Borzdov, “Electron scattering in thin GaAs quantum wires”, Phys. Low-Dim. Struct., 2, pp.87–90, 2006
2. D.V. Pozdnyakov, V.O. Galenchik, V.M. Borzdov, F.F. Komarov, “Peculiar properties of electron transport in single-wall armchair carbon nanotubes”, Proc. SPIE, 6328, pp.0Y-1–9, 2006
3. D.V. Pozdnyakov, V.O. Galenchik, F.F. Komarov, V.M. Borzdov, “Electron transport in armchair single-wall carbon nanotubes”, Physica E: Low-Dim. Syst. Nanostr., 33, pp.336–342, 2006
4. D.V. Pozdnyakov, V.O. Galenchik, A.V. Borzdov, V.M. Borzdov, F.F. Komarov, “Modeling of non-stationary electron-phonon transport in armchair single-wall carbon nanotubes”, in: Physics, Chemistry and Application of Nanostructures. Reviews and Short Notes to Nanomeeting – 2007, edited by V.E. Borisenko, S.V. Gaponenko, V.S. Gurin, World Scientific Publishing Co. Pte. Ltd., Singapore, 2007, pp.245–248
5. A.V. Borzdov, D.V. Pozdnyakov, “Scattering of Electrons in the GaAs/AlAs Transistor Structure”, Phys. Solid State, 49, pp.963–967, 2007
6. D. Pozdnyakov, V. Galenchik, A. Borzdov, V. Borzdov, F. Komarov, “Influence of scattering processes on electron quantum states in nanowires”, Nanoscale Res. Lett., 2, pp.213–218, 2007
7. A.V. Borzdov, D.V. Pozdnyakov, V.M. Borzdov, “Electron drift velocity control in GaAs-in-Al_2O_3 quantum wire transistor structure due to the electron scattering rate alteration”, http://arxiv.org/ftp/arxiv/papers/0806/0806.3181.pdf, pp.1–4, 2008

Penetration of quantum-mechanical current density under semi-infinite rectangular potential barrier as the consequence of the interference of the electron waves in semiconductor 2D nanostructures

V.A Petrov, A.V.Nikitin
Institute of Radio Engineering and Electronics, Russian Academy of Sciences,
Moscow, 101999, Russia, vicanpet@mtu-net.ru

In the present work, theoretical investigation of the influence of the electron interference effects on the inhomogeneous spatial distribution of the probability current density j_x (x, z) (or a quantum-mechanical current density ej_x (x, z), e is the electron charge) for the electron waves spreading along the x-axis in a semiconductor 1D or 2D nanostructures certain type [1,2] is continued.

We theoretically investigated behaviour of the ej_x (x, z) at falling of the electron wave on rectangular semi-infinite potential barrier (a potential wall) in height V_0 in semiconductor 2D nanostructure. We have considered a situation when in 2D nanostructure, consisting in the direction of propagation of the electron wave two rectangular quantum wells (QW) of different width, at the left, from region 1 ($x < 0$, QW_1) on the first quantum-confined electron subband the electronic wave of unit amplitude with energy $E_x < V_0$ on such barrier in region 2 ($x > 0$, QW_2) falls. Different width of the QWs in the regions 1 and 2 provide nonorthogonality of the wave functions in these regions. It results to confuse of the electronic subbands in different regions and to appearance of the electronic interference effects.

As is known [3], at falling of the electron wave with energy E_x (the x-axis is the direction of propagation of the electron wave) on a rectangular potential wall in height V_0 ($x > 0$) under condition of $E_x < V_0$ the quantum-mechanical current density ej_x (x, z) in the region 2 is equal to zero, because of the real exponential exponent of the wave function. Certainly, in this case exists exponentially dumped penetration of wave function of the particle into this region at $x > 0$.

We have shown, that in a situation when the electron wave falls on the first quantum-confined electron subband in QW_1 and longitudinal energy E_x of the particle less than energy of the bottom of the second subband in this region 1 and reflection of the electron wave probably only on same first subband the quantum-mechanical current density ej_x (x, z) in region 2 equally to zero, as well as in [3]. However, if energy of the particle in region 1 is more than energy of the bottom of the second quantum-confined electron subband in QW_1 (for asymmetrical on the z-axis nanostructure), or the bottom of the third subband in symmetric structure (reflection on even subband owing to symmetry of structure on the z-axis is forbidden) a situation because of the interference of the reflected waves cardinally varies. The possibility of the exit of the reflected wave on the second (for asymmetrical) or on the third (for symmetric) structures on $x \rightarrow -\infty$ results to the situation, when under a barrier the quantum-mechanical current density ej_x (x, z) $\neq 0$ and its amplitude exponentially dumped at $x \rightarrow \infty$. Thus under a barrier there are three areas of distribution of the ej_x (x, z): the central area, in which ej_x (x, z) it is directed in a positive direction of the x- axis and two lateral, in which ej_x (x, z) has a return direction.

We have carried out the numerical analysis of this effect for symmetric on the z-axis semiconductor 2D nanostructure with GaAs parameters. The structure has consisted from consistently located along falling electron wave of two КЯ: QW_1 = 300 Å at $x < 0$ and QW_2 = 350 Å at $x > 0$. Thus it was supposed, that on the boundary at $x = 0$ in region 2 exists semi-infinite potential barrier in height V_0 so energy of a falling particle $E_x < V_0$. We have obtained the dependences of the penetration length of the ej_x (x, z) from the E_x and V_0 . The possible manifestation of the considered effect in other nanostructures are discussed.

[1] V. A. Petrov, A. V. Nikitin, *Micro-and Nanoelectronics 2007*, edited by Kamil A. Valiev, Alexander A. Orlikovsky, Proceedings of SPIE Vol. 7025 (SPIE, Bellingham, WA 2008) 70250O.

[2] V.A. Petrov, A.V.Nikitin, *Journal of Communications Technology and Electronics,*54, pp. 209-217,2009.

[3] L. D. Landau and E. M. Lifshitz, *Quantum Mechanics:Non-Relativistic Theory* (Nauka, Moscow, 1989, 4th ed.;Pergamon, Oxford, 1977, 3rd ed.).

Laser generation in broken-gap heterostructures

I. Semenikhin[1], K. A. Chao[2], A. Zakharova[1]

1. Institute of Physics and Technology of the Russian Academy of Sciences, Moscow, Russia, E-mail address zakharova@ftian.ru 2. Department of Physics, Lund University, Lund, Sweden, and Department of Physics, Chemistry and Biology, Linköping University, Linköping, Sweden, E-mail address chao@ifm.liu.se

Since the pioneering work by Yia-Chung Chang and J. N. Schulman on optical properties of type I and type II superlattices made from zinc-blende materials [1], the broken-gap heterostructures have been investigated extensively. The experiments on the lateral transport and intersubband optical transitions in InAs/GaSb superlattices and InAs/GaSb quantum wells sandwiched by the two wide-gap AlSb barriers grown along the [001] crystal direction discover the unusual electronic band structures with the forbidden energy interval in the in-plane dispersion resultant from the anticrossing and hybridization of electron and hole levels. Such a behavior is because of the bottom of InAs conduction band is below the top of the GaSb valence band. For this reason, the highest heavy-hole level 1hh in GaSb layer can be above the lowest electron level 1e in InAs layer at zero in-plane wave vector. Then the 1hh and 1e levels anticross at some nonzero in-plane wave vector $\vec{k}_{\parallel} \neq 0$ and the hybridization gap is formed between the 1e and 1hh subbands [2]. This hybridization was studied in detail in connection to the transport and optical properties of broken-gap heterostructures. Under a consideration of optical transitions, it was obtained a strong anisotropy of optical matrix elements with respect to different directions of light polarization. The lateral anisotropy of the optical matrix elements and absorption coefficients for the intersubband transitions caused by linearly polarized light is found to be due to effects of bulk inversion asymmetry and specific interface structure described by interface Hamiltonian. However, the absorption coefficients of light polarized along the growth direction are much greater than those for the light polarized in the plane of the structure and depend considerably on electron-hole hybridization.

Because of large values of optical matrix elements for the intersubband transitions between the hybridized 1hh-1e states and the electron-like states in the upper 2e subband in the AlSb/InAs/GaSb/AlSb quantum well for the light polarized along the growth direction, these heterostructures were proposed to use for the infrared laser generation [2]. We have performed here a detailed investigation of the properties of the broken-gap laser of type InAs/AlSb/InAs/GaSb/AlSb/GaSb with n-doped left InAs contact and p-doped GaSb right contact using the eight-band Burt-Foreman envelope function theory and a self-consistent calculation of the Schrödinger and Poisson equations. The electrons from the left contact are injected into the 2e subband states in the well. On the other hand, the electrons from the hybridized 1e-1hh states can transfer effectively into the empty valence band states of the right contact. In this way, we obtained the population inversion between the states of the 2e subband and the 1e-1hh states with the applied bias increasing. We calculated the optical matrix elements and the optical gain in the laser generation regime. We found a giant optical gain for the TM laser modes when the transitions occur between the 2e states and the highest ones from the hybridized 1e-1hh states.

1. Yia-Chung Chang and J. N. Schulman, “Interband optical transitions in GaAs-$Ga_{1-x}Al_xAs$ and InAs-GaAs superlattices”, Phys. Rev. B, 31, 2069, 1985.
2. E. Halvorsen, Y. Galperin, and K. A. Chao, “Optical transitions in broken-gap heterostructures”, Phys. Rev. B, 61, 16743, 2000.

Monte Carlo simulation of submicron three-gate MOSFETs

O. Zhevnyak , V. Borzdov , A. Borzdov, D. Speranski
Belarussian State University, Minsk, Belarus, E-mail: Zhevnyakol@tut.by

Provided success in a miniaturization of active elements of submicron MOSFETs encourages great interest to devices with complex configuration of these elements. The three-gate MOSFETs may be considered as one of the promising transistor construction on basis of silicon technology [1, p.128; 2]. Our work is devoted to investigation of some electric properties of three-gate MOSFETs by means of Monte Carlo simulation of electron transport in these transistors.

In figure 1 the constructive scheme of studied devices is presented. We considered the symmetrical configuration only (i.e. $l_{1G} = l_{2G} = l_{3G} = 0.05$ μm) for transistors with channel length $L_{ch} = 0.2$ μm at room temperature.

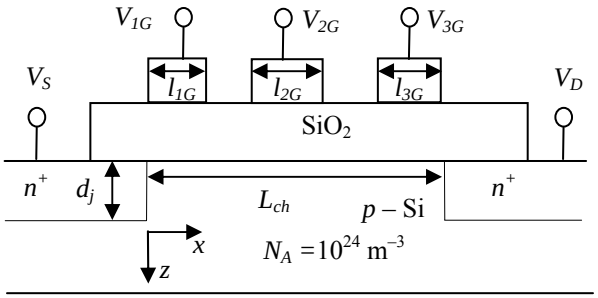

Fig. 1. The studied MOSFETs.

The both Monte Carlo model of electron transport and procedure of self-consistent solution of Poisson equation are the same as in our early works (see, for example, [3; 4]). The influences of bias voltages as well as some constructive parameters of studied MOSFETs on electron transport and drain current in these devices are investigated. It is obtained that by varying of gate voltages and drain junction depth the significant changes of electron properties may be observed. This result proves the necessary of more intensive study of electric properties of three-gate MOSFETs.

In figure 2 and 3 the some of the simulated results are presented for case $d_j = 10$ nm. The curves are corresponded to the following: ***1*** – $V_{1G} = V_{3G} = 2$ V, $V_{2G} = 1$ V, $V_D = 1$ V; ***2*** – $V_{1G} = V_{3G} = 2$ V, $V_{2G} = 1$ V, $V_D = 3$ V; ***3*** – $V_{1G} = V_{3G} = 3$ V, $V_{2G} = 1$ V, $V_D = 1$ V; ***4*** – $V_{1G} = V_{3G} = 3$ V, $V_{2G} = 1$ V, $V_D = 3$ V.

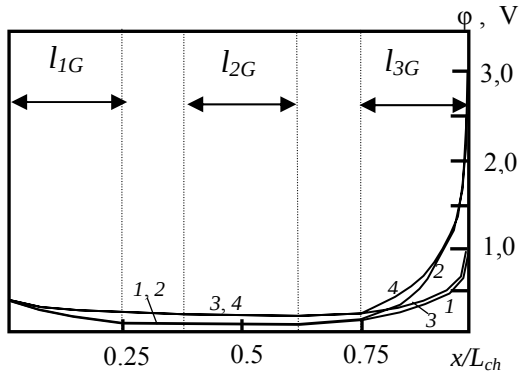

Fig. 2. The electric potential along the channel.

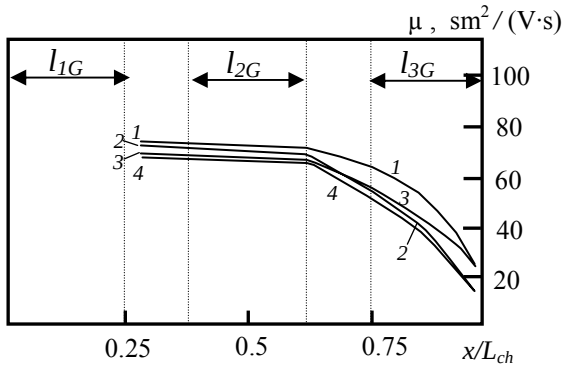

Fig. 3. The electron mobility along the channel.

1. G.Y. Krasnikov. *The constructive and technological features of submicron MOSFETs*. Technosphere, Moscow, Part 1. 2002 (in Russian)
2. W. Y. Choi, B. Y. Choi, D. S. Woo, Y. J. Choi, J.D. Lee, and B.-G. Park, "Side-gate design optimization of 50 nm MOSFETs with electrically induced source/drain", Jpn. J. Appl. Phys. 41/1, pp.2345-2347, 2002
3. V.M. Borzdov, V. O. Galenchik, O. G. Zhevnyak, F. F. Komarov, A. V. Zyazulya, "Ensemble Monte Carlo simulation of submicron n-channel MOSFETs with account of hot electron effect", Proc. SPIE, 5401, pp. 634–641, 2004.
4. V.M. Borzdov, O.G. Zhevnyak, F.F Komarov, V.O. Galenchik. *Monte Carlo simulation of device structures of integrated electronics*. BSU, Minsk, 2007 (in Russian)

SPICE Modeling and TCAD Simulation of Si Vertical Double-Diffused MOSFET

A.V. Sedov[1], V.O. Turin[1], A.M.Tsyrlov[2], and G.I. Zebrev[3]

[1] *Orel State Technical University, Orel, Russia, e-mail:* sedov_a_v@ostu.ru

[2] *JSC "Proton", Orel, Russia, e-mail:* sktb@proton-orel.ru

[3] *National Research Nuclear University "MEPHI", Moscow, Russia, e-mail:* gizebrev@mephi.ru

The Silicon Vertical Double-Diffused MOS field-effect transistor (VDMOSFET) [1] is used widely as a low-voltage switch [2] and continued to be relevant in other applications [3]. In our work we have studied VDMOSFET from optical relay К249КП5Р produced by Proton, JSC, in Orel, Russia. We have used Shichman-Hodges MOSFET compact model for SPICE modeling and the semiconductor drift-diffusion model for 2D isothermal simulations by the finite elements method (FEM) in TCAD Synopsys. By these two methods we have obtained output and transfer characteristics of Si VDMOSFET with good agreement with experimental data. Hence, we make conclusion, that models and computational tools, we have used, are applicable for study of the considered device. By analyzing the results of TCAD FEM simulations, we have found that the high current density in vertical channel of VDMOSFET is a reason for ones specific high on-resistance. Our simulations provide insight into VDMOSFET physics and allow for the device design optimization aimed on the decrease of on-resistance, increase of transconductance, and minimization of an inter-cellar pitch width.

1. A. Blikher. *Physics of power bipolar and field-effect transistors*. L.: Energoatomizdat, 1986 (in Russian)
2. S.C. Sun and J.D. Plummer, "Modeling of the On-Resistance of LDMOS, VDMOS, and VMOS Power Transistors", IEEE Trans. Electron Devices, , vol. 27, no. 2, pp. 356-367, 1980
3. N. Nenadović, V. Cuoco, S. Theeuwen, H. Schellevis, G. Spierings, A. Griffo, M. Pelk, L. Nanver, R. Jos, and J. Slotboom, "RF Power Silicon-On-Glass VDMOSFETs", IEEE Electron Device Lett., vol. 25, no. 6, pp. 424-426, 2004

Modeling of HBT with $Si_{1-X-Y}Ge_XC_Y$ base

K. Petrosjanc , R.Torgovnikov
Moscow State Institute of Electronics and Mathematics, eande@miem.edu.ru

Silicon-Germanium (SiGe) BiCMOS technology is more than 10 years used to produce very high-frequency ICs for variety of consumer electronics – wireless local area networks, automotive radars, cellular phones, optical communications and etc. World-famous companies IBM [1], STM, Sony etc. produce SiGe:C BiCMOS LSIs. For today the peak values of cut-off frequency f_T are about 200 – 230 GHz and the values of 300-350 GHz are expected in nearest future.

The incorporation of low concentrations of carbon into the base region of a $Si_{1-x}Ge_x$ HBT can dramatically suppress boron outdiffusion thus paving the way for further improvements in SiGe HBT performance. The diffusion coefficient of boron in SiGe is reduced by more than one order of magnitude. It leads to reduction of the base region width, and also enables a much higher base doping to be used with intrinsic base resistance value. Highly-doped SiGe:C HBTs in comparison with C-free HBTs demonstrate increased cut-off (f_T) and maximum oscillation (f_{max}) frequencies by 50-70%, and reduced RF noises and ring oscillators delays. Moreover emitter dimensions can be shrunk to reduce power consumption, without loss in RF performance.

In this work we use the Synopsys Sentaurus TCAD system for analysis of SiGe:C structures having potential to complete in analogue, mixed signal, RF power ICs and Systems on a Chip (SoC) where a balance between gain, cut-off frequency and breakdown voltage is necessary. The boron and carbon profiles in SiGe base were obtained to provide a trade-off between gain, cut-off frequency and break-down voltage. High values of f_T x BV_{cbo} product were achieved.

The standard structure of SiGe:C HBT Fig 1 [1] was simulated for different carbon concentrations at a range of 10^{19} cm^{-3} – 10^{20} cm^{-3}. Experimental carbon profile is used as input data in technological simulation and boron diffusivity is corrected according to carbon concentration in base region.

In devise simulation we have used suitable physical models for mobility, bandgap narrowing, avalanche breakdown, Shockley-Read-Hall and Auger recombination. The values of boron diffusivity in SiGe base were determined from experimental data and corrected for every carbon doping level [2].

It was shown that introduction in $Si_{1-X-Y}Ge_XC_Y$ base region low amount of carbon doping y noticeable increases the value of cut-off frequency f_T from 45 to 72 GHz, but at the same time decreases breakdown voltage of collector junction BV_{cbo} from 7.9 to 6.0 V (Table 1.). From the practical consideration the compromise combinations of base width Wb, carbon concentration C, and peak boron concentration N_{BMAX} was chosen to provide high values of cut-off frequency f_T and reasonable values of breakdown voltage BV_{cbo}. High values of f_T x BV_{CB0} product, important for analog and RF power applications, were achieved. The results are in good agreement with experimental data published in [3].

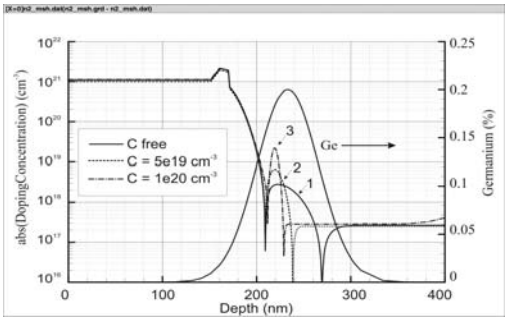

Fig. 1 Simulated doping profiles of SiGe:C HBT for different carbon concentrations in base**.**

Table 1

Carbon concentration C, cm^{-3}	0	$5 \cdot 10^{19}$	10^{20}
Peak of boron concentration in base region N_{BMAX}, cm^{-3}	$3 \cdot 10^{18}$	$7 \cdot 10^{18}$	$3 \cdot 10^{19}$
Base width W_b, nm	60	30	17
DC current gain	90	100	150
Peak of cut-off Frequency f_T, GHz	47	63	72
Collector-base breakdown voltage BV_{CB0}, V	7.9	6.7	6.0
f_Tx BV_{CB0} product	355	420	432

1. B.S. Meyerson, “Silicon:Germanium-based mixed-signal technology for optimization of wired and wireless telecommunications”, IBM Journal of Research and Development, **44**, pp. 391-407, 2000.

2.H. Ruecker, B. Heinemann, “Modeling the Effect of Carbon Dopant on Boron Diffusion”, Proceedings of International Conference Simulation of Semiconductor Processes and Devices, pp. 281-284, SISPAD, -10 Sep 1997.

3.Magnee P. H. C., Hurkx G. A. M., Agarwal P. “SiGe:C HBT Technology for Advanced BiCMOS Processes”, Proceedings of 12th GaAs Symposium pp. 243 – 246, Amsterdam 2004.

Reversible Gate Oxide Defect Recharging in Nanoscale Field Effect Transistors: Charge Annealing, Tunnel Gate Leakage, Random Telegraph Signal and 1/f Noise

G. I. Zebrev, N. Samokhin, D. Batmanova
Micro- and Nanoelectronics Department, National Research Nuclear University "MEPHI", Moscow, Russia,
e-mail address: gizebrev@mephi.ru

It was until the MOSFET gate thicknesses become a few nanometers that the role of the radiation-induced oxide defects has been dramatically changed. In elder technologies with the gate oxide thicknesses of order tens of nanometers the main effect of radiation degradation consisted in buildup of radiation-induced trapped charge and interface traps with accompanying time-dependent relaxation ("anneal") which is known to result in temporal instability of the MOSFET's threshold voltage and transconductance [1]. In modern devices due to the gate oxide thinning this effect becomes negligible. The effect to be dealt with in this report is reversible recharging process due to mutual carrier exchange between the near-interfacial oxide defects and the silicon substrate controlled by the Fermi level position in the Si. This effect is reported in Ref. [2] to be a reason of slow long-term oxide charge relaxation with logarithmic kinetics and fast interface trap reversible recharging. A physics-based rate equation modeling of trap recharging has been developed for the MOSFET devices with ultra-thin gate oxides. The proposed model is shown to describe all effects of slow kinetics (including irreversible logarithmic annealing, 1/f noise, random telegraph signal in nanoscale devices [3], and two-step tunnel gate leakage through radiation-induced defects [4,5]) in a unified manner.

1. V. V. Belyakov, V. S. Pershenkov, G. I. Zebrev, A. V. Sogoyan, A. I. Chumakov, A. Y. Nikiforov and P. K. Skorobogatov, "Methods for the Prediction of Total-Dose Effects on Modern Integrated Semiconductor Devices in Space: A Review", Russian Microelectronics, V.32, pp.25-39, No.1, 2003.
2. V.V. Emelianov, G.I. Zebrev et al., "Reversible Positive Charge Annealing in MOS Transistor During Variety of Electrical and Thermal Stresses," IEEE Trans. Nucl. Sci. V.43(3), 805-809 (1996).
3. M. J. Uren, D. J. Day, and M. J. Kirton, "1/f and random telegraph noise in silicon metal-oxide-semiconductor field-effect transistors," Appl. Phys. Lett.,vol. 47, no. 11, pp. 1195–1197, 1985.
4. L. Larcher, A. Pacagnella et al., IEEE Trans. Nucl. Sci. V.46(6), 1553-1561 (1999).
5. G.I. Zebrev, A.N. Rubantsev et al. "Monte-Carlo atomistic simulation of the gate leakage via tunneling through the oxide defects in nanoscale MOSFETs" (in Russian), MEPHI Scientific Session Proc., V.8, 2008.

Radiation-Hardening-by-Design with Circuit-Level Modeling of Total Ionizing Dose Effects in Modern CMOS Technologies

M. Gorbunov[1] , G. Zebrev[2] , P. Osipenko[1]

1. *Scientific-Research Institute of System Studies, Russian Academy of Sciences, Moscow, Russia, gorbunov@niisi.msk.ru*
2. *Moscow Engineering Physics Institute, Moscow, Russia, gizebrev@mephi.ru*

Modern submicron CMOS ICs are widely used for special applications in ionizing radiation environments. Besides the requirements of high speed operation and low power consumption there are additional demands of low radiation effects sensitivity. High radiation tolerance can be achieved by technology optimization or by design [1]. The former approach is very effective but also very expensive. The latter approach can be implemented on standard commercial technology with high effectiveness and low cost.

Radhard IC designer often needs to compare different hardening methods to increase the effectiveness of the design. Irradiation tests for the whole chip allow estimating the system hardness, but evaluation of the components hardness is much more complicated. Therefore multi-level modeling is essential part of radhard IC design. Multi-level modeling approach involves 3 main levels: physical, circuit (SPICE) and system level. On the first level, radiation effects are modeled with due regard to technology process features. For this purpose many complicated models are developed and 3D simulations are used [2]. It is the most accurate, but the most computationally intensive approach which can not be used for multi-transistor (>10 transistors) circuits. Parameters obtained at physical level can be used for the circuit-level models. These models are usually less accurate and they do not allow obtaining physical process parameters. Nevertheless they can be used for the large circuits simulation and some radiation process parameters can be calculated from electrical characteristics obtained at circuit level [3]. System level operates with "building blocks" from different system hierarchy levels (gates level, register transfer level, etc.). Parameters of each building block (including their radiation effects sensitivity) can be obtained from the circuit level. Hence the circuit level is "the bridge" connecting the physical and system levels.

Standard SPICE models (BSIM, BSIMSOI, EKV, etc.) do not take into account any radiation effects and the integration of physical models to circuit-level simulation still remains a non-solved problem. Designers of radhard ICs often need the effective modeling tool embedded to standard design flow.

Physical model of total ionizing dose (TID) effects previously developed and successfully verified by authors [4] was embedded to BSIM model implemented using Verilog-A language. This tool is fully compatible with standard SPICE simulators (Spectre, UltraSim, HSPICE, ELDO, etc.) and allows taking into account the electrical bias conditions for each transistor during irradiation. Proposed modeling strategy consists of 2 stages. At the first stage radiation parameters of the physical model are obtained from experimental IV characteristics of the test transistors after irradiation. At the second stage obtained parameters values are used for simulation of dose degradation of circuit characteristics. Obtained dose dependencies can be used for system level simulation [5]. This approach was verified using BSIM3v3 and BSIMSOI Spectre models for 0.18 μm CMOS and 0.35 μm SOI CMOS technologies. SPICE modeling results for IV characteristics have excellent correlation with experimental data. Dose dependences of ring-oscillator frequency and gain-bandwidth characteristics of operational amplifier, are qualitatively demonstrated. The radiation-induced parameters mismatch is also clearly obtained.

1. R.C. Lacoe, "Improving Integrated Circuit Performance Through the Application of Hardness-by-Design Methodology," IEEE Trans. on Nucl. Sci., vol. 55, no. 4, August 2008.
2. H.J. Barnaby, M.L. Mclain, I.S. Esqueda, X.J. Chen, "Modeling ionizing radiation effects in solid state materials and CMOS devices," IEEE CICC 2008 Proceedings, pp. 273 – 280, 21-24 Sept. 2008.
3. G.I. Zebrev, M.S. Gorbunov, V.E. Shunkov, *et al.*, "Physical Modeling and Circuit Simulation of Hardness of SOI Transistors and Circuits for Space Applications," RADECS-2006 proceedings.
4. G.I. Zebrev, M.S. Gorbunov, "Modeling of Radiation-Induced Leakage and Low Dose-Rate Effects in Thick Edge Isolation of Modern MOSFETs," IEEE Trans. on Nucl. Sci., vol. 56, no. 4, August 2009.
5. E.O. Mikkola, B. Vermeire, *et al.*, "VHDL-AMS Modeling of Total Ionizing Dose Radiation Effects on CMOS Mixed Signal Circuits", IEEE Trans. on Nucl. Sci., vol. 54, no. 4, August 2007.

Specification of model for the multi-cathode quantum vacuum nano-triode on the base of new experimental data

V. A. Zhukov

St. Petersburg Institute for Informatics and Automation, Russian Academy of Sciences, St. Petersburg, Russia,
E-mail address: valery.zhukov2@gmail.com

In the works [1, 2] the quantum mechanical model explaining the interference oscillations in differential conductivity of the three-cathode vacuum nano-triode [3] has been offered. In the works [2, 4] the model of the vacuum nano-tetrode with possibility of the mode with N- shaped CVC (Current-Voltage Characteristic) has been offered. Out of the later experiments [5, 6] it has become clear that by virtue of specificity of technology the vacuum nano-triode should have not 3 but about 35 nano-cathodes. According to our estimation, from 5 up to 9 of the nano-cathodes can have diameters in an interval of 1.5 ÷ 2.5 nanometers and can give the essential contribution to the common current and CVC of the vacuum nano-triode. Besides that the distances a cathode-grid and a grid-anode can considerably vary. These distances are strongly influencing the operating conditions of the vacuum nano-triode.

In the given work the new model of the vacuum nano-triode is developed. This model is taking into account the greater number (up to 9) of nano-cathodes and a possibility of changing the distances a cathode-grid and a grid-anode. It is shown that the mode with N-shaped CVC could be easily obtained not only in the vacuum nano-tetrode [4] but also in the vacuum nano-triode by means of a little changing the initial geometry of experiment [3]. This happens at performance of a ratio

$$U_g / U_a = (z_g - z_k)/(z_a - z_k) \quad (1)$$

here the values Ug, Ua are potentials on a cathode, on a grid and on an anode, respectively. Values Zk, Zg, Za are coordinates of cathode, grid and anode, respectively. The taking into account of the greater number of nano-cathodes allows to obtain not only qualitative but also the quantitative consent with experiment [3]. As experiment [3] is reproduced on series of samples, the multi-cathode vacuum nano-triode with N-shaped CVC might be used as the switch in the radiative-steady circuits of the integrated vacuum nano-electronics.

This work is supported by the Program of Presidium of Russian Academy of Sciences within framework of the research initiative “The base of fundamental research of nanotechnology and nano-materials”.

1. V. A. Zhukov, “Theory of the Vacuum Nanotriode, Part 1: Explaining the Results of an Experiment”, Russian Microelectronics, **34**, No. 2, pp. 103–110, 2005.
2. V. Zhukov, “Numerical simulation of quantum vacuum nanotriode. Opportunity of quantum interferometers development on metal rings at room temperature”, Proc. SPIE, **5833,** p. 47, 2005.
3. A. A. G. Driscill-Smith, D. G. Hasko, and H. Ahmed, “Quantum interference in vacuum nanotriode” J. Vac. Sci. Technol. **B 18**, pp. 348, 2001.
4. V. A. Zhukov, “Theory of the Vacuum Nanotriode, Part 2: The Possibility of Negative Transconductance”, Russian Microelectronics, **34**, No. 4, pp. 222–228, 2005.
5. A.M. Blackburn, D.G. Hasko, D.A. Williams, “Improved nanotriode fabrication process for multiple gates and reduced leakage current”, Microelectronic Engineering, **73–74**, pp. 797–802, 2004.
6. A.M. Blackburn, D.G. Hasko, D.A. Williams, “In-Vacuum Resonant Tunneling in the Nanopentode”, Abstract of IVNC’ 2005.

The specifics of modeling high-speed integrated amplifiers with high amount of feedback

E.M. Savchenko, A.S. Budyakov
FSUE "Science and Production Enterprise "Pulsar" Moscow, Russia, pulsar@dol.ru

Traditionally the design of low-frequency integrated circuit of amplifiers with high gain (50-100 dB) that are used with high amount of negative feedback is the modeling of schematic and topography of a chip. The specifics of such IC is the necessity to use external feedback circuits, that's why designing of IC with frequencies 500 MHz and more faces the necessity to consider not only IC chip, but also the chip-package system altogether.

One of the main technologies of electric contact between the chip and the package is the wire bonding technology. Wire connections of the IC package is characterized with inductance of several nH and high Q-factor. However the parameters of such inductance depend on reproducibility of technological process, that needs to consider manufacturing tolerance while creating a model.

To create a model of IC package one uses CAD tools of electromagnetic analysis, that allow to calculate S-parametrs of a 3D package model. This kind of modeling is totally the same as real measurements, that's why it's important to consider not only 3D package model, but also mounting elements to measure real parameters of the package. This is important for obtaining correct measurement results and to verify the model. The analysis results in terms of S-parameters convert then into a model with lumped parameters, which is more efficient by schematic time-domain modeling.

In this work one compares the results obtained using different approaches of modeling of amplifiers with high gain and are discussed the specifics of IC package model creation and verification.

Formation of Ge/Cu ohmic contacts to *n*-GaAs with atomic hydrogen pre-annealing step

E. Erofeev[1], V. Kagadei[2]
1 Scientific Research Institute of Electrical Communication Systems, Tomsk, Russia, erofeev@sibmail.com
2. Research and production company "Micran", Tomsk, Russia, vak@micran.ru

Recently the demand for microwave GaAs *p*-HEMT monolithic integrate circuits (MMIC) increases in the high frequency applications such as space communications, auto radar, all whether landing and imaging (50–300 GHz). To enhance the high frequency performance, it is essential to have short gate lengths on nanoscale level (90–70 nm). To this end, thin ohmic metal system with good edge definition is required for the exact gate alignment with E-beam nanolithography. The conventional NiGeAu ohmic contact has been widely used for *n*-GaAs devices. However, due to the inhomogeneous reactions between GaAs and NiGeAu layer, the contact may have a high contact resistance, poor thermal reliability and a rough surface morphology. The Pd/Ge system has been proposed as an alternative contact scheme on *n*-type GaAs. In comparison with the AuGeNi ohmic system, the PdGe-based ohmic contact has a better surface morphology and a better contact edge definition, but the contact resistance degraded after isothermal annealing due to As out-diffusion [1]. Thermal stability of the Pd/Ge contacts has been improved using several overlayers such Ti/Au, Ti/Pt/Au, Ti/W by suppression of the As out-diffusion. However, in the nanoscale gate length process, this thick ohmic contact may induce a poor edge definition after alloying which can cause to the problem such as gate misalignment. Recently, was found [2] that thin films of Cu_3Ge compound forms an ohmic contact to *n*-type GaAs with a low specific contact resistivity, high thermostability, excellent surface morphology and contact edge definition. All these results suggest a great potential of Cu-Ge alloys for nanoscale GaAs MMIC.

The work purpose is investigation of the opportunities of the Ge/Cu ohmic contacts improvement by introduction of the pre-annealing step in atomic hydrogen into the process flow.

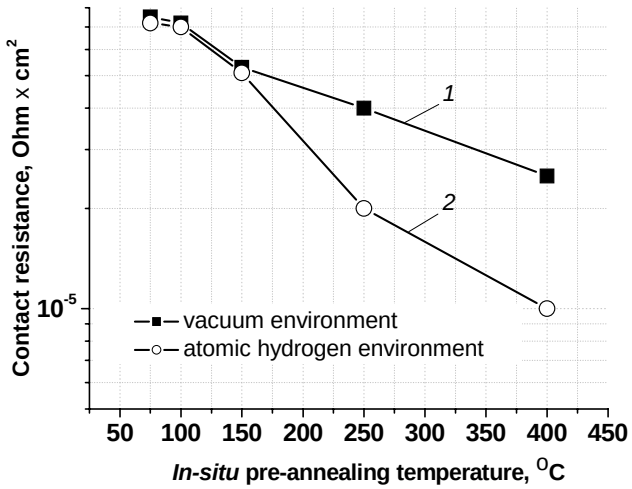

Fig.1. Dependence of the specific contact resistance of Ge/Cu ohmic contacts versus the *in-situ* pre-annealing temperature (t = 30 min) in vacuum (1) and atomic hydrogen (2) environment.

The Si-doped samples *n-i*-GaAs ($n \cong 2\times10^{17}$ cm^{-3}, d = 0.12 μm) were used in experiments. For the GaAs native oxides removal the samples were processed in H_2SO_4 (1:10) water solution within 3 min. Contact layers of Ge/Cu with Ge concentration ranging from 20 to 45 at.% were prepared by depositing a Ge layer first followed by a Cu layer by the electron beam or the thermal evaporation methods in a vacuum with a base pressure 10^{-6}–10^{-7} torr. Then pre-annealing was carried out *in situ* in the deposition chamber in a pressure of 10^{-6}–10^{-7} torr in atomic hydrogen flow $5\times10^{15}cm^{-2}s^{-1}$ at temperature T = 60–400 °C during time t = 1-60 min. After lift-off process for the ohmic contact topology formation the samples were *ex-situ* annealed by the rapid thermal annealing (T = 320–460 °C, t = 30–300 s). Specific contact resistance ρ was measured by the TLM method.

That have been shown, that *in-situ* pre-annealing with atomic hydrogen of Ge/Cu ohmic contacts allows to reduce the minimal value of the specific contact resistance by factor 2–2,5 (fig. 1). The peculiarity of the novel process of the ohmic contact formation has been considered. The problems of the contact pads edge definition and the mechanism responsible for discovered phenomenon has been discussed.

1. E. D. Marshall, B. Zhang, L. C. Wang, P. F. Jiao, T. Sawada, "Microstructure studies of PdGe ohmic contacts to n-type GaAs formed by rapid thermal annealing", J. Appl. Phys, **62**, p. 942, 1987
2. M. O. Aboelfotoh, S. Oktyabrsky, and J. Narayan, " Electrical and microstructural characteristics of GeCu ohmic contacts to *n*-type GaAs", J. Mater. Res., **12**, 9, pp. 2325 – 2332, 1997

Hf-based barrier layers for Cu-metallization

Denisenko Yu.I.[1], Gusev V.N.[1], Khorin A.I.[1,2], Orlikovsky A.A.[1], Rogozhin A.E.[1], Rudakov V.I.[1], Vasiliev A.G.[1,3]

1. *Institute of Physics and Technology, Russian Academy of Sciences, Moscow, Russia, ellipsoid@yandex.ru*
2. *Moscow State Institute of Radio-engineering, Electronics and Automation, Moscow, Russia, horin@ftian.ru*
3. *Federal State Unitary Enterprise "Scientific & Product Enterprise "Pulsar", Moscow , Russia*

It is well known that due to interaction between Cu and Si in the regions of source and drain copper interconnections should not be in direct contact with Si. Now the barrier function is performed by TiN_x layers. However this material has some drawbacks: Ti absorbs oxygen during deposition, it requires rather large concentration of N and layer of TiN_x should be quite thick to assure low diffusion of Cu. In this study the barrier properties of Hf-based thin films were investigated. Hafnium nitride films (15nm) and multilayer Hf-Si structures (50 alternate 0,2 nm-Hf and 0,4 nm-Si layers) were prepared by electron beam evaporation. Hf-Si sandwiches were annealed at 700ºC and 900ºC for 2 min to form silicide. Then 100 nm thick copper layers were deposited on the samples. For the $Cu/HfN_x/Si$ contact system the interfacial reactions between Cu, Hf and Si were observed after annealing at 500ºC for 30 min by profile Auger analysis. The HfN_x barrier fails and Cu atoms penetrate into the Si substrate. On the other hand Auger analysis results for $Cu/HfSi_x/Si$ structure showed that there were not diffusion of Cu atoms in barrier layer and Si substrate. Findings demonstrate that hafnium silicide barrier layers can be used to prevent interfacial reactions between copper interconnections and silicon regions of source and drain.

Properties of HfO_2 films on Si-substrate obtained by electron beam vapor deposition

A.V. Ershov, S.N. Zubkov, V.V. Karzanov, S.V. Khazanova, O.N. NIkolaeva, D.A. Nikolichev

Nizhni NovgorodUniversity im.N.I.Lobachevskogo, NIzhni Novgorod, Russia,
ett@phys.unn.ru

High-*k* dielectrics are nowadays being subject of great study in order to replace SiO_2 in metal-oxide-semiconductor field-effect transistor. HfO_2 is among the most promising of such materials. However properties of this technologically important material have not sufficiently investigated up to now. In particular the many questions are challenged about quality of the interface with Si-substrate, thermodynamic stability in contact with Si.

This report is devoted to investigations of films properties HfO_2, obtained by electron beam vapor deposition. As substrate we use Si –plate KEF-4.5 и KDB-12, previously cleared out from native oxide. For exception of atmosphere effects layer of SiO_2 covers surface of the films. The annealing of the structures was conducted under nitrogen ambient in a wide range of temperature (500-1100°C) in typical tube reactor for 30 min. We performed detailed investigation of obtained samples using photoluminescence (PL), EPR, XPES diagnostic methods.

Analyzing the data from different investigations, we suppose following description. The main type of defects in as-deposited films is oxygen vacancies, which keep their concentration at the thermal treatment up to 800°C. Our results show that interface Si-HfO_2 enclose paramagnetic centers with surface density about 10^{14} $см^{-2}$ related to dangling Si-bonds. Ordinary annealing processes result in chemical reaction between HfO_2 and interface materials. While Si-HfO_2 interface is sufficiently stable, region of SiO_2-HfO_2 during annealing transform to hafnium silicate. Besides during the thermal treatment at the temperature of 500-800 °C the films have tendency to appearance of HfO_x nonstoichiometric complexes. It is supposed they are responsible for PL band in the range of 500-600 nm which peak has red shifting with increasing of annealing temperature. The annealing at 800-900°C leads to more stable interface and to reduction of PL. At the same time state density on the Si-HfO_2 interface decreased more than on the order. One can assume that cleaning out of the native oxide from substrate allow to get stable interface Si-HfO_2. It should be noted that thermal treatment at the temperature over 1000 °C has no affect to the properties of our structures.

Some peculiarities in the formation functional films by sol-gel and electrophoretic technologies

N. Korobova[1], S. Timoshenkov[2] , A.Shabanova[3]

1.Kazakh National University, Almaty, Kazakhstan. korobova3@mail.ru; 2. Moscow Institute of Electronic Technology, Moscow, Russia, spt@miee.ru; 3. National Engineering Academy, Almaty, Kazakhstan.

The development of new improved type of functional films on the conception of multiphase structure has been carried out in this paper. Metal alkoxide solutions were used for application of thin films by electrophoretic deposition technique. We succeeded in preparation of amorphous, crystalline and composite films. Specific features of the preparation technique were considered. Microstructure of the films was examined as well as their physical properties. TEM analyses reveals that films deposited from aging sols and heat-treated at temperatures 300 - 400 °C contain small whiskers and nanocrystallites. The alteration in crystallization behavior of Al_2O_3 whiskers was discussed in terms of aging starting sols before electrophoretic deposition. In the second part of the report superconducting and piezoelectric ultra-fine uniform film preparation has been discussed. Thick film fabrication of high temperature oxide superconductors is one of the most important techniques for the extensive applications of these materials. For the development of polycrystalline conductors for high-current electric power transmission, YBCO and BSCCO compounds in the form of thick films have been identified through microstructural characterization as having the proper local crystallographic texture and grain boundary orientation for strongly linked current. The apparent metastability of all the superconductors in the YBCO and BSCCO systems could become an important consideration in optimizing routes for their preparation and processing at low temperature. We report the results of experiments in which a small amount of organic binder is added to the HTS layer, with a consequent reduction in crack formation and an increase in J_c. Our present study concerns the roles of an organic polymer poly(ethylene glycol) (PEG) as chemical modifier in the precursor for coating formation. HTS coatings were deposited by electrophoresis method on Ag wire at 150- 250 V/cm and 60-120 s. After the coatings were dried at 100 ^{0}C, they were heated slowly (at a rate of 2 ^{0}C/min) up to 800 - 850 ^{0}C in the air [1]. Microstructures of these films were examined by scanning electron microscopy (SEM) and by transmission electron microscopy (TEM), and XRD was used to investigate crystal-structure development. In the third part we want to report about a newly developed sol-gel process to synthesize dense YBCO thick films with $BaTiO_3$ additives and BSCCO films with PbO additives using electrophoretic deposition and metal alkoxide sol/particle suspensions. We successfully produce dense (YBCO+ $BaTiO_3$) and (BSCCO + PbO) ceramics at rather low temperatures, compared with the sintering temperatures used in conventional methods. The thick films of HTS were prepared by electrophoretic deposition, using pre-sintered powder with barium titanate addition in the form of $BaTi(OR)_6$ solution and oxide in the form of $Pb(OR)_2$ in suspensions for electrophoresis. The conditions for applied voltage and deposition times for electrophoretic deposition of HTS thick films were studied in detail [2]. To summarize, the aging time of the solution affects the grain size: the longer the solution is aged, the bigger the grains. Prolonged firing times produce larger grains and pores, suggesting that grain growth and pore coarsening take place at the same time. This preliminary report represents the beginning of more extensive studies into the variety of organic additives and applications. Many experiments are in progress to decrease the width of the superconducting transition, the morphology of the films, and the application of organic additives. The electromagnetic properties can be improved by increasing the magnetic flux pinning effects with $BaTiO_3$ or PbO additions and increasing the dimensions of grains in order to reduce the detrimental influence of grain boundaries.

1. N. Korobova, A. Lavrisheva, A. Shabanova, S. Timoshenkov, O. Jharkova, " Preparation Peculiarities of Superconducting Films" - Int. Conf. of Korea Institute of Maritime Information & Communication Sciences (ICKIMICS 2009), 24-29 June, 2009.p.10

2. Patent RK N20707 " Method of high temperature superconducting coating preparation", N. Korobova, T. Ketegenov, O. Tyumenceva. Publ. in Bulletin N1 (05.01.2009)

The peculiarities of creating composite glasses for multilayer structures, MEMS structures included

S. Timoshenkov [1], O. Orlov O.[2]

1. *Moscow Institute of Electronic Technology, Moscow, , Russia, E-mail spt@miee.ru*
2. *Mikron JSC, Moscow, Russia, E-mail o_orlov@mikron.ru*

The main requirements for glass-like materials used in producing multilayer structures, MEMS structures included are:

- Surface wettability and sufficient adhesion;
- Chemical resistance /water-resistance/
- Heat resistance
- Stability of characteristics
- Closeness of the glass and the semiconductor coefficient of expansion (α)
- Phase composition stability.

The factors influencing the process are:
Temperature /T/, time /τ /, pressure /p/, viscosity /η/, the state of surface, the surface energy /the energy of interaction/, wettability and adhesion, activators, catalysts, pollutants [1,2]. These main parameters are governed by the following equations:

$$\lg \tau = A_1 + \frac{B_1}{T_1} \qquad \lg p = A_2 + \frac{B_2}{T_2} \qquad \lg \eta = A + \frac{B}{T},$$

where A_1, B_1, A_2, B_2 A, B are constants.

This paper presents the study of the layers based on composite glasses $BaO\text{-}Al_2O_3\text{-}SiO_2$ and $B_2O_3\text{-}SiO_2$. To obtain films based on glass, targets pressed from powder were used with powder particles size of 0.1 mkm. The powder was synthesized in high frequency induction plasma with the subsequent powder sputtering on wafer using the method of high frequency magnetron sputtering (or depositing 3 - 20 mkm thick glass layers on silicon wafer by pulverization. It results in a loose porous layer, and the following annealing at the temperature of 1200°C is necessary).

It should be noted that these glasses can be used for producing SOI structures. In this case the mechanisms of joining are:

Mechanical adherence,
Components diffusion,
Chemical interaction,
Embedding of the elements into the glass structure and formation of new bonds,
Formation of a new phase.

It is demonstrated, that obtained glass layers $BaO\text{-}Al_2O_3\text{-}SiO_2$ display sufficient adhesion; Coefficient of expansion and silicon coincidence in the temperature range of 20-400°C, heightened temperature span (the temperature of the beginning of deformation being 850°C), chemical resistance /can be etched only in the solution of HF/; their inductive capacity K=12 and they demonstrate stable characteristics and phase constitution. Obtained glass layers display sufficient adhesion; KTLE and silicon coincidence in the temperature range of 20-300°C, intermediate temperature span (the temperature of the beginning of deformation being 400°C), they demonstrate decreased chemical resistance /can be etched in the solutions of acids and H_2O/; their inductive capacity K=8 and they demonstrate stable characteristics and phase constitution.

Glass-like system	Components content by analysis, mol %	$\alpha \cdot 10^{-7}$, degree^{-1}, (in the temperature interval °C)	Tg, °C
$BaO\text{-}Al_2O_3\text{-}SiO_2$ $B_2O_3\text{ - }SiO_2$	9 BaO - 12 Al_2O_3 - 79 SiO_2 39.26 - 44.55 B_2O_3	33 (20 -400) 43 (20 -300) - 49 (20 -300)	850 400

1. S.M. Sze. *Physics of Semiconductor Devices.* John Willey and Sons, New York, 1981
2. B. Bogdanovich and others *Technologies and research procedures of SOI structures* , Moscow, 2003, pp.181-201

Electron Beam Lithography using PMMA as negative resist

E.N. Zhikharev, S.N. Averkin, V.A. Kalnov
Institute of Physics and Technology of Russian Academy of Science, Moscow, Russia, E-mail zhikharev@ftian.ru

PMMA is commonly used as a positive electron resist. In this case the electron beam irradiation causes molecular chain break and developer can remove the irradiated area of the PMMA film. At the same time the cross-links of polymer molecules occur and a hard insoluble material appears. At lower doses the scission of molecular chain dominates, at dose of 2-3 order higher polymerization process dominates. It was proposed (1) that at high doses better resolution of resist can be achieved. In (2) the resolution of PMMA as negative resist was shown about 12 nm. So, in spite of the fact that PMMA as negative resist demonstrates very little sensitivity, it can be used for creation of principal parts in modern electron beam nanotechnologies. To exactly transfer the image of feature into the underlying layer it is necessarily to know the feature profile (usually line profile).

This work is devoted to scanning electron microscopy study of line profiles formed in PMMA as negative electron resist and transferring such lines into the metal layer. The structures (series of lines) were produced in resist on silicon plates and on silicon plates coated with composition of 100nm silicon oxide and 40nm tungsten. The lithograph Raith-150 was utilized for such purpose. The direction of lines orientated perpendicular to one of the crystallographic direction in substrate. The line were formed long, the length was 1mm in order to successfully chip the plate and to study the structure profile in SEM. The beam focusing on the silicon plate was better than one on the composition with oxide due to charging effect in oxide. At least 5nm focusing accuracy for only silicon and 15nm for composition with oxide were provided. Resist thickness varied in 50-80nm range. After the exposure the samples were developed in common developer for PMMA MIBK:IPA=1:3. The area of about 1 micrometer around the created line was exposed by scattered electrons with the dose suitable for positive developing during the exposing of the central line with the dose forming negative image. This makes the developed structures visible without microscope and helps to chip the wafer correctly. Beam energy was 10 keV, dose about 300 times to necessary one for positive exposure.

The obtained line profile of PMMA is represented in Fig.1. The walls of line profile are almost vertical, such form of line is perspective for plasma etch process through this mask.

The profile of partially etched tungsten film with negative PMMA mask similar to line in Fig.1 is represented on Fig.2. To study the degradation rate of mask the etching was interrupted when part of PMMA line left. It can be seen that at this stage of etching the polymer height decreased from 80 to 26nm, 27nm of tungsten were etched. The line width slightly decreased due to etching of sidewalls.

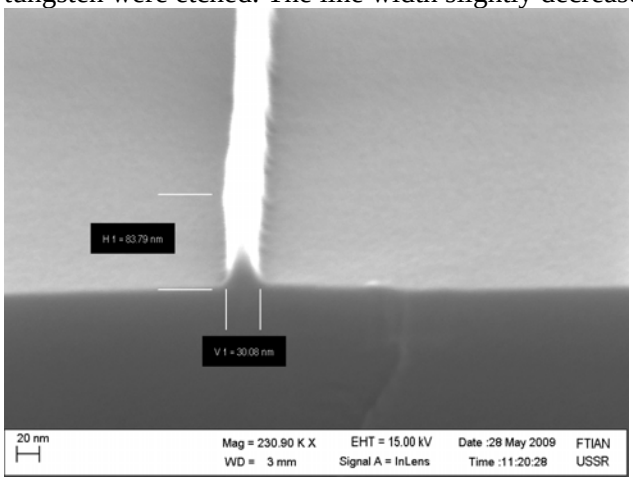

Fig.1 The cross-section of the line produced from PMMA as negative resist.

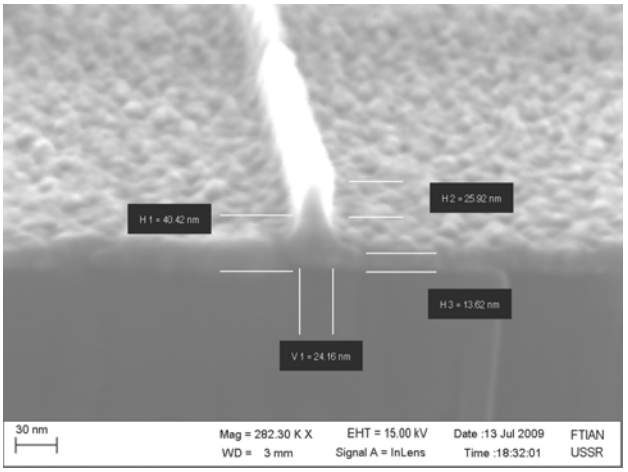

Fig.2 The cross-section of the line produced by plasma etching of tungsten using negative PMMA line as a mask.

1. Everhart T E *Materials for microlithography (ASC Symp Series 266)*, ed L F Thompson, C G Wilson and J M J Frechet, pp 5-10, 1984
2. A C F Hoole, M E Welland A N Broers "Negative PMMA as a high-resolution resist-the limits and possibilities" Semicond. Sci. Technol. **12** 1166-1170 1997.

Application of virtual scanning electron microscope to determine the parameters of atom nanolithograph microlenses

A. Zablozkiy[1], E. Shehin[1], A. Kuzin[1], A. Baturin[1], P. Melentiev[2], D. Lapshin[2], V. Balykin[2]

1. *Moscow Institute of Physics and Technology, Dolgoprudny, Russia, zalexx@gmail.com.*
2. *Institute of Spectroscopy Russian Academy of Sciences, Troitsk , Russia, melentiev@isan.troitsk.ru*

Atom nanolithography technique based on an atom pinhole camera [1] allows making nanostructures with typical sizes less then 50 nm. In atom pinhole camera beam of neutral atoms passes through a metal mask with the given geometry (typical structure sizes $\boldsymbol{Z}$ = 20 - 200 micrometers), forming a "luminous object". Atoms passed through the mask come to membrane placed at a distance $\boldsymbol{L}$ = 5 cm form the mask. This membrane is located at a distance $\boldsymbol{l}$ = 5 microns from the substrate and contains a large number of identical "microlenses" – holes with diameter $\boldsymbol{z}$ = 20 – 200 nm. Each of the microlenses forms individual image of "luminous object" on the substrate with "reducing power" $\boldsymbol{M} = \boldsymbol{L}/\boldsymbol{l} = 10^4$ times. As a result, array of identical nanostructures is formed on the substrate. Array of microlenses is created in the 50 nm thick Si_3N_4 films (Ted Pella Inc.) by focused ion beam microscope Quanta 3D DualBeam (FEI Co.).

Characteristic (critical) dimension of these nanostructures depends of the microlenses parameters. In order to create structures with a characteristic size less than 50 nm, microlenses also must have a diameter less than 50 nm. Thus *in-situ* determination of the microlenses parameters is necessary for operative technology control. However size of the microlens is comparable to the effective size of electron probe of SEM that leads to a discrepancy between the measured parameters of the microlens and their true values [2].

In some cases it is possible to overcome that difficulty by complementing the result of SEM measurement with the data obtained by simulation of these measurements. This approach is called "virtual scanning electron microscope" [3]. The proposal is to complement common order of measurements ("object – measurements – experimental image of the object – parameterization of the object image – object model – parameters of the object model") by the following sequence: "parameterized model of the object – simulation of measurements – simulated image of the object – parameterization of the simulated image – comparison between parameters of the simulated image and the experimental one – fitting parameters of the object model to get a better coincidence of image parameters – reliable parameters of the object model".

This approach allows determining form of the microlens and its parameters – the value of the top and bottom diameter. Application of the proposed approach has allowed adjusting parameters of microlenses membrane and atom pinhole camera. It leads to significantly improvement of nanostructures' parameters (critical dimension, homogeneity) created by atom nanolithography. As a result minimum stable characteristically dimension of these structures have been reduced to 30 nm.

1. P.N. Melentiev, A.V. Zablotskiy, D.A. Lapshin, E.P. Sheshin, A.S. Baturin, V.I. Balykin "Nanolithography based on an atom pinhole camera", Nanotechnology. V. 20, N. 23, 235301, 2009
2. Yu.A. Novikov, A.V. Rakov "Secondary electron emission of relief surface of solid body", Proceedings of Prokhorov General Physics Institute of Russian Academy of Sciences, 55, pp. 3-99, 1998
3. A.V. Zablotskiy, A.S. Baturin, V.S. Bormashov, R.M. Kadushnikov, N.A. Shturkin "Computer simulation of scanning electron microscope for nanometrology", Russian Nanotechnology, N 2, pp. 40-48, 2007

Features of relief formation at silicon surfaces by etching with focused ion beam

N. Gerasimenko[1], A. Chamov[1,2], E. Novoselova[2], V. Khanin[2]
1. Moscow Institute for Electronic Engeneering, Moscow, Russia, rmta@miee.ru.
2. JSC Mikron, Moscow, Russia.

The unusual changes of a relief of etched profile were formed out during etching of singlecrystal silicon by the focused ion beam [FIB]. Especially, periodic ledges, which shape depending on parameters of ion beam (density and scanning modes) were generated on those walls along the depth of an etched profile.

Probably the formation process of periodic structure is connected with that the ion beam is not absolutely perpendicular to a surface of wafer and during profile formation falls on wall surfaces at small angle. For checking this assumption, deviation of ion beam from normal to irradiated surface has been realised so that at the beginning beam arrives at the one of walls by small angle. It is visible original formation of periodic profile is taking place that exactly on this wall.

Represented results are compared with those of series published in a world literature for formation of periodic nanostructures by irradiation of silicon surface at small angels [1]: in both cases parallel located periodic structures which represent alternation of ledges and hollows are generated.

As for our understanding existing in a world literature explanation of this effect based on anisotropic sputtering of surface are not quite correspond to the facts. We propose another explanation of this observable phenomenon.

It is well known that change of mechanical properties of material occurs under radiation treatment is in consequence of radiation-stimulated viscous flow which appearance caused by introduction of radiation structural defects. This phenomenon can be more expressed by influence of dense flow of accelerated particles (FIB). In this case observable effects can be compared with nature phenomena in liquid and loose environments: sea ripples, barkhans in desert.

1. E. Chason, M.J. “Aziz Spontaneous formation of patterns on sputtered surfaces”, Scripta mater., V. 49. – No 10, pp.953-959, 2003

Modification of electrophysical behavior of surface adjacent to FIB milling area

A.A. Chouprik, A.A. Kuzin, A.V. Zablotskiy
Moscow Institute of Physics and Technology, Dolgoprudny, Russia,
E-mail: chouprik@ckpmipt.ru

The focused ion beam (FIB) microscope has gained widespread use in fundamental materials studies and technological applications over the last several years because it offers both high-resolution imaging and flexible micromachining in a single platform [1]. FIB can do direct fabrication or patterning by controlling ion exposure locally. In comparison with optical lithography, the advantage over the focused ion beam (FIB) is that it can produce arbitrarily shaped patterns with height variations on the sample without expensive masks and multiple processes. FIB patterning saves processing steps and time, and it can be exploited to develop prototypes of micro- and nanoelectronic devices. One of the important applications of FIB milling is fabrication of multilayer metal-oxide-semiconductor structures for investigation of electrophysical properties of gate insulator. The continued scaling of electronic devices to smaller and smaller size faces the problem of the replacement of the conventional SiO_2 gate insulator with a high dielectric constant (high-*k*) oxide. In next generation complementary metal-oxide-semiconductor devices, the high-*k* candidate must have a SiO_2-free interface with the semiconductor. Multilayer metal-oxide-semiconductor structures based on different oxides with small lateral size may be created by FIB milling of extensive multilayer samples. But processing of materials using a kiloelectronvolt FIB often result in undesirable consequences impairing quality of made structures including the nano-modification of materials surface adjacent to FIB milling area through deposition, amorphization, implantation, and sputtering. Electron-beam induced current, scanning ion microscopy, electron energy-loss spectroscopy, X-ray energy dispersive spectroscopy et al. are used for investigation of surface modification. Atomic force microscopy is one of the most appropriate tools for such investigations for its high spatial resolution and nondestructive analysis. Spreading resistance method and Kelvin probe microscopy (KPM) are used for analysis of electrophysical behavior modification of surface adjacent to FIB milling area of metal-oxide-semiconductor structures.

Focused Ga^+ ion beam milling of Ag(50 nm)/SiO_2(10 nm)/Si and Ni(25 nm)/ HfO_2(4 nm)/SiO_2(1 nm)/Si [2] structures was carried out using FEI Quanta200 3D SEM/FIB dual beam workstation. Localized milling was achieved using bitmap file control. The beam overlap and dwell time are defined as 50% and 3 µs, respectively.

The measured by KPM surface potential maps (fig. 1) are associated with variation in the contact potential difference (CPD) at the specimen surface. KPM measurements reveal that irradiation/implantation with the focused Ga^+ ion beam induce not highly localized modification of the CPD within the previously homogeneous top layers. Significant characteristic differences in the CPD are observed on samples processed by FIB with different parameters of influence. The measured by spreading resistance method current maps are associated with variation in the conductance at the specimen surface. Comparison of CPD and current maps for samples processed by FIB with different parameters of influence give important information about electrophysical behavior of surface adjacent to FIB milling area.

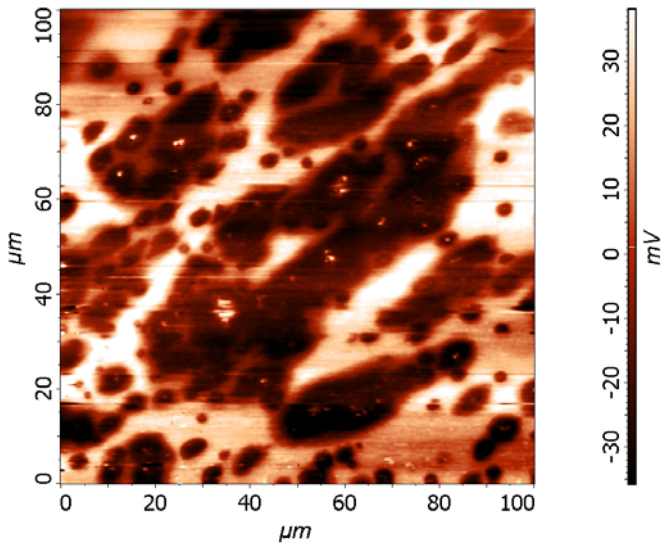

Fig.1. Surface potential distribution over surface of Ag film of Ag/SiO_2/Si structure adjacent to FIB milling area

1. C.A.Volkert, A.M. Minor, MRS bulletin, 32, pp. 389-399, 2007
2. Yu. Lebedinskii, A. Zenkevich, E. Guseva, J. Appl. Phys. 101, pp. 074504, 2007

Formation of buried borosilicate layers by means of ion implantation

A. Churilov, S. Krivelevich, R. Seljukov
Yaroslavl branch of Physicotechnological Institute, Russian Academy of Sciences Yaroslavl, Russia,
S.Krivelevich@mail.ru

One of a possible ways of silicon on insulator (SOI) technology development is ion synthesis of buried dielectric layers of desired composition. This method is the further development of a traditional SIMOX and ITOX processes [1]. Such layers application allows eliminating of some of these technologies shortcomings. The main of them is expensiveness of SOI structures caused by large doses of oxygen implantation and high temperatures of post-implantation heat treatment. Earlier it was shown [2] that temperature and implantation dose reduction is possible if dioxide layer is replaced by the buried layer of silicate glasses, in particular by layers of borosilicate and phosphorosilicate glasses. Application of such glasses reveals new opportunities for element base advancement of modern MIS LSI and the LSI of the next generations.

In present work the properties of structures formed by oxygen and boron implantation in silicon were investigated. For samples preparation the implantation of O_2^+ into (100) Si substrates with energy 300 keV and doses $1{,}2\cdot10^{17}$ sm^{-2}, $2\cdot10^{17}$ sm^{-2}, $3{,}4\cdot10^{17}$ sm^{-2} was carried out. Afterward the wafers were annealed at temperature 900°C in the environment of dry oxygen during 5 minutes. Then boron implantation was carried out at energy of B^+ ions – 100 keV, at implantation dose - $8\cdot10^{16}$ sm^{-2}. The implanted wafers were repeatedly annealed at 900°C in the environment of dry oxygen. Then annealing was repeated at temperature 1050°C. Oxygen and Si depth distribution was detected by means of electronic Auger-spectroscopy. Besides the concentration distributions of boron was measured by SIMS depth profiling.

The obtained structures were studied also by IR-spectroscopy method. Measurements of IR absorption spectrum were performed at Fourier-spectrometer IFS-113v at a room temperature in the range of wavenumbers 4000 – 400 sm^{-1}. Silicon substrates with the films of borosilicate glass were used as reference samples. All basic bands, characteristic for borosilicate glass films are observed on the sample implanted by O_2^+ with a dose of $3{,}4\cdot10^{17}$ sm^{-2}. However, the absorption bands corresponding bridge bond Si-O-Si oscillation (ν=1100 sm^{-1}, ν=810 sm^{-1}, ν=455 sm^{-1}) were slightly broadened in comparison with reference sample. The amplitude ratios of these bands also differ from amplitude ratio observed for reference samples. The bands corresponding to valence oscillations B-O and B-O-Si bonds were less pronounced. At the same time the results of Auger analysis reveal that the buried layer with nearly constant through depth concentration of oxygen and Si is formed by implantation of $3{,}4\cdot10^{17}$ sm^{-2} O_2^+ dose and further annealing. Width of this layer makes about 70 nm, and a concentration ratio of elements approaches to stoichiometric ratio corresponding SiO_2. It allows to assert that at implantation of molecular oxygen dose $3{,}4\cdot10^{17}$ sm^{-2} into silicon and its annealing at temperature 1050°C the buried layer of borosilicate glass is formed.

Reduction of an implantation dose of molecular oxygen to $2\cdot10^{17}$ sm^{-2} does not result in essential changes of spectra form in comparison with samples of the previous series. It is noteworthy that bands related to B-O and B-O-Si bonds oscillation in these spectra are weaker. At the same time the measurements carried out by means of electronic Auger–spectroscopy have shown that in this case the oxygen concentration in the implanted layer is less stoichiometric and approximately amounts 33 at. %. SIMS measurements of boron concentration distribution in the implanted samples have revealed that it practically does not depend on a dose of implanted molecular oxygen. The maximum boron concentration in all cases remains almost constant and makes about $4{,}5\cdot10^{16}$ sm^{-3}. It is quite admissible that in this case the buried layer contains nanoclusters, including oxygen and boron alongside with silicon atoms. The further reduction of molecular oxygen implantation dose has led to essential distortion of spectra. The basic band of absorption (ν=1100 sm^{-1}) was considerably broadened and shifted to low frequencies.

Thus, the results of present work show that by means of ion implantation the creation of buried layers of borosilicate glass is feasible.

1. K. Bernstein and N. J. Rohrer. *SOI Circuit Design Concepts.* Kluwer Academic Publ., New York, 2002
2. S.A. Krivelevich, Y.I. Denisenko and A.A. Tsyrulev, “Ionic synthesis of silica-based glasses: prospect, simulation and applied aspects”, *Micro- and Nanoelectronics 2003*, K.A. Valiev, A.A. Orlikovsky (Eds.), Proc. of SPIE, 5401. pp. 119-128, 2004

Fast atom beam formation of inert and chemically active substances in an extensive source of ions for application in the technological processes

Y. Maishev, S. Shevchuk, T. Matveev.
. Institute of Physics and Technology RAS, Moscow, Russian Federation,
E-mail: shevchuk@ftian.ru

ULSI industrial process involves a submicron structures formation. All modern formation methods are concerned with charged particles usage (plasma chemical or ion-beam processing). Disadvantages of these methods are related to the defects due to the trapped charge [1] or plasma emission which arises under the action of UV-VUV [2]. Thus for the precision submicron structures etching process realization it is necessary to eliminate both surface charge brought by the plasma ions and the defects which appear under UV and VUV plasma emission influence. One of the promising solutions of these tasks is the development of neutral particles source and the technologies for submicron structure etching with fast atoms beams and dielectric thin films deposition from the fast atom beam.

In the presented work an extensive beam source with cold cathode was used for neutral particles beam formation. A neutralization system and fast atom beam separation system was investigated for this ion beam source. In the neutralization system the recharge of ions is implemented both on the own gas target in the neutralization channel and on the walls of the neutralization system. Residual ions were removed from the fast atom beam in the separation system. Thus we achieved high neutralization coefficient for inert and reactive working substances.

Experimental investigation of the fast atom beam source was done in the work. Fast atom beam with 100% neutralization was obtained. Processes of the etching by various inert and chemically active gases (argon, oxygen, CF_4, sulfur hexafluoride of a diamond like film and dioxide silicon film) were conducted in various operating modes of a source. Rates of etching and neutralization coefficient were calculated. Experiments on deposition of a diamond like film from a fast molecular beam of C_6H_{12} in various operating modes of a source were implemented. On the basis of the experimental data the optimum conditions for fast atom beam formation of inert and chemically active working substances were found.

1. Kinoshita T., Hane M., McVittee J.P., “Notching as an example of charging in uniform high density plasmas”, J. Vac. Sci. Technol.B, **V.14** pp.560-565, 1996.
2. M. Okigawa, Y. Yshikawa, Y. Ichihashi, S. Samukawa, “Ultraviolet-induced damage in fluorocarbon plasma and its reduction by pulse-time-modulated plasma in charge coupled device image sensor wafer processes”, J. Vac. Sci. Technol.B, **V.22**, pp.2818-2822, 2004.

Microwave plasma assisted single crystal diamond films growth and its application in microelectronics

A.L. Vikharev[1], A.M. Gorbachev[1], A.B. Muchnikov[1], D.B. Radishev[1], A.A. Altukhov[2], A.V. Mitenkin[2], M.P. Dukhnovsky[3], V.E. Zemlyakov[3]

1. Institute of Applied Physics, Russian Academy of Sciences, Nizhny Novgorod, Russia, E-mail address (val@appl.sci-nnov.ru). 2. ITC «UralAlmazInvest», Moscow, Russia, E-mail address (UAI-Co@yandex.ru). 3. FSUE «Istok», Fryazino, Russia, E-mail address (duhnovskyimp@mail.ru).

Recently, single crystal diamond became known as attractive material for micro- and nanoelectronics. It is caused by a number of outstanding properties of single crystal diamond, such as: highest thermal conductivity (22 W•cm-1•K-1 and more in isotopically-pure samples), broad transparency from the deep UV to the far IR and RF region of the electromagnetic spectrum, record-breaking carrier mobility, high breakdown voltage (up to 107 V•cm-1) and unique mechanical properties. Microwave plasma assisted chemical vapor deposited (CVD) single crystal diamond can demonstrate the properties of both a very good insulator (band gap 5.5 eV) and a wide band gap semiconductor (if doped).

In this paper we studied the conditions of high quality single crystal diamond films growth in a 2.45 GHz microwave plasma assisted CVD reactor. Single crystal diamond layers (thickness up to 300 microns) were grown on polished orthogonal natural diamond type IIa substrates at different growth parameters.

The CVD single crystal diamond layers were characterized by Raman spectroscopy, X-ray diffraction spectroscopy, SEM, AFM and optical microphotography. Grown CVD single crystal diamond layers were doped by boron ions and annealed. Electrophysical properties of grown layers were investigated.

Plasma damage and restoration of CVD low-k materials

Evgeny Smirnov[1] , Abdelkarim Ferchichi, Larry Zhao and Mikhail R. Baklanov

IMEC, 75 Kapeldreef, 3001 Leuven, Belgium;
1also at Moscow Institute of Electronic Technology (Technical University)

Materials with low dielectric constant (low-k) are required as interlayer dielectrics for on-chip interconnects of ultra-large-scale integrated (ULSI) devices to provide high speed, low dynamic power dissipation and low cross-talk noise. The k value reduction is obtained by the selection of appropriate chemical compounds in the film and by introduction of porosity.

Advanced low-k films are mainly based on Silica with 10-15% of organic hydrophobic groups. These groups are needed to avoid moisture adsorption that increases the dielectric constant. The hydrophobic groups are normally bonded to Si atom in SiO4/2 matrix. To reach a k-value below 3.0, introduction of artificial porosity is needed. Advanced low-k materials have porosity 30-50% and pore size close to 2-2.5 nm. The porosity creates number of integration challenges. One of the most difficult challenges is related to diffusion of active radicals into the films and further reaction with the film components.

In this work, the damage of SiCOH low-k films during the exposure in etch (fluorocarbon plasma) and strip (CO2 and NH3 based) plasmas in industrial CCP chamber is studied using FTIR spectroscopy, Ellipsometric porosimetry (EP), Water contact angle (WCA) and test structures based on special Planar capacitors (p-cap), designed for evaluation of electrical characteristics of thin films.[1] Then, the damaged films received restoration treatments based on silylation by silane derivatives in a special chamber integrated into the etch cluster. It allowed to transfer the etched wafers to the restoration chamber in vacuum condition without expose to air. As an alternative restoration method, the wafers immediately after plasma etch were exposed in CH4 plasma in the same plasma chamber.

Ellipsometric porosimetry data showed that intensive ion radiation in CCP chamber provides partial pores sealing when the low-k films are exposed. For this reason the degree of plasma damage was much less than observed in TCP chambers (FTIR data). However, this damage decreases WCA suggesting significant hydrophilization of the top surface. The both above suggested restoration treatments increases surface contact angle but FTIR data do not show significant reduction of hydrophilicity. Therefore, the restoration treatments were efficient only for surface hydrophobisation (restoration) while the bulk of low-k materials remains damaged. These phenomena are in good agreement with the results of electrical evaluation done by p-cap structures. The most important conclusion that is obtained from this research is that the major challenge of restoration treatment is limited penetration of restoration agents into the pores. The pore sealing that is normally considered as a positive sign of RIE, in this case plays a negative role.

[1] L.Zhao et al. IEEE International Interconnect Technology Conference (IITC), Sapporo, 2009.

Optimization of parameters of deep plasmachemical process of silicon etchings for elements MEMS

Vinogradov A.I., Zaryankin N.M., Mikhajlov Yu.A., Prokopiev E.P., Timoshenkov S.P.
Moscow Institute of Electronic Technology (Technical University), TU- MIET, Zelenograd, proezd 4806, bulding 5, Moscow, Russia, ,E-mail:spt@miee.ru

Process of deep etching of silicon is one of the basic and responsible step in technology of manufacturing of many sensitive elements (SE) structures MEMS [1]. It is also one of the most complex step, because of necessity to perform simultaneously the several, sometimes difficultly compatible conditions. Deep etching process should provide correct reproduction of geometrical structure SE, quite high etching rate, high selectivity to a mask. At the same time it is necessary to provide also the good quality (roughness) as lateral surfaces of a structure, and its bottom. In some cases decreasing or elimination of ARDE (aspect ratio difference of etching) effect is necessary etc.

Presence of several parameters which influence on the necessary process result, makes a way of searching the optimum (or close to optimum) etching result more difficult. A logical solution of this problem is using of statistical methods of planning and analysis of experiment [2]. Such methods allow us to reduce the number of experiments which are necessary for optimization of technological process. In addition, results of one series of experiments are sometimes enough for improvement at once several parameters.

Processes of deep plasmachemical etchings were performed using etcher AMS 200 (Alcatel, France). So-called Bosch-process, which consists of periodic alternation of short passivation- (gas C_4F_8) and etching- (gas SF_6) stages, was used. Typical value of selectivity which Alcatel company shows by delivery of the equipment is quite high and equals to about 75 to a photoresistive mask (PRM). But some practical applications require increasing this number. In particular, for etching trench deeper than 100 microns, the above-stated value of selectivity to a photoresistive mask are not enough. For etching on depth 200 μ and more (thinning process) it is necessary to use a metal mask or a mask from silicon dioxide. This circumstance complicates the technological process, considerably increasing number of steps. Therefore optimization of selectivity Si/PRM and Si/SiO_2 has been performed in the present work. Also the opportunity to decrease the ARDE effect has been investigated.

Processes of deep plasmachemical silicon etching were investigated using methods of planning of multifactorial experiments. It is established that pressure increasing simultaneously with bias power decreasing cause an increasing selectivity of silicon to a photoresistive mask and a SiO_2 mask. The recipe for deep etching of silicon with selectivity 300 to a photoresistive mask and 1200 to SiO_2 mask are obtained as a result of movement along a gradient.

It is revealed, that heterogeneity of silicon etching depth in trenches with different width (ARDE effect) decreases with increasing duration of passivation stage compare to etching stage. By movement along a gradient conditions at which heterogeneity of etching is essentially lowered are found.

Results of the fulfilled researches have been utilized during manufacturing the sensitive elements of micromechanical accelerometer and gyroscope.

1. I.I.Amirov, O.V.Morozov, M.O.Izyumov, V.A.Kal'nov, K.A.Valiev, A.A.Orlikovsky. // Microsystem technics. 2004. №12. P.15-18.
2. Achnazarova S.L., Kafarov V.V.// Optimization of experiment in chemical technology. M.: High school, 1983.
3. McAuley S.A., Ashraf H., Atabo L., Chambers A., Hall S., Hopkins J., Nicholls G. Silicon micromashining using a high – density plasma source // J.Phys. D: Appl. Phys. 2001. V. 34. P.2769 – 2774.
4. Rangelow I. W. Critical tasks in high aspect ratio silicon dry etching for microelectromechanical systems // J. Vac. Sci. Technol. 2003. V. A21. N 4. P. 1550 – 1562.

Formation of periodical nanostructures on semiconductors using solid alumina template

A.Belov, S.Gavrilov, V.Shevyakov
Moscow Institute of Electronic Techologies (Techincal University), E-mail: belov@dsd.miee.ru

Nanostructural materials are of practical and scientific interest both for understanding the fundamental electronic, magnetic, optical, thermodynamic, and mechanical properties of materials with nanometer sizes and for producing structures with radically new physical properties on their basis, resulting in significant increases in the functional characteristics of electronic and optical devices. Fabrication of nanodimensional structures is possible with the use of microelectronic technology. For this purpose, one can apply expensive methods of photolithography of deep and ultradeep ultraviolet, electrolithography, and X-ray lithography. Currently, methods based on using self-organization and self-formation, which are called non-lithographic methods, are actively being developed. These methods of fabrication of nanostructures are based on applying nanoporous materials as matrices for deposition or technological masks for etching, doping, etc. The analysis of data on porous semiconductors and dielectrics showed that a very promising material for the creation of nanostructures is porous anodic aluminum oxide.

In this work, we suggest the method of "dry" etching of silicon through a mask of porous aluminum oxide, which enables us to optimize this technology to the highest degree.

As initial materials, we chose silicon wafers, on the surface of which titanium and aluminum films of 30 nm and 2μm thick, respectively, were deposited layer-by-layer by magnetron sputtering. The deposition of the titanium film is caused by the necessity of having increased adhesion ability for the upper layer and reproducibility of the oxidizing process over the entire thickness of the aluminum layer. The two-stage anodization of deposited aluminum film formed a porous aluminum oxide mask. The final moment of the film anodization process was determined from the sharp increase in the anodized sample cathode voltage caused by the onset of formation of poreless titanium oxide layer. The obtained structures were ion-etched in argon. During the etching, we supported the working pressure in the chamber at a level of 2 10^{-3} Torr. The ion current was 0.1 A at an accelerating voltage of 7 kV. At the path of ion transportation, a hot tungsten cathode was located for the ion neutralization. Thus, the structure was bombarded with accelerated neutral particles. This prevented the polarization of aluminum oxide and resulted in efficient access of bombarding particles to the bottom part of oxide pores. In figure presented AFM image of the silicon substrate surface after selective removal of the solid oxide mask from it, and (b) profile of cross section of this structure

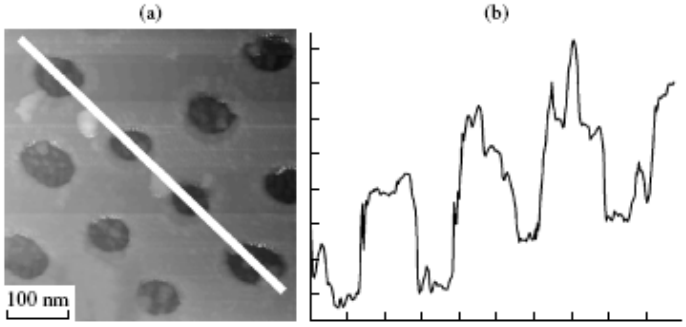

As a result of etching by accelerated argon atoms, it was possible to visualize the silicon substrate characterized by a nanoprofile surface, the pits in which represent as a whole the pattern of pores of the aluminum oxide solid mask. Due to its developed surface, this silicon structure can be used to form efficient elements of photodetection devices, environmental control sensors with increased sensitivity, etc.

Thus, the method using protection by the solid mask of porous alumina and subsequent "dry" etching is efficient for nanoprofiling various materials. The most acceptable method for etching through this mask is that based on the bombardment of structures with accelerated neutral atoms, in particular, argon atoms leading to an increased reproducibility of forming a nanoprofile. One of the advantages of the method proposed in this study is the possibility of using the solid masks, which are of great importance for the aspect ratio of pores. The fabricated silicon structures with the nanoprofile surface can be used in the creation of efficient elements of photodetection devices, environmental control sensors with increased sensitivity, etc.

The effect of a plasma treatment on the residual stresses of metallic cantilever structures

I.I. Amirov, V.V. Naumov

Yaroslavl branch of the Physics-Technology Institute of RAS, Yaroslavl, Russia, amirov@yf-ftian.ru

Film stress is crucial for stringent MEMS/NEMS design. Thin film structures deform undesirably as a result of residual stress. Bimaterial cantilever structures are always initially curved because of the imbalanced residual stress in the two layers. Therefore it is important to control the stress and stress gradient in the metal cantilever structures in order to obtain a flat metal cantilever after releasing [1, 2]. Stress level in the final structure may be different from the as-deposited state, because the film undergoes various micromachining processes, with various thermal cycles in different process steps and exposure to plasma treatment in the dry release process. The goal of the work is to investigate the influence of the plasma treatment of three layer Cr/Al/Cr cantilever structure (CS) on its residual stress. In the curvature-based approach to the film stress, the residual strain is derived from the measured curvature.

The three layer Cr/Al/Cr (50/250/50 nm) CS are fabricated using a surface micromachining technique with a amorphous Si layer (2 μm) as the sacrificial material. The cantilever structures are released upon the removal of the sacrificial layer using isotropic dry etching in low-pressure SF_6 plasma. Released Cr/Al/Cr cantilever structures are always found to be curved (Fig.1). Theirs treatment are performed in high density rf-inductive Ar and O_2 plasma at the different ion bombardment. The profile of the gradient strain is then derived from the curvatures measured during the continuous treatment of the top Cr or Al of the CS in plasma. The conditions of treatment were following; P=0,2 Pa, Q=10-20 sccm, W=800 W, W_{sb}=0-100 W. The time of treatment is equal 2-15 min.

It is shown that, during treatment Ar and O_2 plasma the beam deflection CS decreases, and a flat metal cantilever is observed. But in some case can be nonmonotonic, complicating the design. The rate of decrease of beam deflection was higher in O_2 plasma. The relationship between the residual strain and bending curvature is developed. The mechanisms of influence of plasma treatment on the stresses are discussed.

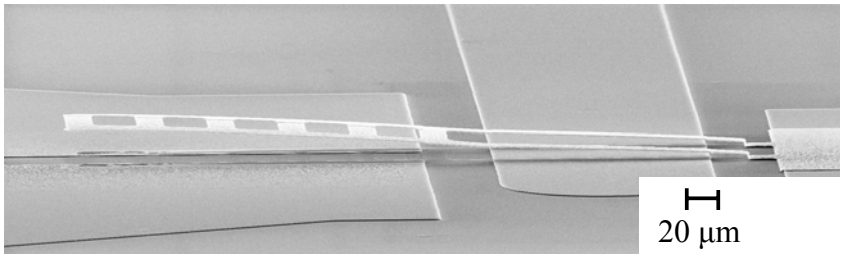

Fig1. A SEM image of a three layer Cr/Al/Cr cantilever structure

1. S. Huang, X. Zhang. Study of gradient stress in biomaterial cantilever structures for infrared applications. J. Micromech. Microeng. 17 (2007) 1211–1219

2. J. G. Boyd, S-H. Kim, S. Mani. Methodology for using residual stresses for self-assembly during deposition and etching of microstructures under external load. J. Micromech. Microeng. 17 (2007) 452–461

Kinetics of the GaAs etch process in the Cl_2 dc glow discharge plasma

A. Dunaev, S. Pivovarenok, A. Efremov, V. Svettsov
Ivanovo State University of Chemistry & Technology, Ivanovo, Russia, efremov@isuct.ru

GaAs is a highly perspective material for future micro- and nano-electronics due to the combinations of such favorable properties as low bandwidth and high mobility of charge carriers. This allows one to use GaAs in a wide number of high frequency devices and integral components. Also, the GaAs is a basic material for a quantum nano-electronics on AlGaAs hetero-junctions that also requires an accurate patterning of the GaAs-based structures.

From previous works, it is known that the patterning of GaAs requires the chlorine-containing gas chemistry which provides high etch rates in a combination with the acceptable etch anisotropy and etch selectivity over the photoresist. In this work, we carried out an investigation of the GaAs etch kinetics in order to understand deeper the GaAs etch mechanism in the Cl_2-based plasmas as well as to examine the ability of optical emission spectroscopy (OES) for the remote process control.

The experiments were carried out in a flow-type reactor made from the glass. The reactor has a cylindrical geometry with a radius of 3 cm and the discharge zone length of 40 cm. The etched samples (the fragments of a standard polished wafer with a size of 2x2 cm approx.) were placed on the level of the reactor wall with no additional bias. The operating parameters were the gas pressure (40–120 Pa), the discharge current (20–60 mA) and the gas flow rate (2-8 sccm). The GaAs etch rates were measured gravimetrically according to the change of the sample mass after the plasma treatment.

It was found that the gravimetric kinetic curves (Fig. 1) have an initial non-linear region $\Delta\tau$ where the etch rate depends on the etch time. This can be caused by such effects as 1) the formation of the Cl adsorbed layer which is necessary to start the reaction; 2) the etching of the native oxide layer which reacts slowly with both Cl and Cl_2; and 3) the non-uniform etch of the sample surface due to the initially non-uniform distribution of the active surface sites. The domination of the third reason follows from the fact that $\Delta\tau \to 0$ for the samples with a preliminary removed polished layer. With the change of operating parameters, the behavior of $\Delta\tau$ contradicts with the ion flux but follows the fluxes of both Cl2 and Cl. This allows one to assume the adsorption-desorption processes as the limiting stage. For the steady-state etch regime ($t >> \Delta\tau$, where t is the ethc time) the GaAs etch rate correlates linearly with the fluxes of neutral species. Such situation is typical for the kinetic regime of the heterogeneous plasma-assisted chemical reaction and corresponds to the first-order etch kinetics.

The OES diagnostics indicated the presence of Cl, GaCl and Ga in a gas phase while the Cl_2 was not detected because of the low sensitivity in the short wavelength region. The most stable, intensive and reproducible maximums are the Cl atom lines 725.6 nm and 837.6 nm as well as the resonant Ga lines 403.3 nm and 417.3 nm. From Fig. 2, it can be seen that intensities of the resonant Ga lines reach the steady-state values also after the some initial period which is in good agreement with the gravimetric measurements. A near-to-constant intensity of Cl lines corresponds to a constant Cl atom density and confirms the kinetic regime of the etch process.

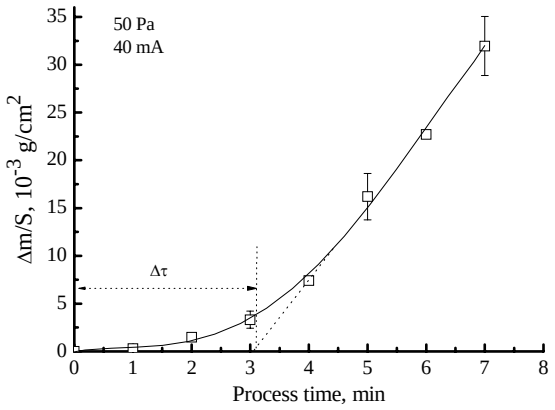

Fig. 1. The gravimetric kinetic curve.

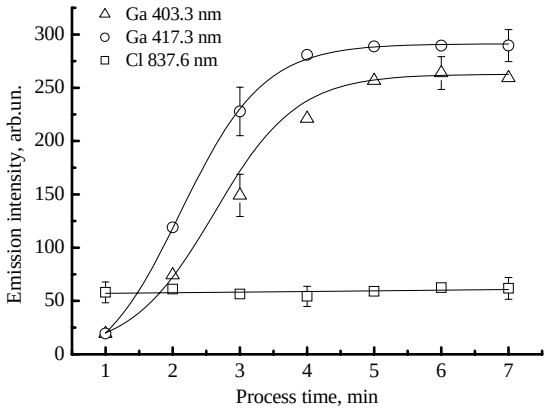

Fig. 2 The spectral kinetic curves. The conditions correspond to Fig. 1.

Plasma parameters and composition in HCl/X (X=Cl_2, H_2, Ar) dc glow discharges

A. Efremov, V. Svettsov, S. Lemehov
Ivanovo State University of Chemistry & Technology, Ivanovo, Russia, efremov@isuct.ru

The HCl-based gas mixtures have evident perspectives in modern micro- and nano-electronics technology being used for several purposes. The main advantage of the binary gas mixture plasma compared with the single gas process is that the gas mixing ratio gives an additional tool to adjust plasma parameters and composition and thus, to optimize the etch result. Particularly, it was found that the HCl-based plasmas provide improving etch selectivity of Si/SiO_2 and Si/photoresist compared with the fluorine-containing plasmas. Since the HCl shows much lower dissociation degrees than that for Cl_2 under the same operating conditions, the highly anisotropic etching is also expected for the materials which are traditionally patterned in the chlorine-containing plasmas, and namely for the A^2B^3 and A^3B^5 group semiconductors and metals Al, Cu, Pt, Au, etc. And finally, the HCl-based plasmas do not suffer from the carbon polymerization or from the re-deposition of the solid compounds resulting from the plasma chemical reactions of unsaturated radicals in a gas phase, as it was repeatedly mentioned for the traditionally used chlorine-containing gases CCl_4, BCl_3 and $SiCl_4$. However, the development and optimization of the etch process using the HCl-based gas mixtures is retarded by the insufficient knowledge how the additive gas influences both plasma parameters and densities of active species.

In this work we carried out the study of plasma parameters and active species kinetics in HCl/X (X=Cl_2, H_2, Ar) dc glow discharges using the 0-dimensional self-consistent model. The set of equations included: 1) The steady-state Boltzmann kinetic equation without accounting for both electron-electron collisions and the second-order impacts; 2) The plasma conductivity equation; 3) The balance equations for neutral and charged particles in a steady-state approximation; 4) The quasi-neutrality conditions for densities of charged particles as well as for their fluxes to the reactor wall. The output parameters were electron energy distribution function (EEDF), mean electron energy and drift rate, transport and kinetic coefficients of neutral and charged species, their volume-average densities and fluxes. As the self-consistency criterion, we used the balance equation for electrons in the approximation of "effective" diffusion coefficient. In order to provide the adequacy criteria for the model, the calculations were performed for the pressures of 20–300 Pa and the discharge currents of 3–30 mA that correspond to our work on diagnostics of the HCl plasma [1].

It was found that the HCl molecules are the dominant neutral species in pure HCl plasma, and the HCl dissociation degree is less than 25%. The steady-state densities of HCl dissociation products are noticeably influenced by the atom-molecular processes, such as R1: $H + HCl \rightarrow H_2 + Cl$ ($k_1 \sim 5\times10^{-14}$ cm^3/sec), R2: $H + Cl_2 \rightarrow HCl + Cl$ ($k_2 \sim 2\times10^{-11}$ cm^3/sec) and R3: $Cl + H_2 \rightarrow HCl + H$ ($k_3 \sim 8\times10^{-14}$ cm^3/sec). The fast decay of H atoms in R1 and R2, which also represent the additional channels for the formation of Cl atoms, results in a disproportion between Br and H densities providing [Cl]>[H]. It was found that even the small (less than 15%) additions of Cl_2 and H_2 to HCl result in the non-additive changes in plasma composition due to the shift in the quasi-equilibrium of R1–R3. Particularly, the addition of Cl_2 up to 15% suppressed the H atom density by more that the order of magnitude while the addition of H_2 results in a domination of H atom flux compared with that for Cl atoms. The addition of Ar does not influence directly the kinetics of R1–R3 but results in the noticeable changes in electron energy distribution and thus, in the electron impact kinetics. This is effect is similar to that obtained for the Cl_2/Ar plasmas [2] and is explained by lower collisional electron energy loss in the Ar-rich plasmas that causes an increase in mean electron energy. The dissociation of HCl due to the interaction with the metastable Ar: $HCl + Ar^m(^3p_{0\text{-}2}) \rightarrow H + Cl + Ar$ was found to be negligible. The reason is the low ($\sim10^{12}$–10^{13} cm^{-3}) density of $Ar^m(^3p_{0\text{-}2})$ because of both low excitation rate (low cross-section, high threshold) and fast heterogeneous decay.

1. **A.M. Efremov , G.H. Kim , D.I. Balashov , C.I. Kim**, Vacuum 81 (2006) 244–250.
2. **A.M. Efremov , Dong-Pyo Kim, Chang-Il Kim**, Thin Solid Films 435 (2003) 232–237.

Emission Tomography Algorithm Optimization: Applications for Microelectronic Plasma Equipment

A.V. Fadeev, K.V. Rudenko, V.F. Lukichev, A.A. Orlikovsky.

Lab. of Microstructuring and Submicron Devices, Institute of Physics & Technology, Russian Academy of Sciences, Moscow, Russia; e-mail: rudenko@ftian.ru

Optical emission tomography is a promising method for analysis of the lateral distribution of the particle density in plasma chambers that is critical for plasma tools design and for process design in microelectronic technology on 200-350 mm wafers. It concerns the distributions of uncharged chemically active radicals especially where reliable, built-in and cost efficient diagnostic techniques not developed at present. In this investigation, we propose the improvement an algorithm [1, 2] of the tomography reconstruction of the 2D distribution of plasma components in reactor chamber across the wafer when their spectrally resolved optical emission collected by fun-like sensors at an extremely small number of optical ports (viewpoints number tend to limit of two points). Chosen geometry of the data collection is compatible with the existing types of plasma reactors. The algorithm was tested for artificially created phantoms in a computing experiment and was applied to an actual plasma reactor [2].

The starting point is the model of 2D concentration field of plasma radical particles. That field is represented by superposition of non-interacting "elementary" inhomogeneities (smooth Gaussian-like functions) built over the flat average lateral distribution. The algorithm includes:

(1) Separation procedure for flat component for 2D-distribution from tomographic data;

(2) Reconstruction of "pure" inhomogeneities field by well-known tomography technique (i.e. maximum of entropy method) and determination at this step the parameters of "elementary" peak with maximum of amplitude in order to eliminate its contribution from input set of beam integrals (input data);

(3) Repeating the step (2) up to depletion of dynamic range of peaks limited by experimental conditions;

(4) Value iterations of parameters for founded peaks with minimum standard deviation adjustment of beam integrals of reconstructed 2D-field to respect on input data.

This investigation had improved the step (4) because of it gave the big error for phantoms with special geometry relatively viewpoints. It was revealed that multidimensional optimization for set of elementary peaks stopped at local minimum and not reached the global one. In that selected cases (example is phantom in Fig.1a), the original maximum of entropy technique at step (2) (Fig. 1b) gives wrong parameters for eliminating elementary peak for extremely ill-posed problem for two viewpoints. We have used the iterations in more wide neighborhoods of peak parameter values and took in account the physical limitations on elementary peaks originated from plasma nature. It allowed obtaining the reconstruction demonstrated at Fig. 1c with error 18% against 61% under non-optimized algorithm. The testing of updated algorithm on statistically large numbers of randomly generated phantoms had shown the error of reconstruction within 1 – 20 % for 2D-field of purified inhomogeneities. Accounting for addition of flat component in distribution in actual plasmas, the suggested technique has better accuracy for those plasma subjects.

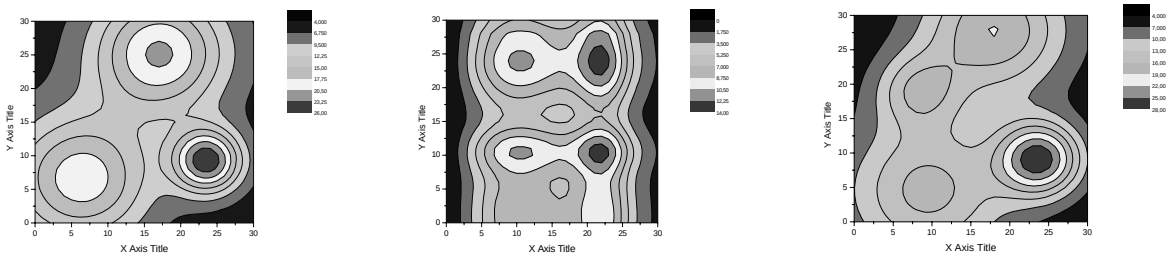

Fig.1.
a) phantom b) maximum entropy reconstruction c) final reconstruction result

1. K.V. Rudenko, F.V. Fadeev, A.A. Orlikovsky, and K.A. Valiev. Tomographic reconstruction of space plasma inhomogeneities in wide aperture plasma sources under strong restriction on the points of view, Proc. of SPIE v. 5401 (SPIE, Bellingham, WA, 2004), p. 79-83

2. A.V. Fadeev, K.V. Rudenko, V.F. Lukichev, A.A. Orlikovsky. Emission Tomography of Plasma in Technological Reactors of Microelectronics. Russian Microelectronics, 2009, Vol. 38, No. 2, pp. 95–109.

Characterization of GaSb(001) surface under pre-growth processing

M.S.Dunaevskii[1], E.V.Kunitsina[1], T.V.L'vova[1], A.N.Semenov[1], B.Y.Meltser[1], J.V.Terentyev[1]

1. Ioffe Physico-Technical Institute, Russian Academy of Sciences, Saint-Petersburg,, Russia,
E-mail addres: Mike.Dunaeffsky@mail.ioffe.ru

The antimonide of gallium and its solid solutions can be used as a medium for 2-5 mkm infra-red optoelectronic devices. Properties of the GaSb-based heterostructures depend on the degree of planarity and crystalline perfection of the GaSb-substrates. One of the main problems of the epitaxial growth of GaSb-based structures is the high chemical activity of GaSb surface and, as a result, the high rate of growth of its native oxide. The pre-epitaxial chemical passivation of the A^3B^5 substrates makes it possible to essentially improve the structural characteristics of the epitaxial layers grown at the substrates [1].

In this work thermal annealing and Na_2S treatment were used for pre-epitaxial chemical passivation of GaSb(001) substrates. The properties of passivated and annealed GaSb-substrates and GaSb/GaInAsSb heterostructures were analyzed by scanning probe microscopy (SPM), transmission electron microscopy (TEM) and photoluminescence (PL) methods.

Using the photoluminescence measurements from the surface of Na_2S-passivated GaSb, the solution concentration and duration of the Na_2S treatment were varied to select the regime corresponding to the maximum PL intensity. SPM studies were used to investigate an influence of the Na_2S-passivation of GaSb (001) substrates on structural properties of molecular beam epitaxy (MBE) grown heterostructures. The GaSb surface reconstructions during the ultra high vacuum (UHV) annealing were monitored by the reflection high-energy electron diffraction (RHEED).

Surface morphology of two group samples, identical before chemical treatment, was studied by SPM after UHV annealing. It was shown by SPM, that non-passivated epi-ready GaSb-substrates demonstrate rough topography (rms~6-8nm) after the UHV annealing. From the transformation of RHEED patterns during the annealing it was possible to measure the critical annealing temperature $T_g=560^0C$, which is necessary to remove the gallium oxide from the substrate. This value for non-passivated GaSb-substrates is high enough and close to temperatures of reactive etching of GaSb. Thus, standard pre-epitaxial procedure is not effective for epi-ready GaSb-substrates and leads to reactive etching and roughening of GaSb surface.

In case of the Na_2S-passivated GaSb-substrates low temperature annealing $T_g<400^0C$ is enough to get clear (3x1) RHEED reflexes, what is the evidence of smooth and clean GaSb surface. It was shown by SPM images, that the surface in this case is formed by flat terraces with rms~0.3-0.5nm. Thus, the result of sulfide passivation procedure is the removal of the gallium oxide and formation of thin layer of S-atoms, which passivate the GaSb surface.

There were also studied structural properties of GaSb/$Ga_{0.78}In_{0.22}As_{0.18}Sb_{0.82}$ heterostructures grown by MBE at the GaSb-substrates after the standard pre-epitaxial procedure (sample S1) and Na_2S-passivation procedure (sample S2). The images of cross-sectional transmission electron microscopy (XTEM) demonstrate the difference in the density of defects at the GaSb/$Ga_{0.78}In_{0.22}As_{0.18}Sb_{0.82}$ interface for S1 and S2 samples. XTEM images demonstrate the presence of dislocations at the GaSb/$Ga_{0.78}In_{0.22}As_{0.18}Sb_{0.82}$ interface in case of S1 sample, thus revealing poor structural properties of these heterostructures. On the contrary, in case of S2 sample XTEM shows no dislocations at the interface. So, Na_2S-passivation of GaSb drastically improves the crystalline perfection of the heterostructures grown at these substrates.

The results of this work demonstrate that the chemical Na_2S-passivation of GaSb(001) ensures the formation of planar surface without roughening or introducing additional defects to the surface. Na_2S-passivation decrease temperature of pre-epitaxial oxide removal annealing below 400^0C, what helps to avoid reactive etching of GaSb. Also, the passivation decrease density of interfacial defects and enhance crystallographic perfection of GaSb/GaInAsSb heterostructures grown at the GaSb(001)-substrates.

1. I.V.Sedova, T.V.L'vova, V.P.Ulin, S.V.Sorokin, A.V.Ankudinov, V.L.Berkovits, S.V.Ivanov, P.S.Kop'ev, "Sulfide passivating coatings on GaAs(100) surface and conditions of MBE growth of II-VI/GaAs", Semiconductors, **36**, pp.54-59, (2002)

Measurements samples temperature and dynamics of recrystallization of implanted silicon at rapid thermal processing

Ya. Fattakhov, M. Galyautdinov, B. Farrakhov, M. Zakharov

Kazan Physical Technical Institute of the Russian Academy of Sciences
Sibirsky Trakt 10/7, Kazan, 420029, Russia, fattakhov@kfti.knc.ru.

In our work the method for fast measurement of temperature on the surface of implanted silicon under rapid thermal processing was suggest and realized. The given method is based on using of Fraunhofer diffraction and realized on the samples of silicon are heated up to temperatures of melting (Tm=1412 ^{o}C) by powerful light pulse. The temperature of silicon was defined by angle changing measurement of the diffraction of the probing laser beam. The diffraction angle changed owing to increase of the period of the diffraction-grid at the dynamic thermal expansion of a crystal. Our structures on a silicon surface with period 4 μm formed by ion implantation. He-Ne laser with λ = 0.6328 μm as a probing beam radiation was used. The measured signal was registered in system symmetric diffraction maximum of the fifth order.

For an example in fig.1 the curves of temperature changes as a result of heating of the sample by pulses of incoherent light with duration τ_p = 3.49 s and density of power P = 60 W/cm^2 and photos of displacement diffraction maximums of the fifth order for the given mode is shown.

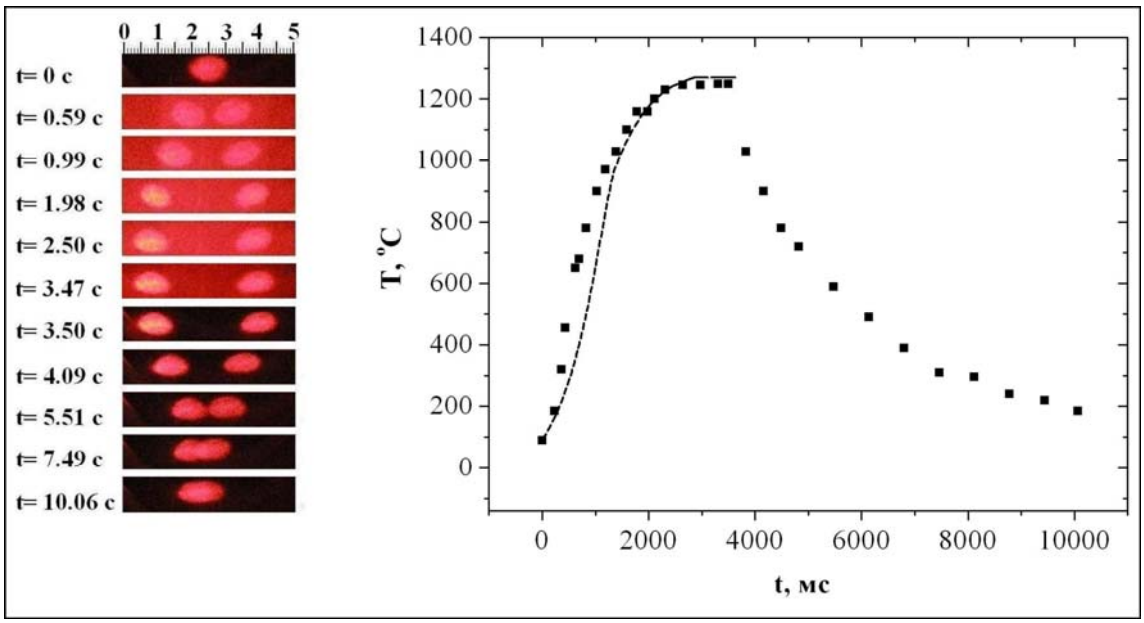

Fig.1. Dynamics of displacement diffraction maximums and the corresponding curves of temperature dependence from time at pulse heating (■–experiment, --- – calculation).

1. Ya.V.Fattakhov, M.F.Galyautdinov, T.N.L`vova, M.V.Zakharov, I.B.Khaibullin. Nuclear Instruments and Methods B, 257, Issues 1-2, pp. 222-226, 2007.
2. DesAutels G.L., Powers P., Brewer C., Walker M., Burky M., and Anderson G. Appl. Opt., 47, № 21, pp 3773-3777, 2008.

Features of electron direct tunneling through an ultrathin oxide under the non-stationary depletion of a n-Si surface

G.V.Chucheva, E.I.Goldman, Yu.V.Gulyaev, A.G.Zhdan
The Institute of Radio Engineering and Electronics Russian Academy of Sciences,
141190, Fryazino, Moscow Region, Russia, E-mail: gvc@.ms.ire.rssi.ru

The conductivity of the ultrathin (h<5nm) oxide in metal–oxide–semiconductor (MOS)-structures is defined by electron direct tunneling through the potential barrier, formed by a gate insulator [1]. At the same time the transparency of the barrier already at the zero-voltage between a field electrode (FE) and a semiconductor (V_g=0) is so great, that tunnel current becomes measured practically all at once after breaking of the detailed balance. Within the range of not too greater voltage drops on oxide V_i, corresponding to the depletion of the semiconductor, electrons on the Fermi level of the FE for the tunnel transition in a semiconductor, in addition to the barrier-oxide it is necessary to overcome else and the classically forbidden region in Si. This region appears therefore that the bottom of the conduction band of the semiconductor at the Si-SiO_2 interface (IF) under V_g=0 is situated above the Fermi level of the FE. With the increase V_i the bottom of the conduction band of the silicon is lowered under the Fermi level of the FE, and indicated range disappears. Thereby, the current–voltage (I-V)-characteristic of the circuit of the FE - Si must to contain to features, connected with the limitation of the electronic flow by the forbidden region in a semiconductor, as well as with its disappearance under the certain V_g.

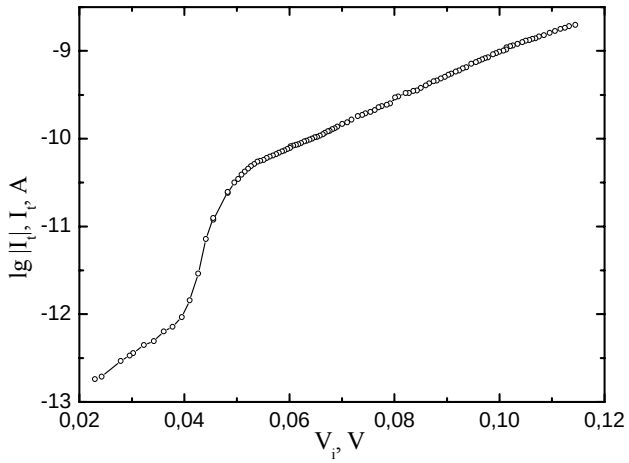

Fig.1.The experimental I-V-characteristic of investigated Si-MOS-structures

Exactly, under small values $|V_g|$ the tunnel current will be defined by the thermo-autoemission with the FE, growing with the increase $|V_g|$ on the typical thermo-autoemission law, taking into account the reduction and following disappearance of the additional barrier. Further, with growing $|V_g|$ the tunnel current will be defined by the classical law of the direct tunneling through the barrier, created by a gate insulator. Thereby, between the initial region of the tunnel I-V-characteristic and the region of the I-V-characteristic, appearing after the disappearance of the additional barrier must to exist the region of the sharp growth of the current. Calculations of the tunnel I-V-characteristic, taking into account considered circumstance, show that initial and final (after the disappearance of the additional barrier) of regions of dependencies of the tunnel current I_t from the V_i must to follow of the law: $lgI_t \propto |V_i|$.

In fig.1 the experimental I-V-characteristic of the tunnel conductivity of Al-SiO_2-n-Si-structures with the oxide thickness of 4nm are presented. I-V-characteristics are measured under the room temperature; steps of the depletion voltage with the amplitude before –20V are applied on structures. Initial values of the tunnel current are registered under each voltage step. This current has the step form before the moment of the time t≤1s. As is seen from the fig.1, observed I-V-characteristics are agreed well with above stated presentations. The developed approach to investigations of the conductivity of structures with ultrathin oxide in the regime of the non-equilibrium depletion possess the certain methodical advantage. This approach allows to identify the tunnel I–V– characteristic in coordinates of I_t – V_i the without use with difficulty realized method of voltage-capacitance characteristics in given conditions.

Work was supported by the Russian Foundation for Basic Research (grant 08-07-00360-a).

1. S.M.Sze. *Physics of Semiconductor Devices.* John Willey and Sons, New York, 1981.

Investigations of nanostructured porous PbTe films with X-ray diffractometry and reflectometry

S.P. Zimin[1], V.M. Vasin[1], E.S. Gorlachev[2], A.P. Petrakov[3], S.V. Shilov[3]
1. Yaroslavl State University, Russia, zimin@uniyar.ac.ru. 2. Yaroslavl Branch of the Institute of Physics and Technology, Russian Academy of Sciences, Russia, egorlachev@yandex.ru. 3. Syktyvkar State University, Russia, petrakov@syktsu.ru

In reference [1] a new method for the fabrication of porous nanostructured lead telluride films with electrochemical treatment of $PbTe/CaF_2/Si(111)$ epitaxial structures in the Norr solution was proposed. It was demonstrated that during anodizing with current density of 6 mA/cm^2 a formation of a mesoporous structure of lead telluride with a porosity value of about 50% takes place. The effective radius of PbTe nanoparticles was determined to be equal to 13 nm. Triple-crystal X-ray diffractometry results analysis showed that pores have spherical voids with an average dimension of 40 nm.

The aim of the present work was to perform X-ray diffractometry and reflectometry investigations of lead telluride porous films obtained with the anodizing current density of 2 and 4 mA/cm^2 with a duration of 10-20 min. PbTe films with *n*-type conductivity were grown on Si(111) substrates by molecular beam epitaxy using a 2 nm thin CaF_2 buffer layer. The lead telluride epitaxial layers with a 5.3 μm thickness were deposited at a substrate temperature of 400°C and a growth rate of 1 $\mu m \cdot h^{-1}$. Anodizing was carried out in the vertical type electrochemical cell with a platinum upper cathode. Norr solution was used as an electrolyte. The presence of microdefects of different nature in the samples has been studied using the methods of total external X-ray reflection and X-ray triple-crystal diffractometry (TCD) with the $Cu_{K\alpha 1}$ radiation (λ=1.54 Å).

Integral curves of X-ray reflectometry based on the effect of total external reflection for lead telluride films before and after anodic electrochemical treatment were measured with a sample deviation in the range of 5-25 arcmin. Considerable decrease of the critical angle, which was observed after anodizing, is explained by the decrease of X-ray density due to the pore formation. The calculations showed that the porosity value *P* (ratio of the total volume of the pores to the overall film volume) in the near-surface region of the anodized films is in the range from 40 to 70%.

Average pore dimensions along the sample surface L_x and at a right angle to the sample surface L_z were evaluated from TCD curves. According to the kinematic approach [2],

$$L_x \approx \lambda / 2\Delta\theta_x \sin\theta_B, \quad (1)$$

where $\Delta\theta_x$ is the width of the diffusive peak on the triple-crystal curve obtained in the mode of the scanning with the crystal-sample at a constant analizator (detector) angle of turn, θ_B is Bragg angle. Dimension of the pores along the surface normal is:

$$L_z \approx \lambda / 2\Delta\theta_z \cos\theta_B, \quad (2)$$

where $\Delta\theta_z$ is the width of the diffusive peak in the mode when the angle of turn of the analizator is two times larger than the angle of turn of the sample ($\theta/2\theta$-mode). The double-crystal rocking curves and TCD curves after a rotation around a surface normal at the angle φ=90° were measured as well for these samples. It was possible to determine the state of the propagation of the pores, which form at different angles to the surface, thus creating an intricate network of twisted pores. The dependence of the values L_x (39-81 nm) and L_z (72-96 nm) from anodizing conditions variation is analysed.

This work was performed with the financial support of the "Scientific potential development of higher school" Program (Project 2.1.1/466).

1. S.P. Zimin, E.A. Bogoyavlenskaya, E.Yu. Buchin, A.P. Petrakov, H. Zogg, D. Zimin, "Formation of porous nanostructured lead telluride films by anodic electrochemical etching method", Semicond. Sci. Technol., 24, 2009 (accepted for publication)
2. A.A. Lomov, D.Yu. Prokhorov, R.M. Imamov, D. Nohavica, P. Gladkov, "Characterization of porous InP(001) layers by triple-crystal x-ray diffractometry", Crystallography Reports, 51, No. 5, pp. 754-760, 2006

Relationship between modification of electrophysical properties and structural characteristics in semiconductor nanosized heterostructures$In_xAl_{1-x}As/In_yGa_{1-y}As/In_xAl_{1-x}As/InP$

R.M. Imamov[1], I.A. Subbotin[1], G.B. Galiev[2], I.S. Vasil'evsky[2], E.A. Klimov[2]

[1]*Shubnikov Institute of Crystallography RAS, Moscow, Russia, E-Mail: grondo@mail.ru.*
[2.]*Institute of UHF Semiconductor Electronic, Moscow, Russia*

Semiconductor nanosized heterostructures $In_xAl_{1-x}As/In_yGa_{1-y}As/In_xAl_{1-x}As/$ grown by molecular beam epitaxy on InP substrates are actively used now for creating of microwave transistors and integral microschemes operating in frequency range 100 GHz because of their new properties and record electrophysical characteristics. These objects are used for the development of communication systems with high density of information (throughput density).

In the present work the investigation of relationship of electrophysical properties modification and structural parameters of the set of the $In_xAl_{1-x}As/In_yGa_{1-y}As/In_xAl_{1-x}As/InP$ samples with different thickness of layer's contain were held. In such system of solid triple compounds high contain of InAs (from 53% to 70 – 80%) is provided. Depending on layer's composition (molar contribution of In, Al or Ga) formation of quantum well of necessary depth and thickness (10 – 25 nm) is provided. Two-dimensional electron gas is formed inside the quantum well by Si doping. Electrophysical characteristics of the samples containing different molar contribution of InAs as inside the quantum well and in buffer layer at different temperatures are measured. Structural diagnostics of samples were held by using high-resolution x-ray diffractometry. Structural parameters of layers and interfaces' characteristics were determined by measured rocking curves analysis. As a result it was established that increasing of molar contribution of InAs in pseudo-morphous channel $In_yGa_{1-y}As$ leads to increasing of electron mobility and concentration and the structural quality of the sample significantly improves. Lattice parameters mismatch of the layers leads to decreasing of mobility and degradation of structural perfection of grown samples because of genesis of large strain in the layers and forming of dislocations of noncompliance especially when contribution of InAs in the buffer layer decreases. When deviation from isomorphous buffer content $In_{0,52}Al_{0,48}As$ (up to 5-6 %) is not large relating to InP substrate the mobility of electrons in the channel remains high. This work was supported by President of Russian Federation grant for the young scientists (№138.2008.2.), program of RAS presidium (№27) and grant of leading scientific schools (№1955.2008.2.)

Characterization of Polymer Semiconductors with TOF-Sims and FTIR

V. Bachurin[1], A. Churilov[1], O. Kolesnikov[1], A. Rudy[2], S. Simakin[1]
1. Yaroslavl branch of Institute of Physics and Technology, Russian Academy of Sciences, Yaroslavl, Russia,
vibachurin@mail.ru *2. Yaroslavl State University, Yaroslavl, Russia,* rudy@uniyar.ac.ru

A large number of studies have been devoted to conducting polymers in the last time after the discovery of the drastic enhancement of conductivity after doping. Polymers of the polyaniline group including the hydrogen chloride, hydrogen bromide, sulfonic acid have conductivity up to 10^{-1} $Ohm^{-1}cm^{-1}$ and are very interesting for use its in a solar cell. Characterization of polyaniline in base form (conductivity $\sigma = 10^{-10}$ $(Ohm \cdot cm)^{-1}$), its HCl salt (σ =0.05 $(Ohm \cdot cm)^{-1}$) and composite Pani-TiO_2 HCl salt (σ =0.4 $(Ohm \cdot cm)^{-1}$) using Fourie infrared spectroscopy (FTIR) and time-of-flight secondary ion mass-spectrometry (TOF-SIMS) was the aim of this work.

The samples were prepared as pressed polymer powders. IR study was carried with help of BRUKER IFS 113v facility in the range 600-1700 cm^{-1}. It was found that base form of polyaniline (formula scheme depicted below) corresponds to emeraldine base (y~0.5) [1]. The changes of position and form of spectral lines were observed for polyaniline compounds.

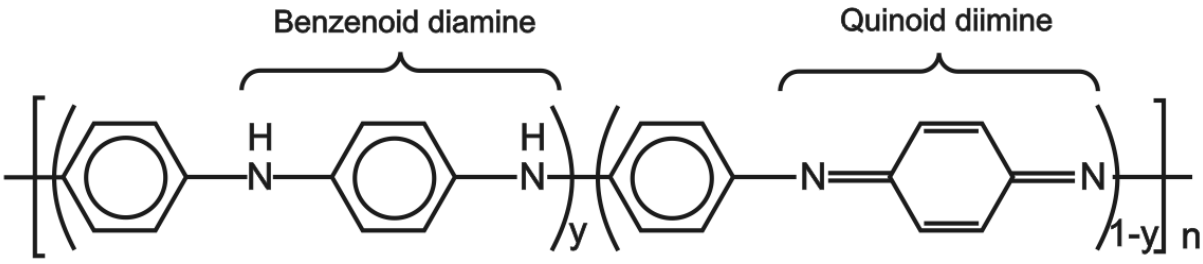

Chemical analysis of the samples was made on ION TOF-SIMS V experimental set up. 25 keV Bi^+, Bi_3^+ and 50 keV Bi_3^{++} primaries used to obtain mass spectra of secondary ions (1-800 a.u.m./q). The sample surface was cleaned by 1 keV Cs^+ ion bombardment before the measurements. The most experiments were carried out with Bi_3^+ ion beam because intensity of secondary ions was one order more in compare with other primaries. Dynamic range of analytical signal is 5 orders. It was established that the most intense have secondary ions which correspond to fragments of aniline monomer and polyaniline in emeraldine base and its compounds. The obtained results permit to make up the table of identified mass peaks and its intensities what is necessary for principal components analysis (PCA) [2] of polyaniline and its salts and composites.

1. S. Quillard, G. Louran and S. Lefrant, “Vibrational analysis of polyaniline”, Phys. Rev. B, 50, pp. 12496-12508, 1994
2. M.C. Biesinger, P-Y. Paepegaev, N.S. Mclntyre, R.R. Harbottle and N.O. Petersen , “Principal componennt analysis of TOF-SIMS images of organic monolayers”, Anal. Chem., 74, pp.5711-5716, 2002

General mechanism of the electric inactivity of the impurity atoms in chalcogenide vitreous semiconductors

G. A. Bordovsky, R.A. Castro, P.P. Seregin, Y.M. Stepanov
Herzen State Pedagogical University of Russia, Saint-Petersburg, Russia,
E-mail: recastro@fromru.com

The aim of the present work is the study of impurity states in chalcogenide vitreous semiconductors containing two-electronic centers with negative correlation energy (U- centers). For the study of electron and coordination states of the impurity atoms the methods of Mossbauer, dielectric and photoelectronic spectroscopy were used.

It was found the existence of general mechanism responsible for absence of the impurity conductivity in the chalcogenide glasses containing the U- centers. For the glasses containing the competing U- centers (for example, Ge and Sn) this mechanism is the following:

if a glass contains the U- centers of type I then their energy levels are positioned in the valence band (beneath the levels formed by chalcogenide atoms), Ge and Sn atoms are stabilized in states with non-saturated chemical bonds (Ge^{2+}, Sn^{2+}) so there is an "non-doping" effect for such centers (examples are Ge^{2+} and Sn^{2+} centers in a structural lattice of $Pb_{15-x}Sn_xGe_{28.5}S_{56.5}$ and $Pb_{17-x}Sn_xGe_{27}Se_{56}$ glasses);

if a glass contains the U- centers of type II then their energy levels are positioned in the bandgap (acceptor levels close to the top of the valence band, donor levels close to a bottom of a conductivity zone with Ge levels above Sn levels), Ge atoms are stabilized in Ge4+ state, tin atoms - in Sn^{2+} and Sn^{4+} states, the absence of the impurity conductivity for Sn centers is explained by the pinning of Fermi level between energy levels formed by Ge donor and acceptor centers (an example - Sn^{2+} centers in (As_2Se_3)-(SnSe)-(GeSe) glasses);

Gubanov-Mott model is a special case for the U- centers of type II when the doubled concentration of the acceptor centers in the structural lattice of glass exceeds the total Ge and Sn concentration (for example - tin atoms in (As_2Se_3)-(SnSe)-(GeSe) glasses).

Broadband dielectric spectroscopy of As_2Se_3 modified layers

N.I. Anisimova, V.A. Bordovsky, R.A. Castro, G.I.Grabko, D.S. Kirbiatev, Y.M. Stepanov
Herzen State Pedagogical University of Russia, Saint-Petersburg, Russia,
E-mail address: recastro@fromru.com

The electric and dielectric properties of modified chalcogenide glasses have been the subject of extensive studies in recent years in view of new prospects for applications of these materials in optoelectronics. However the nature of donor and acceptor impurities in several cases is still not well understood, and is under discussion. The aim of this research is the study of the dielectric relaxation processes in thin layers of As_2Se_3 doping by bismuth.

The $As_2Se_3(Bi)_x$ (x=0, 10 at. %) layers with thickness d ~ 1.0μm were obtained by method of joint-frequency atomization of the glass (As_2Se_3) and the modifier (Bi) onto silicate substrate at pressure of $8x10^{-3}$ mm Hg in the argon atmosphere. All samples had a sandwich configuration with aluminum electrodes and a contact area 15.0 ± 0.3 mm^2. The dielectric permittivity (ε') and dielectric tg δ were measured in the frequency range of 10^{-2} to 105 Hz and in the temperature range of -40 to +70 ^{0}C by using a High-Resolution Dielectric Analyzer (Novocontrol Concept 41).

All films of non-modified As_2Se_3 undergo a Debye-type relaxation. In modified films three relaxation processes and two phase transitions are revealed in the studied temperature range. The relaxation process occurring at the lowest temperature is associated with the local mobility of the glassy chains. At higher temperatures, there occurs an intensive relaxation process that can be attributed to space-charge relaxation or manifestation of the normal relaxation mode.

It is known that the addition of bismuth gives birth to Bi2Se3 clusters in the glassy matrix [1]. The composition of the clusters and the matrix changes with the increasing bismuth concentration. This fact explains the observed structural changes. The empirical data were sufficient fitted using the Havriliak-Negami equation. The temperature dependence of the parameter α is discussed.

1. R.A. Castro, G.A. Bordovsky, V.A. Bordovsky, N.I. Anisimova, "Correlation between bismuth concentration and distribution of relaxators in As2Se3(Bi)x layers", Journ. of Non-Cryst. Sol., 352, pp. 1560-1562, 2006.

Author Index

Author Index

Author Index

Author Index

Author Index

Author Index

Author Index

Author Index

Author Index